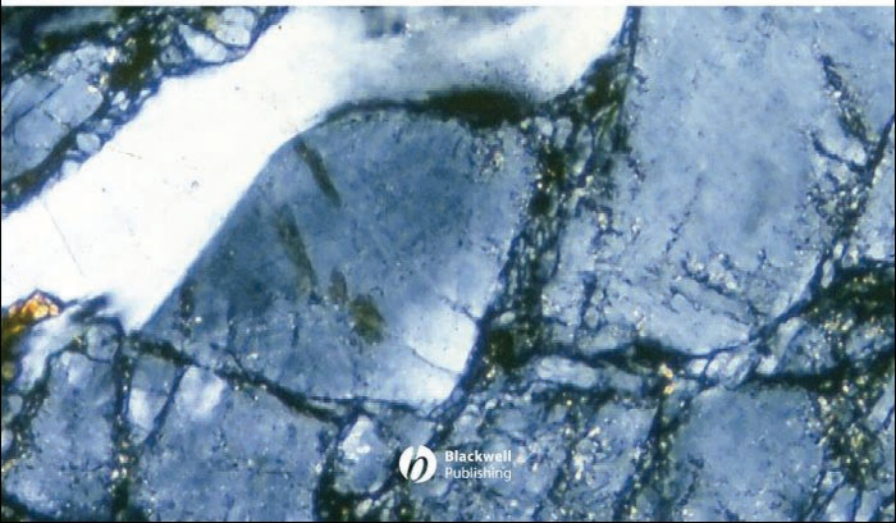




Stephen M. Rowland, Ernest M. Duebendorfer, and Ilsa M. Schiefelbein

# STRUCTURAL ANALYSIS & SYNTHESIS

A LABORATORY COURSE IN  
STRUCTURAL GEOLOGY THIRD EDITION



# Structural Analysis and Synthesis



**A well-armed field party, mapping the geology of Weathertop, in the southeastern Bree Greek Quadrangle. The view is toward the north along the intrusive contact between the Cretaceous Dark Tower Granodiorite, on the right, and the cliff-forming Devonian Lonely Mountain Quartzite, on the left.**

# Structural Analysis and Synthesis

## A Laboratory Course in Structural Geology

Third Edition

Stephen M. Rowland  
University of Nevada, Las Vegas

Ernest M. Duebendorfer  
Northern Arizona University

Ilsa M. Schiefelbein  
ExxonMobil Corporation, Houston, Texas



© 2007 by Stephen M. Rowland, Ernest M. Duebendorfer, and Ilsa M. Schiefelbein  
© 1986, 1994 by Blackwell Publishing Ltd

BLACKWELL PUBLISHING  
350 Main Street, Malden, MA 02148-5020, USA  
9600 Garsington Road, Oxford OX4 2DQ, UK  
550 Swanston Street, Carlton, Victoria 3053, Australia

The right of Stephen M. Rowland, Ernest M. Duebendorfer, and Ilsa M. Schiefelbein to be identified as the Authors of this Work has been asserted in accordance with the UK Copyright, Designs, and Patents Act 1988.

All rights reserved. No part of this publication may be reproduced, stored in a retrieval system, or transmitted, in any form or by any means, electronic, mechanical, photocopying, recording or otherwise, except as permitted by the UK Copyright, Designs, and Patents Act 1988, without the prior permission of the publisher.

First edition published 1986 by Blackwell Publishing Ltd  
Second edition published 1996  
Third edition published 2007

1 2007

*Library of Congress Cataloging-in-Publication Data*

Rowland, Stephen Mark.

Structural analysis and synthesis: a laboratory course in structural geology. — 3rd ed. / Stephen M. Rowland, Ernest M. Duebendorfer, Ilsa M. Schiefelbein.

p. cm.

Includes bibliographical references and index.

ISBN-13: 978-1-4051-1652-7 (pbk. : acid-free paper)

ISBN-10: 1-4051-1652-8 (pbk. : acid-free paper)

1. Geology, Structural—Laboratory manuals. I. Duebendorfer, Ernest M. II. Schiefelbein, Ilsa M. III. Title.

QE501.R73 2006

551.8'078—dc22

2005021041

A catalogue record for this title is available from the British Library.

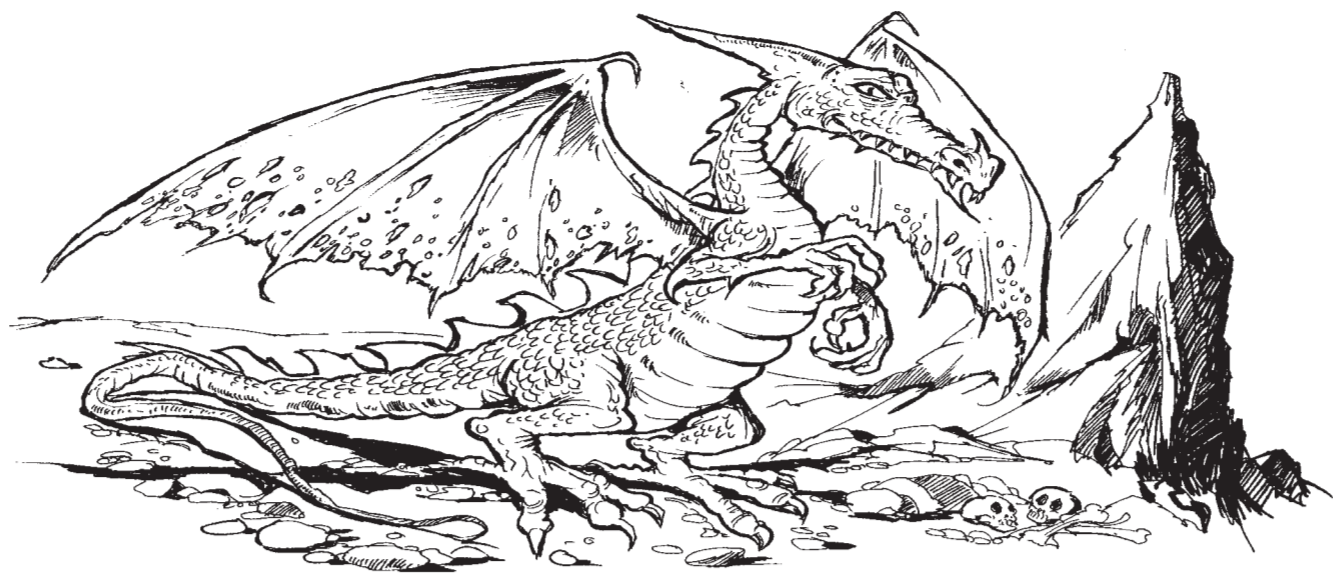
Set in 10/12pt Sabon  
by SPi Publisher Services Pondicherry, India  
Printed and bound in Singapore  
by Markono Print Media Pte Ltd

The publisher's policy is to use permanent paper from mills that operate a sustainable forestry policy, and which has been manufactured from pulp processed using acid-free and elementary chlorine-free practices. Furthermore, the publisher ensures that the text paper and cover board used have met acceptable environmental accreditation standards.

For further information on  
Blackwell Publishing, visit our website:  
[www.blackwellpublishing.com](http://www.blackwellpublishing.com)

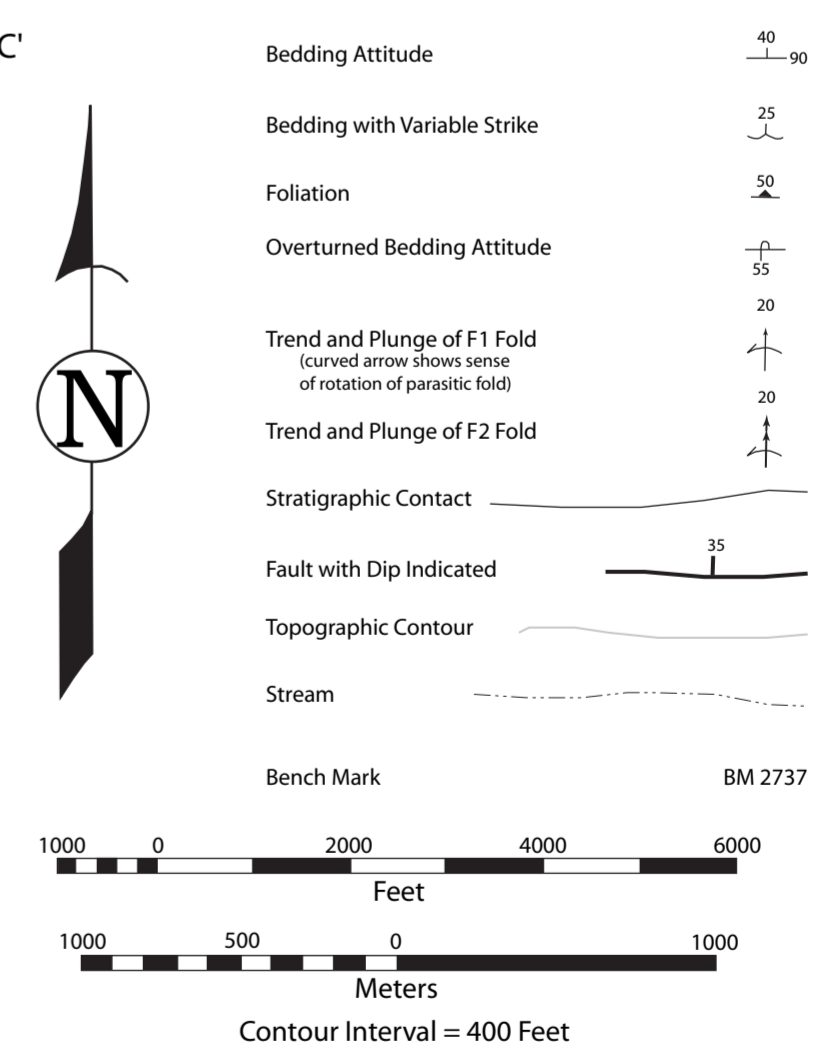
# Dedication

This edition is lovingly dedicated to the memory of artist Nathan F. Stout (1948–2005), our friend and colleague, who drafted all of the numbered figures. Nate spent his career as the Geoscience Department illustrator at UNLV. He hung on just long enough to complete this project, and then he slipped away. If you find any of his artwork especially attractive or helpful, think about Nate. He drew them just for you.



**Bree Creek Quadrangle**

Thd	Pliocene
Helm's Deep Sandstone	Miocene
Tr	
Rohan Tuff	
Tg	Tertiary
Gondor Conglomerate	
Tdd	
Dimill Dale Diatomite	
Tmm	
Misty Mountain Limestone	Eocene
Tm	
Mirkwood Shale	Paleocene
Tts	
The Shire Sandstone	
Tb	Paleocene
Bree Conglomerate	
Te	Paleocene
Edoras Formation (evaporites and nonmarine)	
Kdt	Cretaceous
Dark Tower Granodiorite	Mississippian
Mr	
Rivendell Dolomite	Devonian
Dlm	
Lonely Mountain Quartzite	Silurian
Sm	
Moria Slate	Ordovician
Omt	
Minas Tirith Quartzite	Ordovician
Omt	
Mt. Doom Schist	Ordovician



SMR©2007



# Contents

- Preface, x
- Read This First, xii
- 1 Attitudes of Lines and Planes, 1**
  - Objectives, 1
  - Apparent-dip problems, 3
  - Orthographic projection, 4
  - Trigonometric solutions, 8
  - Alignment diagrams, 9
- 2 Outcrop Patterns and Structure Contours, 11**
  - Objectives, 11
  - Structure contours, 14
  - The three-point problem, 15
  - Determining outcrop patterns with structure contours, 16
  - Bree Creek Quadrangle map, 20
- 3 Interpretation of Geologic Maps, 21**
  - Objectives, 21
  - Determining exact attitudes from outcrop patterns, 21
  - Determining stratigraphic thickness in flat terrain, 23
  - Determining stratigraphic thickness on slopes, 23
  - Determining stratigraphic thickness by orthographic projection, 25
  - Determining the nature of contacts, 26
  - Constructing a stratigraphic column, 28
- 4 Geologic Structure Sections, 31**
  - Objective, 31
  - Structure sections of folded layers, 32
  - Structure sections of intrusive bodies, 33
  - The arc method, 33
  - Drawing a topographic profile, 34
  - Structure-section format, 36
- 5 Stereographic Projection, 38**
  - Objective, 38
  - A plane, 40
  - A line, 40
  - Pole of a plane, 42
  - Line of intersection of two planes, 42
  - Angles within a plane, 43
  - True dip from strike and apparent dip, 44
  - Strike and dip from two apparent dips, 44
  - Rotation of lines, 46
  - The two-tilt problem, 47
  - Cones: the drill-hole problem, 48
- 6 Folds, 53**
  - Objectives, 53
  - Fold classification based on dip isogons, 56
  - Outcrop patterns of folds, 57
  - Down-plunge viewing, 59
- 7 Stereographic Analysis of Folded Rocks, 61**
  - Objectives, 61
  - Beta ( $\beta$ ) diagrams, 61
  - Pi ( $\pi$ ) diagrams, 62
  - Determining the orientation of the axial plane, 62



- Constructing the profile of a fold exposed in flat terrain, 62  
Simple equal-area diagrams of fold orientation, 63  
Contour diagrams, 65  
Determining the fold style and interlimb angle from contoured pi diagrams, 67
- 8 Parasitic Folds, Axial-Planar Foliations, and Superposed Folds, 69**  
Objectives, 69  
Parastic folds, 69  
Axial-planar foliations, 70  
Superposed folds, 72
- 9 Faults, 76**  
Objectives, 76  
Measuring slip, 78  
Rotational (scissor) faulting, 80  
Tilting of fault blocks, 82  
Map patterns of faults, 82  
Timing of faults, 83
- 10 Dynamic and Kinematic Analysis of Faults, 85**  
Objectives, 85  
Dynamic analysis, 85  
Kinematic analysis, 90
- 11 A Structural Synthesis, 95**  
Objective, 95  
Structural synthesis of the Bree Creek Quadrangle, 95  
Writing style, 97  
Common errors in geologic reports, 98
- 12 Rheologic Models, 99**  
Objective, 99  
Equipment required for this chapter, 99  
Elastic deformation: instantaneous, recoverable strain, 99  
Viscous deformation: continuous strain under any stress, 100  
Plastic deformation: continuous strain above a yield stress, 101  
Elasticoplastic deformation, 102  
Elasticoviscous deformation, 102  
Firmoviscous deformation, 104  
Within every rock is a little dashpot, 104
- 13 Brittle Failure, 107**  
Objective, 107  
Equipment required for this chapter, 107  
Quantifying two-dimensional stress, 107  
The Mohr diagram, 109  
The Mohr circle of stress, 110  
The failure envelope, 111  
The importance of pore pressure, 115
- 14 Strain Measurement, 118**  
Objectives, 118  
Equipment required for this chapter, 118  
Longitudinal strain, 118  
Shear strain, 119  
The strain ellipse, 119  
Three strain fields, 120  
The coaxial deformation path, 121  
The coaxial total strain ellipse, 124  
Noncoaxial strain, 125  
The noncoaxial total strain ellipse, 126  
Deformed fossils as strain indicators, 127  
Strain in three dimensions, 128  
Quantifying the strain ellipsoid, 129
- 15 Construction of Balanced Cross Sections, 131**  
Objectives, 131  
Thrust-belt “rules,” 131  
Recognizing ramps and flats, 132  
Relations between folds and thrusts, 133  
Requirements of a balanced cross section, 136  
Constructing a restored cross section, 137  
Constructing a balanced cross section, 138
- 16 Deformation Mechanisms and Microstructures, 141**  
Objectives, 141  
Deformation mechanisms, 141  
Fault rocks, 144  
Kinematic indicators, 146  
S-C fabrics, 147  
Asymmetric porphyroclasts, 148  
Oblique grain shapes in recrystallized quartz aggregates, 149  
Antithetic shears, 149

**17 Introduction to Plate Tectonics, 152**

Objectives, 152

Fundamental principles, 152

Plate boundaries, 154

Triple junctions, 154

Focal-mechanism solutions  
("beach-ball" diagrams), 155

Earth magnetism, 160

Apparent polar wander, 162

B: Geologic timescale, 167

C: Greek letters and their use in this book, 168

D: Graph for determining exaggerated dips  
on structure sections with vertical  
exaggeration, 169

E: Conversion factors, 170

F: Common symbols used on geologic maps,  
171

G: Diagrams for use in problems, 172

**Appendices**A: Measuring attitudes with a Brunton  
compass, 165**References, 289****Further Reading, 291****Index, 297**

# Preface

This book is intended for use in the laboratory portion of a first course in structural geology. Structural geology, like all courses, is taught differently by different people. We have tried to strike a balance between an orderly sequence of topics and a collection of independent chapters that can be flexibly shuffled about to suit the instructor. Chapter 5 on stereographic projection, for example, may be moved up by those instructors who like to engage their students with stereonets as early as possible, and Chapter 12 on rheologic models may be moved up by those who start with an introduction to stress and strain.

There is, however, an underlying strategy and continuity in the organization of the material. As is explicit in the title, this book is concerned with both the analysis and synthesis of structural features. There is a strong emphasis on geologic maps throughout, and most of the first 10 chapters involve some interaction with a contrived geologic map of the mythical Bree Creek Quadrangle. The folded Bree Creek map will be found in an envelope at the back of the book. Before beginning work on Chapter 3 the student is asked to color the Bree Creek Quadrangle map. More than mere busy work, this map coloring requires the student to look carefully at the distribution of each rock unit. The Bree Creek Quadrangle becomes the student's "map area" for the remainder of the course. Various aspects of the map are analyzed in Chapters 2 through 10 (except for Chapter 6); in Chapter 11 these are synthesized into a written summary of the structural history of the quadrangle. Some instructors will choose to skip this syn-

thesis, but we hope that most do not—students need all the writing practice they can get. We have placed the synthesis report in Chapter 11 so that it would not be at the very end of the semester, to allow some writing time. Chapters 12 through 17, in any case, contain material that is less conducive to this teaching approach.

We have written each chapter with a 3-hour laboratory period in mind. In probably every case, however, all but the rarest of students will require additional time to complete all of the problems. The instructor must, of course, exercise judgment in deciding which problems to assign, and many instructors will have their own favorite laboratory or field exercises to intersperse with those in this book. To facilitate field exercises, we have included an appendix on the use of the Brunton compass.

No instructor assigns all 17 chapters of this book within a first course in structural geology. But our feedback from instructors has informed us that each of the chapters is important to some subset of instructors. Some chapters that cannot be explored in detail in the available laboratory time can still be profitably studied by the student. For the student who is frustrated about not having sufficient time to complete all of the chapters, we suggest that you consider proposing to your instructor that you enroll for a credit-hour or two of independent study next semester or quarter, and complete them at that time, perhaps in conjunction with a field project.

An instructor's manual is available from the publisher to assist the laboratory instructor in the use of this book.

The third edition represents a thorough revision of the book, beginning with the addition of a new co-author, Ilsa Schiefelbein, who took a fresh look at our approach. We scrutinized every line of every chapter, and we made many changes that had been suggested by students and lab instructors. In addition, all of the figures were redrafted to maximize clarity. Then, having completed a draft that we thought was nearly perfect, we subjected it to the critical eyes of reviewers Rick Allmendinger and Terry Naumann, who suggested many more ways of improving the presentation. We gratefully acknowledge their efforts; we incorporated as many of their suggestions as we possibly could, and the book is significantly better because of them.

In addition to many small improvements throughout, we made two format changes that will make the book easier to use for the student. The first of these concerns the placement of tear-out maps and exercises. In earlier editions these tear-out sheets were interspersed throughout each chapter. For this edition we have moved them all to Appendix G, which will reduce the clutter within the chapters. The second change is in the format of the Bree Creek Quadrangle map. In previous editions of the book, the Bree Creek map consisted of six separate sheets that the student was obliged to cut out and tape together. Furthermore, some of the edges did not match perfectly. For this edition we have gone to a single, large, folded-map format, which eliminates those pesky map problems.

Serendipitously, cultural events beyond our control conspired to make the Bree Creek map even more engaging than it might have been in the past. To many of the students who used earlier editions of this book, the names Gollum, Baggins, Dark Tower, and Helm's Deep, among many others that appear on the map, carried no particular significance. Nearly all students will now recognize the source of these names. We hope that this adds an additional measure of enjoyment to the use of this book.

It is our pleasure to acknowledge some people who played important roles in the development of

previous editions of this book. The core of the book was strongly influenced by courses taught by Edward A. Hay, Othmar Tobisch, Edward C. Beutner, and James Dietrich. Several of the map exercises in Chapter 3 were originally developed by geology instructor extraordinaire Edward A. Hay, now retired from De Anza College. The multiply deformed roof pendant on the Bree Creek map is adapted from an exercise presented to his students by USGS geologist James Dietrich, when he taught one quarter at U.C. Santa Cruz. And rock samples that appear in the exercises of Chapter 14 were photographed from the collection of U.C. Santa Cruz professor Othmar Tobisch, who kindly made them available for our use. The "plate game" of Chapter 17 was inspired by a similar exercise developed by the late Peter Coney of the University of Arizona.

We will not repeat here the long list of people who contributed in various important but smaller ways to the first and second editions; we hope it will suffice to say that their contributions are still valued, and we hope that they can share in the satisfaction of seeing that the book has lived on to help another generation of students explore the basic principles of structural geology.

Finally, we are sincerely pleased to acknowledge our partners at Blackwell Publishing: Ian Francis, Delia Sandford, Rosie Hayden, and copyeditor Jane Andrew. They helped us muster the energy and enthusiasm to take on the task of preparing a third edition, in the face of competing commitments, and they patiently worked with us through every step of the process.

S.M.R., E.M.D., and I.M.S

### **A Note to Faculty**

To request your Instructor's Resource CD-ROM please send an email to this address: [artworkcd@bos.blackwellpublishing.com](mailto:artworkcd@bos.blackwellpublishing.com)

## Read This First

You are about to begin a detailed investigation of the basic techniques of analyzing the structural history of the earth's crust. Structural geology, in our view, is the single most important course in the undergraduate curriculum (with the possible exception of field geology). There is no such thing as a good geologist who is not comfortable with the basics of structural geology. This book is designed to help you become comfortable with the basics—to help you make the transition from naive curiosity to perceptive self-confidence.

Because self-confidence is built upon experience, in an ideal world you should learn structural geology with real rocks and structures, in the field. The field area in this laboratory manual is the Bree Creek Quadrangle. The geologic map of this quadrangle is located in an envelope at the back of the book. This map will provide continuity from one chapter to the next, so that the course will be more than a series of disconnected exercises.

Most of the things that you will do in this laboratory course are of the type that, once done, the details are soon forgotten. A year or two from now, therefore, you will remember what kinds of questions can be asked, but you probably will not remember exactly how to get the answers. A quick review of your own solved problems, however, will allow you to recall the procedure. If your solutions are neat, well labeled, and not crowded together on the paper they will be a valuable archive throughout your geologic career.

In most of the chapters, we have inserted the problems immediately after the relevant text, ra-

ther than putting them all at the end of the chapter. The idea is to get you to become engaged with certain concepts—and master them—before moving on to the next concepts. We all learn best that way. Appendix G contains pages that are intended to be removed from the book and turned into your lab instructor as part of a particular problem's solution. We recommend that you place all of your completed lab exercises in a three-ring binder after they have been graded by your instructor and returned to you.

You will need the equipment listed below. A zippered plastic binder bag is a convenient way to keep all of this in one place.

- Colored pencils (at least 15)
- Ruler (centimeters and inches)
- Straightedge
- Graph paper (10 squares per inch)
- Tracing paper
- Protractor
- Drawing compass
- Masking tape
- Transparent tape
- 4H or 5H pencils with cap eraser
- Thumbtack (store it in one of the erasers)
- Drawing pen (e.g., Rapidograph or Mars)
- Black drawing ink
- Calculator with trigonometric functions.

If structural geology is the most important course in the curriculum, it should also be the most exciting, challenging, and meaningful. Our sincere hope is that this book will help to make it so.



# Attitudes of Lines and Planes

## Objectives

- Solve apparent-dip problems using orthographic projection, trigonometry, and alignment diagrams.
- Become familiar with the azimuth and quadrant methods for defining the orientations of planes, lines, and lines within planes.

**You will use one or more of these techniques later in the course to construct geological cross sections.**

This chapter is concerned with the orientations of lines and planes. The structural elements that we measure in the field are mostly lines and planes, and manipulating these elements on paper or on a computer screen helps us visualize and analyze geologic structures in three dimensions. In this chapter we will examine several graphical and mathematical techniques for solving apparent-dip problems. Each technique is appropriate in certain circumstances. The examination of various approaches to solving such problems serves as a good introduction to the techniques of solving structural problems in general. Finally, many of these problems are designed to help you visualize structural relations in three dimensions, a critical skill for the structural geologist.

The following terms are used to describe the orientations of lines and planes. All of these are measured in degrees, so values must be followed by the  $^{\circ}$  symbol.

**Attitude** The orientation in space of a line or plane. By convention, the attitude of a plane is

expressed as its *strike* and *dip*; the attitude of a line is expressed as *trend* and *plunge*.

**Bearing** The horizontal angle between a line and a specified coordinate direction, usually true north or south; the compass direction or azimuth.

**Strike** The bearing of a horizontal line contained within an inclined plane (Fig. 1.1). The strike is a line of equal elevation on a plane. There are an infinite number of parallel strike lines for any inclined plane.

**Dip** The vertical angle between an inclined plane and a horizontal line perpendicular to its strike. The direction of dip can be thought of as the direction water would run down the plane (Fig. 1.1).

**Trend** The bearing (compass direction) of a line (Fig. 1.2). Non-horizontal lines trend in the down-plunge direction.

**Plunge** The vertical angle between a line and the horizontal (Fig. 1.2).

**Pitch** The angle measured *within* an inclined plane between a horizontal line and the line in question (Fig. 1.3). Also called **rake**.

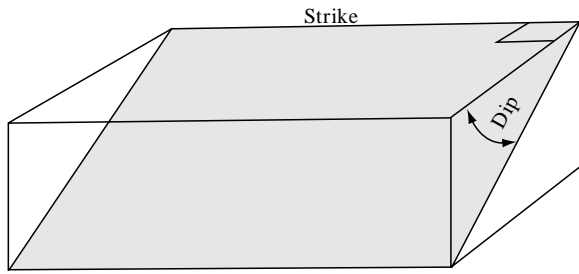


Fig. 1.1 Strike and dip of a plane.

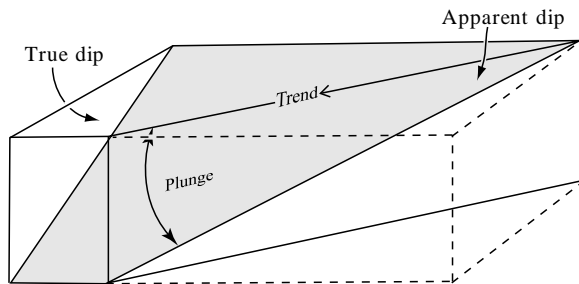


Fig. 1.2 Trend and plunge of an apparent dip.

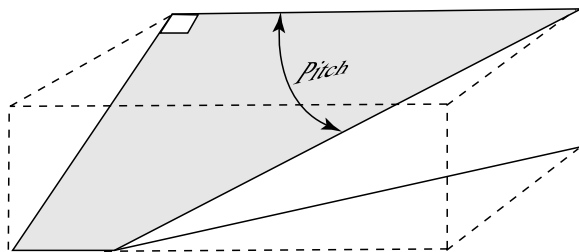


Fig. 1.3 Pitch (or rake) of a line in an inclined plane.

**Apparent dip** The vertical angle between an inclined plane and a horizontal line that is not perpendicular to the strike of the plane (Fig. 1.2). For any inclined plane (except a vertical one), the true dip is always greater than any apparent dip. Note that an apparent dip may be defined by its trend and plunge or by its pitch within a plane.

There are two ways of expressing the strikes of planes and the trends of lines (Fig. 1.4). The *azimuth* method is based on a  $360^\circ$  clockwise circle; the *quadrant* method is based on four  $90^\circ$  quadrants. A plane that strikes northwest–southeast and dips  $50^\circ$  southwest could be described as  $315^\circ, 50^\circ\text{SW}$  (azimuth) or  $\text{N}45^\circ\text{W}, 50^\circ\text{SW}$  (quadrant). Similarly, a line that trends due west and plunges  $30^\circ$  may be described as  $30^\circ, 270^\circ$  (sometimes written as  $30^\circ \rightarrow 270^\circ$ ) or  $30^\circ, \text{N}90^\circ\text{W}$ . For azimuth notation, always use three digits (e.g.,  $008^\circ, 065^\circ, 255^\circ$ ) so that a bearing cannot be confused with a dip (one or two digits). In this book, the strike is given before the dip, and the plunge is given before the trend. To ensure that you become comfortable with both azimuth and quadrant notation, some examples and problems use azimuth and some use quadrant. However, we strongly recommend that you use the azimuth convention in your own work. It is much easier to make errors reading a bearing in quadrant notation (two letters and a number) than in azimuth notation (a single number). In addition, when entering orientation data into a computer program or spreadsheet file, it is much faster to enter azimuth notation because there are fewer characters to enter.

Notice that because the strike is a horizontal line, either direction may be used to describe it. Thus a strike of  $\text{N}45^\circ\text{W}$  ( $315^\circ$ ) is exactly the same as  $\text{S}45^\circ\text{E}$  ( $135^\circ$ ). In quadrant notation, the strike is

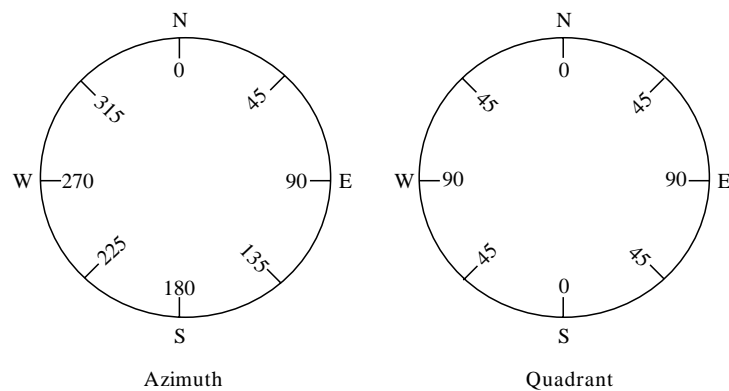


Fig. 1.4 Azimuth and quadrant methods of expressing compass directions.

commonly given in reference to north (N45°W rather than S45°E). In azimuth notation the “right-hand rule” is commonly followed. The right-hand rule states that you choose the strike azimuth such that the surface dips to your right. For example, the attitude of a plane expressed as 040°, 65°NW could be written as 220°, 65° using the right-hand rule convention because the 65°NW dip direction would lie to the right of the 220° strike bearing.

The dip, on the other hand, is usually not a horizontal line, so the down-dip direction must somehow be specified. The safest way is to record the compass direction of the dip. Because the direction of dip is always perpendicular to the strike, the exact bearing is not needed; the dip direction is approximated by giving the quadrant in which it lies or the cardinal point (north, south, east, or west) to which it most nearly points. If the right-hand rule is strictly followed, it is possible to specify the dip direction without actually writing down the direction of dip.

Solve Problems 1.1, 1.2, and 1.3.

**Apparent-dip problems**

There are many situations in which the true dip of a plane cannot be measured accurately in the field

**Problem 1.1**

Translate the azimuth convention into the quadrant convention, or vice versa.

a) N12°E	f) N37°W
b) 298°	g) 233°
c) N86°W	h) 270°
d) N55°E	i) 083°
e) 126°	j) N3°W

**Problem 1.2**

Circle those attitudes that are impossible (i.e., a bed with the indicated strike cannot possibly dip in the direction indicated).

a) 314°, 49°NW	f) 333°, 15°SE
b) 086°, 43°W	g) 089°, 43°N
c) N15°W, 87°NW	h) 065°, 36°SW
d) 345°, 62°NE	i) N65°W, 54°SE
e) 062°, 32°S	

or cannot be drawn on a cross-section view. Any cross section not drawn perpendicular to strike displays an apparent dip rather than the true dip of a plane (except for horizontal and vertical planes).

**Problem 1.3**

Fault surfaces sometimes contain overprinted slip lineations (fault striae). Such slip lineations can be used to determine the orientation of slip on a fault, and, therefore, whether the motion on the fault was strike-slip, dip-slip, or oblique-slip. A geology student who was just learning to use a Brunton compass recorded the orientations of five slip lineations on one fault surface. The strike and dip of the fault surface is 320°, 47°NE. The student’s five recorded lineation orientations are recorded in the table below.

Determine which lineation orientations are feasible and which ones must represent a mistake on the part of the student because the given orientation does not lie within the fault plane. Give a brief explanation for each of your five answers. For the valid lineation orientations, indicate which type of fault motion is indicated.

Lineation (plunge and trend)	Feasible? (yes or no)	Explanation	Type of motion indicated (strike-slip, dip-slip, or oblique-slip)
a) 34°, due north			
b) 0°, 140°			
c) 33°, N66°W			
d) 47°, 050°			
e) 75°, due north			



Apparent-dip problems involve determining the attitude of a plane from the attitude of one or more apparent dips, or vice versa. The strike and dip of a plane may be determined from either: (1) the strike of the plane and the attitude of one apparent dip, or (2) the attitudes of two apparent dips.

There are four major techniques for solving apparent-dip problems. These are: (1) orthographic projection, (2) trigonometry, (3) alignment diagrams (nomograms), and (4) stereographic projection. Stereographic projection is described in Chapter 5. The other three techniques are discussed in this chapter.

Throughout this and subsequent chapters the following symbols will be used:

- $\alpha$  (alpha) = plunge of apparent dip
- $\beta$  (beta) = angle between the strike of a plane and the trend of an apparent dip
- $\delta$  (delta) = plunge of true dip
- $\theta$  (theta) = direction (trend) of apparent dip.

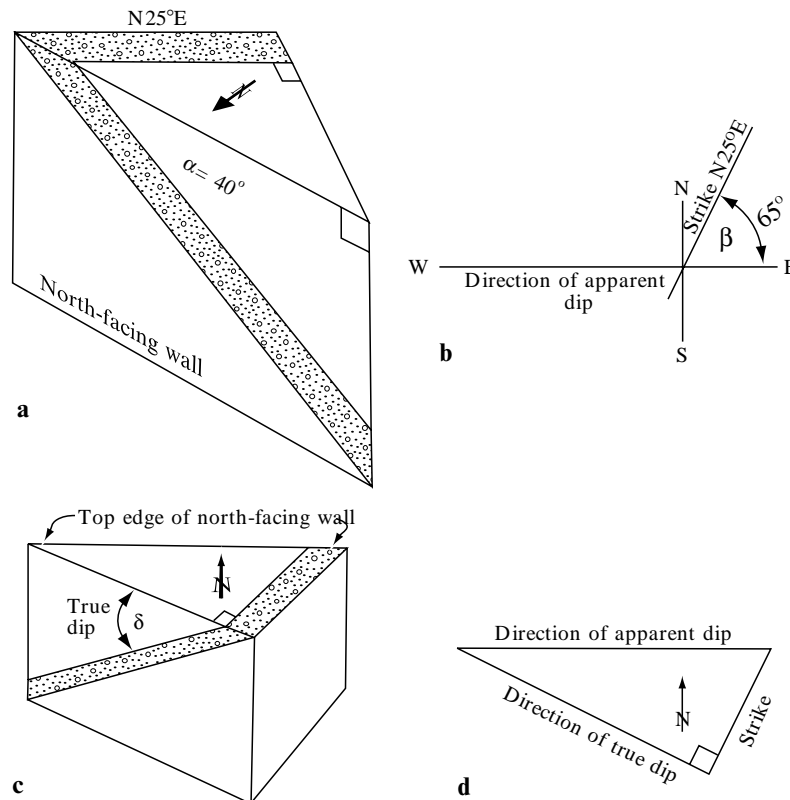
## Orthographic projection

One way to solve apparent-dip problems is to carefully draw a layout diagram of the situation. This technique, called orthographic projection, is more time-consuming than the other approaches, but it helps you to develop the ability to visualize in three dimensions and to draw precisely.

### Example 1.1: Determine true dip from strike plus attitude of one apparent dip

Suppose that a quarry wall faces due north and exposes a quartzite bed with an apparent dip of  $40^\circ$ , N $90^\circ$ W. Near the quarry the quartzite can be seen to strike N $25^\circ$ E. What is the true dip?

Before attempting a solution, it is crucial that you visualize the problem. If you cannot draw it, then you probably do not understand it. Figure 1.5a shows the elements of this problem.



**Fig. 1.5** Solution of Example 1.1. The dashed lines are fold lines. (a) Block diagram. (b) Step 1 of orthographic solution. (c) Block diagram looking north. (d) Orthographic projection of step 2. (e) Block diagram of step 3. (f) Orthographic projection of step 3. (g) Block diagram of step 4. (h) Orthographic projection of step 4.

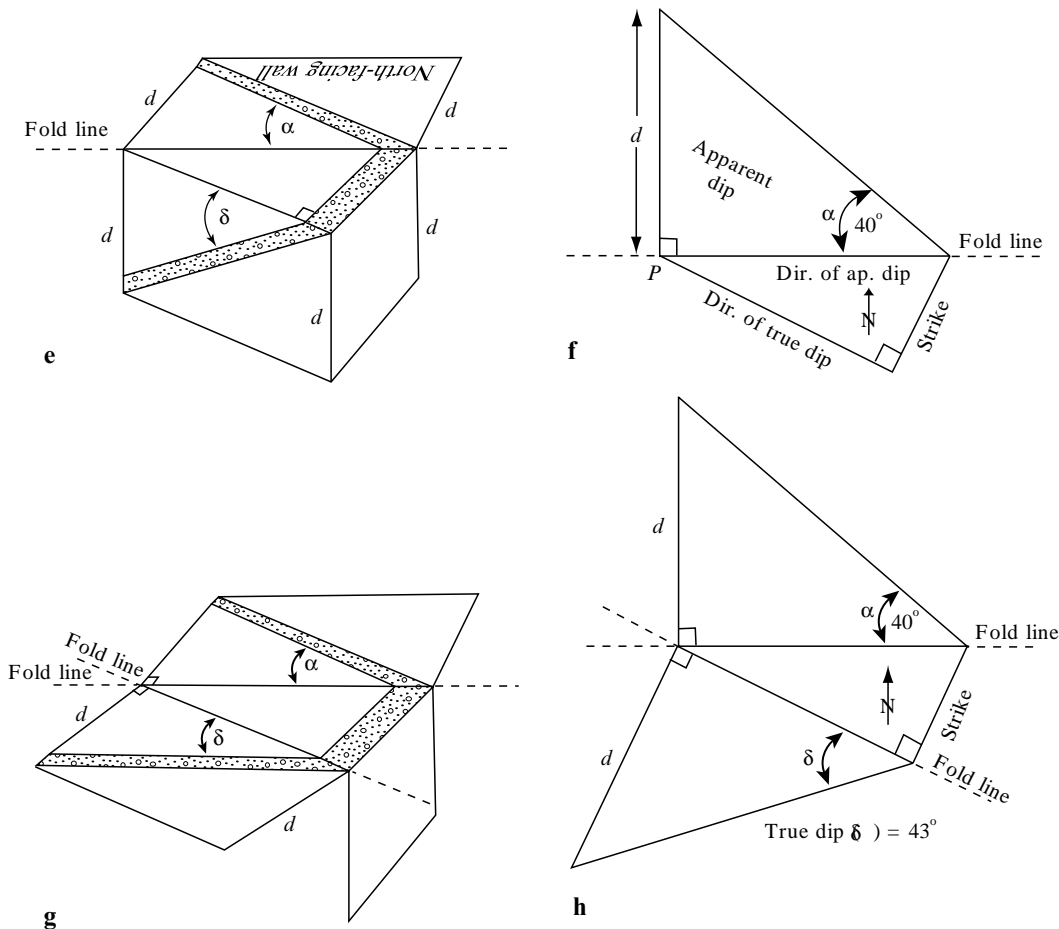
*Solution*

- 1 Carefully draw the strike line and the direction of the apparent dip in plan (map) view (Fig. 1.5b).
- 2 Add a line for the direction of true dip. This can be drawn anywhere perpendicular to the strike line but not through the intersection between the strike and apparent-dip lines (Fig. 1.5c,d).
- 3 Now we have a right triangle, the hypotenuse of which is the apparent-dip direction. Imagine that you are looking down from space and that this hypotenuse is the top edge of the quarry wall. Now imagine folding the quarry wall up into the horizontal plane. This is done graphically by drawing another right triangle adjacent to the first (Fig. 1.5e,f). The apparent-dip angle, known to be  $40^\circ$  in this problem, is measured and drawn directly adjacent

- to the direction of the apparent-dip line. Since the apparent dip is to the west, the angle opens to the west on the drawing. The line opposite angle  $\alpha$  is of length  $d$  and represents the depth to the layer of interest at point  $P$  (Fig. 1.5f).
- 4 Finally, the direction of true dip is used as a fold line, and another line of length  $d$  is drawn perpendicular to it (Fig. 1.5g,h). The true dip angle  $\delta$  is then formed by connecting the end of this new line to the strike line. Because the true dip is to the northwest, angle  $\delta$  opens toward the northwest. Angle  $\delta$  is measured directly off the drawing to be  $43^\circ$ .

If you have trouble visualizing this process, make a photocopy of Fig. 1.5h, fold the paper along the fold lines, and reread the solution to this problem.

Solve Problems 1.4 and 1.5.



**Fig. 1.5** (Continued)

**Problem 1.4**

Along a railroad cut, a bed has an apparent dip of  $20^\circ$  in a direction of  $N62^\circ W$ . The bed strikes  $N67^\circ E$ . Using orthographic projection, find the true dip.

**Problem 1.5**

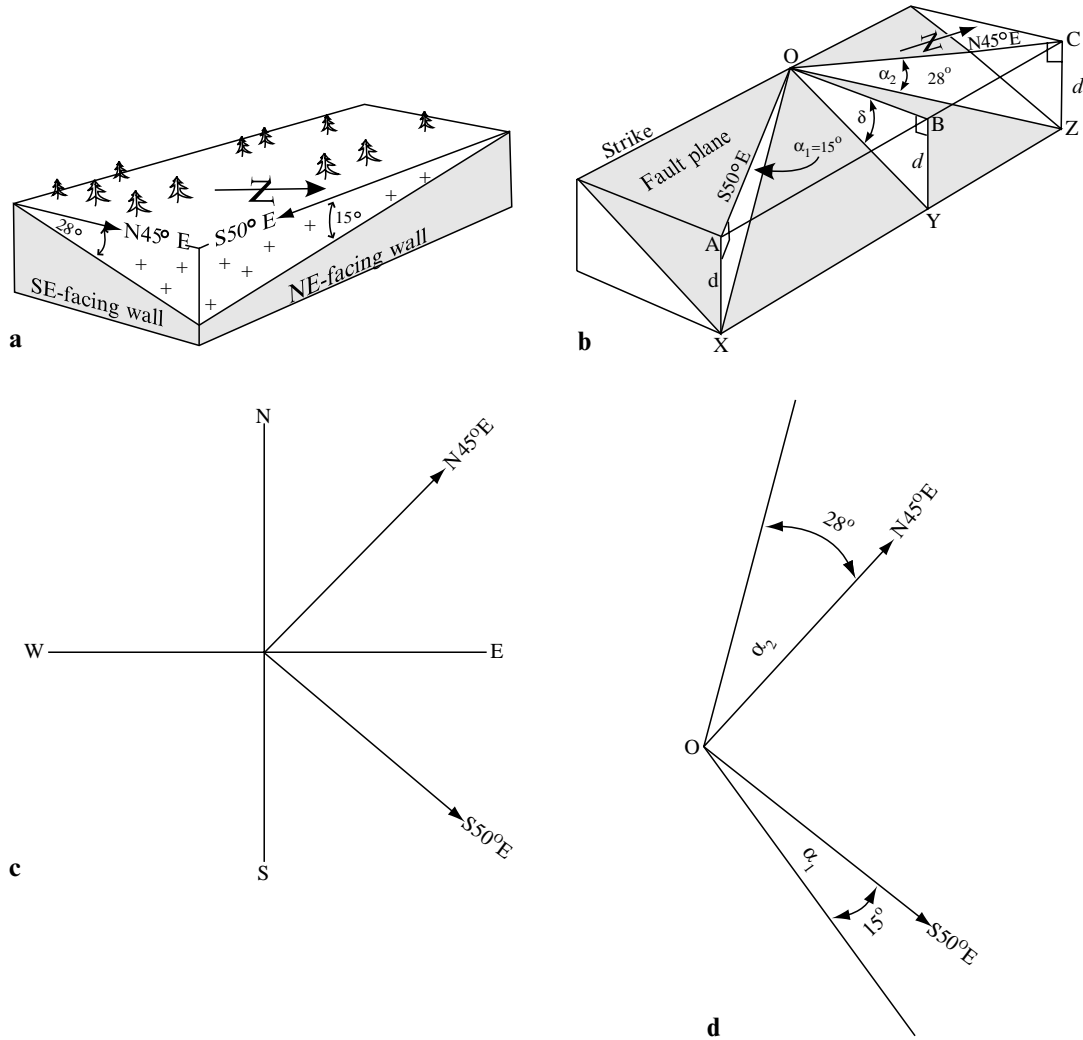
A fault has the following attitude:  $080^\circ, 48^\circ S$ . Using orthographic projection, determine the apparent dip of this fault in a vertical cross section striking  $295^\circ$ .

**Example 1.2: Determine strike and dip from two apparent dips**

Suppose that a fault trace is exposed in two adjacent cliff faces. In one wall the apparent dip is  $15^\circ$ ,  $S50^\circ E$ , and in the other it is  $28^\circ$ ,  $N45^\circ E$  (Fig. 1.6a). What is the strike and dip of the fault plane?

*Solution*

- 1 Visualize the problem as shown in Fig. 1.6b. We will use the two trend lines,  $OA$  and  $OC$ , as fold lines. As in Example 1.1, we will use a vertical line of arbitrary length  $d$ . Draw the two trend lines in plan view (Fig. 1.6c).
- 2 From the junction of these two lines (point  $O$ ) draw angles  $\alpha_1$  and  $\alpha_2$  (Fig. 1.6d). It does not



**Fig. 1.6** Solution of Example 1.2. (a) Block diagram. (b) Block diagram showing triangles involved in orthographic projection and trigonometric solutions. (c) Step 1 of orthographic solution. (d) Step 2. (e) Step 3. (f) Step 4. (g) Steps 5 and 6.

really matter on which side of the trend lines you draw your angles, but drawing them outside the angle between the trend lines minimizes the clutter on your final diagram.

- 3 Draw a line of length  $d$  perpendicular to each of the trend lines to form the triangles COZ and AOX (Fig. 1.6e). Find these points on Fig. 1.6b. The value of  $d$  is not important, but it must always be drawn exactly the same length because it represents the depth to the layer along any strike line.
- 4 Figure 1.6e shows triangles COZ and AOX folded up into plan view with the two apparent-dip trend lines used as fold lines. As shown in Fig. 1.6b, line AC is horizontal and parallel to the fault plane; therefore it defines the fault's strike. We may therefore draw line AC on the diagram and measure its trend to determine the strike (Fig. 1.6f); it turns out to be N22°W.
- 5 Line OB is then added perpendicular to line AC; it represents the direction of true dip (Fig. 1.6g).
- 6 Using line OB as a fold line, triangle BOY (as shown in Fig. 1.6b) can be projected into the horizontal plane, again using length  $d$  to set the position of point Y (Fig. 1.6g). The true

dip  $\delta$  can now be measured directly off the diagram to be 30°.

Solve Problems 1.6 and 1.7.

**Problem 1.6**

A fault plane is intersected by two mine adits. In one adit the plunge and trend of the apparent dip is 20°, N10°W, and in the other it is 32°, N85°W. Use orthographic projection to determine the attitude of the fault plane.

**Problem 1.7**

A bed strikes 065° and dips 40° to the south. Two vertical cross sections need to be drawn through this bed, one oriented north-south and the other oriented east-west. By orthographic projection determine the apparent dip on each cross section.

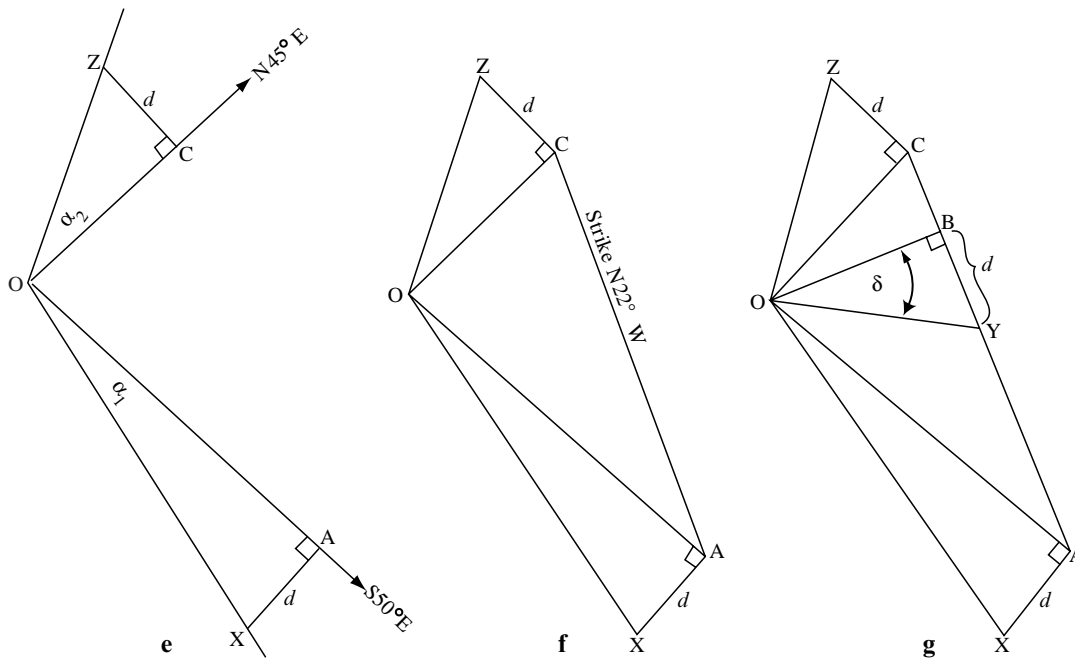


Fig. 1.6 (Continued)

### Trigonometric solutions

Apparent-dip problems can be done much faster and more precisely trigonometrically, especially with a calculator. This method is particularly suitable when very small dip angles are involved. Even when the angles are not drawn orthographically, however, you should sketch a block diagram in order clearly to visualize the problem. Programs to solve apparent-dip problems on programmable calculators are discussed by De Jong (1975).

Refer to Fig. 1.6b for the following derivation:

$$\begin{aligned} AX &= BY \\ \tan AOX &= \frac{AX}{OA} = \frac{BY}{OA} \\ \tan AOX &= \frac{BY}{OB(\sec AOB)} \\ \tan AOX &= \frac{OB(\tan BOY)}{OB(\sec AOB)} \\ &= \frac{\tan BOY}{\sec AOB} \\ &= \tan BOY \cos AOB \end{aligned}$$

or, using symbols,

$$\tan \alpha = (\tan \delta)(\cos \text{angle between true- and apparent-dip directions}) \quad (1.1)$$

or

$$\tan \delta = \frac{\tan \alpha}{\cos \text{angle between true- and apparent-dip directions}} \quad (1.2)$$

or

$$\tan \delta = \frac{\tan \alpha}{\sin \beta} \quad (1.3)$$

#### Example 1.3: Determine true dip from strike plus attitude of one apparent dip

Example 1.1 is a convenient problem of this type to solve trigonometrically. The strike of a bed is known to be  $025^\circ$  but we do not know the dip. An apparent dip is  $40^\circ$ ,  $270^\circ$ , and angle  $\beta$  (between the strike of the bed and the trend of the apparent dip) is  $65^\circ$  (Fig. 1.5b).

$$\begin{aligned} \alpha &= 40^\circ, \tan 40^\circ = 0.839 \\ \beta &= 65^\circ, \sin 65^\circ = 0.906 \end{aligned}$$

### Solution

From equation 1.3,

$$\begin{aligned} \tan \delta &= \frac{\tan \alpha}{\sin \beta} = \frac{0.839}{0.906} = 0.926 \\ \delta &= 42.8^\circ \end{aligned}$$

#### Example 1.4: Determine strike and dip from two apparent dips

Because two apparent dips with trend  $\theta$  are involved, they will be labeled  $\theta_1$  and  $\theta_2$ , which correspond to the two apparent-dip angles  $\alpha_1$  and  $\alpha_2$ .  $\theta_1$  should represent the more gently dipping of the two apparent dips.

This type of problem has two steps. The first step is to determine the angle between the true-dip direction and  $\theta_1$ . The relevant trigonometric relationships are as follows:

$$\begin{aligned} \tan \text{angle between } \theta_1 \text{ and true-dip direction} &= (\csc \text{angle between } \theta_1 \text{ and } \theta_2) \\ &\quad \times [(\cot \alpha_1)(\tan \alpha_2) - (\cos \text{angle between } \theta_1 \text{ and } \theta_2)] \end{aligned} \quad (1.4)$$

Using Example 1.2, we have the situation shown in Fig. 1.6c,d.

$$\begin{aligned} \theta_1 &= 130^\circ (\text{S}50^\circ\text{E}) & \alpha_1 &= 15^\circ \\ \theta_2 &= 45^\circ (\text{N}45^\circ\text{E}) & \alpha_2 &= 28^\circ \\ \text{angle between } \theta_1 \text{ and } \theta_2 &= 85^\circ \end{aligned}$$

### Solution

From equation 1.4,

$$\begin{aligned} \tan \text{angle between } \theta_1 \text{ and true-dip direction} &= (\csc 85^\circ)[(\cot 15^\circ)(\tan 28^\circ) - (\cos 85^\circ)] \\ &= 1.004[(3.732)(0.532) - (0.087)] \\ &= 1.004[1.985 - 0.087] = 1.91 \\ \text{angle between } \theta_1 \text{ and true-dip direction} &= 62.3^\circ \end{aligned}$$

This angle is measured from  $\theta_1$  in the direction of  $\theta_2$ . In this case the computed angle ( $62.3^\circ$ ) is less than the angle between  $\theta_1$  and  $\theta_2$  ( $85^\circ$ ). The true-dip direction, therefore, lies between  $\theta_1$  and  $\theta_2$ .  $\theta_1$  is  $130^\circ$  ( $\text{S}50^\circ\text{E}$ ) so the direction of true dip is  $130^\circ - 62^\circ = 68^\circ$  ( $\text{N}68^\circ\text{E}$ ). Examination of Fig. 1.6b shows that this is a reasonable dip

direction. A dip direction of N68°E corresponds to a strike of N22°W, which agrees with our orthographic projection solution.

If the angle between  $\theta_1$  and the true-dip direction is determined to be greater than the angle between  $\theta_1$  and  $\theta_2$ , then the angle is measured from  $\theta_1$  toward and beyond  $\theta_2$ .

Once the true-dip direction (and therefore the strike direction) has been determined, equation 1.3 is used to determine  $\delta$ :

$$\begin{aligned} \tan \delta &= \frac{\tan \alpha}{\sin \beta} \\ \alpha &= 15^\circ, \quad \tan \alpha = 0.268 \\ \beta &= \text{angle between } 130^\circ(\text{S}50^\circ\text{E}) \\ &\quad \text{and } 158^\circ(\text{S}22^\circ\text{E}) = 28^\circ \\ \sin \beta &= 0.469 \\ \tan \delta &= \frac{0.268}{0.469} = 0.571 \\ \delta &= 30^\circ \end{aligned}$$

**Problem 1.8**

Solve Problem 1.4 using trigonometry.

**Problem 1.9**

Solve Problem 1.5 using trigonometry.

**Problem 1.10**

A mining company is planning to construct an underground coal mine within a thin coal seam that dips 2° due east. You are the mine engineer, and it is your task to make sure that the mine adits do not fill with water. This requires that each adit has a slope of no less than 1°. In what directions may adits be oriented within the coal seam such that their slope is 1° or steeper?

**Problem 1.11**

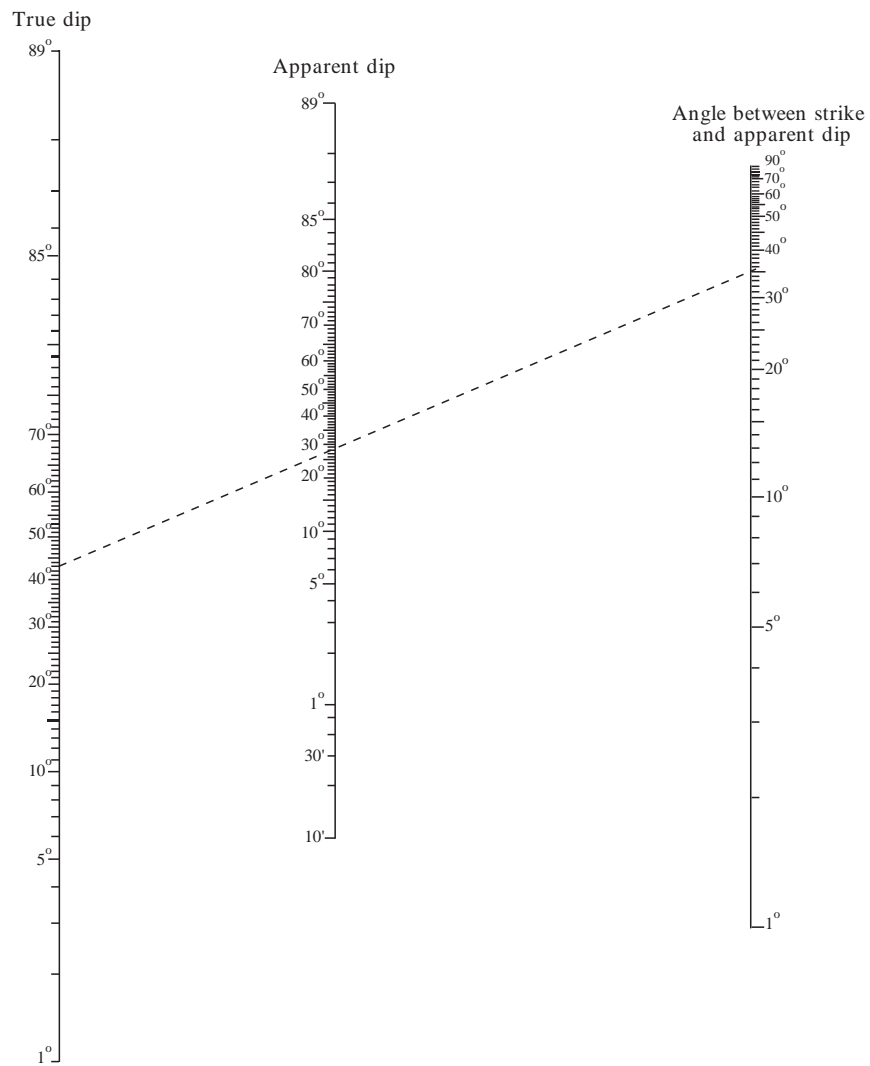
The apparent dip of a fault plane is measured in two trenches. In one trench the apparent dip is 4° toward the southwest in a trench wall that has a bearing of 220°. In the second trench the apparent dip is 7° toward the east in a trench wall that has a bearing of 100°. Trigonometrically determine the direction and angle of true dip.

**Alignment diagrams**

Alignment diagrams (nomograms) usually involve three variables that have a simple mathematical relationship with one another. A straight line connects points on three scales. Figure 1.7 is an alignment diagram for  $\delta$ ,  $\alpha$ , and  $\beta$ . If any two of these variables are known, the third may be quickly determined. This technique is particularly convenient for determining apparent-dip angles on geologic structure sections that are not perpendicular to strike, as discussed in Chapter 4.

**Problem 1.12**

Solve Problems 1.4 and 1.5 using the alignment diagram (Fig. 1.7).



**Fig. 1.7** Alignment diagram (nomogram) for use in solving apparent-dip problems. Place a straight edge on the two known values to determine the unknown value. As shown on the diagram, if the true dip of a plane is  $43^\circ$  and the angle between the strike and the apparent dip direction is  $35^\circ$ , then the apparent dip is  $28^\circ$ . After Palmer (1918).

## Outcrop Patterns and Structure Contours

### Objectives

- **Determine the general attitude of a plane from its outcrop pattern.**
- **Draw structure-contour maps.**
- **Solve three-point problems.**
- **Determine the outcrop patterns of planar and folded layers from attitudes at isolated outcrops.**

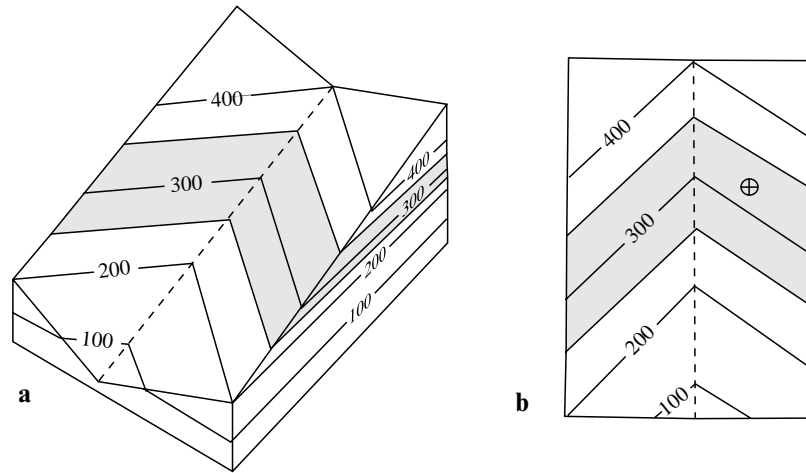
Because the earth's surface is irregular, planar features such as contacts between beds, dikes, and faults typically form irregular outcrop patterns. In situations where strike and dip symbols are not provided (such as on regional, small-scale maps), outcrop patterns can serve as clues to the orientations of the planes. Following are seven generalized cases showing the relationships between topography and the outcrop patterns of planes as seen on a map. As you examine Figs 2.1 through 2.7, cover the block diagram (parts a) and try to visualize the orientation of the bed from its outcrop pattern in map view (parts b). Note the symbols that indicate attitude.

- 1 Horizontal planes appear parallel to contour lines and "V" upstream (Fig. 2.1).
- 2 Vertical planes are not deflected at all by valleys and ridges (Fig. 2.2).
- 3 Inclined planes "V" updip as they cross ridges (Fig. 2.3).
- 4 Planes that dip upstream "V" upstream (Fig. 2.4).
- 5 Planes that dip downstream at the same gradient as the stream appear parallel to the stream bed (Fig. 2.5).
- 6 Planes that dip downstream at a gentler gradient than the stream "V" upstream (Fig. 2.6).
- 7 Planes that dip downstream at a steeper gradient than the stream bed (the usual case) "V" downstream (Fig. 2.7).

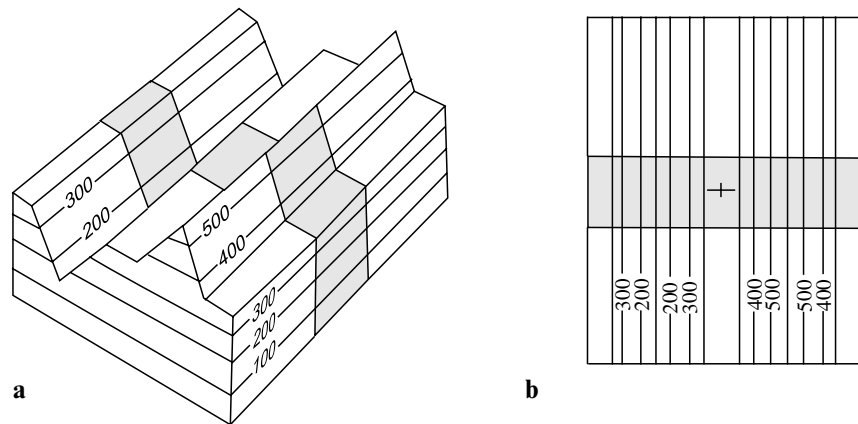
### Problem 2.1

On the geologic map in Fig. G-1 (Appendix G) draw the correct strike and dip symbol in each circle to indicate the attitude of Formation B and each dike. To verify your attitude symbols, Fig. G-2 can be cut out and folded to form a block model of this map. Appendix F shows standard symbols for geologic maps.

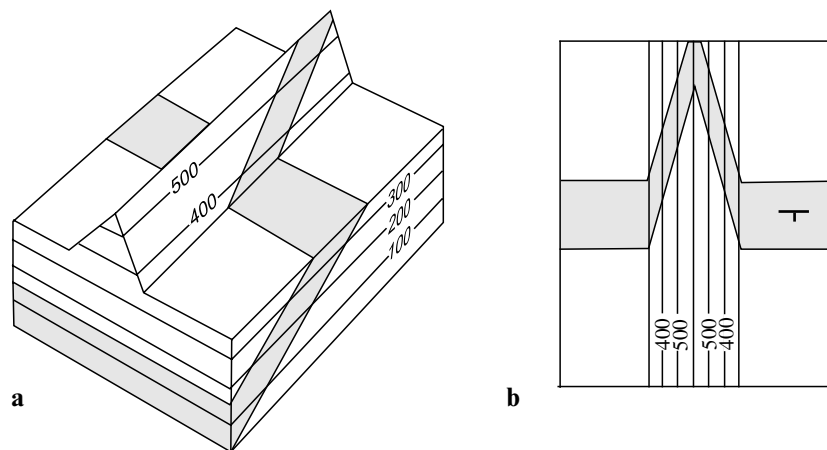




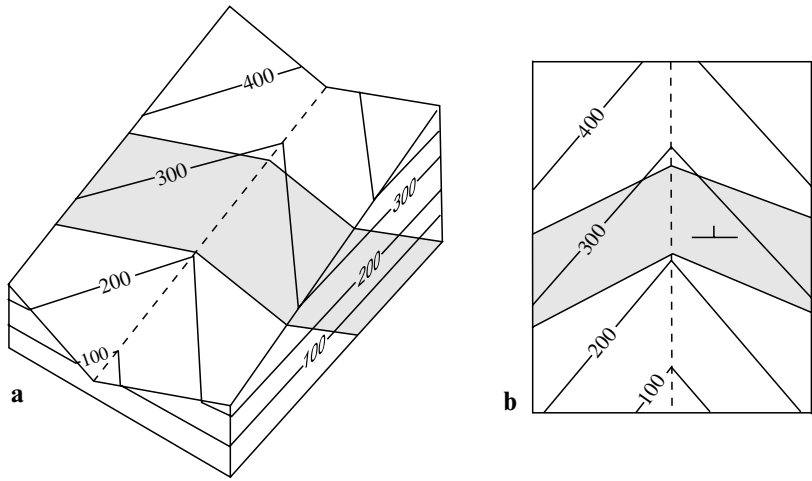
**Fig. 2.1** Horizontal plane in a stream valley. (a) Block diagram. (b) Map view.



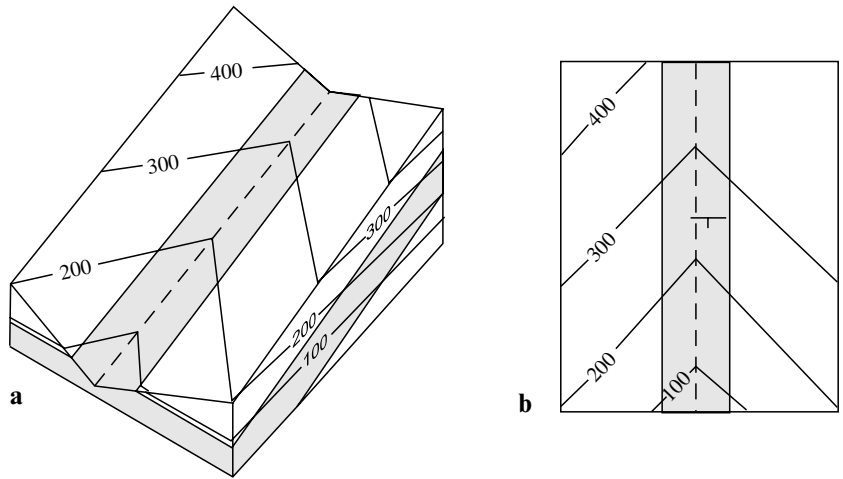
**Fig. 2.2** Vertical plane crossing a ridge and valley. (a) Block diagram. (b) Map view.



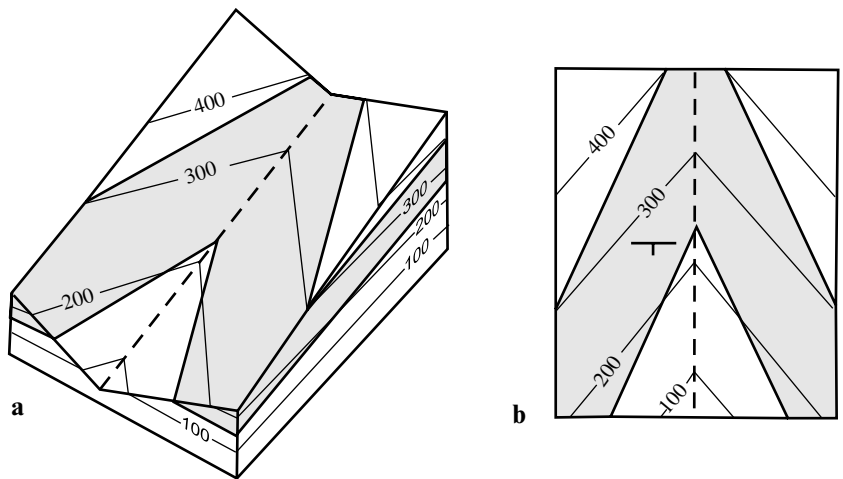
**Fig. 2.3** Inclined plane crossing a ridge. (a) Block diagram. (b) Map view.



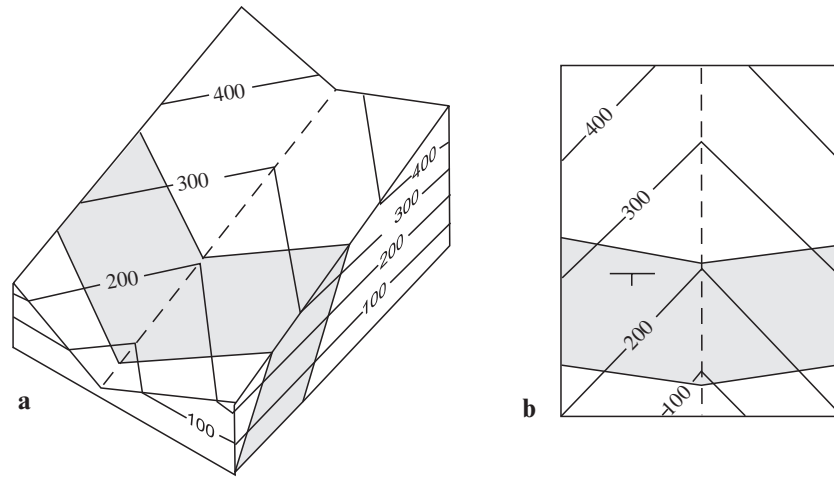
**Fig. 2.4** Inclined plane dipping upstream. (a) Block diagram. (b) Map view.



**Fig. 2.5** Plane dipping parallel to stream gradient. (a) Block diagram. (b) Map view.



**Fig. 2.6** Plane dipping downstream more gently than the stream gradient. (a) Block diagram. (b) Map view.



**Fig. 2.7** Plane dipping downstream more steeply than the stream gradient. (a) Block diagram. (b) Map view.

### Structure contours

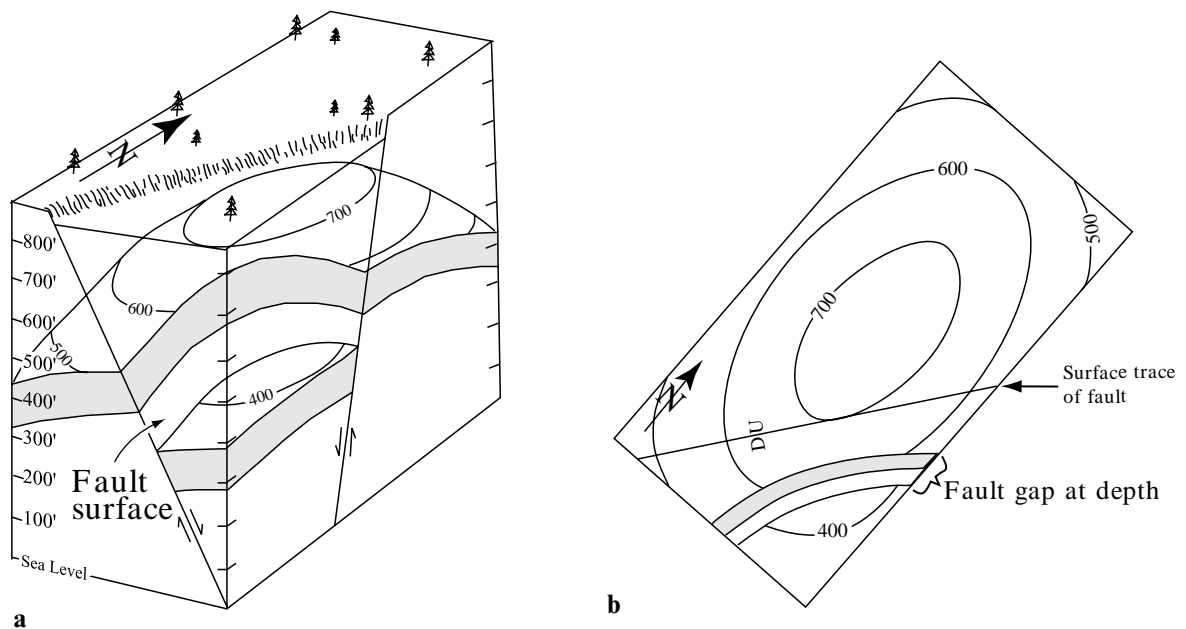
A contour line is one that connects points of equal value. On a topographic map, each contour line connects points of equal elevation on the earth's surface. A *structure contour* is a line that connects points of equal elevation on a structural surface, such as the top of a formation.

Structure-contour maps are most commonly constructed from drill-hole data. See Fig. 2.8, for example, which shows a faulted dome. Notice that, unlike topographic contours, structure contours sometimes terminate abruptly. Gaps in the

map indicate normal faults, and overlaps indicate reverse faults.

Structure-contour maps help geologists recognize structures in the subsurface. They are used extensively in petroleum exploration to identify structural traps and in hydrology to characterize the subsurface configurations of aquifers. The objective here will be to introduce you to structure-contour maps so that you are generally familiar with them and can use them to determine outcrop patterns later in the chapter.

Figure G-3 (Appendix G) is a map showing the elevation (in feet) of the top of a formation in 26



**Fig. 2.8** Block diagram (a) and structure-contour map (b) of a faulted dome. D, down; U, up.

drill holes. This area is in the northeastern corner of the Bree Creek Quadrangle, and the formation involved is the Bree Conglomerate. The geologic map of the Bree Creek Quadrangle may be found in an envelope at the back of this book. As explained later in this chapter, you will use it often as you work through the following chapters.

There are various techniques for contouring numerical data such as the elevations in Fig. G-3. In the case of geologic structure contours, there are usually not enough data to produce an unequivocal map, so experienced interpretation becomes extremely valuable. Although there are computer programs that will draw contour lines between data points, such a program cannot substitute for the judgment of an experienced geologist. For example, if four structure contours must pass between two elevation points, a computer program may space these contours at equal intervals. If the geologist has independent evidence that the surface to be contoured steepens toward one of the elevation points, he or she can draw the structure contours accordingly (i.e., progressively closer together) to depict the steepening surface.

### Problem 2.2

Draw structure contours on Fig. G-3. Use a 400-ft contour interval (including 0, 400, 800, 1200, etc.). Assume that, unlike the example in Fig. 2.8, this surface is not broken by faults, so your structure contours should be continuous.

If you do not know how to begin, here is a suggestion. Find a point, such as the 799-ft point, with an elevation that is close to the elevation of one of the contour lines. You know that the 800-ft contour passes very close to this point, but where does it go from there? To the east and northeast are two points with elevations of 1013 ft and 516 ft; 800 lies between these two elevations, so the 800-ft contour must pass between these two points, closer to the 1013-ft point than to the 516-ft point. Once you have a few lines drawn, the rest will fall into place. Your structure contours should be smooth, subparallel lines. Use a pencil; this is a trial-and-error operation. Be sure to label the elevation of each structure contour as you draw it.

When you are finished you should be able to recognize some folds. Using the symbols in Appendix F, draw appropriate fold symbols on your structure-contour map. Also draw a few strike-and-dip symbols on the map, but without specifying the amount of dip.

### The three-point problem

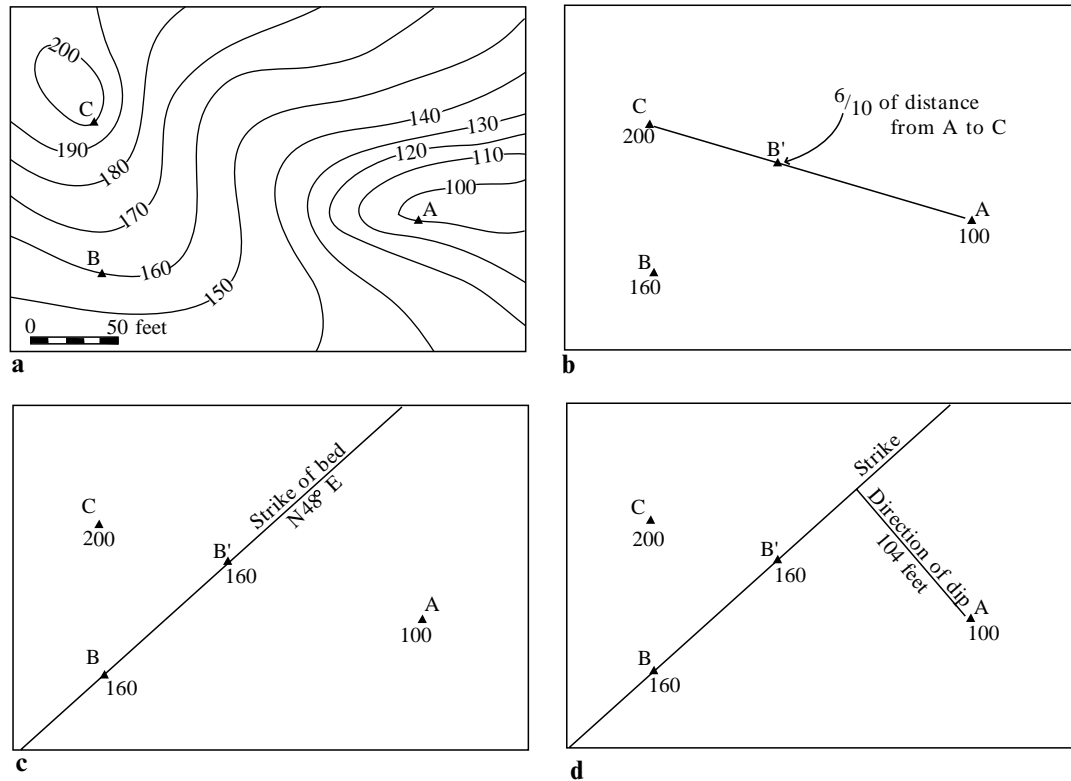
In many geologic situations, a bedding plane or fault surface may crop out at several localities. If the surface is planar and the elevations of three points on the surface are known, then the classic “three-point” problem can be used to determine the attitude of the plane. Consider Fig. 2.9a, which shows three points (A, B, C) on a topographic map. These three points lie on the upper surface of a sandstone layer. The problem is to determine the attitude of the layer. We will solve this problem in two different ways, using first a structure-contour approach, then a two-apparent-dip approach.

#### Solution 1

- 1 Place a piece of tracing paper over the map, and label the three known points and their elevations. On the tracing paper draw a line connecting the highest of the three points with the lowest. Take the tracing paper off the map. Now find the point on this line that is equal in elevation to the intermediate point. In Fig. 2.9b, point B has an elevation of 160 ft, so point B', the point on the AC line that is equal in elevation to point B, lies 6/10 of the way from point A (100 ft) to point C (200 ft).
- 2 The bed in question is assumed to be planar, so B' must lie in the plane. We now have two points, B and B', of equal elevation lying in the plane of the bed, which define the strike of the plane. The structure-contour line B-B' is drawn, and the strike is measured with a protractor to be N48°E (Fig. 2.9c).
- 3 The direction and amount of dip are determined by drawing a perpendicular line to the strike line from point A, the lowest of the three known outcrop points (Fig. 2.9d). The amount of dip can be determined trigonometrically as shown:

$$\tan \delta = \frac{\text{change in elevation}}{\text{map distance}} = \frac{60'}{104'} = 0.57$$

$$0.57 = \tan 30^\circ, \delta = 30^\circ$$



**Fig. 2.9** Solution of a three-point problem using a combination of graphical and trigonometric techniques. (a) Three coplanar points (A, B, and C) on a topographic map. (b) Location of a fourth point, B', at the same elevation as point B. (c) Line B-B' defines the strike of the plane. (d) Dip-direction line perpendicular to the line B-B'.

### Solution 2

Another approach to solving a three-point problem is to convert it into a two-apparent-dip problem, as follows:

- 1 Draw lines from the lowest of the three points to each of the other two points (Fig. 2.10a). These two lines represent apparent-dip directions from B to A and from C to A.
- 2 Measure the bearing and length of lines CA and BA on the map (Fig. 2.10b), and determine their plunges:

$$\theta_1 = 80^\circ, \theta_2 = 107^\circ$$

$$\tan \alpha_1 = \frac{\text{diff. in elevation}}{\text{map distance}} = \frac{60'}{198'} = 0.303$$

$$\tan \alpha_2 = \frac{100'}{204'} = 0.490$$

- 3 Use equation 1.4 to find the true-dip direction, and then use equation 1.3 to find the amount of dip.

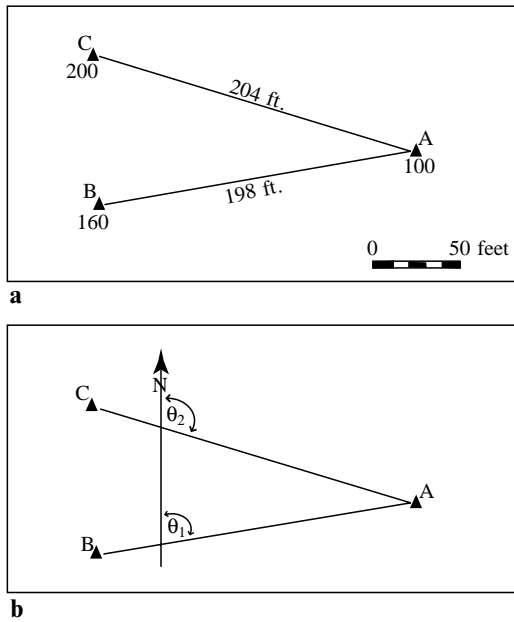
### Problem 2.3

Points A, B, and C in Fig. G-4 are oil wells drilled on a level plain, and all of the wells tap the same oil-bearing sandstone. The depth (*not the elevation!*) of the top of this sandstone in each well is as follows: A = 5115 ft, B = 6135 ft, and C = 5485 ft.

- 1 Determine the attitude of the sandstone.
- 2 If a well is drilled at point D, at what depth would it hit the top of the sandstone?

### Determining outcrop patterns with structure contours

Earlier we discussed structure-contour maps derived from drill-hole data. Structure-contour maps may also be constructed from surface data. Suppose, for example, that an important horizon is exposed in three places on a topographic map,



**Fig. 2.10** Three-point problem converted to a two-apparent-dip problem. (a) Three coplanar points. Lines are drawn to the lowest of the three points from the other two points. (b) Apparent-dip directions  $\theta_1$  and  $\theta_2$ .

as in Fig. 2.9a. If this horizon is planar we can determine its outcrop pattern on the map by the following technique.

- 1 On a piece of tracing paper draw the structure contour that passes through the middle elevation point (Fig. 2.9b,c).
- 2 Find the true dip as described above under the three-point problem.
- 3 Draw structure contours parallel to the line B–B' (Fig. 2.9c). In order to determine the outcrop pattern, these structure contours must have a contour interval equal to (or a multiple of) the contour interval on the topographic map. They also must represent the same elevations. Because the surface we are dealing with in this example is assumed to be planar, the structure contours will be a series of straight, equidistant, parallel, lines. The spacing can be determined trigonometrically:

$$\text{map distance} = \frac{\text{contour interval}}{\tan \delta}$$

In this example the spacing turns out to be 17.5 ft in plan view (Fig. 2.11a). Point B is at an elevation of 160 ft, which is conveniently also the elevation of a topographic contour.

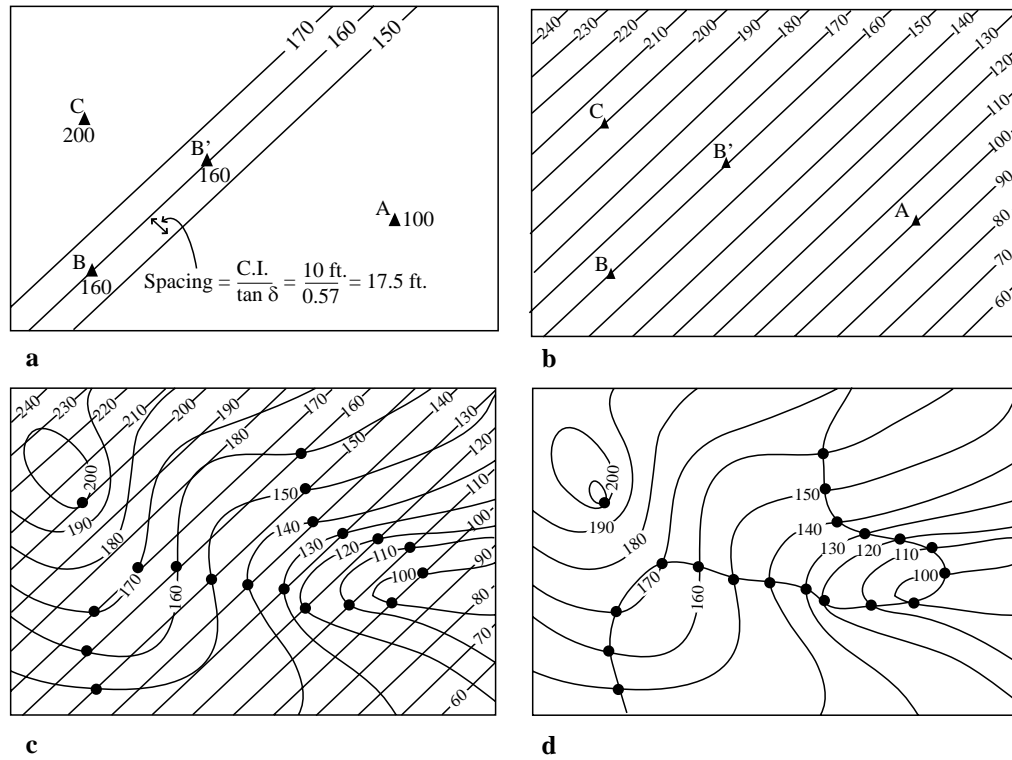
Points on the bedding plane with known elevations (points A and C in this problem) should serve as control points; that is, lay the tracing paper over the map and make sure that the elevations of known outcrop points match their elevations on the structure-contour map. If the surface is not quite planar but changes dip slightly, adjustments can constantly be made on the structure-contour map. Figure 2.11b shows the completed structure-contour map for this example.

- 4 Superimpose the structure-contour map and the topographic map (Fig. 2.11c). Every point where a structure contour crosses a topographic contour of equal elevation is a surface outcrop point. The outcrop line of the plane is made by placing the structure-contour map beneath the topographic map and marking each point where contours of the same elevation cross. A light table may be necessary to see through the topographic map. Connect the points of intersection to display the outcrop pattern on the topographic map (Fig. 2.11d).

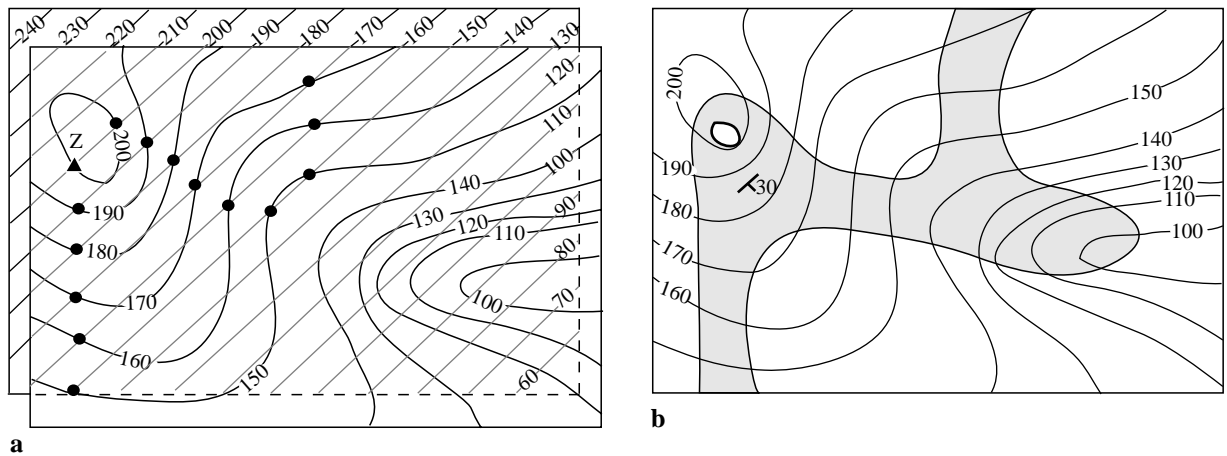
This same technique can be used to locate a second surface that is parallel to the first. Suppose that the contact shown in Fig. 2.11d is the top of a bed, and we wish to determine the outcrop pattern of the bottom as well. If a single outcrop point on the topographic map is known, then the outcrop pattern can easily be found using the structure-contour map already constructed for the bed's upper surface as follows:

- 1 Position the structure-contour map beneath the topographic map such that the bottom surface outcrop point (or points) lies (lie) at the proper elevation on the structure-contour map. With the structure contours parallel to their former position, proceed as before. In Fig. 2.12a, point Z, at an elevation of 200 ft, is a known outcrop point of the bottom of the bed. The structure-contour map has been moved so that the 200-ft structure contour passes through point Z, and the predicted outcrop points have been located as before.
- 2 Once the upper and lower contacts are drawn on the topographic map, the outcrop pattern of the bed can be shaded or colored (Fig. 2.12b).

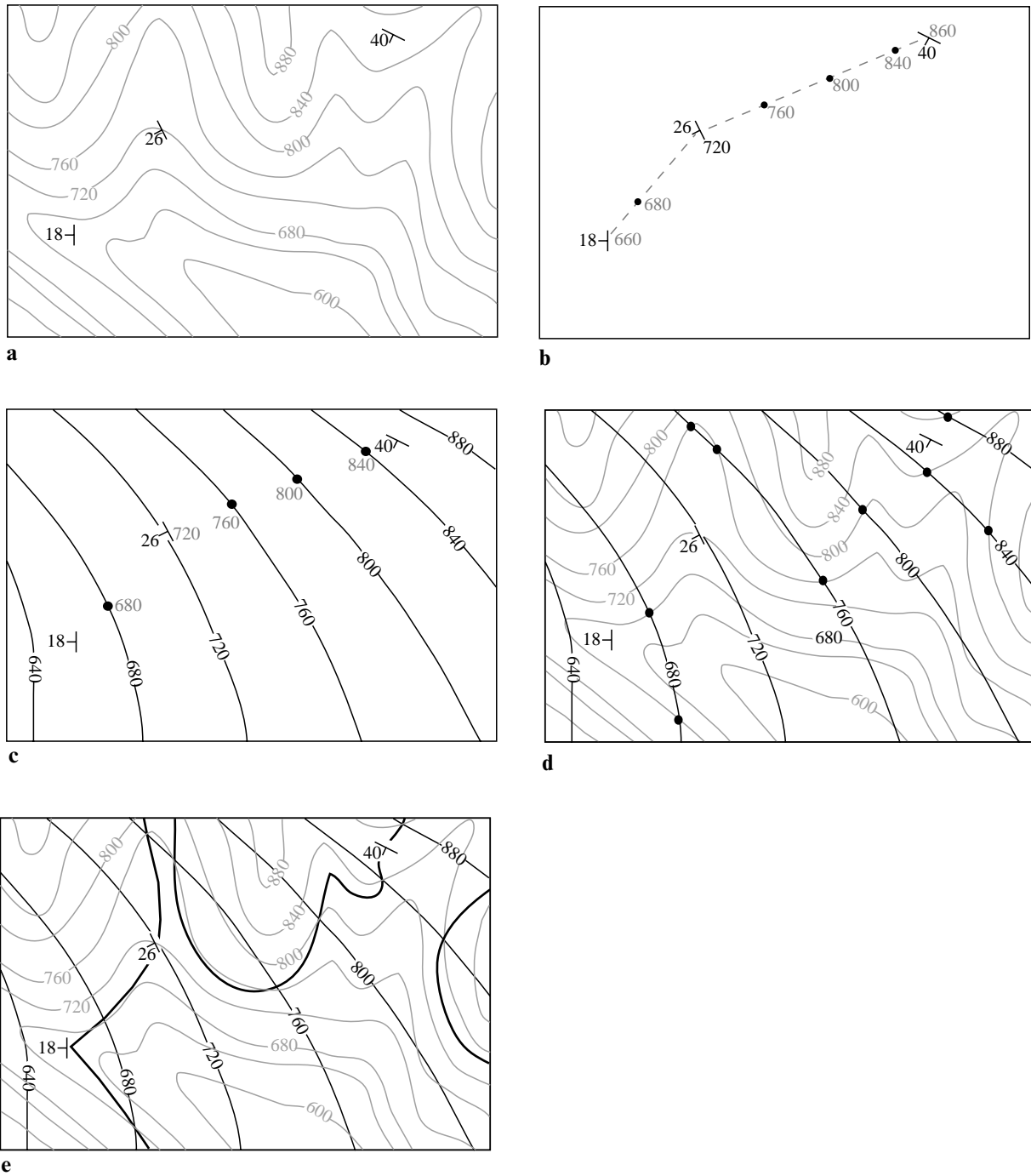
This technique for locating the intersection of a geologic surface with the surface of the earth may be used even when the surface is not a plane, as long as a structure-contour map can be constructed. In Fig. 2.13a, for example, three attitudes



**Fig. 2.11** Determination of outcrop pattern using structure contours. (a) Three structure contours on a base map (from Fig. 2.9c). (b) Structure-contour map. (c) Structure-contour map superimposed on a topographic map. (d) Outcrop pattern of a plane on a topographic map.



**Fig. 2.12** (a) Structure-contour map from Fig. 2.11 shifted such that the 200-ft structure contour lies on point Z. Point Z is a point where the bottom of a layer is exposed. The top of this same layer is exposed at points A, B, and C from Fig. 2.9a. (b) Outcrop pattern of this layer, which dips 30° to the southeast.



**Fig. 2.13** Determination of outcrop pattern of a gently folded surface using structure contours. (a) Attitude of a gently folded marker bed at three points on a topographic map. (b) Interpolation of elevations between points of known elevation. (c) Structure-contour map of a gently folded bed. (d) Structure-contour map superimposed on topographic base. (e) Inferred outcrop pattern of marker bed.



of a marker bed are mapped, and all are different. If we assume a constant slope and a gradual change in dip between outcrop points, a structure-contour map may easily be constructed as follows:

- 1 Arithmetically interpolate between the known elevation points to locate the necessary elevation points on the surface (Fig. 2.13b).
- 2 Draw smooth parallel structure contours parallel to the strikes at the outcrop points (Fig. 2.13c).
- 3 Superimpose the structure contour map and the topographic map, and mark the points where contours of equal elevation intersect (Fig. 2.13d).
- 4 Connect these intersection points to produce the outcrop map (Fig. 2.13e).

#### Problem 2.4

Figure G-5 is a topographic map. Points A, B, and C are outcrop points of the upper surface of a planar coal seam. Point Z is an outcrop point of the base of the coal seam.

- 1 Determine the attitude of the coal seam.
- 2 Draw the outcrop pattern of the coal seam.
- 3 Determine the thickness of the coal seam. Attach any drawings and computations you use.

#### Bree Creek Quadrangle map

Beginning in Chapter 3, many of the exercises in this book will deal with the structures of the mythical Bree Creek Quadrangle. A geologic map of this quadrangle, copied from the original map that Aragorn smuggled out of the Mines of Moria, is found in the back of this structure manual. This map records a variety of structures and structural relationships, and it will provide you with problems of appropriate complexity throughout the course. Before continuing on to Chapter 3, lightly color the Bree Creek Quadrangle map. More than mere busywork, coloring a map forces you to look closely at the distribution of various rock units. For maximum contrast, avoid using similar colors, such as red and orange, for rock units that consistently occur adjacent to one another on the map. Because you will be using this map often, it is important that you treat it carefully.

## Interpretation of Geologic Maps

### Objectives

- **Determine the exact attitude of a plane from its outcrop pattern.**
- **Determine stratigraphic thickness from outcrop pattern.**
- **Determine the nature of contacts from outcrop patterns and attitudes.**
- **Construct a stratigraphic column.**

Every geologic project relies on the geologic maps available at the time of the investigation. You may be asked to check a geologic map for accuracy or to map an area in greater detail. Even if your particular project does not involve direct field-work, it is essential that you have the skills necessary to interpret published geologic maps.

Geologic maps are drawn primarily from observations made on the earth's surface, often with reference to topographic maps, aerial photographs, or satellite images. The purposes of a geologic map are to show the surface distributions of rock units, the locations of the interfaces or *contacts* between adjacent rock units, the locations of faults, and the orientations of various planar and linear elements. Standard geologic symbols used on geologic maps are shown in Appendix F.

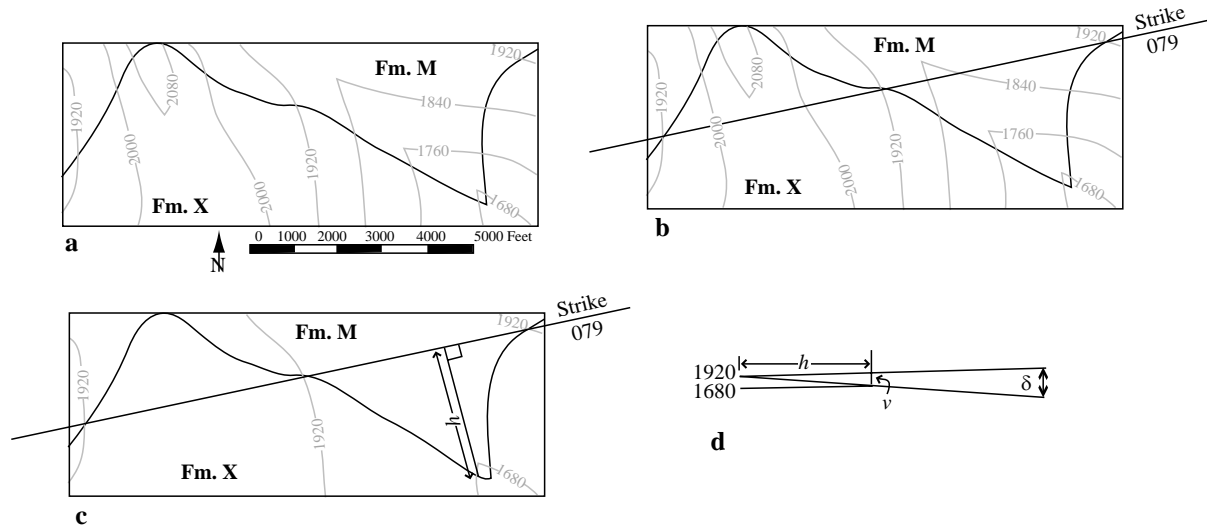
Some aspects of constructing a geologic map, such as the defining of rock units, are quite subjective and are done on the basis of the geologist's interpretations of how certain rocks formed. This being the case, many neatly inked, multicolored maps belie the uncertainty that went into their construction.

Accompanying this manual is a geologic map of the Bree Creek Quadrangle. An important teaching strategy of this book is to have you analyze the map in detail throughout the course, one step at a time, and then to have you synthesize it all into a cohesive structural history. The analysis begins with this chapter; the synthesis will come in Chapter 11.

It is important to keep in mind that topographic and geologic maps are projections onto a horizontal surface. Therefore, distances measured on maps are horizontal distances ("as the crow flies"), not actual ground distances.

### Determining exact attitudes from outcrop patterns

Because the strike of a plane is a horizontal line, any line drawn between points of equal elevation on a plane defines the plane's strike. Figure 3.1a is a geologic map with two rock units, Formation M and Formation X. The contact between these two rock units crosses several topographic contours. To find the strike of the contact, a straight



**Fig. 3.1** Technique for determining the attitude of a plane from its outcrop pattern. (a) Contact between Formation M and Formation X. (b) The line connecting points of equal elevation defines strike. (c) A perpendicular is drawn to a point of contact at a different elevation. (d) Dip angle  $\delta$  is found from  $\tan \delta = v/h$ .

line is drawn from the intersection of the contact with the 1920-ft contour on the west side of the map to the intersection of the contact with the 1920-ft contour on the east side of the map (Fig. 3.1b). The strike of this contact is thus determined to be  $079^\circ$ , as measured directly on the geologic map.

Remembering the rules of Vs from Chapter 2, it should be clear to you from the outcrop pattern in Fig. 3.1a that the beds dip toward the south. To determine the exact dip, draw a line that is perpendicular to the strike line from another point of known elevation on the contact. In Fig. 3.1c, a line has been drawn from the strike line to a point where the contact crosses the 1680-ft contour. The length of this line ( $h$ ) and the change in elevation ( $v$ ) from the strike line to this point yield the dip  $\delta$  with the following equation (Fig. 3.1d):

$$\tan \delta = \frac{v}{h}$$

The solution to this example is:

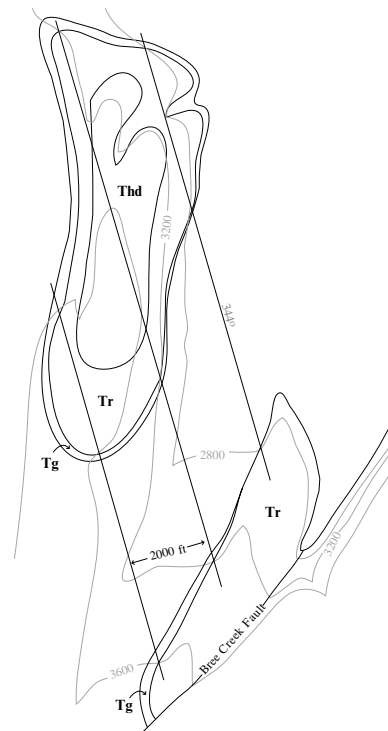
$$\tan \delta = \frac{v}{h} = \frac{240}{3000} = 0.08$$

$$\delta = 5^\circ$$

This method for determining attitudes from outcrop patterns can be used only if the rocks are not folded.

Figure 3.2 shows the Neogene (Miocene and Pliocene) units of the northeastern block of the Bree Creek Quadrangle. Straight lines have been drawn

connecting points of known elevation on the bottom contact of the Rohan Tuff, unit Tr. The strike, measured directly on the map with a protractor, is  $344^\circ$ , and the dip is  $11^\circ$ NE as determined by:



**Fig. 3.2** Neogene units in the northeastern portion of the Bree Creek Quadrangle. Tg, Gondor Conglomerate; Thd, Helm's Deep Sandstone; Tr, Rohan Tuff.

**Problem 3.1**

On the Bree Creek Quadrangle map determine the exact strike and dip of the Miocene and Pliocene units and label the map accordingly with the appropriate symbol. List each attitude in the space below as well as on your map. Use the lower contact of each unit, because the upper contact may have been eroded.

After determining the strike and dip of each formation, try to visualize the geology in three dimensions. Make sure that the attitude you determined is in agreement with the outcrop pattern. (A page for you to write your answers to Problems 3.1, 3.2, and 3.3 is provided on Fig. G-6, Appendix G.)

	Thd	Tr	Tg
<i>Northeastern fault block</i>			
Northern exposures	_____	_____	_____
Southern exposures	_____	_____	_____
<i>Central fault block</i>			
Northern area	_____	_____	_____
Galadriel's Ridge	_____	_____	_____
Southwestern area	_____	_____	_____
<i>Western fault block</i>			
Gandalf's Knob	_____	_____	_____
Southern exposures	_____	_____	_____

$$\tan \delta = \frac{v}{b} = \frac{400}{2000} = 0.2$$

$$\delta = 11^\circ$$

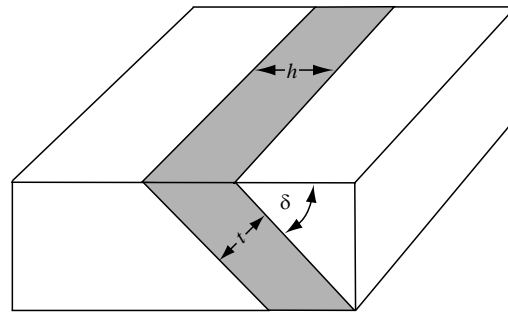
But what is the attitude of the southern outcrop of the Rohan Tuff? Even though no two points of equal elevation can be found on the bottom contact, notice that the points of known elevation lie on the same straight lines drawn for the northern outcrop. This is strong evidence that the attitude of the southern outcrop of Rohan Tuff is exactly the same as that for the northern one. This kind of reasoning is typical of what must become routine when interpreting geologic maps. But become careful! This approach assumes that the base of the Rohan Tuff is planar. Many sedimentary and volcanic deposits have non-planar bases.

Solve Problem 3.1.

**Determining stratigraphic thickness in flat terrain**

If the attitude of a rock unit is known, it is usually possible to determine its approximate stratigraphic thickness from a geologic map. If a unit is steeply dipping, and if its upper and lower contacts are exposed on flat or nearly flat terrain, then the thickness is determined from the trigonometric relationships shown in Fig. 3.3.

$$t = b \sin \delta$$



$$t = b \sin \delta$$

**Fig. 3.3** Trigonometric relationships used for determining stratigraphic thickness *t* in flat terrain from dip  $\delta$  and map width *b*.

where *t* is stratigraphic thickness, *b* is horizontal thickness (width in map view), and  $\delta$  is dip.

Solve Problem 3.2.

**Determining stratigraphic thickness on slopes**

The thickness of layers exposed on slopes may be determined trigonometrically if, in addition to dip  $\delta$  and map width *b*, the vertical distance *v* (i.e., difference in elevation) from the base to the top of the layer is known. Figure 3.4a shows a situation in which the layer and the slope are dipping in the same direction. Relevant angles have been added in Fig. 3.4b, from which the following derivation is made:

### Problem 3.2

The Paleogene (Paleocene through Oligocene) units of the Bree Creek Quadrangle were folded and then eroded nearly flat. Determine the approximate stratigraphic thickness of each of these Paleogene units. To do this, for each unit find a place that is not in the hinge zone of a fold, where the topography is nearly flat, where both the upper and lower contacts are exposed, and where the dip is fairly constant. The horizontal distance  $h$  must be measured perpendicular to the strike. A good place to measure the Bree Conglomerate, for example, is where Galadriel's Creek crosses it in the southwestern corner of the map. In places where the dip is not completely consistent you may have to use an average dip. (Because of the large contour interval on this map and the absence of completely flat terrain, thickness determinations will be somewhat variable.)

Tmm \_\_\_\_\_ (NE corner at 1600-ft contour)

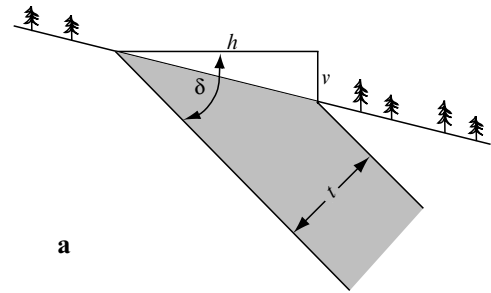
Tm \_\_\_\_\_ (W of Galadriel's Ridge at 36°W dip)

Tts \_\_\_\_\_ (NE corner at 2000- and 2400-ft contours)

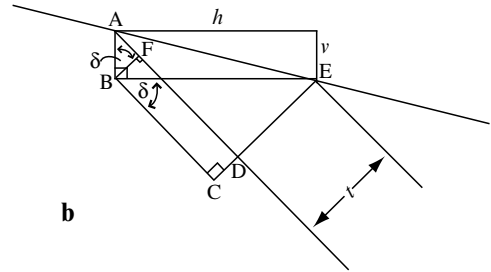
Tb \_\_\_\_\_ (at Galadriel's Creek)

Te \_\_\_\_\_

$$\begin{aligned}
 t &= DE = CE - CD \\
 \delta &= CBE = ABF \\
 \sin CBE &= \frac{CE}{BE} = \frac{CE}{h} \\
 CE &= h \sin CBE = h \sin \delta \\
 \cos ABF &= \frac{BF}{AB} = \frac{BF}{v} \\
 \cos \delta &= \frac{BF}{v} = \frac{CD}{v} \\
 CD &= v \cos \delta \\
 t &= h \sin \delta - v \cos \delta
 \end{aligned}$$



a



b

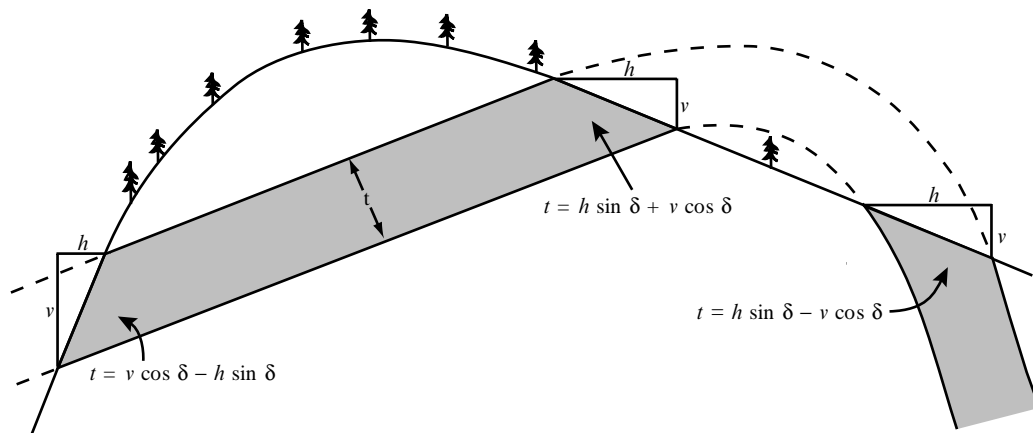
**Fig. 3.4** Determining stratigraphic thickness  $t$  on slopes. (a) Lengths  $h$  and  $v$  and dip angle  $\delta$  are needed to derive  $t$ . (b) Geometry of derivation.

This relationship applies to situations where bedding dips more steeply than topography and both dip in the same direction (right-hand example in Fig. 3.5). Similar trigonometric derivations can be used to show that in situations where bedding dips more gently than topography and both dip in the same direction (left-hand example in Fig. 3.5), the equation becomes:

$$t = v \cos \delta - h \sin \delta$$

Where bedding and topography dip in opposite directions (middle example of Fig. 3.5) the equation becomes:

$$t = h \sin \delta + v \cos \delta$$



**Fig. 3.5** Three combinations of sloping topography and dipping layers, with the appropriate formula for each.

### Determining stratigraphic thickness by orthographic projection

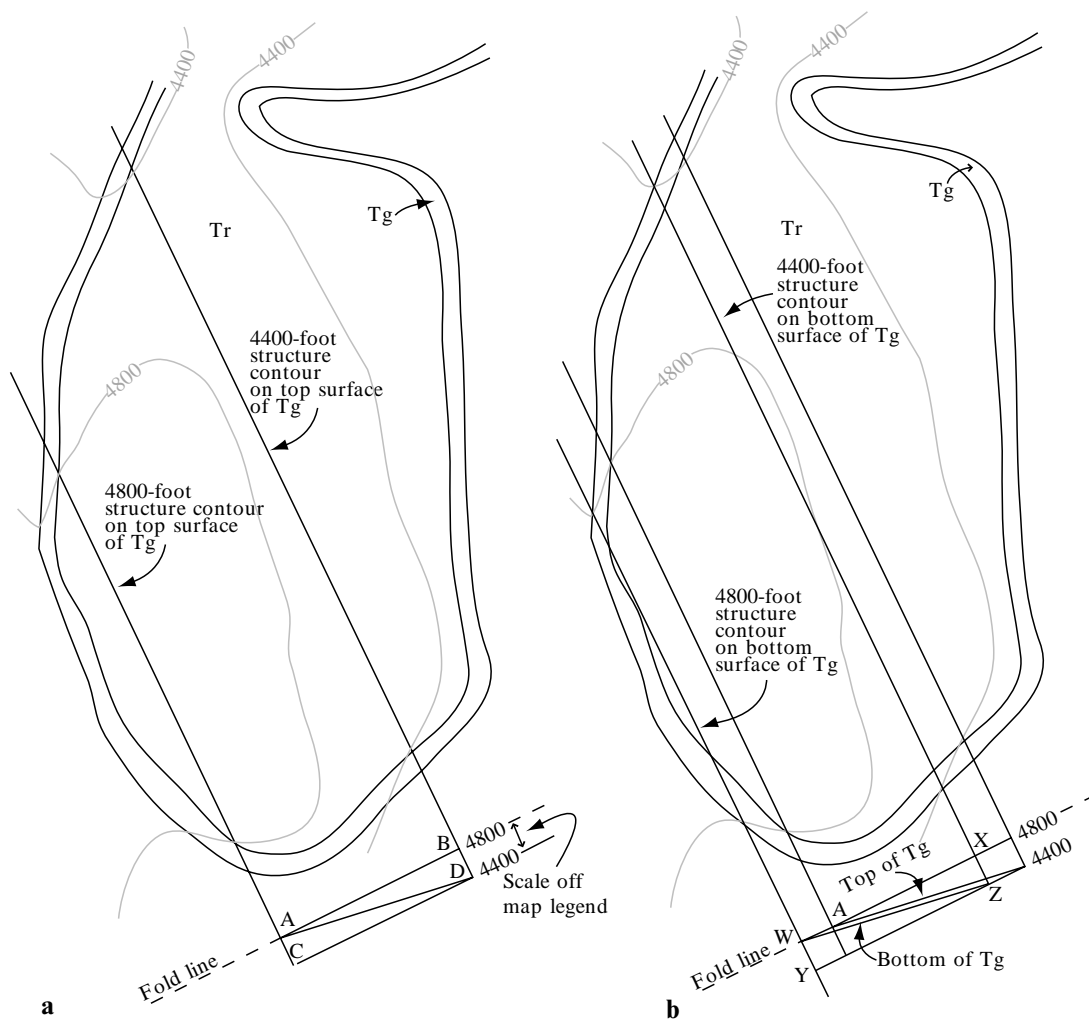
In some situations the preceding trigonometric techniques for determining stratigraphic thickness cannot be used. On the Bree Creek map, for example, the 400-ft contour interval does not allow the difference in elevation from the base to the top of a unit to be precisely determined. In such cases orthographic projection can be used to determine stratigraphic thickness.

Suppose you want to determine the thickness of the Gondor Conglomerate (Tg) at Galadriel's Ridge in the Bree Creek Quadrangle. Begin by finding two points of equal elevation at the same stratigraphic level. A line between such points defines the strike (as discussed above). In Fig. 3.6a one such line is drawn through the top of Tg at 4800 ft, and another is drawn through the top of Tg at 4400 ft.

The object of this construction is to draw a vertical cross-section view perpendicular to strike. This view will be folded up into the horizontal plane.

Line AB is drawn perpendicular to the two strike lines (Fig. 3.6a). This will represent the 4800-ft elevation line in the orthographic projection. A second line, CD, is now drawn, also perpendicular to the two strike lines. Line CD represents the 4400-ft elevation line. The distance between lines AB and CD is taken directly off the map legend. Next we draw line AD, which represents the eastward-dipping top of Tg in orthographic projection.

Repeating this same procedure with the bottom contact of Tg results in points W, X, Y, and Z (Fig. 3.6b). Line WZ represents the base of Tg in orthographic projection, and the thickness can be measured directly off the diagram. The precision is primarily limited by the scale of the map. In this example Tg can be measured to be about 100 ft thick.



**Fig. 3.6** Technique for determining stratigraphic thickness by orthographic projection. (a) Plotting top surface. (b) Plotting bottom surface and deriving the thickness.

### Problem 3.3

Determine the approximate thickness of the Neogene units in the areas indicated. (Both the Helm's Deep Sandstone and the Rohan Tuff have quite variable thicknesses. The Rohan Tuff was tilted and partly eroded prior to the deposition of the Helm's Deep Sandstone, and the Helm's Deep Sandstone has no upper contact. Where appropriate, determine the range of thicknesses.)

	Thd	Tr	Tg
Gollum Ridge	_____		
Gandalf's Knob	_____		
Galadriel's Ridge		_____	_____
Mirkwood Creek			_____
North of Edoras Creek	_____		

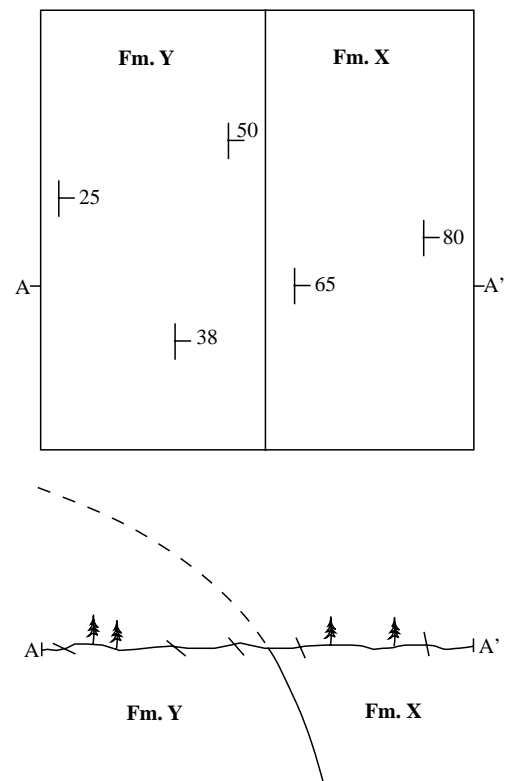
### Determining the nature of contacts

A contact is the surface between two contiguous rock units. There are three basic types of contacts: (1) depositional, (2) fault, and (3) intrusive. It is important to be able to interpret the nature of contacts from geologic maps whenever possible. Following are a few map characteristics of each type of contact.

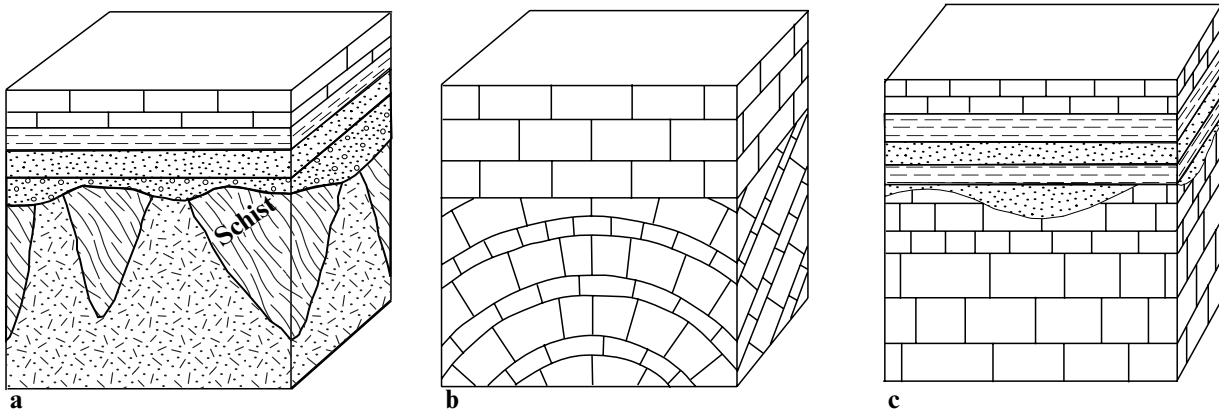
Where sedimentary or volcanic rocks have been deposited on top of other rocks, the contact is said to be *depositional*. If adjacent rock units have attitudes parallel to one another, and there is no evidence of erosion on the contact, then the contact is a *conformable depositional* contact. On the map, conformable contacts display no abrupt change in attitude across the contact. In Fig. 3.7, for example, although the dips in Formation X are steeper than those in Formation Y, there is a gradual steepening across the contact. A cross-section view is shown below the map view.

If a demonstrable surface of erosion or non-deposition separates two rock units then the contact is an *unconformity* — a buried erosion surface. There are three basic types of unconformities (Fig. 3.8): (1) nonconformities (sediments deposited on crystalline rock), (2) angular unconformities (sediments deposited on deformed and eroded older sediments), and (3) disconformities (sediments deposited on eroded but undeformed older sediments). Notice that a disconformity would be indistinguishable from a conformable contact on a geologic map because in both cases the beds are parallel across the contact. Disconformities can only be recognized in the field. In the case of a nonconformity, the strike of the sedimentary layers is parallel to the contact (Fig. 3.9a). In angular unconformities the layers overlying the unconformity are always parallel to the contact, while those beneath it are not (Fig. 3.9b).

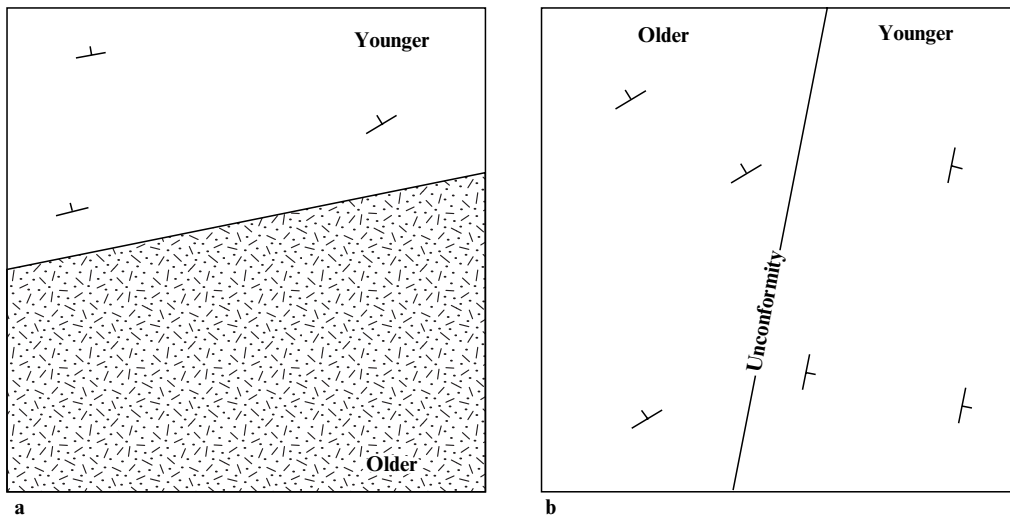
*Fault contacts* are best diagnosed in the field on the basis of fault gouge, slickensides, offset beds, and geomorphic features. On geologic maps, faults are often conspicuous because of the rock units that are truncated. Figure 3.10 shows a contact that is best interpreted as a fault because of the strong discordance of strike and the fact that neither unit strikes parallel to the contact.



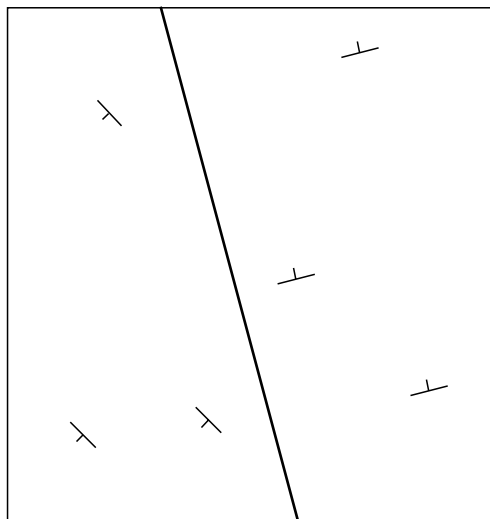
**Fig. 3.7** Conformable depositional contact. Map view above and vertical structure section below.



**Fig. 3.8** Three types of unconformities: (a) nonconformity, (b) angular unconformity, and (c) disconformity.



**Fig. 3.9** (a) Nonconformity and (b) angular unconformity in map view.

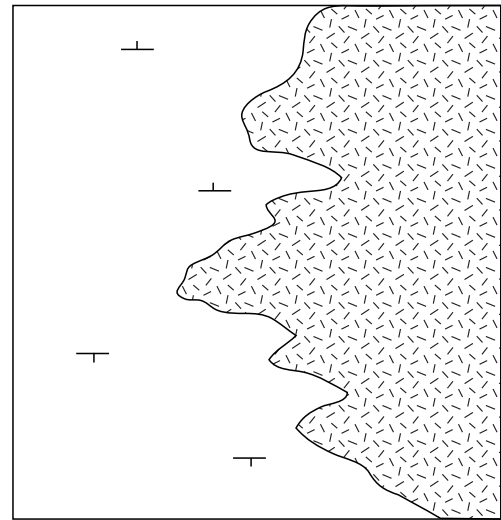


**Fig. 3.10** Fault contact in map view.



*Intrusive contacts* are obvious where the intrusive rocks have clearly been injected into the country rock. As in the case of faults, this is best determined in the field. Figure 3.11 shows an unequivocal intrusive contact, but sometimes intrusive contacts are not so jagged and cannot be easily distinguished from faults. Intrusions such as sills may even be parallel to the bedding of the country rock, making the contact appear to be a nonconformity.

While the nature of a contact may not always be clear in map view, a geologist drawing a structure section (cross-section view) must show the nature of the contact. In Fig. 3.12a, a geologic map is shown with two possible structure sections. Figure 3.12b interprets the contact between the gabbro and Formation M as an unconformity, while Fig. 3.12c interprets the same contact as a fault. The fact that the strike of the beds in Formation M exactly parallels the contact makes the unconformity the preferred interpretation. A fault, or even an intrusive contact, cannot be ruled out, however, without examining the contact in the field.



**Fig. 3.11** Intrusive contact in map view.

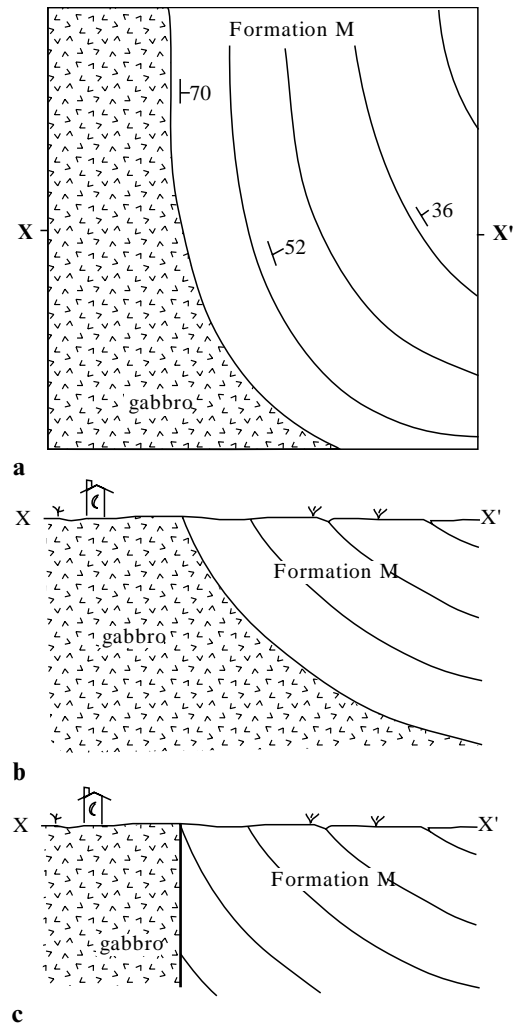
### Problem 3.4

Figure G-7 consists of three geologic maps, each of which has two topographic profiles below it. For each map there are at least two possible interpretations for the contact. Sketch two geologically plausible structure sections for each map, as was done in Fig. 3.12. In the space provided below each set of diagrams, indicate which of your two structure sections you consider most likely to be correct, and briefly *give your reasons*.

These structure sections should be quick sketches that show relationships between adjacent rock units. You do not need to be concerned with each apparent dip; merely approximate the dips freehand.

### Constructing a stratigraphic column

A stratigraphic column is a thumbnail sketch of the stratigraphy of an area, showing the relationships between rock units and thicknesses of strata. It is usually a composite of several stratigraphic sections measured at different locations. Stratigraphic columns are extremely useful tools for summarizing the history of deposition and erosion of an area and for comparing the geology of one area with that of other areas. A stratigraphic column does not summarize the structural history of



**Fig. 3.12** Geologic map with two alternative structure-section interpretations. (a) Geologic map. (b) Unconformity interpretation. (c) Fault interpretation.

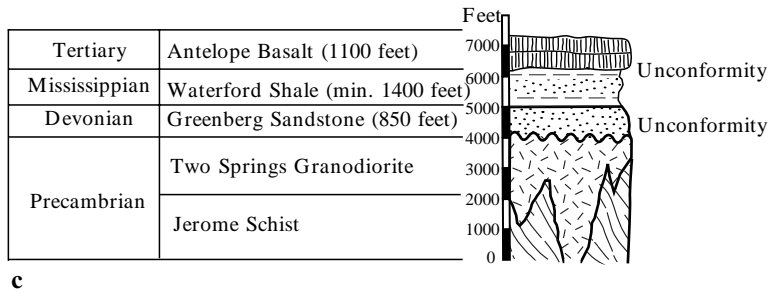
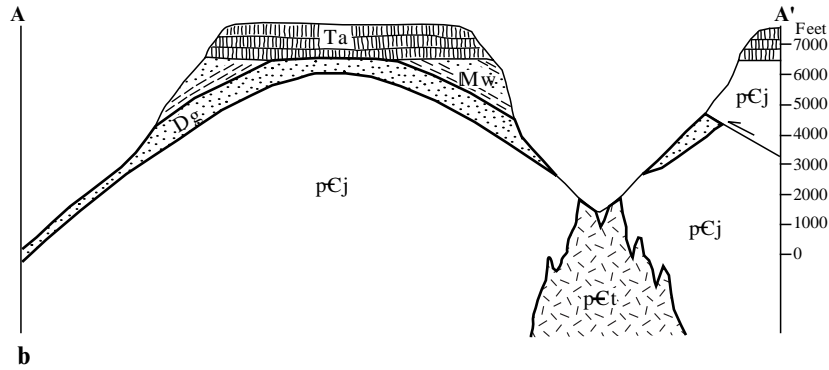
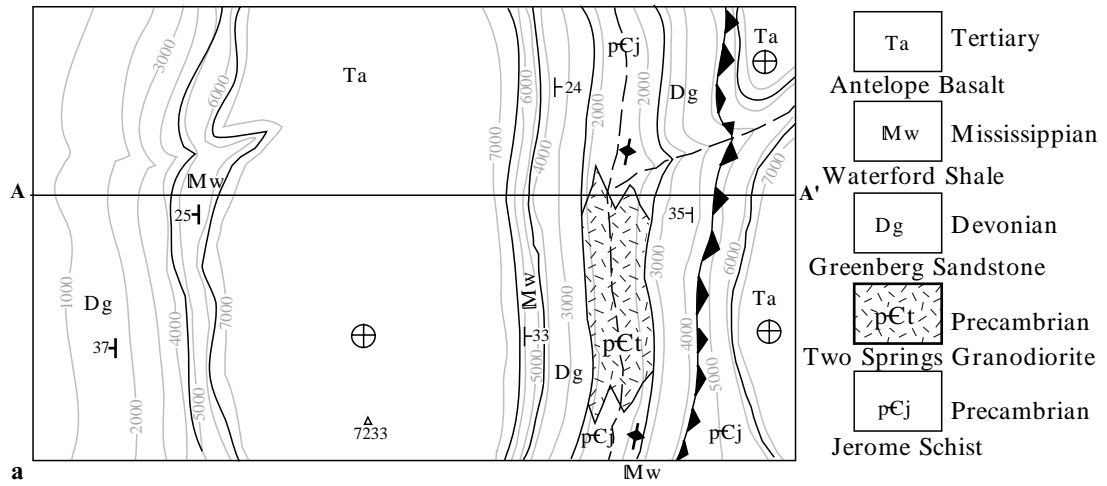
an area because folds and faults are not shown. It is, nonetheless, a first step in understanding an area's structural history. For your work with the Bree Creek Quadrangle, a stratigraphic column will be very handy.

Figure 3.13 contains a geologic map (Fig. 3.13a), an accompanying structure section (Fig. 3.13b), and a stratigraphic column (Fig. 3.13c). The construction of structure sections is discussed in detail in Chapter 4. Notice that the structure section shows the structural and stratigraphic relationships in a specific locality, line A-A'. The stratigraphic column, on the other hand, shows the generalized stratigraphic relationships over a larger area. For example, even though the Antelope Basalt lies unconformably on the Jerome Schist in the eastern part of the map,

in the stratigraphic column the Antelope Basalt appears overlying the Waterford Shale, the youngest unit it overlies in the area. If you have trouble seeing how the map, structure section, and stratigraphic column relate to one another, try coloring one or more of the units on all three diagrams.

### **Problem 3.5**

On a piece of graph paper construct a stratigraphic column for the Cenozoic and Mesozoic units of the Bree Creek Quadrangle. Choose a scale that allows your column to fit comfortably on a single sheet of paper.



**Fig. 3.13** (a) Geologic map, (b) corresponding structure section, and (c) stratigraphic column.

## Geologic Structure Sections

### Objective

- Learn to draw geologic structure sections through folded and faulted terrain.

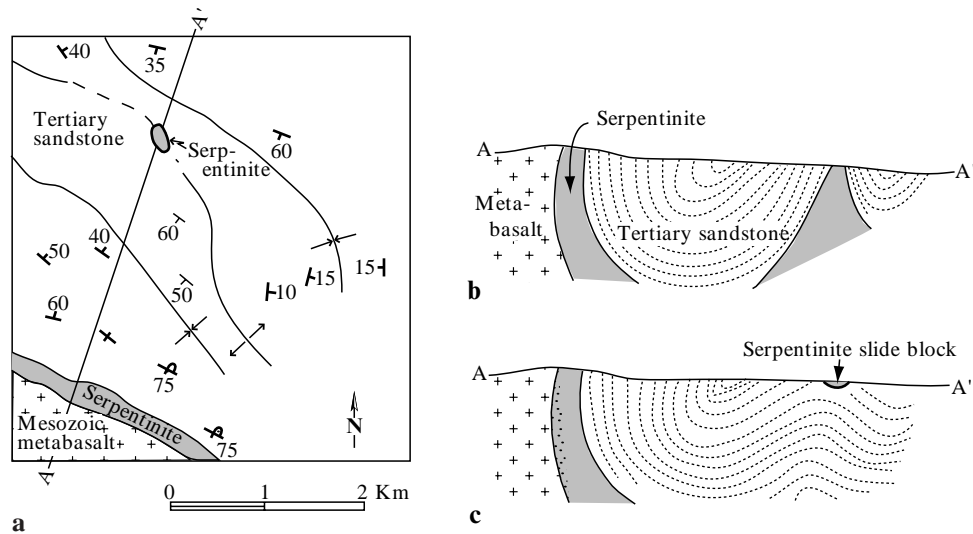
A geologic map is a two-dimensional representation of geologic features on the earth's surface. In order to provide a third dimension, it is standard practice to draw one or more *vertical structure sections*. These are vertical cross sections of the earth showing rock units, folds, and faults. Structure sections are widely used as the basis for geologic interpretations in petroleum and mineral exploration, hydrological studies, assessment of geologic hazards, and in basic research. By convention, structure sections are usually drawn with the west on the left. Structure sections oriented exactly north–south are usually drawn with the north on the left.

Under the best of circumstances, drill core and geophysical data are available to help the geologist “see” into the earth, but many structure sections are based solely on a geologic map. Geologists use their understanding of the geometry and kinematics of structures to project the mapped geology into the subsurface, but this is still inferential. As such, structure sections must be regarded as interpretations that are subject to change with the appearance of new information.

By way of example, examine the geologic map in Fig. 4.1a and the two structure sections based on it. The map shows three groups of rocks: Mesozoic metabasalt, serpentinite, and Tertiary sand-

stone. The serpentinite occurs as a continuous band between the metabasalt and the sandstone in the southwestern part of the map and as a small patch within the sandstone in the northern part of the map. The original interpretation (Fig. 4.1b) accounts for the northern outcrop of serpentinite as occurring in the core of a partially eroded anticline. However, additional fieldwork revealed that the northern patch of serpentinite is more likely a large landslide block that long ago slid off the southern serpentinite mass (Fig. 4.1c). Far from being a trivial difference, these two interpretations imply rather different styles of folding as well as predicting completely different stability and permeability characteristics for the entire length of the anticlinal axial trace.

When you are drawing a structure section, remember that, in general, it should be geometrically possible to unfold the folds and recover the fault slip in order to reconstruct an earlier, less deformed or undeformed state. In other words, your structure section should be *retrodeformable*. Structure sections in which great care is taken concerning retrodeformation are called *balanced structure sections*. An introduction to the construction and retrodeformation of balanced structure sections is presented in Chapter 15. For many situations, if you make sure that sedimentary units



**Fig. 4.1** Geologic map with two contrasting interpretations of structure section A–A'. Generalized from Dibblee (1966). (a) Geologic map. (b) Original structure section in which the northern serpentinite block is interpreted as the exposed core of an anticline. (c) Revised structure section in which the northern exposure of serpentinite is interpreted as a landslide block.

maintain a constant thickness (unless you have evidence to the contrary) and that the hanging walls of faults match the footwalls, you will be on the right track. In some structurally complex regions, particularly where faulting has moved rocks into or out of the plane of the structure section, it may not be possible to draw a strictly balanced structure section.

### Structure sections of folded layers

The geometry of folds is discussed in Chapter 6. In this chapter we are concerned with the mechanics of drawing structure sections through folded beds, not with the mechanics or kinematics of the folding.

The simplest structure sections to draw are those that are perpendicular to the strike of the bedding. Figure 4.2 shows a geologic map with all beds striking north–south. Section A–A' is drawn east–west, perpendicular to the strike. Each bedding attitude and each contact is merely projected parallel to the fold axis to the topographic profile oriented parallel to the section line. On the topographic profile each measured dip is drawn with the aid of a protractor. Using these dip lines on the topographic profile as guides, contacts are drawn as smooth, parallel lines. Dashed lines are used to show eroded structures. Show as much depth below the earth's surface as the data permit.

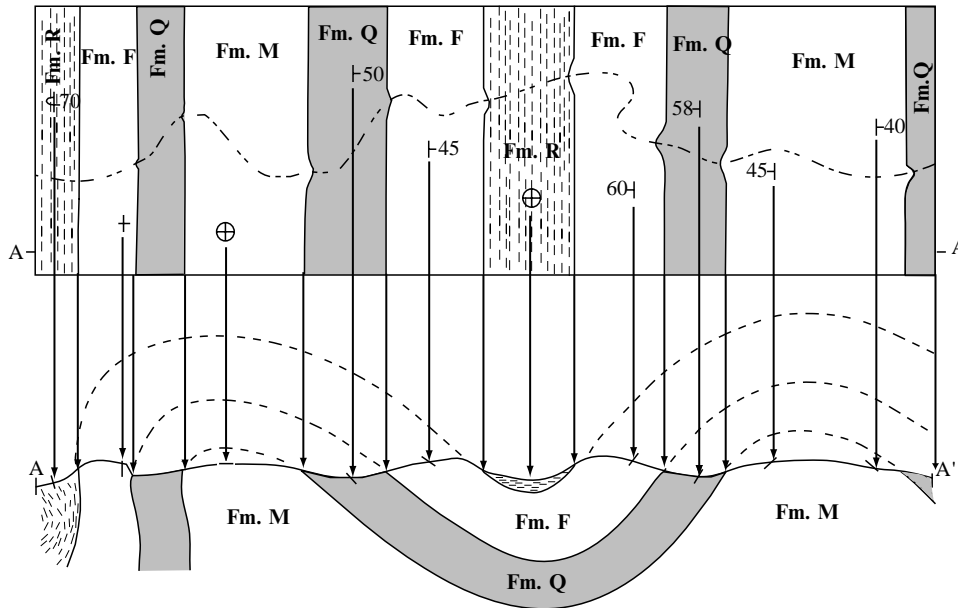
### Problem 4.1

Draw structure section A–A' on Fig. G-8 (Appendix G).

In very few cases are the strikes of the beds all parallel, as they are in Fig. 4.2. The section line, therefore, rarely can be perpendicular to all of the strikes. When the section line intersects the strike of a plane at an angle other than  $90^\circ$ , the dip of the plane as it appears in the structure section will be an apparent dip. Recall that the apparent dip is always less than the true dip.

The quickest way to determine the correct apparent dip to draw on the structure section is to use the nomogram in Fig. 1.7. Figure 4.3 shows a geologic map in which the strike of Formation B has been projected along the strike to line X–X' and then perpendicular to X–X' to the topographic profile. The angle between the strike and the section line is  $35^\circ$ , the true dip is  $43^\circ$ , and the apparent dip is revealed by the alignment diagram to be  $28^\circ$ , which is the angle drawn on the structure section.

Some rock units have highly variable strikes, and judgment must be exercised in projecting attitudes to the section line. Attitudes close to the section line should be used whenever possible. If the dip is variable, the dip of the contact may have to be taken as



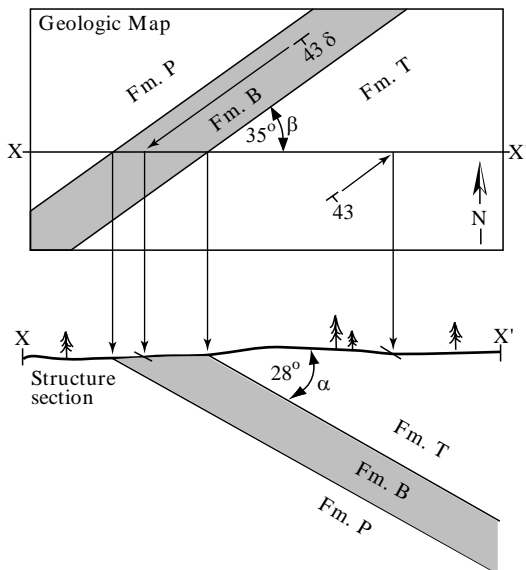
**Fig. 4.2** Basic technique for drawing a geologic structure section perpendicular to the strike of the bedding. Arrows show transfer of attitudes from map to section. Dashed lines represent beds that have been eroded away.

the mean of the dips near the section line. The attitudes should be projected parallel to the fold axis, which in the case of plunging folds will not be parallel to the contacts. In all cases, it is important to study the entire geologic map to aid in the construction of structure sections. Critical field relationships

that must appear on your structure section may not be exposed along the line of section.

**Structure sections of intrusive bodies**

Tabular intrusive bodies, such as dikes and sills, present no special problem. Irregular plutons, however, are problematic because in the absence of drill-hole or geophysical data it is impossible to know the shape of the body in the subsurface. Such plutons are usually drawn somewhat schematically in structure sections, displaying the presumed nature of the body without pretending to show its exact shape. For an example, see Fig. 4.4.



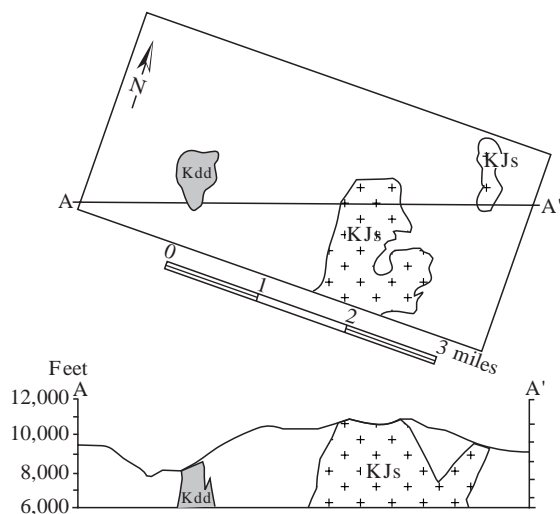
**Fig. 4.3** Geologic map and corresponding structure section drawn at an angle to strike. Dip on map becomes an apparent dip on the structure section.

**Problem 4.2**

Draw structure section A-A' on Fig. G-9. Determine each apparent dip, using either the alignment diagram in Fig. 1.7 or trigonometry.

**The arc method**

A more precise, but not necessarily more accurate, technique than freehand sketching for drawing structure sections is called the arc (or Busk) method. It has proved to be particularly useful in regions of



**Fig. 4.4** Example of a structure section with intrusive bodies. After Huber and Rinehart (1965).

basins and domes or gently folded areas where beds have been folded by flexural slip and retain a constant thickness. Such folds are sometimes called *concentric* folds, for reasons that will become clear.

The arc method is based on the following two premises: (1) the transition from one dip to the next is smooth, and (2) bed thickness is constant. “Volume problems” (loss of volume) at the cusps of folds are completely ignored, which is why this technique is only appropriate for gently folded layers.

Consider the map and topographic profile in Fig. 4.5. Each attitude on the map has been projected to the topographic profile. Instead of sketching freehand, however, a drawing compass is used to interpolate dips between the measured points. The steps are as follows.

- 1 With the aid of a protractor, draw lines perpendicular to each dip on the topographic profile. Such lines have been drawn in Fig. 4.5b perpendicular to dips a, b, and c. Extend them until they intersect.
- 2 Each point of intersection of the lines perpendicular to two adjacent dips serves as the center of a set of concentric arcs drawn with a drawing compass. Point 1 on Fig. 4.5c is the center of a set of arcs between the perpendiculars to dips a and b. Point 2 serves as the center from which each arc is continued between the perpendiculars to dips b and c.
- 3 The process is continued until the structure section is completed. Figure 4.5d shows the completed structure section. Notice that

some arcs were drawn with unlikely sharp corners in order for thicknesses to remain constant.

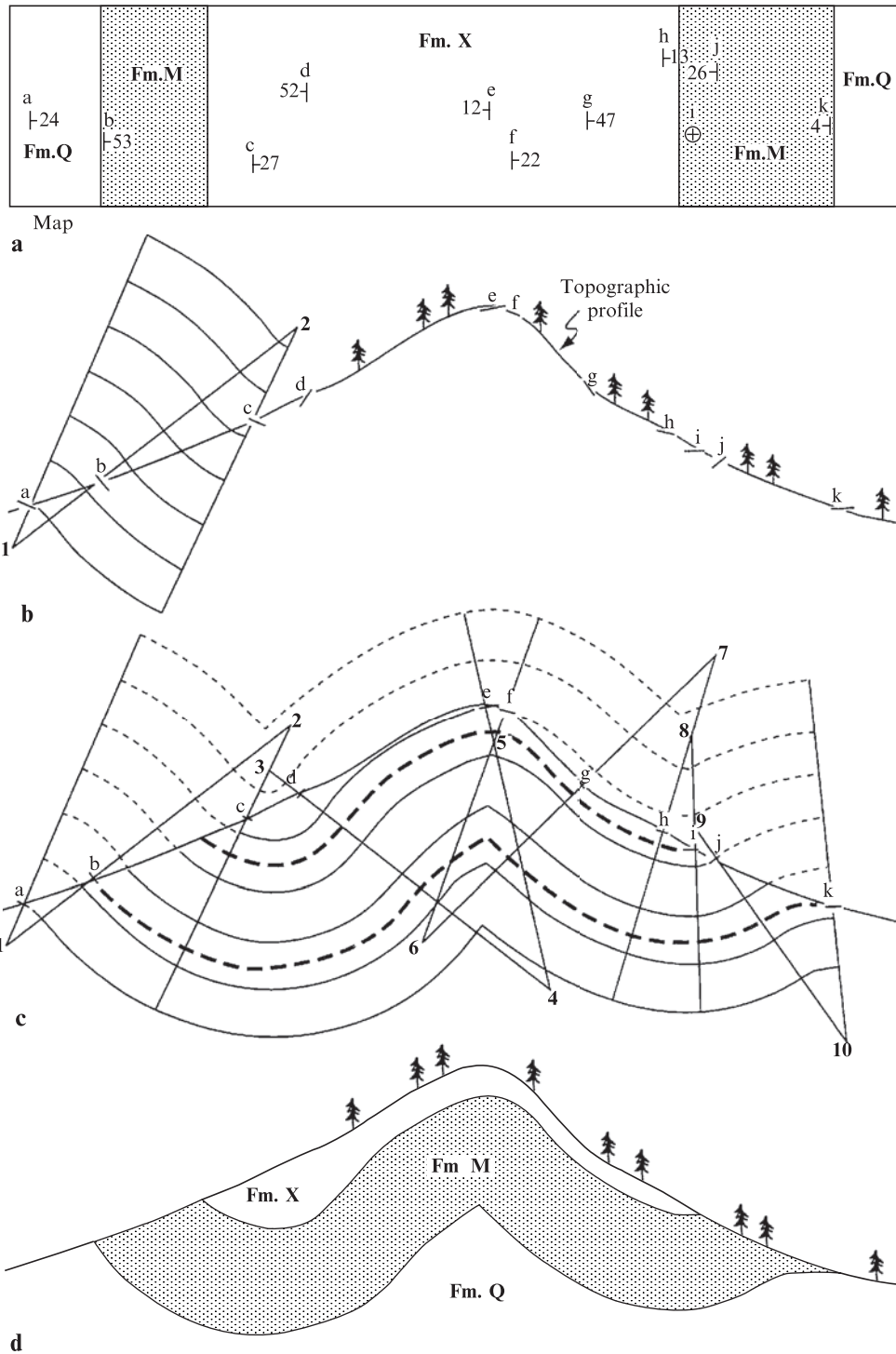
### Problem 4.3

An exploration oil well was drilled at the point shown on Fig. G-10 and the units encountered are shown on the structure section. The oil-bearing Eagle Bluff Limestone was encountered at a depth of 7200 ft. Using the arc method, draw a structure section. Indicate the point on the map where you, as a consulting geologist, would recommend drilling for oil. How deep must a well be drilled at this point to penetrate the upper surface of the Eagle Bluff Limestone?

### Drawing a topographic profile

Up to this point in this chapter, in all of the examples and problems, a topographic profile has been provided. Topographic profiles show the relief at the earth’s surface along the top of the structure section. Usually you will have to construct your own topographic profile. The technique for drawing a topographic profile one is as follows:

- 1 Draw the section line on the map (Fig. 4.6a).
- 2 Lay the edge of a piece of paper along the section line, and mark and label on the paper each contour, stream, and ridge crest (Fig. 4.6b).
- 3 Scale off and label the appropriate elevations on a piece of graph paper (Fig. 4.6c). Graph paper with 10 or 20 squares per inch is ideal for 7.5-minute quadrangle maps because the scale is 1 inch = 2000 ft. Notice that the map scales on Fig. 4.6a and 4.6b are the same as the vertical scale on Fig. 4.6c and 4.6d. It is very important that the vertical and horizontal scales are the same on structure sections. This is a very common oversight. If the scale of the structure section is not the same as the scale of the map then the dips cannot be drawn at their nominal angle.
- 4 Lay the labeled paper on the graph paper and transfer each contour, stream, and ridge crest point to the proper elevation on the graph paper (Fig. 4.6c).
- 5 Connect the points (Fig. 4.6d).



**Fig. 4.5** Arc method for drawing structure sections of folded beds. (a) Geologic map. (b) Topographic profile with beginning arcs. (c) Completion of arcs. (d) Completed structure section.



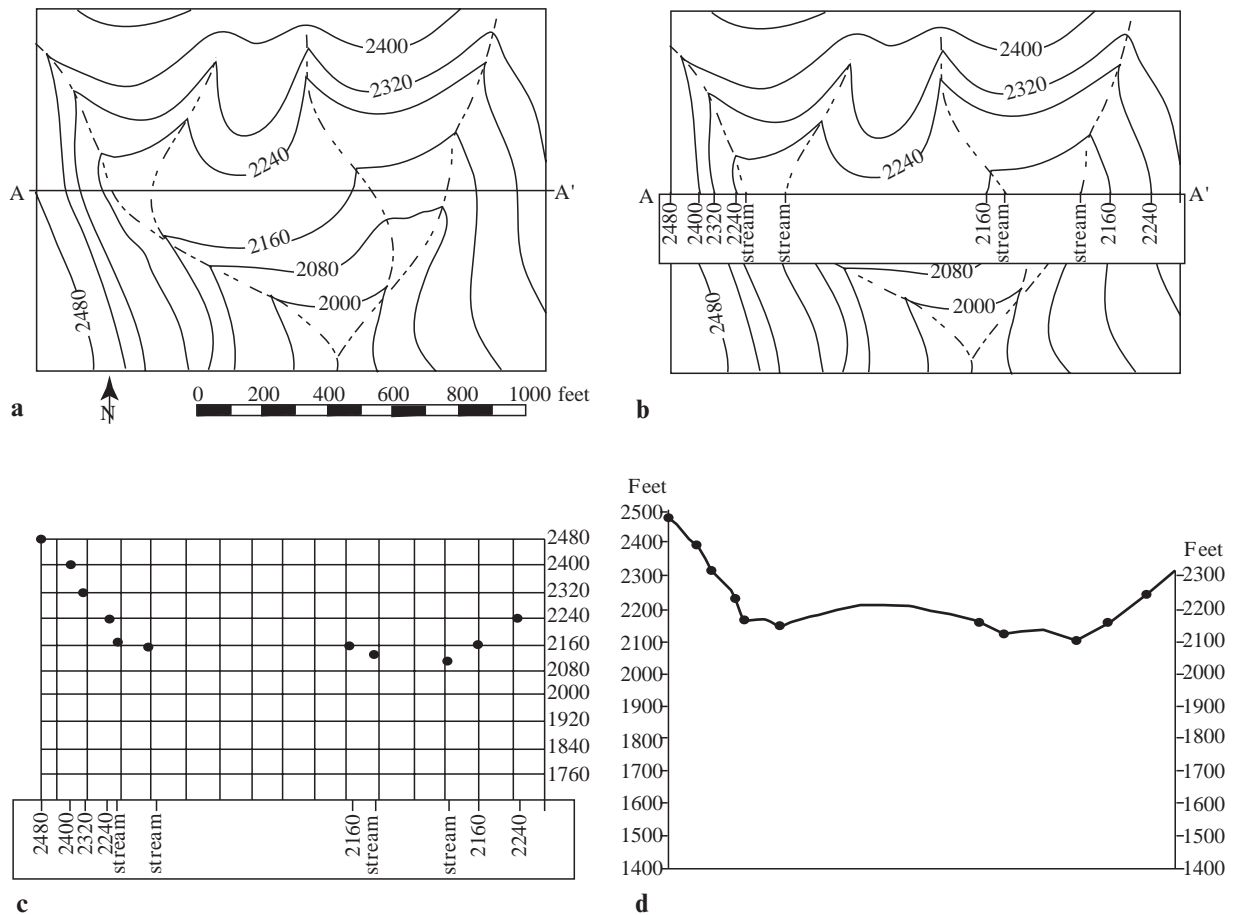
**Box 4.1** A note about vertical exaggeration

For routine structure sections, including all that you draw for exercises in this book, be sure that the vertical and horizontal scales are exactly the same. This means that there is **no vertical exaggeration**. However, there are circumstances under which vertical exaggeration is desired. For example, suppose you are preparing a structure section for an interpretive display at a state park; you might want to exaggerate the vertical scale to emphasize topographic features in the park. In such cases, use Appendix D to determine the adjusted dip of beds in the structure section, and be sure to indicate the amount of vertical exaggeration on the drawing (e.g., “4 × vertical exaggeration”). If there is no vertical exaggeration on a structure section, write “No vertical exaggeration” or “V : H = 1 : 1” beneath the section.

**Structure-section format**

Formal structure sections should include the following characteristics:

- 1 A descriptive title.
- 2 Named geographical and geologic features such as rivers, peaks, faults, and folds should be labeled.
- 3 The section should be bordered with vertical lines on which elevations are labeled.
- 4 All rock units should be labeled with appropriate symbols.
- 5 Standard lithologic patterns should be used to indicate rock type.
- 6 A legend should be included that identifies symbols and scale.
- 7 Vertical exaggeration, if any, should be indicated; if none, indicate “no vertical exaggeration”.



**Fig. 4.6** Technique for drawing a topographic profile. (a) Draw section line on map. (b) Transfer contour crossings, streams, and other features to another sheet of paper. (c) Transfer points to proper elevation on cross-section sheet. (d) Connect points in a way that reflects the topographic subtleties recorded on the map.

- 8 Depositional and intrusive contacts should be thin dark lines; faults should be thicker dark lines.
- 9 Construction lines should be erased.
- 10 Rock units should be colored as they are on the map.

#### **Problem 4.4**

Draw topographic profiles and structure sections A–A' and B–B' on the Bree Creek Quadrangle map. Draw them as neatly and accurately as possible, and color each unit on the structure sections as it is colored on your map. Because the map shows that the Tertiary section rests on a Cretaceous crystalline basement, you must show the crystalline basement beneath the Tertiary rocks on your structure section. These structure sections will later become part of your synthesis of the structural history of the Bree Creek Quadrangle.

Use your thickness measurements from Problems 3.2 and 3.3. Units should maintain a constant thickness in your structure section unless you have evidence to the contrary.

Remember that structure sections involve a great deal of interpretation and that, until someone drills a hole, there is no single correct answer. But your structure section must make sense and be compatible with the geology shown on the map. As in all scientific interpretations, the best solution is the simplest one that is compatible with the available data.

In the northeastern part of the map area, someone did drill holes. Problem 2.2 (Fig. G-3) involved the drawing of a structure contour map on the upper surface of the Bree Conglomerate. Use your completed structure contour map to determine the depth of the Bree Conglomerate in the eastern half of structure section A–A'.

Be sure that your structure sections have all of the 10 features listed above.

## Stereographic Projection

### Objective

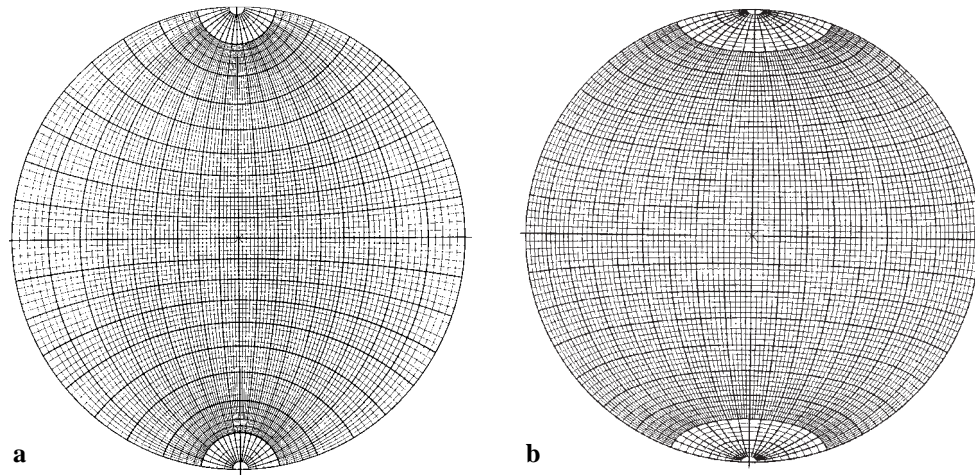
- **Use stereographic projection to quantitatively represent three-dimensional, orientation data (such as the attitudes of lines and planes) on a two-dimensional piece of paper.**

An extremely useful technique for solving many structural problems is stereographic projection. This involves the plotting of planes and lines on a circular grid or net. Many computer programs are available, both commercially and as freeware, that will plot and manipulate structural data on stereonet in different and powerful ways. However, in this chapter we introduce you to some of these techniques and encourage you to complete the problems in the traditional way—by hand. Plotting and manipulating structural data by hand forces you to visualize the connection between the orientations of structures in the field or on a map and the sometimes complex patterns of lines plotted on the stereonet. Your ability to correctly interpret stereograms, regardless of how they are generated, will be severely limited if you are not adept at plotting and manipulating structural data by hand.

Two types of nets are in common use in geology. The net in Fig. 5.1a is called a stereographic net; it is also called a Wulff net, after G. V. Wulff, who adapted the net to crystallographic use. The net in Fig. 5.1b is called a Lambert equal-area net, or Schmidt net. In common geologic parlance, both of these nets are referred to as stereonets.

The two nets are constructed somewhat differently. On the equal-area net, equal areas on the reference sphere remain equal on the projection. This is not the case with the stereographic net. The situation is similar to map projections of the earth; some projections sacrifice accuracy of area to preserve spatial relationships, while others do the opposite. In preserving area, the equal-area net does not preserve angular relationships. The construction of the equal-area net does allow the correct measurement of angles, however, and this net may reliably be used even when angular relationships are involved. In structural geology the relative density of data points is often important, so most structural geologists use the equal-area net. In crystallography, angular relationships are especially important, so crystallographers use the Wulff net. In this book, we will use the equal-area net exclusively.

The equal-area net is arranged rather like a globe of the earth, with north–south lines that are analogous to meridians of longitude and east–west lines that are analogous to parallels of latitude. The north–south lines are called *great circles* and the east–west lines are called *small circles*. The perimeter of the net is called the *primitive circle* (Fig. 5.2);



**Fig. 5.1** Nets used for stereographic projection. (a) Stereographic net or Wulff net. (b) Lambert equal-area net or Schmidt net.

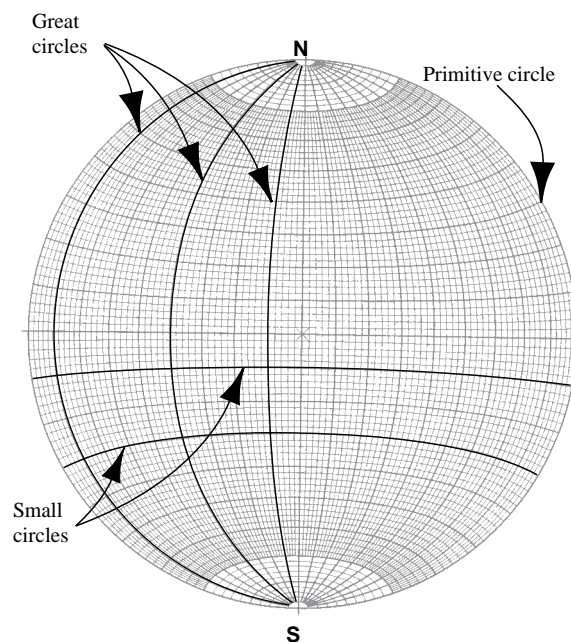
here “primitive” has the mathematical sense of “fundamental.”

Unlike crystallographers, who use the net as if it were an upper hemisphere, structural geologists use it as a lower hemisphere. To visualize how elements are projected onto the net, imagine looking down into a large bowl in which a cardboard half-circle has been snugly fitted at an angle. The exposed diameter of the half-circle is a straight line, and the curved part of the half-circle describes a curve on the bottom of the bowl. Figure 5.3a is an oblique view of a plane within a bowl; the plane strikes north–south and dips  $50^\circ$ W. Figure 5.3b is an equal-area projection of the same plane. Notice that the dip of the plane,  $50^\circ$  in this case, is measured from the perimeter of the net. The great circles on the net represent a set of planes having the same strike and all possible dips. The primitive circle represents a horizontal plane. Although north and south poles are labeled in Figs 5.2 and 5.3, geographic coordinates are actually attached to the data on the tracing paper that you will lay over your net, rather than to the underlying net. By rotating the tracing paper, a great circle corresponding to any plane may be drawn. Similarly, we will refer to the straight line that corresponds to the equator in Figs 5.2 and 5.3 as the “east–west line,” even though it has no fixed geographic orientation.

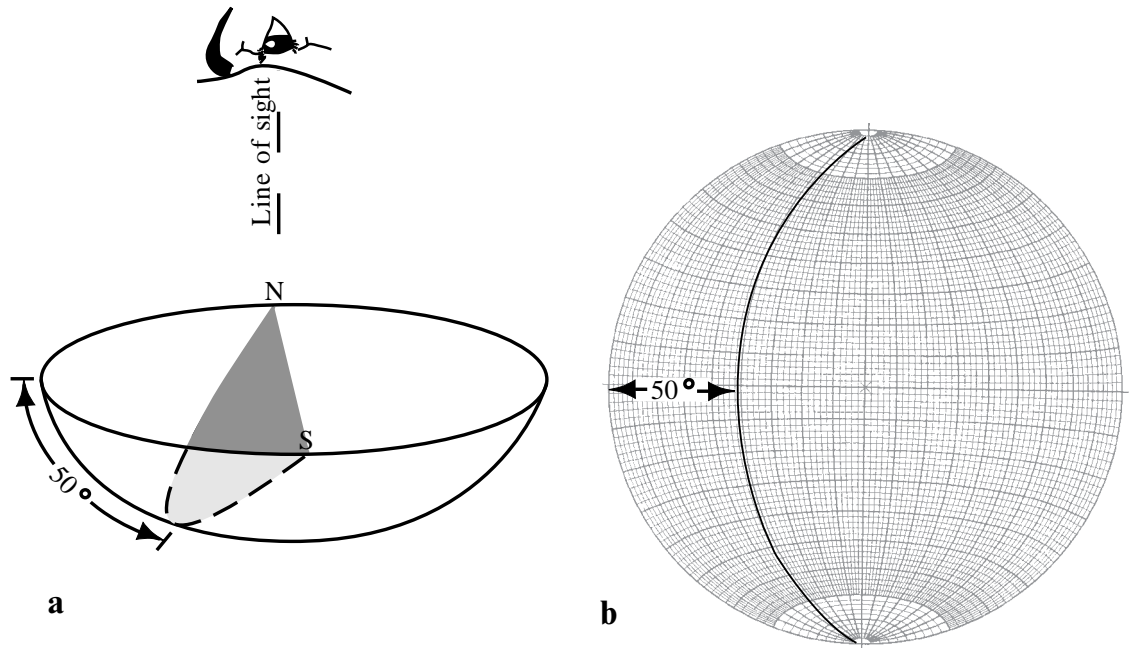
Figure G-11 (Appendix G) is an equal-area net for use in this and succeeding chapters. You will project lines and planes onto the net by placing a piece of tracing paper over the net and rotating the tracing paper on a thumbtack located at the center

of the net. Your net will be heavily used, so it is a good idea to tape it to a piece of thin cardboard to protect it and to ensure that the thumbtack hole does not get larger. Place a rubber eraser on the thumbtack when your net is not in use, to avoid impaling yourself.

Following are several examples of stereographic projection. Work through each of them on your own net.



**Fig. 5.2** Main elements of the equal-area projection.



**Fig. 5.3** Oblique lower-hemisphere view of the projection of a plane striking north-south and dipping  $50^\circ$  west. (a) Oblique view. (b) Equal-area projection.

### A plane

Suppose a plane has an attitude of  $315^\circ$ ,  $60^\circ$ SW. It is plotted on the equal-area net as follows:

- 1 Stick a thumbtack through the center of the net from the back, and place a piece of tracing paper over the net such that the tracing paper will rotate on the thumbtack. A small piece of clear tape in the center of the paper will prevent the hole from getting larger with use.
- 2 Trace the primitive circle on the tracing paper (this step may be eliminated later), and mark the north and south poles.
- 3 Find  $315^\circ$  on the primitive circle, mark it with a small tick mark on the tracing paper and label it  $315^\circ$  (Fig. 5.4a).
- 4 Rotate the tracing paper so that the  $N45^\circ W$  mark is at the north pole of the net (Fig. 5.4b).
- 5 Southwest is now on the left-hand side of the tracing paper, so count  $60^\circ$  inward from the primitive circle along the east-west line of the net and put a mark on that point.
- 6 Without rotating the tracing paper, draw the great circle that passes through that point (Fig. 5.4b).

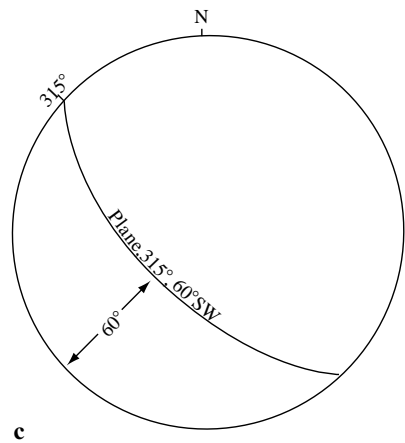
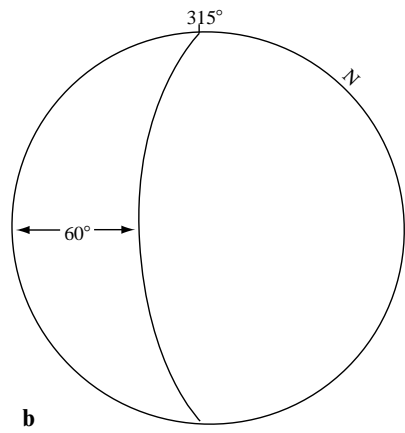
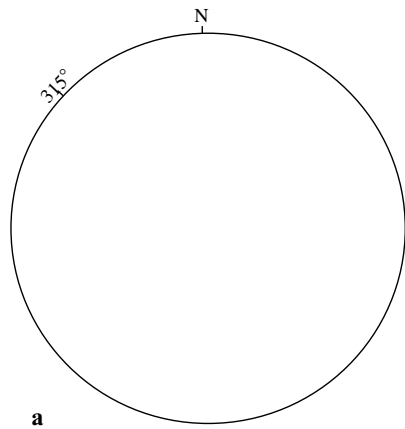
- 7 Finally, rotate the paper back to its original position (Fig. 5.4c).

### A line

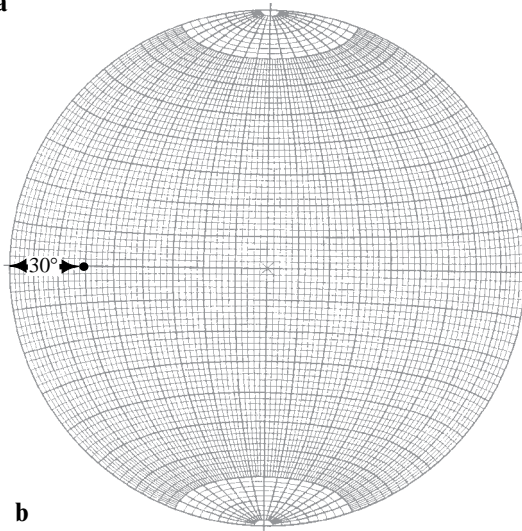
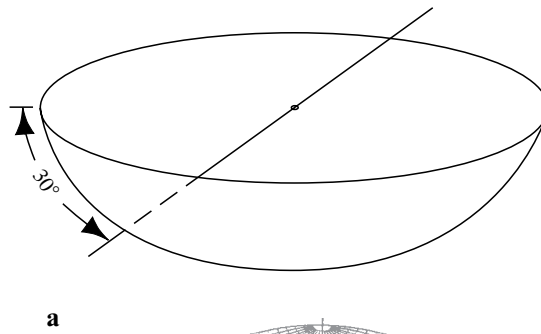
While a plane intersects the hemisphere as a line, a line intersects the hemisphere as a single point. Figure 5.5a is an oblique view of a line that trends due west and plunges  $30^\circ$ , and Fig. 5.5b is an equal-area net projection of this line. Imagine this line passing through the center of the sphere and piercing the lower hemisphere.

Consider a line that has an attitude of  $32^\circ$ ,  $S20^\circ E$ . Here is how such a line projects onto the net:

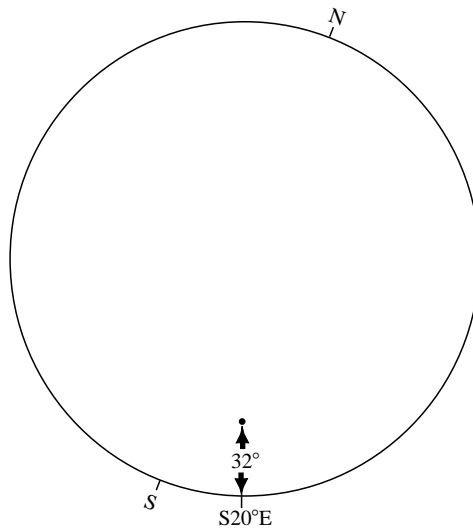
- 1 Mark the north pole and  $S20^\circ E$  on the tracing paper.
- 2 Rotate the  $S20^\circ E$  point to the bottom ("south") point on the net. (The north, west, or east points work just as well. Only from one of these four points on the net may the plunge of a line be measured.)
- 3 Count  $32^\circ$  from the primitive circle inward, and mark that point (Fig. 5.6).
- 4 Rotate the paper back to its original orientation.



**Fig. 5.4** Projection of a plane striking  $315^\circ$  and dipping  $60^\circ$  SW. (a) Plotting of strike. (b) Projection of plane with tracing paper rotated so that the strike is at the top of the net. (c) Tracing paper rotated back to original position.



**Fig. 5.5** Projection of a line that plunges  $30^\circ$  due west. (a) Oblique view. (b) Equal-area projection.



**Fig. 5.6** Projection of a line that plunges  $32^\circ$ , S20°E.

### Pole of a plane

By plotting the pole to a plane it is possible to describe the plane's orientation with a single point on the net. The pole to a plane is the straight line perpendicular to the plane,  $90^\circ$  across the stereonet from the great circle that represents the plane. If a plane strikes north–south and dips  $40^\circ$  west, its pole plunges  $50^\circ$  due east (Fig. 5.7).

Suppose a plane has an attitude of  $N74^\circ E$ ,  $80^\circ N$ . Its pole is plotted as follows:

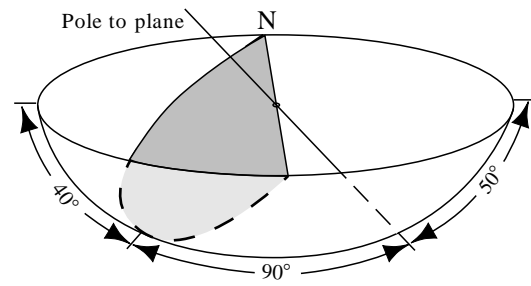
- 1 Mark the point on the tracing paper that corresponds to  $N74^\circ E$ . Then rotate the tracing paper so that this point lies at the north pole of the net, as if you were going to plot the plane itself. The great circle representing this plane is shown by the dashed line in Fig. 5.8.
- 2 Find the point on the east–west line of the net where the great circle for this plane passes, and count  $90^\circ$  in a straight line across the net. This point is the pole to the plane. Mark this point, record the plunge, and also make a tick mark where the east–west line meets the primitive circle. Then rotate the tracing paper back to its original position and determine the direction of plunge. As shown in Fig. 5.8, the pole to this plane plunges  $10^\circ$ ,  $S16^\circ E$ .

In this way the orientation of numerous planes may be displayed on one diagram without cluttering it up with a lot of lines.

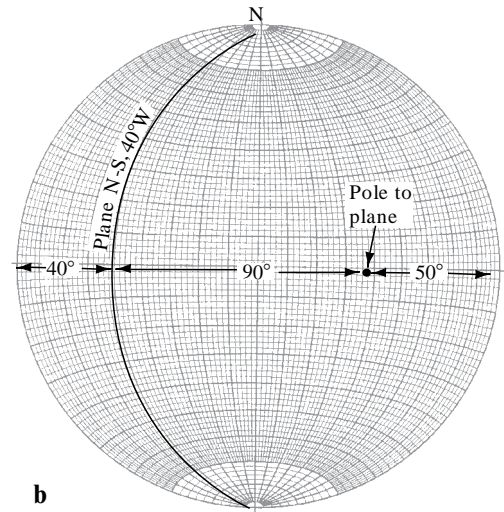
### Line of intersection of two planes

Many structural problems involve finding the orientation of a line common to two intersecting planes. Suppose we wish to find the line of intersection of a plane  $322^\circ$ ,  $65^\circ SW$  with another plane  $060^\circ$ ,  $78^\circ NW$ . This line is located as follows:

- 1 Draw the great circle for each plane (Fig. 5.9).
- 2 Rotate the tracing paper so that the point of intersection lies on the east–west line of the net. Mark the primitive circle at the closest end of the east–west line.
- 3 Before rotating the tracing paper back, count the number of degrees on the east–west line from the primitive circle to the point of intersection; this is the plunge of the line of intersection.

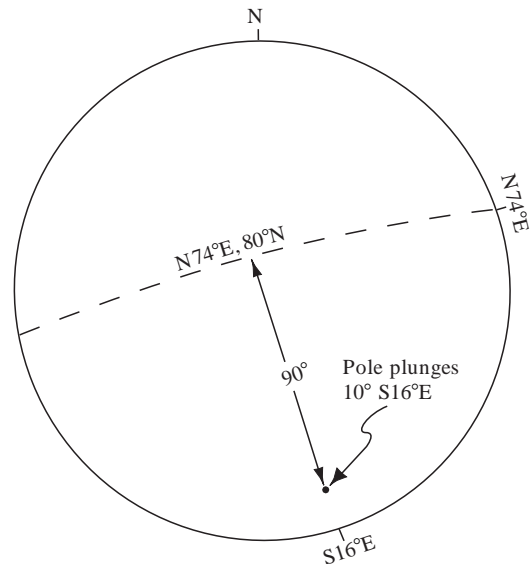


a



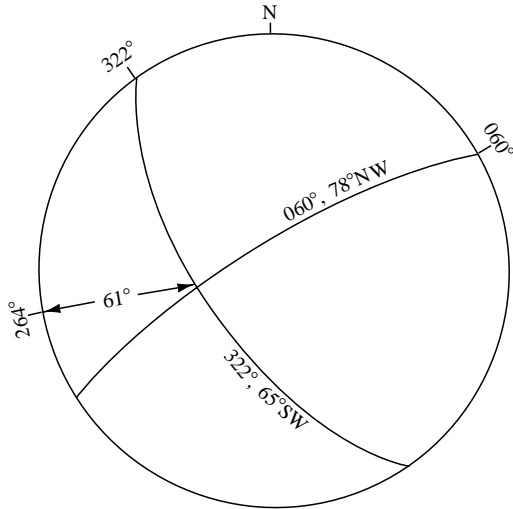
b

**Fig. 5.7** Projection of a plane ( $N-S$ ,  $40^\circ W$ ) and the pole to the plane. (a) Oblique view. (b) Equal-area projection.



**Fig. 5.8** Projection of a pole to a plane.

- 4 Rotate the tracing paper back to its original orientation. Find the bearing of the mark made on the primitive circle in step 2. This is the trend of the line of intersection. The line of intersection for this example plunges  $61^\circ$ ,  $264^\circ$ , as seen in Fig. 5.9.

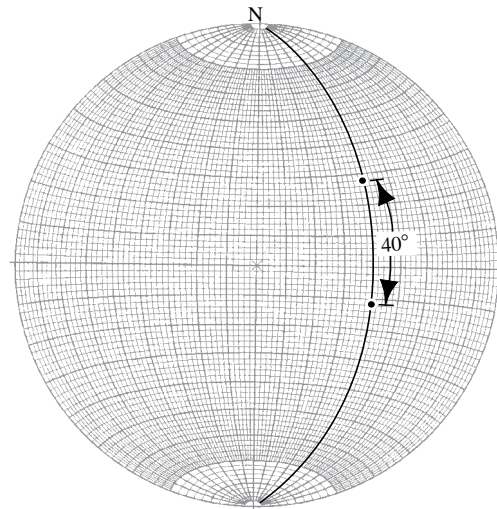


**Fig. 5.9** Projection of the line of intersection of two planes. The attitude of the line of intersection is indicated.

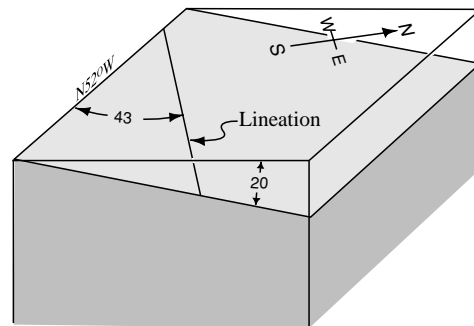
### Angles within a plane

Angles within a plane are measured along the great circle of the plane. In Fig. 5.10, for example, each of the two points represents a line in a plane that strikes north-south and dips  $50^\circ$ E. The angle between these two lines is  $40^\circ$ , measured directly along the plane's great circle.

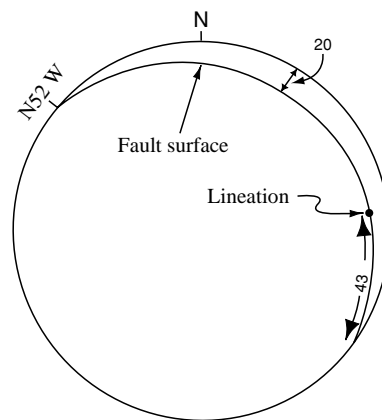
The more common need is to plot the pitch of a line within a plane. Plotting pitches may be useful when working with rocks containing lineations. The lineations must be measured in whatever outcrop plane (e.g., foliation or fault surface) they occur. Suppose, for example, that a fault surface of  $N52^\circ$ W,  $20^\circ$ NE contains a slickenside lineation with a pitch of  $43^\circ$  to the east (Fig. 5.11a). Figure 5.11b shows the lineation plotted on the equal-area net.



**Fig. 5.10** Measuring the angle between two lines in a plane.



a



b

**Fig. 5.11** Pitch of a line in a plane. (a) Block diagram. (b) Equal-area projection.



### True dip from strike and apparent dip

Two intersecting lines define a plane, so if the strike of a plane is known, along with the trend and plunge of an apparent dip, then these two lines may be used to determine the complete orientation of the plane.

Suppose a fault is known to strike  $010^\circ$ , and an apparent dip of the fault plane is measured to have a trend of  $154^\circ$  and a plunge of  $35^\circ$ . The true dip of the fault is determined as follows:

- 1 Draw a line representing the strike line of the plane. This will be a straight line across the center of the net, intersecting the primitive circle at the strike bearing (Fig. 5.12a).
- 2 Make a pencil mark on the primitive circle representing the trend of the apparent dip (Fig. 5.12a).
- 3 Rotate the tracing paper so that the point marking the apparent-dip trend lies on the east–west line of the net. Count the number of degrees of plunge toward the center of the net and mark that point. This point represents the apparent-dip line.
- 4 We now have two points on the primitive circle (the two ends of the strike line) and one point not on the primitive circle (the apparent-dip point), all three of which lie on the fault plane. Turn the tracing paper so that the strike line lies on the north–south line of the net, and draw the great circle that passes through these three points.

- 5 Before rotating the tracing paper back, measure the true dip along the east–west line of the net. As shown in Fig. 5.12b, the true dip is  $50^\circ$ .

### Strike and dip from two apparent dips

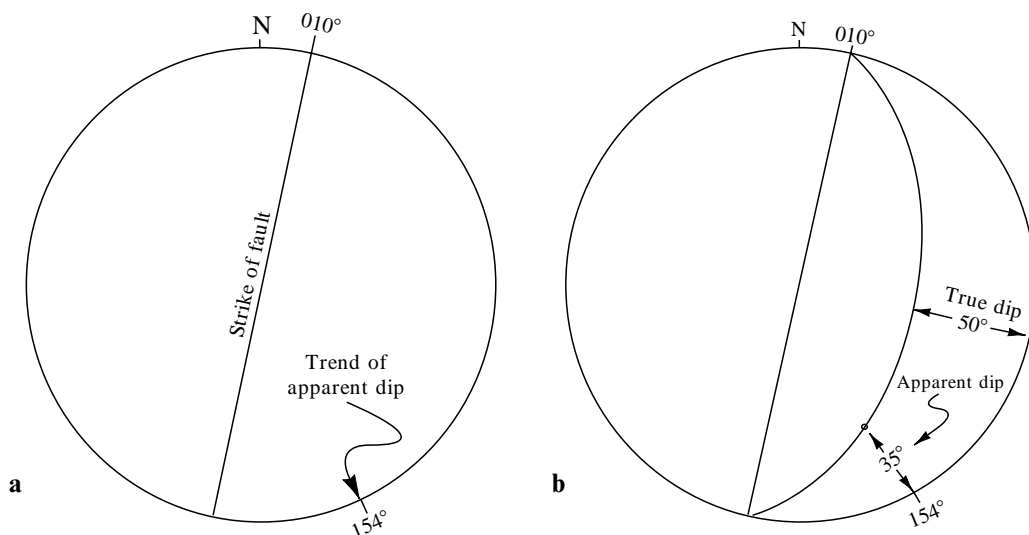
Even if the strike of a plane is not known, two apparent dips are sufficient to find the complete attitude. Suppose two apparent dips of a bed are  $13^\circ$ ,  $S18^\circ E$  and  $19^\circ$ ,  $S52^\circ W$ . The attitude of the plane may be determined as follows:

- 1 Plot points representing the two apparent-dip lines (Fig. 5.13a).
- 2 Rotate the tracing paper until both points lie on the same great circle. This great circle represents the plane of the bed, and the strike and dip are thus revealed. As shown in Fig. 5.13b, the attitude of the plane in this problem is  $N57^\circ W$ ,  $20^\circ SW$ .

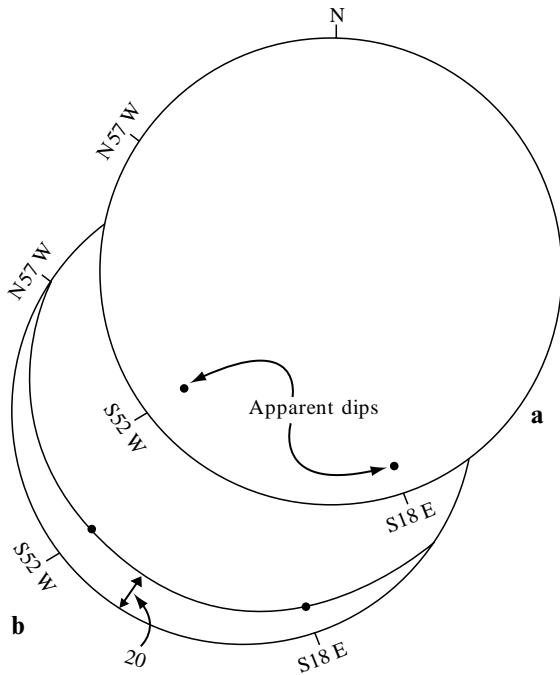
Use stereographic projection to solve the following problems, using a separate piece of tracing paper for each problem.

#### Problem 5.1

Along a vertical railroad cut a bed has an apparent dip of  $20^\circ$ ,  $298^\circ$ . The bed strikes  $067^\circ$ . What is the true dip?



**Fig. 5.12** Determination of true dip from strike and apparent dip. (a) Draw the strike line and trend of apparent dip. (b) Completed diagram showing the direction and degrees of the true dip.



**Fig. 5.13** Determination of strike and dip from two apparent dips. (a) Apparent dips plotted as points on the net. (b) Completed diagram showing the strike and true dip.

### Problem 5.2

In a mine, a fault has an apparent dip of  $14^\circ$ ,  $N90^\circ W$  in one adit and  $25^\circ$ ,  $S11^\circ E$  in another. What is the attitude of the fault plane?

### Problem 5.3

A fault strikes due north and dips  $70^\circ E$ . A limestone bed with an attitude of  $325^\circ$ ,  $25^\circ SW$  is cut by the fault. Hydrothermal alteration along the fault has resulted in an ore shoot at the intersection of the two planes.

- 1 What is the orientation of the ore shoot?
- 2 What is the pitch of the ore shoot in the plane of the fault?
- 3 What is the pitch of the ore shoot in the plane of the limestone bed?

### Problem 5.4

One limb of a fold has an attitude of  $061^\circ$ ,  $48^\circ SE$  and other limb  $028^\circ$ ,  $55^\circ NW$ . What is the orientation of the fold axis?

### Problem 5.5

A coal bed with an attitude of  $N68^\circ E$ ,  $40^\circ S$  is exposed near the bottom of a hill. One adit is to be driven westward along the bottom of the bed from the east side of the hill, and a second adit is to be driven eastward along the bottom of the bed from the west side of the hill. To facilitate drainage of water, as well as the ease of movement of full ore carts out of the mine, each adit is to have a slope of  $10^\circ$ . Determine the bearing of each of the two adits.

### Problem 5.6

You are mapping metamorphic rocks and you notice a lineation within the rocks. At five different outcrops you measure the pitch of the lineation on an exposed planar rock surface (not necessarily the same structural surface at each outcrop). The table below lists the attitude of each exposed surface and the pitch of the lineation on that surface.

Outcrop no.	Attitude of surface	Pitch of lineation
1	$300^\circ$ , $84^\circ NE$	$76^\circ E$
2	$350^\circ$ , $30^\circ E$	$50^\circ N$
3	$040^\circ$ , $70^\circ SE$	$63^\circ SW$
4	$337^\circ$ , $30^\circ W$	$50^\circ S$
5	$272^\circ$ , $45^\circ N$	$59^\circ E$

You hypothesize that this lineation represents a planar fabric within the rock. Test this idea by determining whether these five lineation orientations are coplanar. If so, what is the attitude of the plane?

### Problem 5.7

Two intersecting shear zones have the following attitudes:  $N80^\circ E$ ,  $75^\circ S$  and  $N60^\circ E$ ,  $52^\circ NW$ .

- 1 What is the orientation of the line of intersection?
- 2 What is the orientation of the plane perpendicular to the line of intersection?
- 3 What is the obtuse angle between the shear zones within this plane?
- 4 What is the orientation of the plane that bisects the obtuse angle?
- 5 A mining adit is to be driven to the line of intersection of the two shear zones. For maximum stability the adit is to bisect the obtuse angle between the two shear zones and intersect the line of intersection perpendicularly. What should the trend and plunge of the adit be?
- 6 If the adit is to approach the line of intersection from the southeast, will the full ore carts be going uphill or downhill as they come out of the mine?

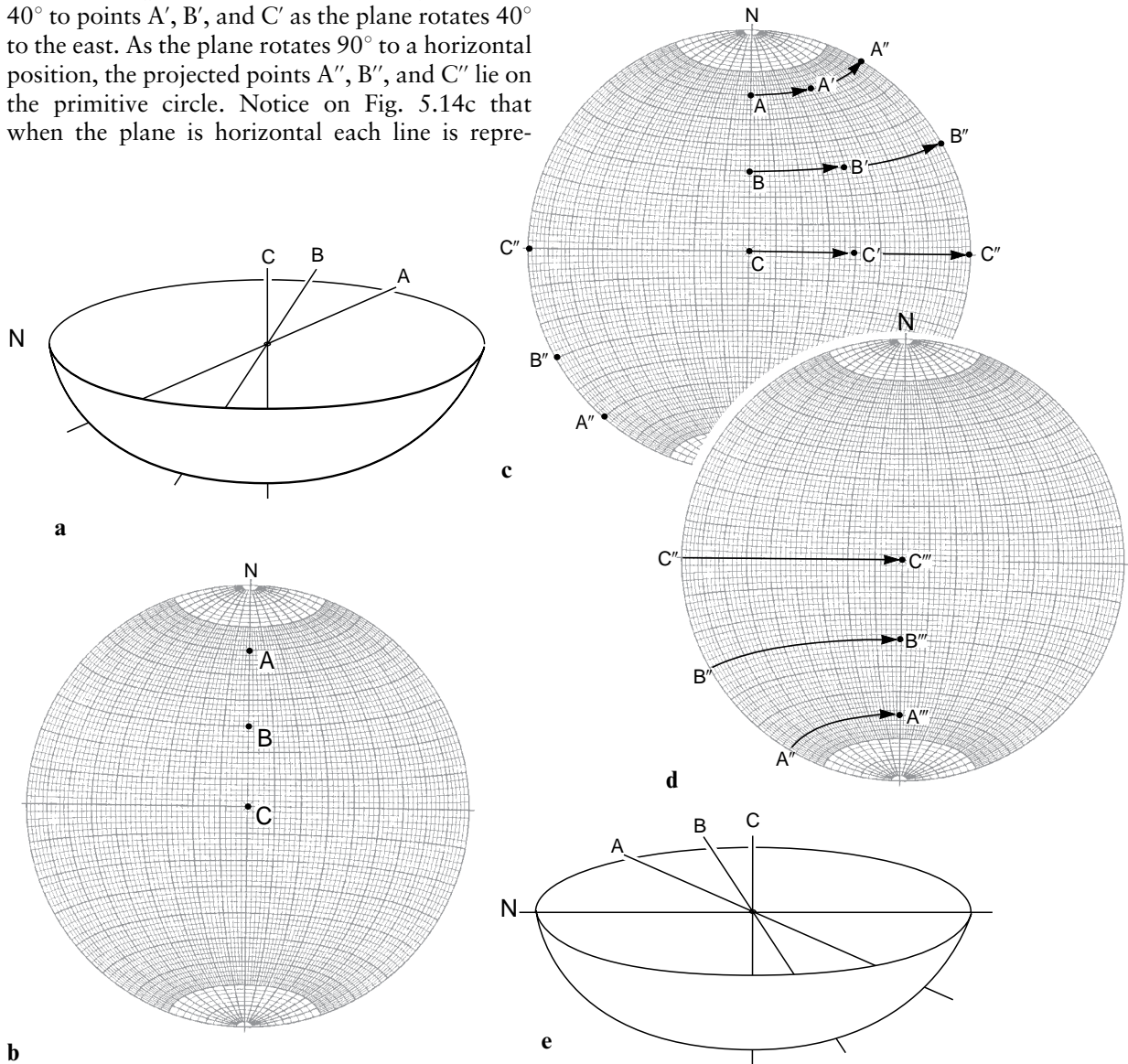
### Rotation of lines

Some types of problems involve the rotation of lines or planes on the stereonet. Imagine three lines—A, B, and C—with plunges of  $30^\circ$ ,  $60^\circ$ , and  $90^\circ$ , respectively, all lying within a vertical, north–south-striking plane. Figure 5.14a is an oblique view of these lines intersecting a lower hemisphere, and Fig. 5.14b shows the same three lines projected on the equal-area net.

As the originally vertical, north–south-oriented plane rotates around the horizontal north–south axis of the net, the projection points of lines within the plane move along the small circles. Figure 5.14c shows points A, B, and C moving in unison  $40^\circ$  to points A', B', and C' as the plane rotates  $40^\circ$  to the east. As the plane rotates  $90^\circ$  to a horizontal position, the projected points A'', B'', and C'' lie on the primitive circle. Notice on Fig. 5.14c that when the plane is horizontal each line is repre-

sented by two points  $180^\circ$  apart on the primitive circle, one in the northeast quadrant and one in the southwest quadrant.

As the plane continues to rotate, A and B leave the northern half of the hemisphere and reappear in the southern half. In other words, when you rotate lines beyond the primitive circle you change from plotting the “head” of the line to plotting its “tail.” This occurs because only the lower hemisphere of the stereonet is used for plotting data. Figure 5.14d shows the projection points of the three lines as the plane in which they lie rotates  $180^\circ$  from its original orientation in Fig. 5.14a.



**Fig. 5.14** Rotation of three coplanar lines. (a) Oblique view. (b) Projection of lines on the equal-area net. (c) Projection of lines rotated  $40^\circ$  (A', B', C') and  $90^\circ$  (A'', B'', C''). (d) Projection of lines rotated  $180^\circ$  from their original positions. (e) Oblique view of the final positions of lines rotated  $180^\circ$ . Lines A, B, and C lie in a north–south-striking vertical plane.

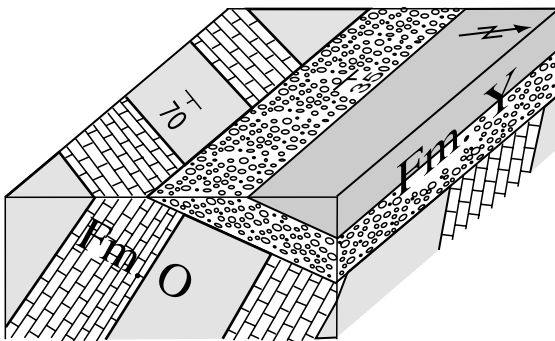
Although in this example the lines being rotated are coplanar, this need not be the case. Lines representing the poles of several variously oriented planes, for example, can be rotated together. The only requirement is that all points must move the same number of degrees along their respective small circles.

### The two-tilt problem

It is not uncommon to find rocks that have undergone more than one episode of deformation. In such situations it is sometimes useful to remove the effects of a later deformation in order to study an earlier one.

Consider the block diagram in Fig. 5.15a. An angular unconformity separates Formation Y (N60°W, 35°NE) from Formation O (N50°E, 70°SE). Formation O was evidently tilted and eroded prior to the deposition of Formation Y, then tilted again. In order to unravel the structural history of this area we need to know the attitude of Formation O at the time Formation Y was being deposited. This problem is solved as follows:

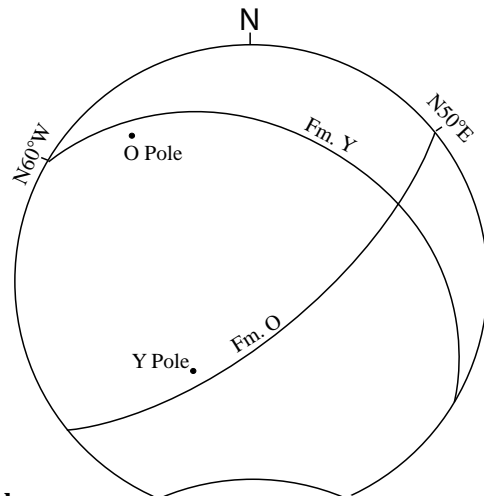
- 1 Plot the poles of the two formations on the equal-area net (Fig. 5.15b).
- 2 We want to return Formation Y to horizontal and measure the attitude of Formation O. The pole of a horizontal bed is vertical, so if we move the Y pole point to the center of the net, Formation Y will be horizontal. Rotate the tracing paper so that Y lies on the east-west line of the net.
- 3 The Y pole can now be moved along the east-west line to the center of the net (Fig. 5.15c). This involves 35° of movement.



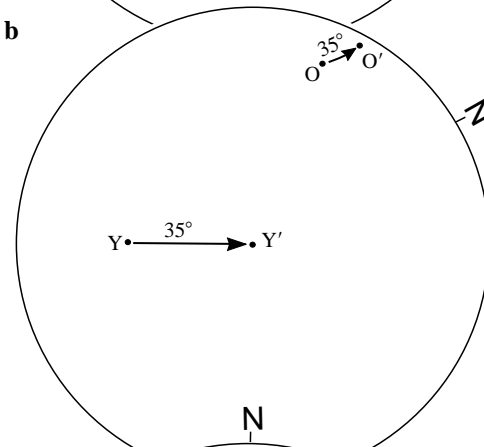
a

The O pole, therefore, must also be moved 35° along the small circle on which it lies, to O' (Fig. 5.15c).

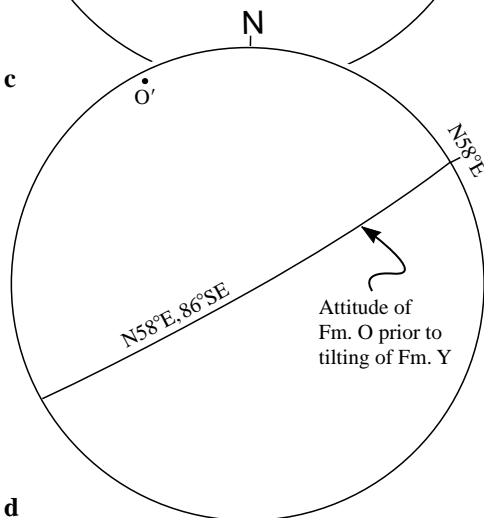
- 4 O' is the pole of Formation O prior to the last episode of tilting. As shown in Fig. 5.15d, the attitude of Formation O at that time was N58°E, 86°SE.



b



c



d

**Fig. 5.15** Two-tilt problem. (a) Block diagram. (b) Plot of attitudes and poles of Formations O and Y. (c) Untilting of Formation Y. (d) Plot of attitude of Formation O prior to tilting of Formation Y.

**Problem 5.8**

The beds below an angular unconformity have an attitude of  $334^{\circ}$ ,  $74^{\circ}\text{W}$ , and those above  $030^{\circ}\text{E}$ ,  $54^{\circ}\text{NW}$ . What was the attitude of the older beds while the younger beds were being deposited?

**Problem 5.9**

Iron-bearing minerals in volcanic rocks contain magnetic fields that were acquired when the magma flowed out onto the earth's surface and cooled. These magnetic fields can be measured to determine the orientation of the lines of force of the earth's magnetic field at the time of cooling. If the north-seeking paleomagnetic attitude in a basalt is  $32^{\circ}$ ,  $\text{N}67^{\circ}\text{E}$ , and the flow has been tilted to  $\text{N}12^{\circ}\text{W}$ ,  $40^{\circ}\text{W}$ , what was the attitude (plunge and trend) of the pretilt paleomagnetic orientation?

**Problem 5.10**

The dip direction of cross-beds in sandstone can be used to determine the direction that the current was flowing when the sand was deposited. A sandstone bed strikes  $320^{\circ}$  and dips  $57^{\circ}\text{SW}$ . Cross-beds within this tilted bed indicate a paleocurrent direction of  $090^{\circ}$ . Rotate the bed to its pretilted orientation and determine the actual paleocurrent direction.

**Problem 5.11**

In the northeastern fault block of the Bree Creek Quadrangle there is a hill that is capped by Helm's Deep Sandstone overlying Rohan Tuff. In Problem 3.1 you determined the attitudes of these two units at this locality. Use stereographic projection to determine the amount and direction of the tilting experienced by this fault block after deposition of the Rohan Tuff but before deposition of the Helm's Deep Sandstone.

**Cones: the drill-hole problem**

In certain problems it is necessary to project a cone onto the net. Suppose, for a simple example, that a hole has been drilled horizontally due north into a cliff. The drill core is shown in Fig. 5.16a. The rock is layered, and the angle between the core axis and the bedding plane is  $30^{\circ}$ . The angle between the pole to the bedding plane and the core axis is  $60^{\circ}$ , the complement of  $30^{\circ}$ .

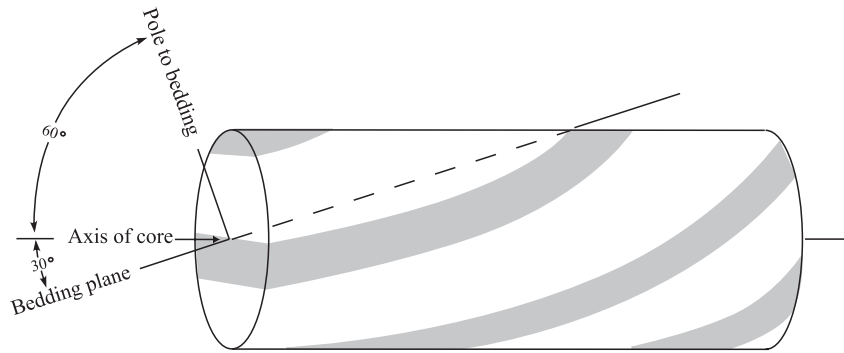
The core rotated as it was extracted from the hole, so the exact orientation of the bedding plane cannot be determined. However, a locus of possible orientations can be defined. Figure 5.16b is an oblique view of the situation, showing a cone with its axis horizontal and trending north-south. The cone represents all possible lines  $30^{\circ}$  from the axis. Lines perpendicular to the sides of the cone, representing poles to the bedding plane, pass through the center of the sphere and intersect the lower hemisphere as two half-circles. As shown in Fig. 5.16c, the equal-area plot of the possible poles to bedding consists of two small circles, each  $60^{\circ}$  from a pole. If a second hole is drilled, oriented differently from the first, two more small circles can be drawn. The second set of circles will have two, three, or four points in common with the first pair of small circles. A third hole results in a unique solution, establishing the pole to bedding.

Consider the following data from three drill holes:

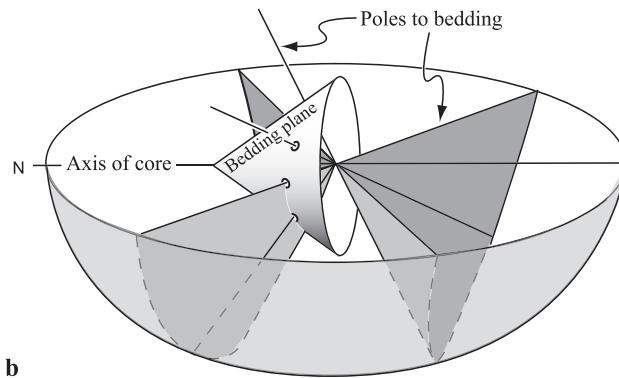
Hole no.	Plunge and trend of hole	Angle between axis of core and bedding	Angle between axis and pole to bedding
1	$74^{\circ}$ , $\text{N}80^{\circ}\text{W}$	$17^{\circ}$	$73^{\circ}$
2	$70^{\circ}$ , $\text{S}30^{\circ}\text{E}$	$18^{\circ}$	$72^{\circ}$
3	$62^{\circ}$ , $\text{N}67^{\circ}\text{E}$	$51^{\circ}$	$39^{\circ}$

What is the attitude of the beds? The solution involves consideration of the holes in pairs. In part A we will consider holes 1 and 2 together, and in part B holes 1 and 3 together. The two parts should be drawn on separate pieces of tracing paper.

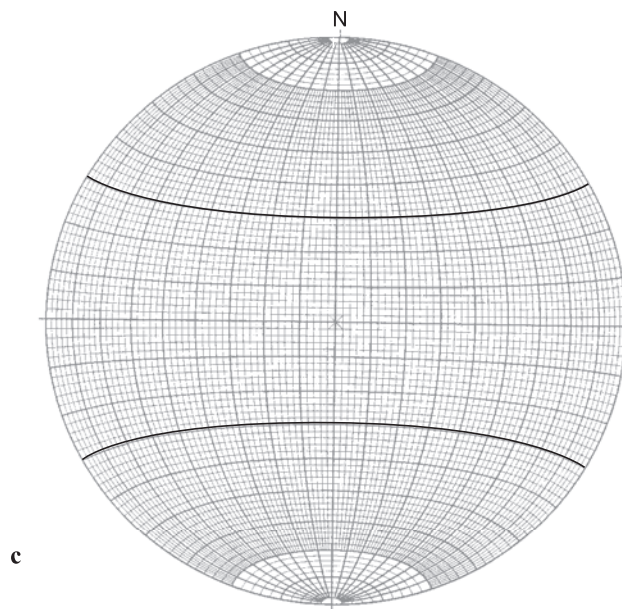
- A1** Plot each hole (Fig. 5.17a).  
**A2** Rotate the tracing paper so that both points lie on the same great circle, which places them in a common plane. In this example the plane dips  $82^{\circ}\text{SW}$ .



a



b



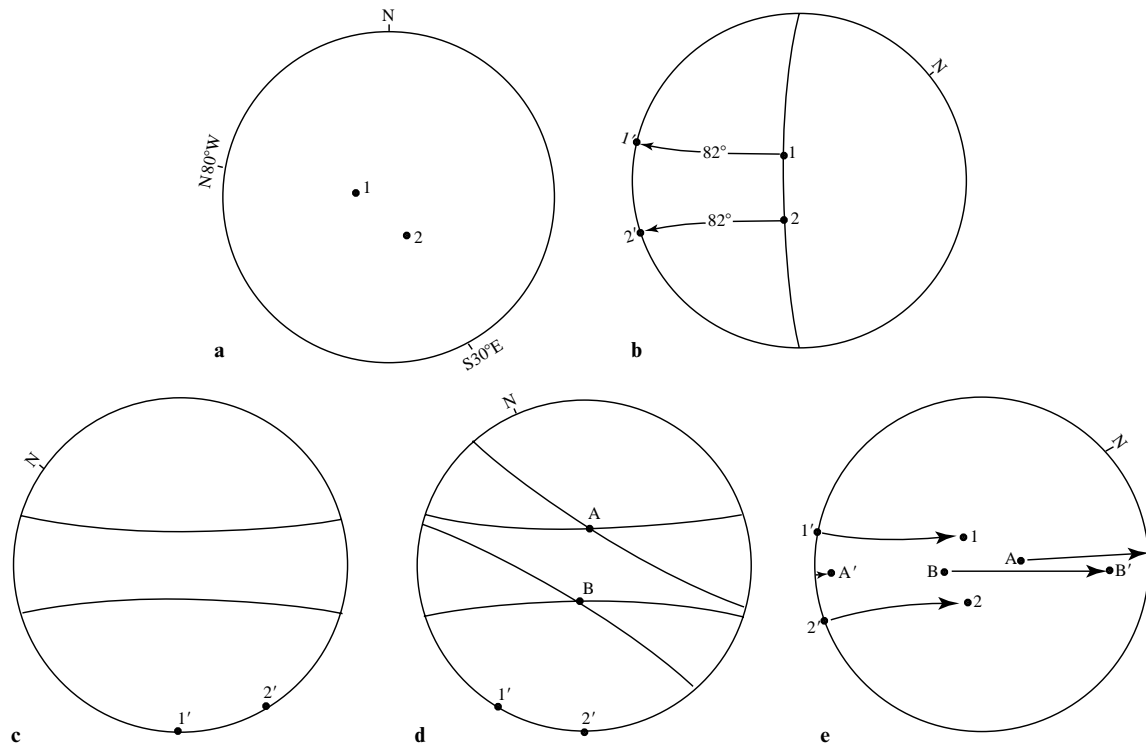
c

**Fig. 5.16** Drill-hole problem. (a) Drill core. (b) Oblique view of the projection of all possible poles to bedding of the drill core. (c) Equal-area projection of all possible poles to bedding of the drill core.

- A3** Rotate the common plane to horizontal. This step moves points 1 and 2 along their respective small circles  $82^\circ$  to points 1' and 2' on the primitive circle (Fig. 5.17b).
- A4** Rotate the tracing paper so that point 1' lies at a pole of the net. In this position, hole 1 has effectively been oriented horizontal and north-south, similar to the core shown in Fig. 5.16a. The angle between the axis of hole 1 and the pole to bedding is  $73^\circ$ , so two small circles, each  $73^\circ$  from a pole, describe all of the possible pole orientations. Figure 5.17c shows these two small circles.
- A5** Now rotate the tracing paper so that point 2' is at a pole of the net. The angle between the axis of hole 2 and the pole to bedding is  $72^\circ$ , so two small circles, each  $72^\circ$  from a pole, describe the possible orientations of the pole to bedding. As shown in Fig. 5.17d, the two sets of small circles cross at points A and B. Depending on the orientations of the two

cores, there may be from one to four points of intersection.

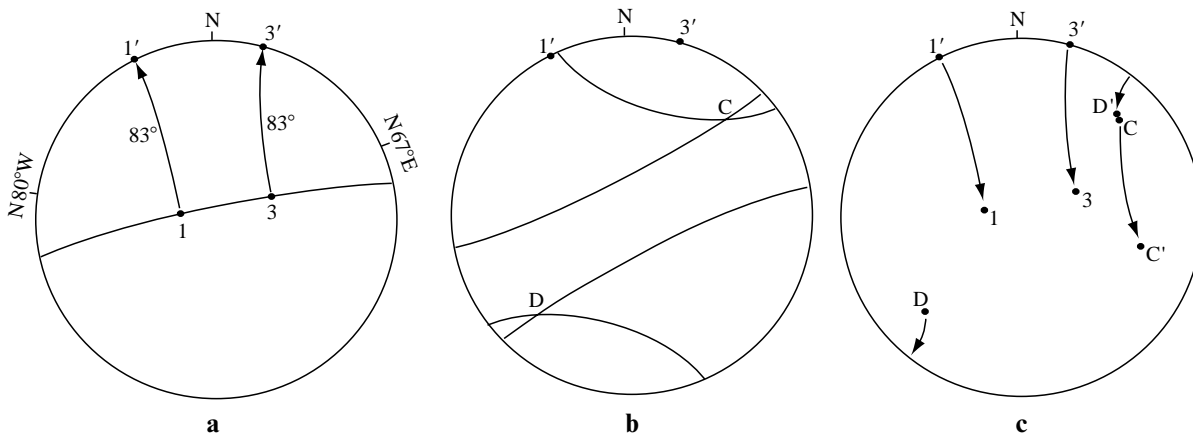
- A6** The points of intersection have been determined with the cores in a horizontal plane. The cores must be returned to their proper orientation for the orientations of the points of intersection to be determined. To do this, rotate the tracing paper so that points 1 and 2 again lie on a common great circle, as in step A2. Points 1' and 2' are imagined to move  $82^\circ$  back to 1 and 2, and points A and B move  $82^\circ$  along small circles in the same direction to points A' and B', as shown in Fig. 5.17e. Notice that point A, after moving  $72^\circ$ , encounters the primitive circle. In order to complete its  $82^\circ$  excursion it reappears  $180^\circ$  around the primitive circle and travels an additional  $10^\circ$ . Points A' and B', thus located, are both possible poles to bedding in this problem.



**Fig. 5.17** Part A of drill-hole solution. (a) Plot of orientations of holes 1 and 2. (b) Location of the plane that is common to both drill-hole orientations and rotation of this plane so that it is horizontal. (c) Plot of small circles that together represent the cone of the possible bedding-plane poles relative to hole 1. (d) Same for hole 2. Points A and B are points common to both pairs of small circles. (e) Determination of orientation of poles A and B by rotating them back to their original orientations. A third hole must be analyzed to determine which pole is the correct one.

- B1** Holes 1 and 3 will now be considered together on a separate piece of tracing paper. Figure 5.18a shows cores 1 and 3 plotted, rotated to a common great circle, and moved to the primitive circle as  $1'$  and  $3'$ . Notice that  $1'$  here is in a different location than  $1'$  in step A3.
- B2** Small circles  $73^\circ$  and  $39^\circ$  from points  $1'$  and  $3'$ , respectively, are drawn, as shown in Fig. 5.18b. The intersection of the two pairs of small circles are points C and D.
- B3** As points  $1'$  and  $3'$  travel  $83^\circ$  back to their original positions as points 1 and 3, points C and D also travel  $83^\circ$  on small circles (Fig. 5.18c).

Either  $C'$  or  $D'$  should be in the same position on the net as  $A'$  or  $B'$ . In this example, points  $B'$  and  $D'$  turn out to be the same point, with an orientation of  $26^\circ$ ,  $N41^\circ E$ . This is the pole to the bedding plane, thus establishing a bedding attitude of  $N50^\circ W$ ,  $64^\circ SW$ . A third solution could be done, with points 2 and 3 considered together, for further confirmation. If no two points are coincident, then either a mistake has been made or the attitude is not consistent from one hole to the next.



**Fig. 5.18** Part B of drill-hole solution. (a) Plot of orientations of holes 1 and 3, and rotation of the common plane to horizontal. (b) Plot of cones of the possible poles to bedding planes relative to holes 1 and 3. (c) Determination of orientations of common poles C and D. Pole  $D'$  coincides with pole  $B'$  (Fig. 5.17e) and is therefore the correct solution.

### Problem 5.12

Using the data from the three drill holes shown below, determine the attitude of bedding.

Hole no.	Plunge and trend of hole	Angle between axis of core and bedding	Angle between axis and pole to bedding
1	$70^\circ$ , $N20^\circ W$	$40^\circ$	$50^\circ$
2	$76^\circ$ , $N80^\circ E$	$65^\circ$	$25^\circ$
3	$68^\circ$ , $S30^\circ W$	$54^\circ$	$36^\circ$





### Objectives

- Describe the orientation and geometry of folds.
- Classify folds on the basis of dip isogons.

Chapters 1 through 5 have been devoted to various techniques of structural analysis. Now it is time to use some of these techniques to describe and analyze folded and faulted rocks. In Chapter 4 you learned techniques for drawing vertical structure sections of folded and faulted rocks, but the emphasis was on the mechanics of drawing the structure sections rather than on the structures themselves. Chapters 6 to 10 are devoted to techniques for analyzing folds and faults.

An understanding of the formation of geologic structures begins with a precise description of the structures themselves. Listed below are the principal terms used to describe the geometric elements and characteristics of folds. Most of the concepts and techniques discussed in Chapters 6 and 7 apply only to cylindrical folds (see below).

**Hinge point** The point of minimum radius of curvature on a fold (Figs 6.1a, 6.2a).

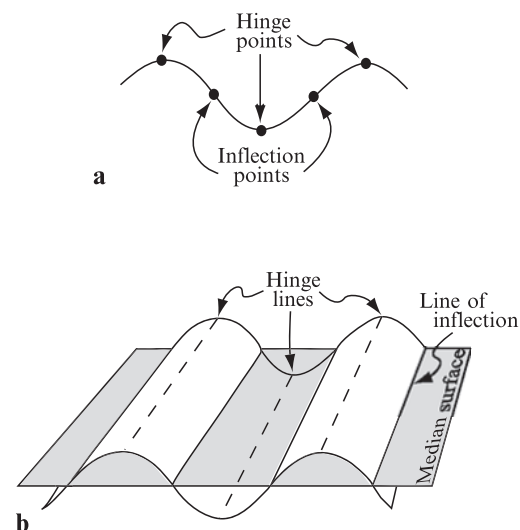
**Hinge line** The locus of hinge points on a folded surface (Fig. 6.1b).

**Inflection point** The point on a fold where the rate of change of slope is zero, usually chosen as the midpoint (Fig. 6.1a).

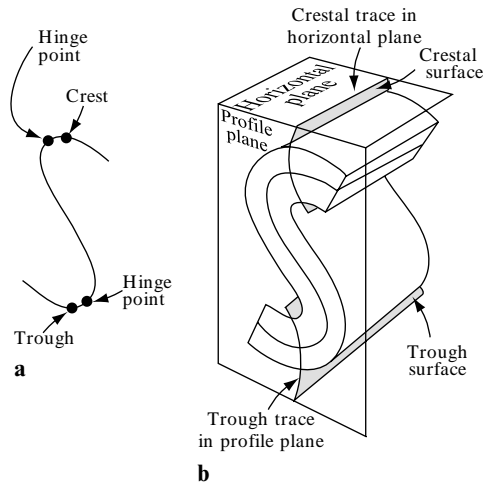
**Line of inflection** The locus of inflection points of a folded surface (Fig. 6.1b).

**Median surface** The surface that joins the successive lines of inflection of a folded surface (Fig. 6.1b).

**Crest and trough** The high and low points, respectively, of a fold, usually in reference to folds with gently plunging hinge lines (Fig. 6.2a).



**Fig. 6.1** Some terms for describing the geometry of folds. (a) Profile view. (b) Block diagram.



**Fig. 6.2** More terms for describing the geometry of folds. (a) Profile view. (b) Block diagram.

**Crestal surface and trough surface** The surfaces joining the crests and troughs, respectively, of nested folds (Fig. 6.2b).

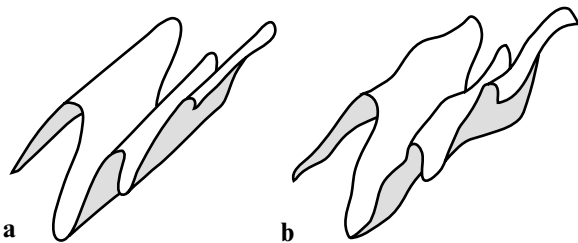
**Crestal trace and trough trace** The lines representing the intersections of the crestal and trough surfaces, respectively, with another surface, usually the surface of the earth (Fig. 6.2b).

**Cylindrical fold** A fold generated by a straight line moving parallel to itself in space (Fig. 6.3a).

**Noncylindrical fold** A fold that cannot be generated by a straight line moving parallel to itself in space (Fig. 6.3b).

**Fold axis** The straight line that generates a cylindrical fold. Unlike the hinge line, the fold axis is not a specific line but rather a hypothetical line defined by its attitude. Only cylindrical folds, or cylindrical segments of folds, have fold axes.

**Symmetric folds** Folds that meet the following criteria: (1) the median surface is planar, (2) the axial plane is perpendicular to the median surface, and (3) the folds are bilaterally symmetrical about their axial planes (Fig. 6.4a).



**Fig. 6.3** (a) Cylindrical folds. (b) Noncylindrical folds.

**Asymmetric folds** Folds that are not symmetric (Fig. 6.4b). Limbs of asymmetric folds are of unequal length.

**Kink fold** A fold characterized by long, relatively straight limbs and narrow, sharp, angular hinges.

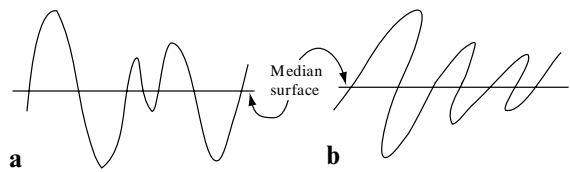
**Profile plane** A plane perpendicular to the fold axis (Fig. 6.5).

**Axial surface** The surface joining the hinge lines of a set of nested folds (Fig. 6.5). Whether or not the folds are cylindrical, the axial surface may or may not be planar.

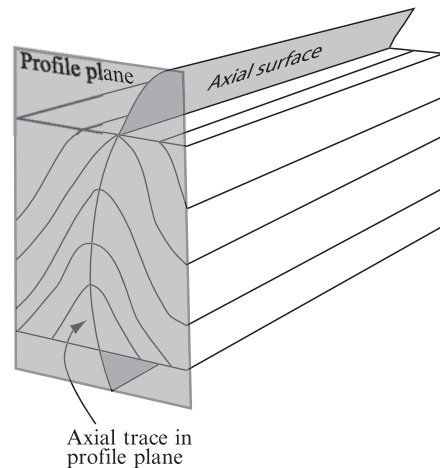
**Axial plane** A planar axial surface (see Fig. 6.8).

**Axial trace** The line representing the intersection of the axial surface and another surface (Fig. 6.5).

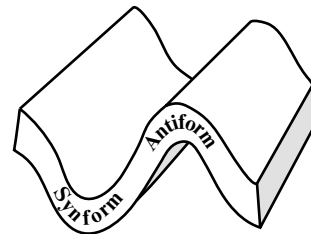
**Synform** A fold that closes downward (Fig. 6.6).



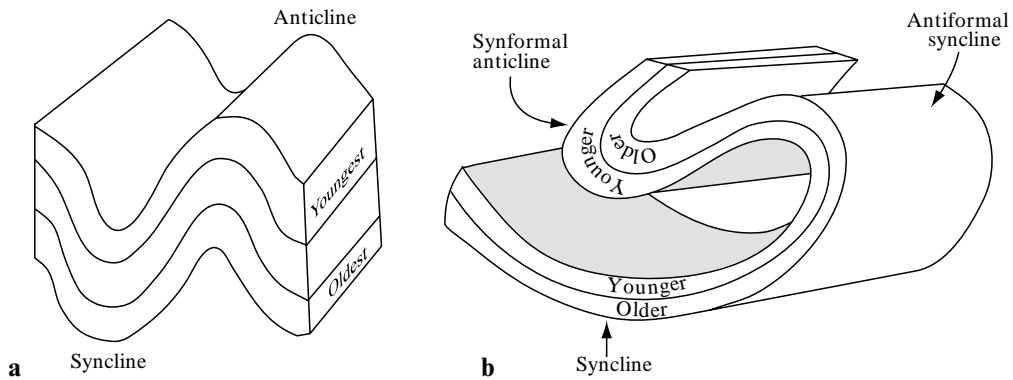
**Fig. 6.4** (a) Symmetric and (b) nonsymmetric folds with varying amplitudes.



**Fig. 6.5** Profile plane and the axial surface of folds.



**Fig. 6.6** Block diagram showing a synform and anti-form.



**Fig. 6.7** Block diagrams showing (a) synclines and anticlines, and (b) how they can differ from synforms and antiforms.

**Antiform** A fold that closes upward (Fig. 6.6).

**Syncline** A fold with younger rocks in its core (Fig. 6.7).

**Anticline** A fold with older rocks in its core (Fig. 6.7).

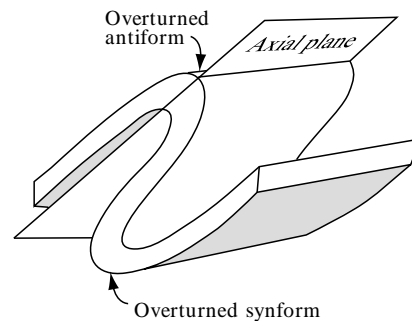
**Overturned fold** A fold in which one limb, and only one limb, has been tilted more than  $90^\circ$ , resulting in both limbs dipping in the same direction (Fig. 6.8).

**Vertical fold** A fold in which the hinge line is vertical or nearly so (Fig. 6.9a).

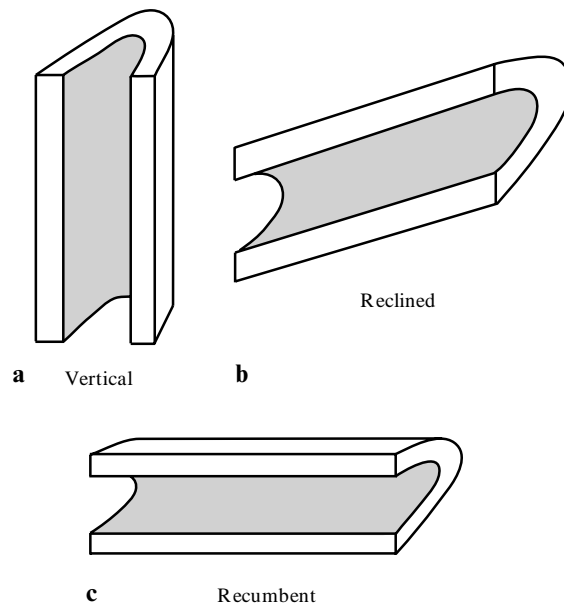
**Reclined fold** An overturned fold in which the axial surface is inclined and the hinge line plunges down the dip of the axial surface (Fig. 6.9b).

**Recumbent fold** An overturned fold in which the axial surface is horizontal or nearly so (Fig. 6.9c).

**Interlimb angle** The angle between adjacent fold limbs. Figure 6.10 shows the terms used to describe folds with various interlimb angles.



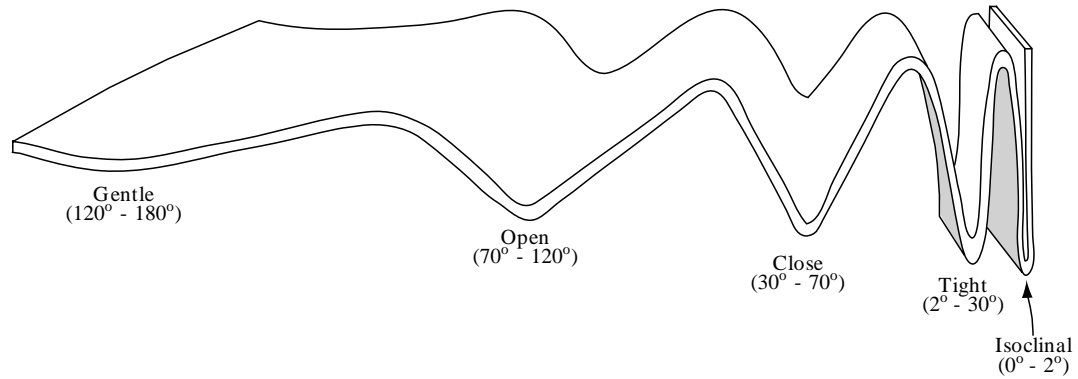
**Fig. 6.8** Block diagram showing overturned folds.



**Fig. 6.9** (a) Vertical, (b) reclined, and (c) recumbent folds.

### Problem 6.1

Figure G-12 (Appendix G) is a block model to be cut out and folded into a three-dimensional block. The surface with the north arrow represents a horizontal surface. You may want to color some of the beds before assembling the block, to enhance the definition of the folds. After you have assembled your block, draw and label the crestal, trough, and axial traces of all of the folds. Then describe the folds in the block. Your description should consist of two or three complete sentences. Be sure to include whether the folds are cylindrical or noncylindrical, symmetric or asymmetric, the attitude of the fold axis and the axial surface, and the interlimb angle.



**Fig. 6.10** Terms used to describe interlimb angles of folds.

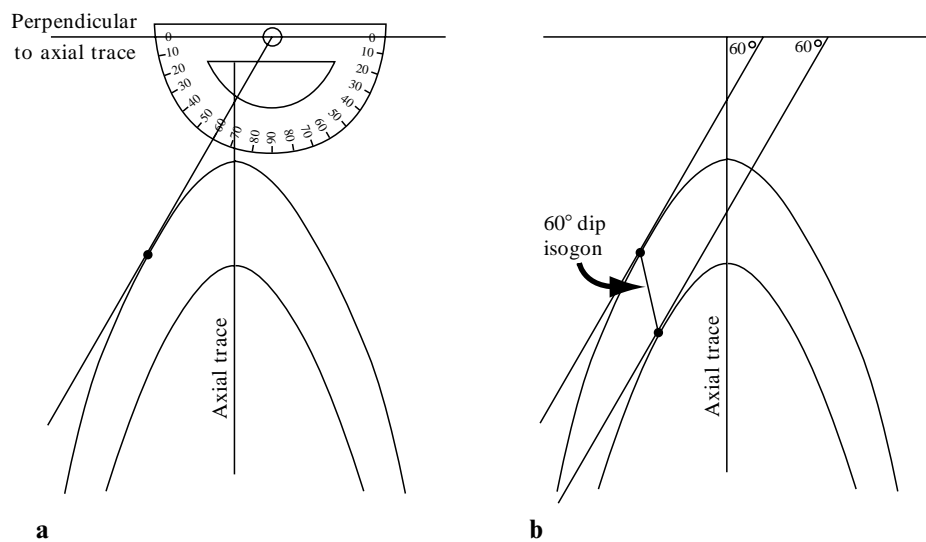
### Fold classification based on dip isogons

Our discussion of folds and folding begins with the geometric description of folds. A widely used geometric classification of folds is based on *dip isogons* (Ramsay, 1967).

Dip isogons are lines that connect points of equal dip on adjacent folded surfaces. They are constructed as shown in Fig. 6.11. The axial trace is drawn on a profile view of the fold, and another line is drawn perpendicular to the axial trace. With a protractor, points along adjacent folded surfaces are located such that tangents to the fold surfaces intersect the perpendicular line at a predetermined angle (Fig. 6.11a). Dip isogons

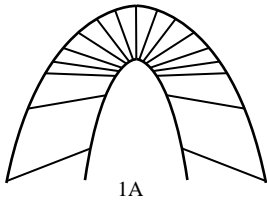
are lines that connect corresponding points on adjacent folded surfaces (Fig. 6.11b).

From the characteristics of the dip isogons structural geologists have defined three classes of folds (Fig. 6.12). Class 1 folds are those in which the dip isogons converge toward the core of the fold. Class 2 folds are those in which the dip isogons are parallel to the axial trace. And Class 3 folds are those in which the dip isogons diverge in the direction of the core of the fold. Class 1 folds may be subdivided further into class 1A (those with strongly convergent isogons), class 1B (those with moderately convergent isogons), and class 1C (those with weakly convergent isogons) (Fig. 6.12). Folds in which dip isogons are every-



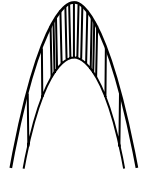
**Fig. 6.11** Construction of dip isogons. (a) Drawing tangents at a predetermined angle. (b) A dip isogon connects points where parallel tangent lines intersect points on adjacent folded surfaces.

## Class 1, convergent isogons

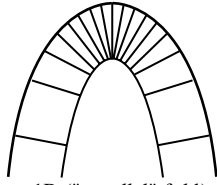


1A

## Class 2, parallel isogons

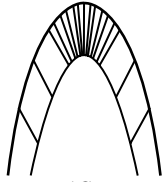
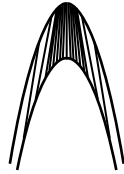


("similar" fold)



1B ("parallel" fold)

## Class 3, divergent isogons



1C

**Fig. 6.12** Classification of folds based on the characteristics of dip isogons. After Ramsay (1967).

where perpendicular to the bedding are classified as parallel folds (class 1B); folds in which dip isogons are parallel to *each other* are called similar folds (class 2). One drawback to the dip isogon method is that it does not work for kink folds (folds with planar limbs and sharp hinges), which are quite common.

It is important to keep in mind that different types of rock respond differently to fold-generating processes in the earth's crust. For this reason, two strata that are nested together in the same fold do not necessarily belong to the same fold class.

### Problem 6.2

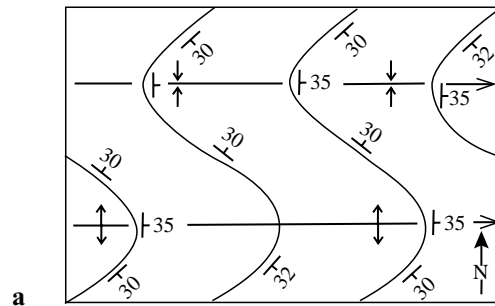
Figure G-13 is a sketch of the profile view of a set of folds exposed in the face of a cliff. First try to visualize the orientations of dip isogons on these folds. Then draw dip isogons at  $10^\circ$  intervals for each of the three layers. Indicate the fold class of each layer.

### Problem 6.3

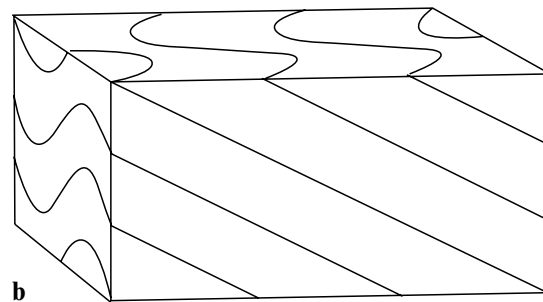
Figure G-14 contains photographs of four rock slabs. First, examine each photograph and try to visualize dip isogons on the folds. Write a description of the class or classes of folds you can visualize in each slab. Then tape a piece of tracing paper over the photographs, and outline at least two layers in each photo. Draw some dip isogons on each folded layer. Finally, for each slab, discuss any new insights you gained by drawing the isogons.

### Outcrop patterns of folds

Figures 6.13 and 6.14 show sets of folds in which the outcrop patterns are identical, but the folds plunge in opposite directions. Clearly, outcrop pattern alone is not sufficient to determine the orientation of a fold. The direction and amount of dip of the axial surface and plunge of the fold axis must also be determined. The outcrop pattern of beds in symmetric folds with vertical axial surfaces, such as those in Figs 6.13 and 6.14, are symmetric on opposite sides of the crestal and trough traces of

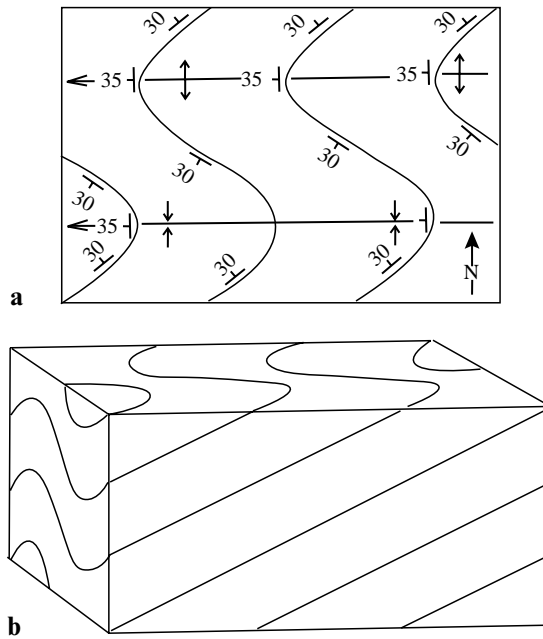


a

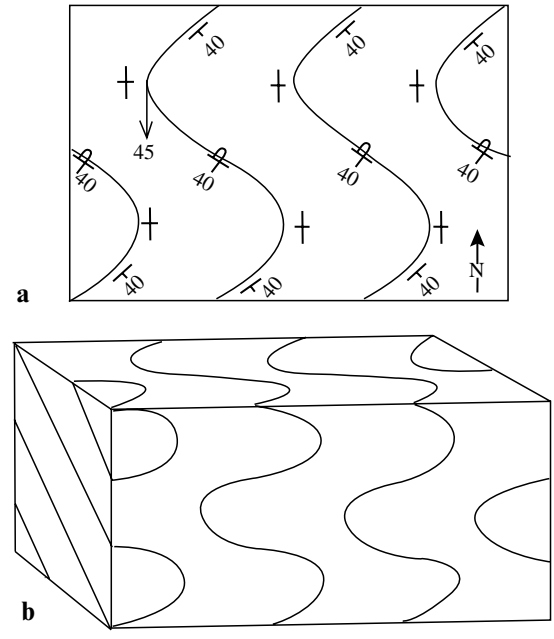


b

**Fig. 6.13** Eastward-plunging folds. (a) Map view. (b) Block diagram.



**Fig. 6.14** Westward-plunging folds. (a) Map view. (b) Block diagram.



**Fig. 6.15** Southward-plunging, overturned folds. (a) Map view. (b) Block diagram.

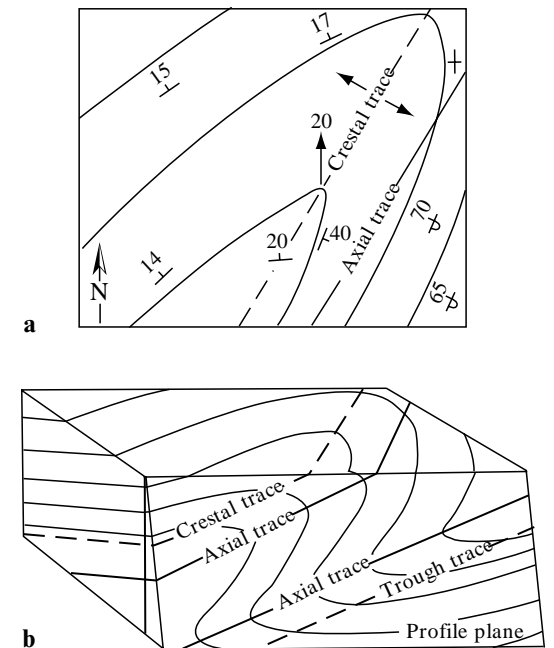
such folds are also axial traces, and the dip at the axial trace is equal to the plunge of the fold axis. The folds shown in Fig. 6.13 plunge  $35^\circ$  due east, and those in Fig. 6.14 plunge  $35^\circ$  due west.

Figure 6.15 shows an outcrop pattern identical to those in Figs 6.13 and 6.14, but here the folds are overturned, and they plunge  $45^\circ$  south. Fold a piece of paper and tilt it to simulate one of the folded layers in Fig. 6.15. Notice that these folds, and all overturned folds, contain vertical beds. The strike of vertical beds in overturned folds is parallel to the trend of the fold axis.

Because the folds in Fig. 6.15 have no unique high and low points, they have no crestal and trough traces. In most cases of plunging folds with tilted axial surfaces, the crestal and trough traces are not axial traces. Sometimes the crestal and trough traces are not even parallel to the axial traces.

Figure 6.16 shows a set of folds in which the axial surface dips northwest, the axis plunges  $20^\circ$  north, and the crestal and trough traces are clearly not axial traces. The axial traces of such folds can only be reliably located in the profile plane.

For any cylindrical fold, the dip of the bedding at the crestal or trough trace is the same as the



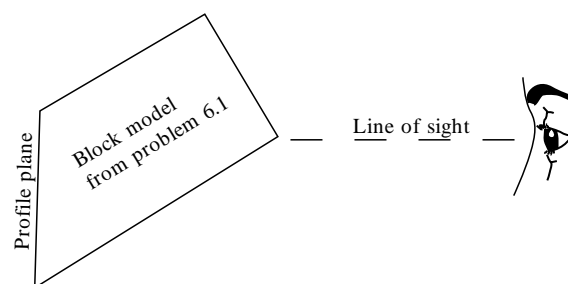
**Fig. 6.16** Example of folds in which the crestal and trough traces are not axial traces. (a) Map view. (b) Block diagram.

trend and plunge of the fold axis. So the crestal and trough traces are the easiest lines to draw on map outcrop patterns of folds.

### Problem 6.4

Figure G-15 contains five geologic maps, each of which contains folded strata. Fold a piece of paper to help you visualize each fold's shape and orientation, then draw crestal and/or trough traces on each map. Use the appropriate symbol (see Appendix F) to indicate the type of fold (syncline or anticline), and indicate the attitude of the fold axis.

Determine the trend and plunge of each fold axis and write these in the space provided below each map.



**Fig. 6.17** Illustration of the down-plunge viewing technique for obtaining a profile view of a fold.

### Down-plunge viewing

Features of folds are best examined in profile view, when your line of sight is parallel to the fold axis. This is apparent in the block model from Problem 6.1, which has an exposed profile plane. A profile plane need not be available, however, to obtain a profile view. Turn the block model around and look parallel to the axis but on the opposite side of the block from the profile plane (Fig. 6.17). The folds should appear the same as in the profile plane. This technique, in which you look “down the plunge” (or “up the plunge” in this case), is an effortless way to obtain a profile view of a fold even in irregular terrain. When you are working with a geologic map on which the trend and plunge of a fold are indicated, you merely place your eye so that your line of sight intersects the map at approximately the same angle as the plunge of the fold axis. Try it on the folds of the Bree Creek Quadrangle. A technique for constructing the profile view of a fold exposed in flat terrain is explained in Chapter 7 (see Fig. 7.6).

### Problem 6.5

Figure G-16 shows the sides and top of a block model of folded layered rocks. The surface with the north arrow represents a horizontal surface. Cut out the pattern, and fold it into a block. Look at the block from different angles until you see a set of cylindrical folds. At this point you are looking down-plunge. If you have trouble, try coloring one or more units.

- 1 Make a drawing of the block as it appears in the down-plunge view, showing the folds.
- 2 What is the approximate attitude of the axial surfaces?
- 3 What is the approximate attitude of the fold axis?
- 4 By comparing the folds with those in Fig. 6.12, determine the classes of folds in the block model and label each fold on your drawing accordingly.





## Stereographic Analysis of Folded Rocks

### Objectives

- Construct beta diagrams and pi diagrams of folds.
- Construct and interpret a contoured equal-area diagram of structural data.

Large-scale folds that are poorly exposed may be impossible to analyze using the techniques discussed in Chapter 6. In such cases, data from isolated outcrops may be combined and analyzed stereographically to characterize the geometry of a fold and the orientations of its elements. Stereographic analysis of the folded Paleogene rocks of the Bree Creek Quadrangle will serve as the major exercise in this chapter.

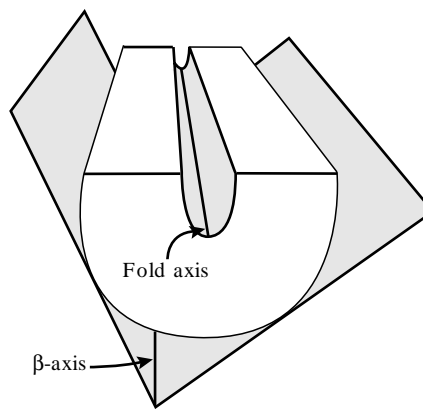
While the techniques described in this chapter will be applied specifically to the analysis of folds, stereographic analysis is also commonly used to study structures such as joints, faults, and cleavages at many scales.

### Beta ( $\beta$ ) diagrams

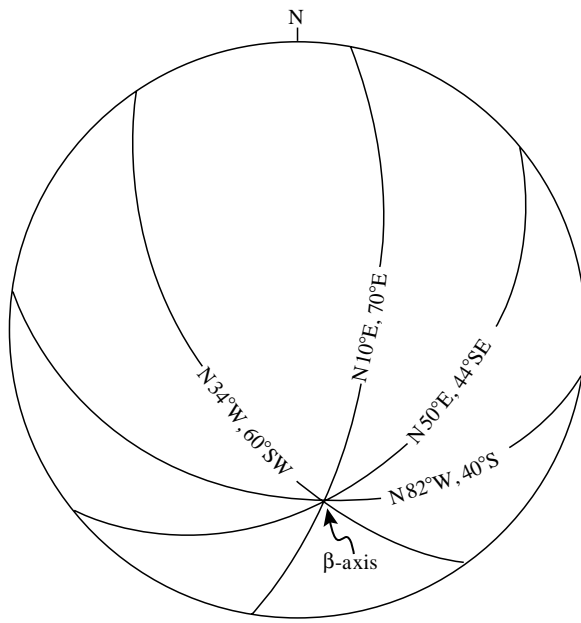
A simple method for determining the orientation of the axis of a cylindrical fold is to construct a  $\beta$ -diagram. Any two planes tangent to a folded surface intersect in a line that is parallel to the fold axis (Fig. 7.1). Such a line is called a  $\beta$ -axis. A  $\beta$ -axis is found by plotting the attitudes of bedding (or some other planar element) on an equal-area net; the  $\beta$ -axis is the intersection line of the planes, which plots as a point on the net.

Suppose, for example, that the following four foliation attitudes are measured at different places on a folded surface: N82°W, 40°S; N10°E, 70°E; N34°W, 60°SW; and N50°E, 44°SE. These attitudes are shown plotted on an equal-area net in Fig. 7.2. The  $\beta$ -axis, and therefore the fold axis, plunges 39°, S7°E.

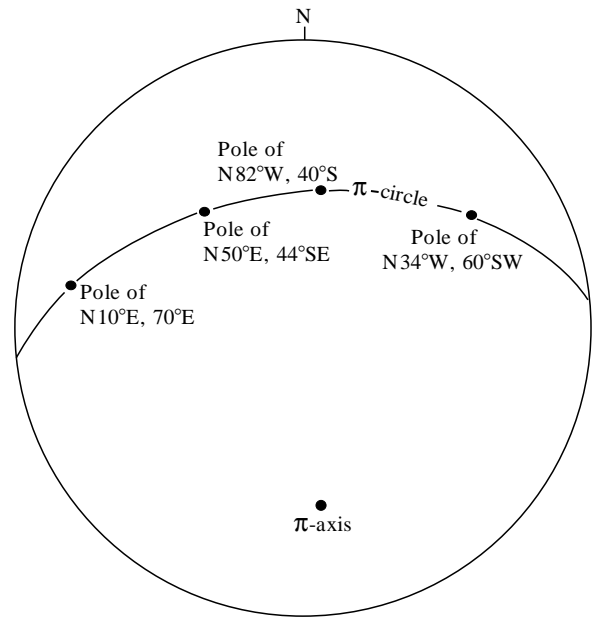
Few folds are perfectly cylindrical, so the great circles will rarely intersect perfectly, even if the



**Fig. 7.1** The  $\beta$ -axis is the intersection of planes tangent to a folded surface.



**Fig. 7.2** Beta diagram. The great circles represent four foliation attitudes of a cylindrical fold intersecting at the  $\beta$ -axis.



**Fig. 7.3** Pi diagram. The  $\pi$ -circle is the great circle common to the four poles of foliations of a cylindrical fold.

folds have a common history. When data from areas with different folding histories are plotted together, distinctively different  $\beta$ -axes will appear.

### Pi ( $\pi$ ) diagrams

A less tedious method of plotting large numbers of attitudes is to plot the poles of a folded surface on the equal-area net. Ideally, in a cylindrical fold these poles will lie on one great circle, called the  $\pi$ -circle. In reality, however, there may be considerable scatter in the distribution of poles and a best-fit  $\pi$ -circle will have to be chosen. The pole to the  $\pi$ -circle is the  $\pi$ -axis, which, like the  $\beta$ -axis, is parallel to the fold axis. Figure 7.3 shows the same four attitudes that were plotted on the  $\beta$ -diagram in Fig. 7.2, and the corresponding  $\pi$ -circle and  $\pi$ -axis. In most cases  $\pi$ -diagrams are more revealing, as well as more quickly constructed, than  $\beta$ -diagrams.

### Determining the orientation of the axial plane

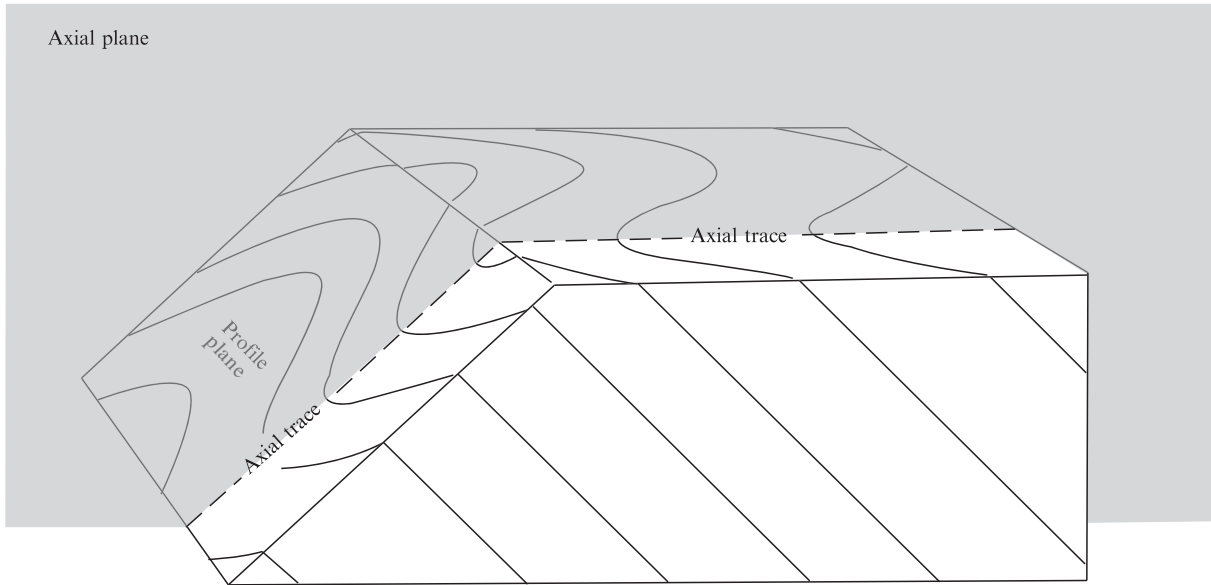
The orientation of a fold is defined not only by the trend and plunge of the fold axis, but also by the attitude of the axial plane. The axial plane can be thought of as a set of coplanar lines, one of which is the hinge line and another is the surface axial

trace (Fig. 7.4). If the axial trace can be located on a geologic map, and if the trend and plunge of the hinge line can be determined, then the orientation of the axial plane can easily be determined stereographically; it is the great circle that passes through the  $\pi$ -axis (or  $\beta$ -axis) and the two points on the primitive circle that represent the surface axial trace (Fig. 7.5).

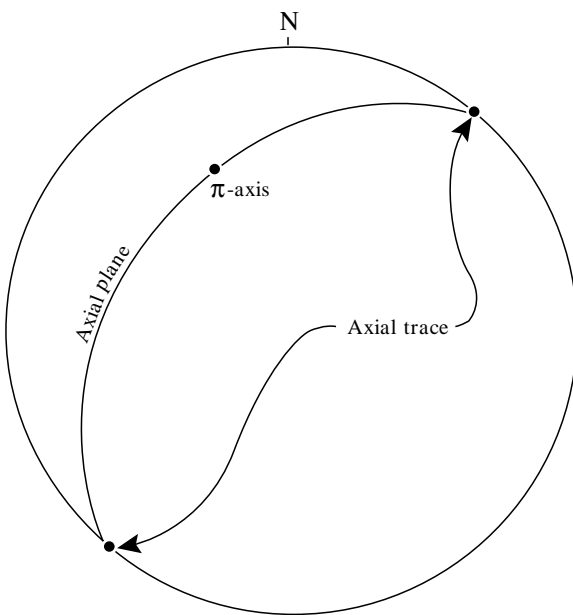
Often the surface axial trace cannot be reliably located on a geologic map. If the folds are well exposed, then a profile view can be constructed (as explained in the next section), and the axial trace can be located in the profile plane and transferred to the geologic map.

### Constructing the profile of a fold exposed in flat terrain

To find the orientation of the axial plane of a fold, it is very useful to know the orientation of the axial trace. This is most reliably located on a profile view of the fold. If the trend and plunge of the fold axis are known, and if the fold is well exposed in relatively flat terrain, then a profile view may be constructed quickly. Consider the fold shown in plan view in Fig. 7.6a. The profile view and surface axial trace are constructed as follows:



**Fig. 7.4** Block diagram of folds showing the profile plane, axial plane, and axial trace.



**Fig. 7.5** Equal-area net plot. The axial plane is the great circle common to the  $\pi$ -axis and the two points on the primitive circle that represent the axial trace.

- 1 Draw a square grid on the map with one axis of the grid parallel to the trend of the fold axis (Fig. 7.6b). The length of the sides of each square,  $d_s$  (surface distance), is any convenient arbitrary length, such as 1 or 10 cm.
- 2 When the surface distance  $d_s$  is projected on a profile plane it remains the same length in the

direction perpendicular to the trend of the fold axis. The sides parallel to the trend, however, will be shortened in the profile view (except in the case of a vertical fold). This is easily confirmed by viewing down-plunge in Fig. 7.6b. The shortened length parallel to the trend of the fold axis we will call  $d_p$  (profile distance). Length  $d_p$  may be determined trigonometrically with the following formula:

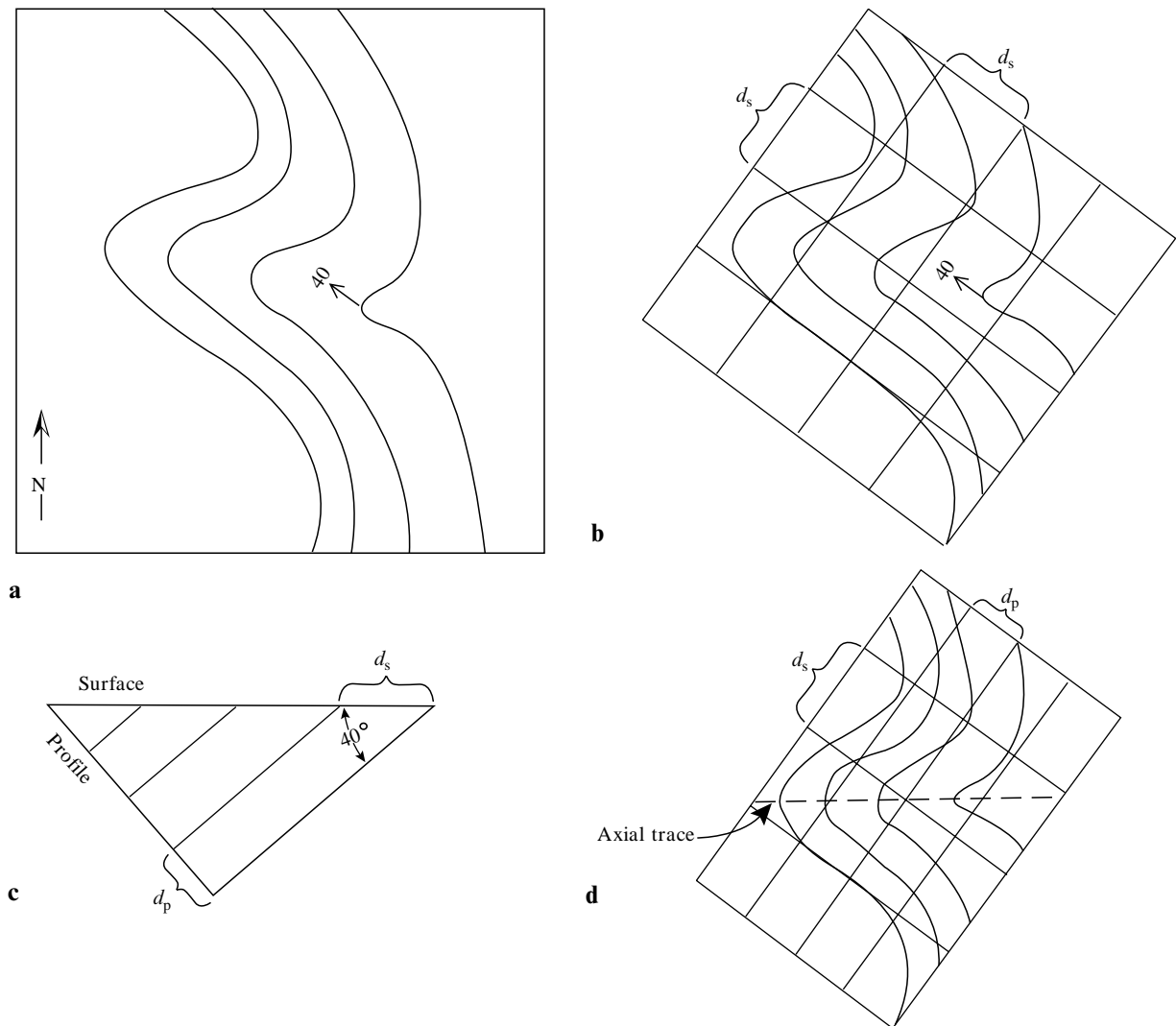
$$d_p = d_s \sin \text{plunge}$$

It can also be determined graphically, as shown in Fig. 7.6c.

- 3 With  $d_p$  now determined, a rectangular grid is drawn that represents the square grid projected onto the profile plane. Points on the square grid in the map view are then transferred to corresponding points on the rectangular grid. The profile view of the fold is then sketched freehand, using the transferred points for control (Fig. 7.6d).
- 4 The axial trace can now be drawn on the profile plane (Fig. 7.6d) and then transferred back to corresponding points on the square grid.

#### Simple equal-area diagrams of fold orientation

The orientation of a fold can be simply and clearly characterized by an equal-area diagram showing

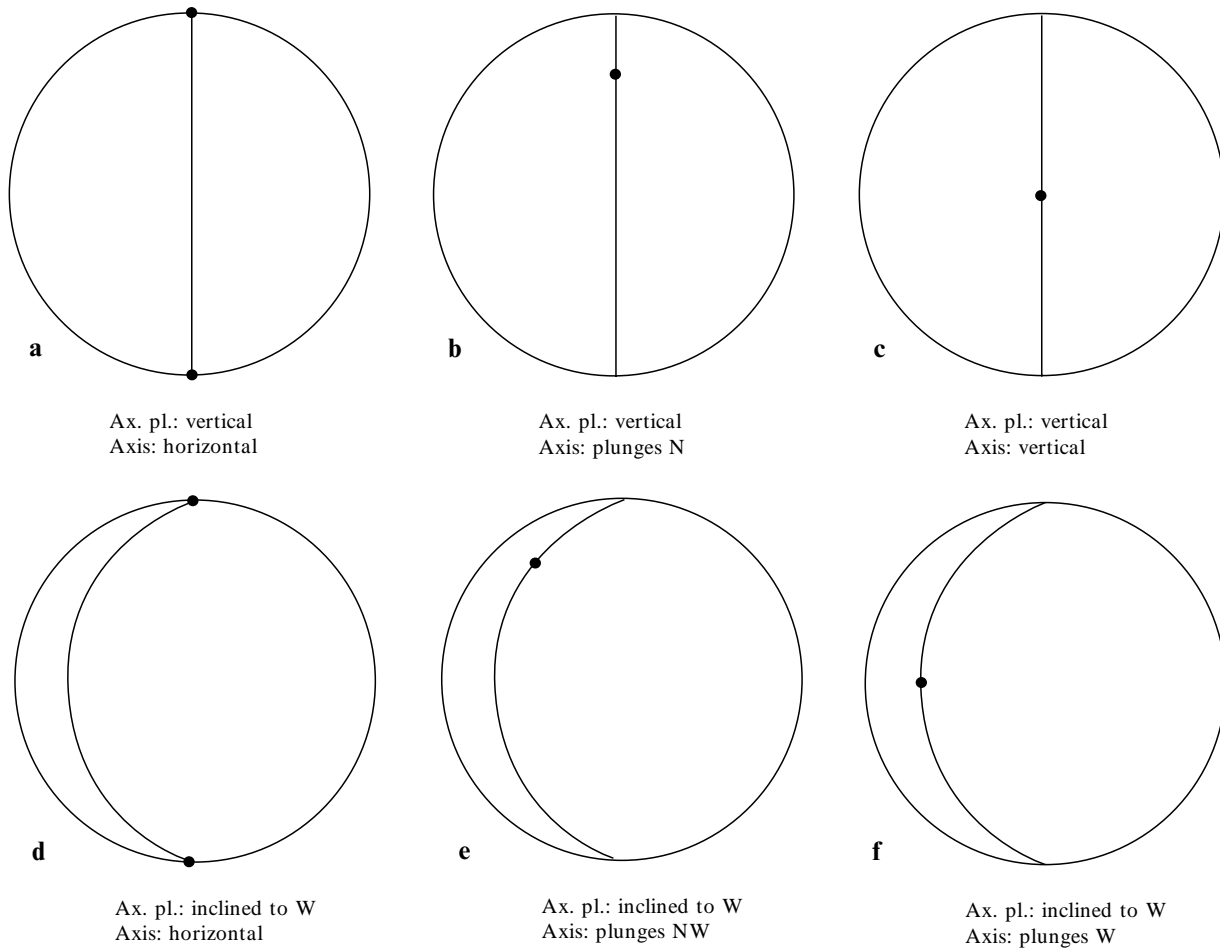


**Fig. 7.6** Method for constructing the profile view of a fold exposed in flat terrain. (a) Map view. (b) Square grid drawn on a map with one axis parallel to the trend of the fold axis. (c) Graphical relationship between the surface distance ( $d_s$ ) and profile distance ( $d_p$ ). (d) Profile view. The fold is drawn using grid intersections for control. The axial trace is drawn onto the fold.

the axial plane and fold axis. Examples of various folds are shown in Fig. 7.7. Picture in your mind's eye what each of these folds would look like. What characteristics of a fold are *not* displayed in such a diagram?

### Problem 7.1

- 1 On separate pieces of tracing paper construct a  $\beta$ -diagram and  $\pi$ -diagram for the folds in Figure G-17 (Appendix G). Determine the trend and plunge of the fold axis.
- 2 Construct a profile view as shown in Fig. 7.6, and draw surface axial traces on the plan view. Determine the strike of the axial plane.
- 3 Draw a simple equal-area diagram, such as those in Fig. 7.7, showing the orientation of these folds.
- 4 Succinctly but completely describe these folds. Include the attitude of the fold axis, attitude of the axial plane, interlimb angle, symmetry, and fold class.



**Fig. 7.7** Simple equal-area diagrams showing orientation of the folds. Ax. pl., axial plane.

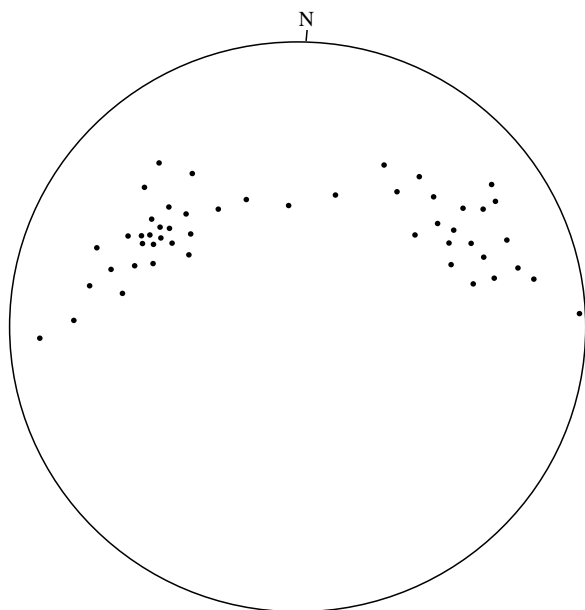
### Contour diagrams

In nature, folds are not exactly cylindrical, so commonly no single  $\beta$ -axis or  $\pi$ -axis emerges on the stereonet. However, if a large number of data are available the orientation of the hinge line may be statistically determined through the use of a contoured equal-area diagram.

Figure 7.8 is an equal-area diagram showing the poles to 50 bedding attitudes. Such a diagram is called a *point diagram* or *scatter diagram*. You could approximately locate a  $\pi$ -circle through the highest density of points, but contouring makes the results repeatable and reliable, as well as providing additional information.

There are computer programs that will quickly contour a set of data points in a scatter diagram, but it is instructive to do it by hand at least one time, to understand the process. Follow these instructions:

- 1 Cut out the center counter and peripheral counter in Fig. G-18 (Appendix G). Use a razor-blade knife to very carefully cut out the holes in the counters, and cut a slit in the peripheral counter as indicated. The holes in the counters are 1% of the area of the equal-area net provided with this book.
- 2 Remove the grid in Fig. G-19, and tape it to a piece of thin cardboard to increase its longevity. The distance between grid intervals is equal to the radius of the holes in the counters.
- 3 Tape the tracing paper containing the point diagram onto the grid such that the center of the point diagram lies on a grid intersection. Tape a second, clean piece of tracing paper over the point diagram. The two pieces of tracing paper should not move while you are counting points.
- 4 You are now ready to start counting points. This is done by placing the center counter on

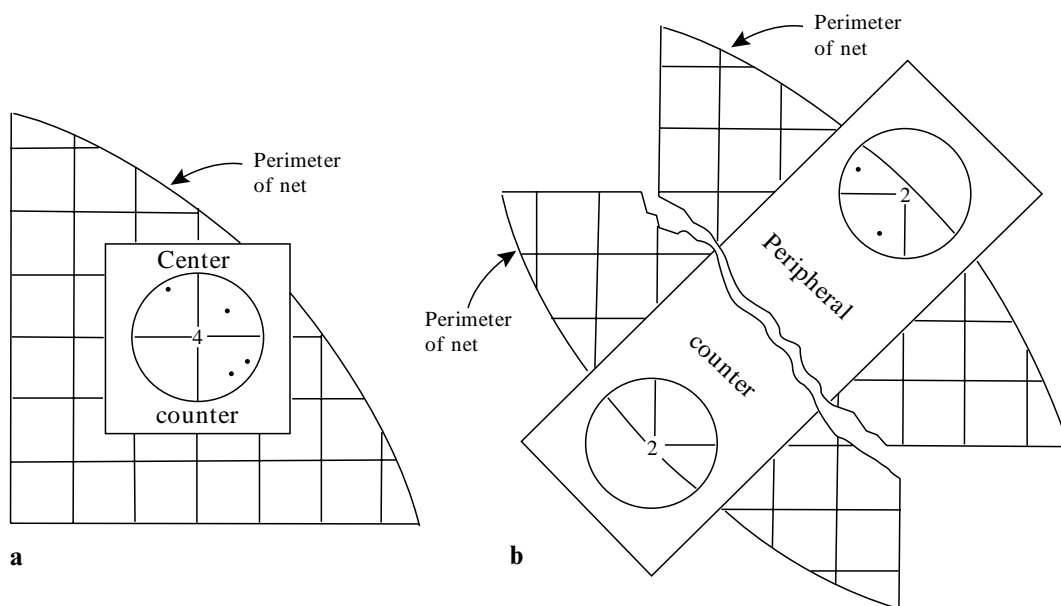


**Fig. 7.8** Point diagram with 50 attitudes plotted.

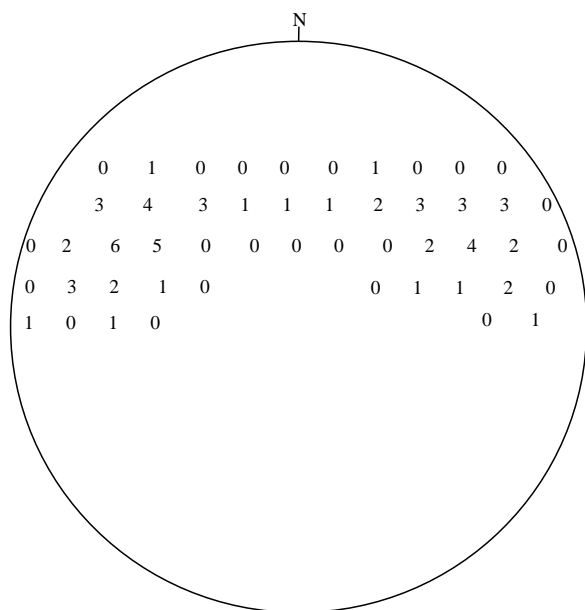
the point diagram such that the hole is centered on a grid intersection (Fig. 7.9a). Count the number of points within the circle, and write that number in the center of the circle on the clean sheet of tracing paper. Systematically move the counter from one grid intersection to the next, recording the number of points

within the 1% circle at each intersection. Each point will be counted more than once.

- 5 On the periphery of the point diagram, where part of the circle of the center counter lies outside the net, the peripheral counter is used (Fig. 7.9b). When the peripheral counter is used the points in both circles are counted, added together, and that number is written at the center of both circles. Figure 7.10 shows the results of counting the points in the point diagram in Fig. 7.8. Each number is a sample of 1% of the area of the point diagram.
- 6 The numbers are contoured as shown in Fig. 7.11a. The result is much like a topographic map, except that the contour lines separate point-density ranges rather than elevation ranges. In the interest of simplicity and clarity, some of the contours can be eliminated. Figure 7.11b shows contours 3 and 5 eliminated and varying shades of gray added. Fifty points were involved in this sample, so each point represents 2% of the total. The contours in Fig. 7.11b, therefore, represent densities of 2, 4, 8, and 12% per 1% area. The contour interval and total number of points represented ( $n$ ) are always indicated, either below the plot or in the figure caption (Fig. 7.11c).
- 7 The highest density regions on such a diagram are called the  $\pi$ -maxima. The great circle that



**Fig. 7.9** Technique for counting points for the purpose of contouring. (a) Use of center counter. (b) Use of peripheral counter. The total number of points in both circles is written at the center of both circles.



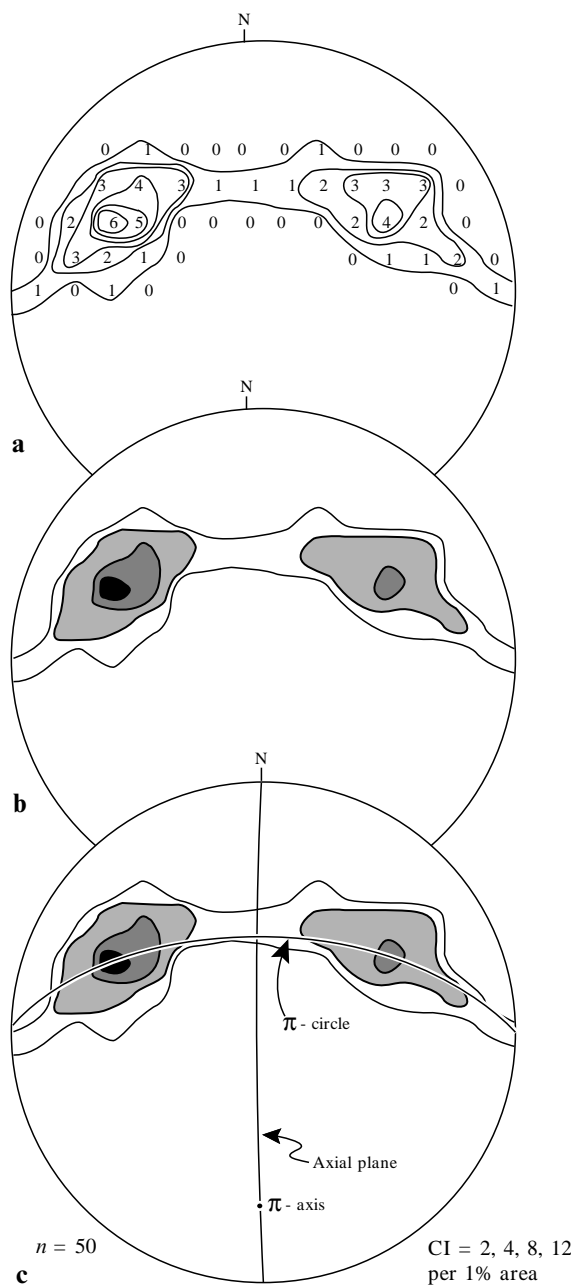
**Fig. 7.10** Results of counting the points in Fig. 7.8.

passes through them is the  $\pi$ -circle, and its pole is the  $\pi$ -axis (Fig. 7.11c). In the case of mildly folded, symmetric folds, the axial plane bisects the acute angle between the  $\pi$ -maxima, as shown in Fig. 7.11c. The attitude of the axial plane is most reliably determined from a combination of the  $\pi$ -axis attitude and the strike of the surface axial trace, the latter being determined by the technique shown in Fig. 7.6.

#### Determining the fold style and interlimb angle from contoured $\pi$ diagrams

In addition to providing a statistical  $\pi$ -axis, contoured  $\pi$ -diagrams indicate the style of folding and the interlimb angle. The band of contours across the diagram is referred to as the *girdle*, and the shape of the girdle reflects the shape of the folds. Figure 7.12a shows a profile and  $\pi$ -diagram of an extreme case of long limbs and narrow hinge zones. Figure 7.12c shows asymmetric folds whose eastward-dipping limbs are longer than the westward-dipping limbs. Figures 7.12b, d, and e are other examples of different styles of folding and their corresponding contoured  $\pi$ -diagrams.

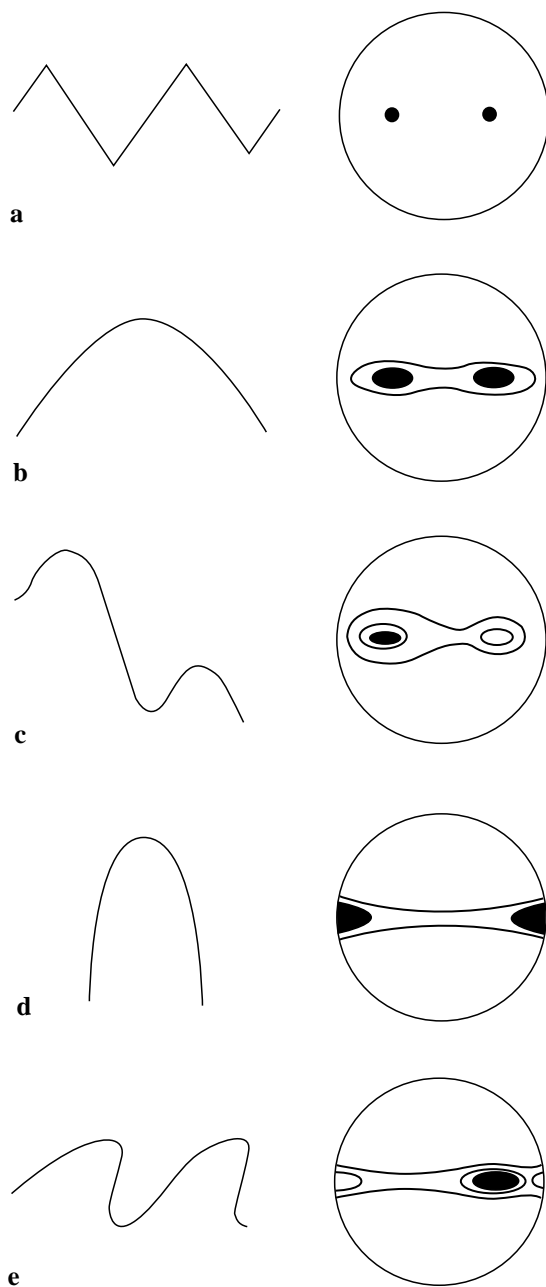
The interlimb angle of a fold can be measured between the two maxima along the  $\pi$ -circle dir-



**Fig. 7.11** Deriving the  $\pi$ -circle. (a) Contours drawn on a point grid. (b) Selected and shaded contours. (c) The  $\pi$ -axis and  $\pi$ -circle are determined from the contour diagram. The axial plane cannot be located with certainty without additional information. CI, contour interval.

ectly off the contoured  $\pi$ -diagram. For upright folds the interlimb angle is  $180^\circ$  minus the angle between the two maxima. For overturned folds the interlimb angle is simply the angle measured directly between the maxima.





**Fig. 7.12** Profiles and corresponding contoured  $\pi$ -diagrams of variously shaped folds (c, d, and e after Ragan, 1985).

### Problem 7.2

Three of the four fault blocks within the Bree Creek Quadrangle contain folded Paleogene rocks for which bedding attitudes are shown on the map. Complete the tasks listed below for each fault block. We suggest that this problem be completed by teams of three students, with each member of the team completing all the tasks for only one of the three fault blocks. Each member of the team should then make copies of his or her results so that each student on the team has data for all three of the fault blocks. These diagrams will be used in Chapter 11 for a structural synthesis of the Bree Creek Quadrangle.

- 1 Construct a contoured  $\pi$ -diagram of the folds involving Paleogene strata.
- 2 Using the technique shown in Fig. 7.6, construct a profile view of the folds.



**Wizard hint:** In the northeastern block, do not include the beds exposed on the Gollum Ridge fault scarp, because this technique can only be used in areas of low relief.

- 3 Draw dip isogons on your profile view and determine the class of each folded layer.
- 4 Describe the folds as succinctly and completely as possible. Your description should include the trend and plunge of the  $\pi$ -axis, attitude of the axial surface, interlimb angle, symmetry, class of folds, and age of folding.
- 5 Figure G-20 is a reference map of the Bree Creek Quadrangle with a circle on each of the three fault blocks involved in this problem. Sketch the contour diagram for each of the three fault blocks in the corresponding circle, similar to those in Fig. 7.11c. Draw the  $\pi$ -axis and axial plane on each circle. Such a reference map is an effective way of summarizing the orientation and geometry of folds in separate areas.

## Parasitic Folds, Axial-Planar Foliations, and Superposed Folds

### Objectives

- Use parasitic folds to locate the axial traces of major folds.
- Reconstruct the structural history of an area that underwent two generations of folding.

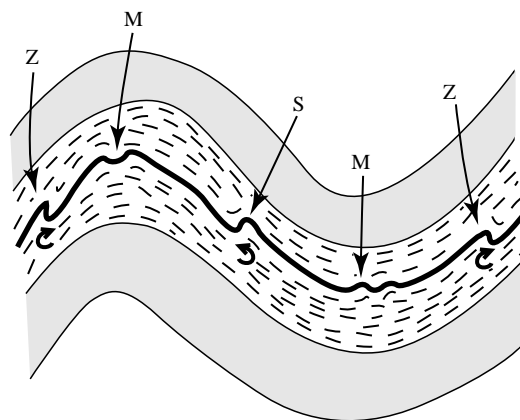
In this chapter you will learn to analyze and interpret folds within folds, refolded folds, and axial-planar foliations. The southeastern portion of the Bree Creek Quadrangle, which up to now has been ignored, will be analyzed as the major exercise in this chapter.

### Parasitic folds

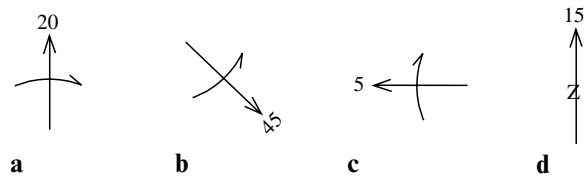
On the limbs and in the hinge zones of large folds one often finds small folds, the axes of which are parallel to the major fold axes. Such small folds are called *parasitic folds*. Parasitic folds that occur in the hinge zone of a larger fold are usually symmetric and are sometimes referred to as *M folds* because of their shape. Those that occur on the limbs of large folds are usually asymmetric and may be referred to as *Z folds* or *S folds*, depending on their shape in profile (Fig. 8.1). A fold that appears as a Z on a south-facing exposure will be an S on a north-facing exposure; however, it will exhibit a consistent sense of asymmetry or rotation with respect to the axial surface of the fold regardless of the view. Z folds record a clockwise sense of rotation and S folds a counterclockwise sense. S (counterclockwise) parasitic folds consistently

occur on the left limbs of synclines viewed in profile, and on the right limbs of anticlines. Z (clockwise) parasitic folds are found on the opposite limbs from S folds (Fig. 8.1).

Examples of map symbols commonly used to show the attitude of the axis and the sense of rotation of a parasitic fold are shown in Fig. 8.2. The straight arrow represents the trend of the fold axis, while the curved arrow shows the sense of



**Fig. 8.1** Types of parasitic folds. The arrows show the sense of rotation.



**Fig. 8.2** Examples of symbols representing variously oriented parasitic folds. North is at the top of the figure. (a) Axis plunges  $20^{\circ}\text{N}$ ; sense of rotation is clockwise. (b) Axis plunges  $45^{\circ}\text{SE}$ ; sense of rotation is counterclockwise. (c) Axis plunges  $5^{\circ}\text{W}$ ; sense of rotation is clockwise. (d) Axis of Z fold plunges  $15^{\circ}\text{N}$ .

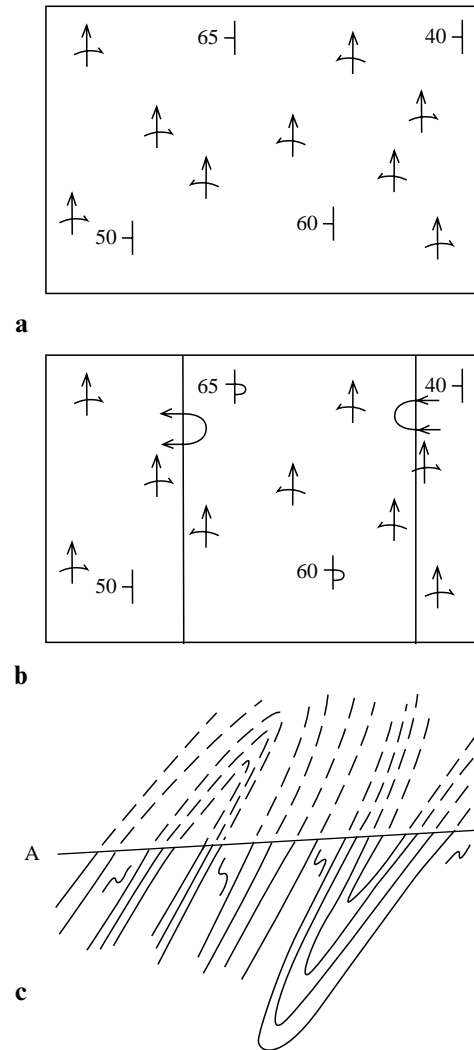
rotation of the parasitic fold as viewed down-plunge on the map or in the field. Alternatively, the actual down-plunge shape of the fold may be used as a map symbol (Fig. 8.2d).

In areas with tight or isoclinal folds that are poorly exposed, parasitic folds may allow the geologist to locate the position of the axial trace of a major fold that cannot be recognized any other way. Consider the map in Fig. 8.3a. Four bedding attitudes all show a westward dip. Without considering the parasitic folds, the structure appears to be a west-dipping homocline. However, the sense of rotation of the parasitic folds reveals the presence of an anticline and syncline and allows the axial traces to be approximately located (Fig. 8.3b). Note also that this analysis indicates that the dips on the shared limb of the two folds are overturned (Fig. 8.3b). The sense-of-rotation arrows point *toward* anticlinal axial traces and *away from* synclinal axial traces. Figure 8.3c is a structure section showing the two folds.

### Problem 8.1

Figure G-21 (Appendix G) contains an oblique view of a small map area showing several outcrops, some with parasitic folds. Each outcrop on the oblique view is represented on the map view (Fig. G-21b) by either a strike-and-dip symbol or a trend-and-plunge symbol. The black layers represent thin limestone beds that are interbedded with shale and sandstone. The limestone bed at one outcrop is not necessarily the same bed as at another outcrop.

- 1 Using small, curved arrows, as in Fig. 8.3, indicate on the map view (Fig. G-21b) the sense of rotation of each parasitic fold.
- 2 Draw the axial traces of the major folds on the map.
- 3 Sketch the structure section A–A' in Fig. G-21c, schematically showing parasitic folds.



**Fig. 8.3** Attitudes of beds and parasitic folds. (a) Map view. (b) Same map with axial traces of the overturned anticline and overturned syncline approximately located. (c) Structure section with the parasitic folds shown schematically.

### Axial-planar foliations

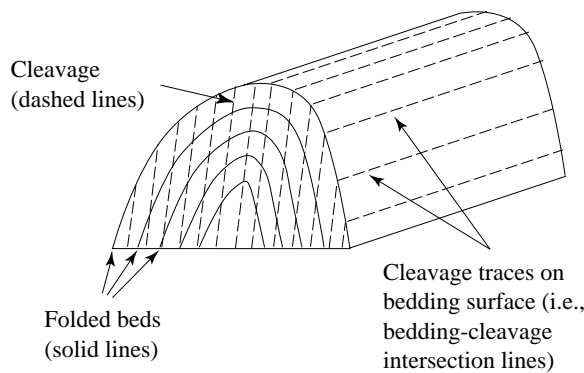
In areas of tight folding, particularly in low- to intermediate-grade metamorphic rocks, a pervasive cleavage or foliation may develop approximately parallel to the axial surface of regional folds. Examine the photograph in Fig. 8.4 closely for an example of axial-planar cleavage.

Although such a fabric may be the most conspicuous planar feature within the rock, it should not be confused with bedding. In many cases, bedding can be recognized in strongly cleaved rocks by looking for distinct bands in the rock.



**Fig. 8.4** Map view of folded interbedded limestone and slate. Note axial-planar cleavage, which is oriented parallel to the axial surfaces of the folds. Rock hammer for scale.

These bands may reflect original differences in composition or texture (i.e., bedding) or the sedimentary protolith. If bedding and cleavage are oblique to one another, the relative orientation of these two planar features may be used to infer



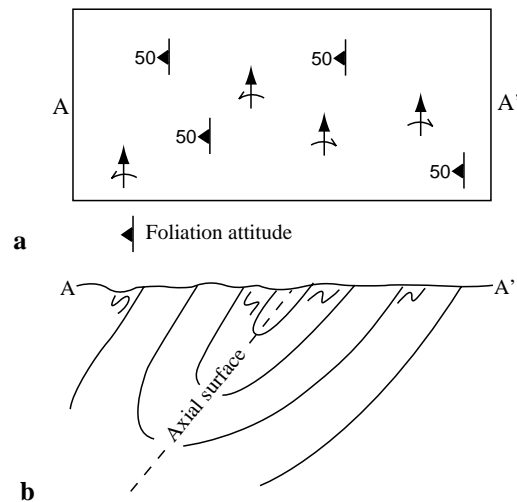
**Fig. 8.5** Antiform showing bedding–cleavage relationships. See text for discussion.

the locations of axial traces of macroscopic folds that may not otherwise be evident in areas of incomplete exposure.

Figure 8.5 shows the relation between bedding and cleavage in an upright antiform. Refer to this figure to help you visualize the following four relations that can be used to provide information about large-scale, regional folds:

- 1 Cleavage dips more steeply than bedding (except on an overturned fold limb). Sketch this, to convince yourself.
- 2 In the hinge area of a fold, the angle between the cleavage and bedding is  $90^\circ$ .
- 3 The tighter the fold, the smaller the angle between the cleavage and bedding.
- 4 Because the cleavage is parallel (or nearly so) to the axial surface of the fold, the orientation of the cleavage can be used to directly infer the orientation of the axial surface.

In nature, differences in rock properties can cause local deviations in the orientation of cleavage surfaces. It is therefore important to acquire cleavage orientation data from different rock units over a relatively large area when using cleavage to infer fold geometry and orientation. Figure 8.6a is a geologic map in which parasitic folds reveal the presence of a syncline; the axial-planar cleavages (or foliations) allow the attitude of the axial surface to be determined (Fig. 8.6b).



**Fig. 8.6** Axial-planar foliations (cleavage). (a) Map showing attitudes of foliations and parasitic folds. (b) Structure section A–A'.

**Problem 8.2**

Figure G-22 is a photograph of an outcrop in the Transantarctic Range of Antarctica. The view shows a cross section of beds of coarse conglomerate and finer-grained conglomerate. The arrow points to an ice axe for scale. Due to the snow and ice, exposures in the area are limited, and the geologist must glean as much information as possible from available outcrops. Place a sheet of tracing paper over the photo. Draw and label the bedding and the cleavage. If these beds represent the limb of an upright fold, would the hinge area of the antiform be to the right or to the left? Explain your answer, and illustrate your explanation with a simple sketch showing the antiform, the cleavage, and the position of this exposure within the antiform.

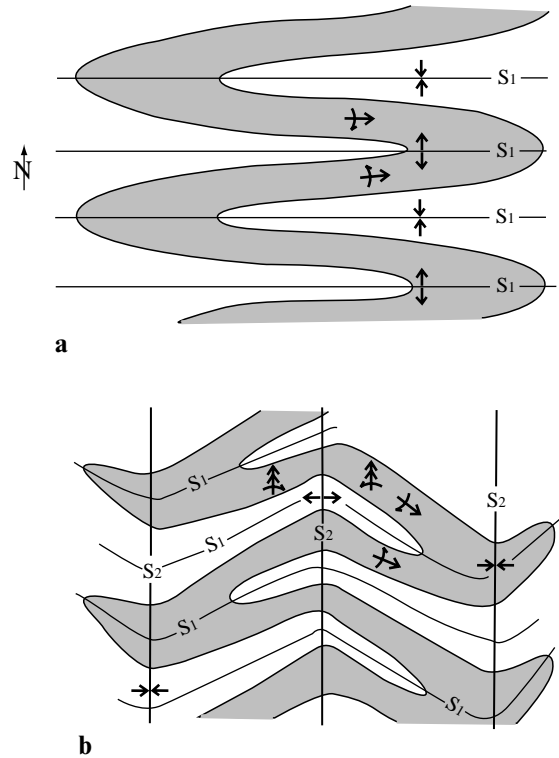
**Problem 8.3**

Figure G-23 contains a geologic map that shows both the bedding and cleavage attitudes. Using the cleavage–bedding relations discussed above, sketch a cross section of the map area showing the form of the folds. There are no contacts between the rock units shown on the map; show the geometry of the folds schematically by sketching the form lines of hypothetical bedding surfaces, as is done in Fig. 8.6.

**Wizard hint:** *Some of the beds are overturned, but the geologist who measured them in the field could not identify which were overturned and which were not. Use relation number 1 above to identify the outcrops where the beds are overturned, and alter the strike-and-dip symbols accordingly.*

**Superposed folds**

A region that has experienced more than one episode of deformation may show complex fold interference patterns in the field and on a geologic map. Consider the simple case shown in Fig. 8.7. The first generation of folding,  $F_1$ , produced folds with east–west-striking axial surfaces (Fig. 8.7a). The second generation of folding,  $F_2$ , produced folds with north–south-striking axial surfaces (Fig. 8.7b). It is clear that the east–west axial



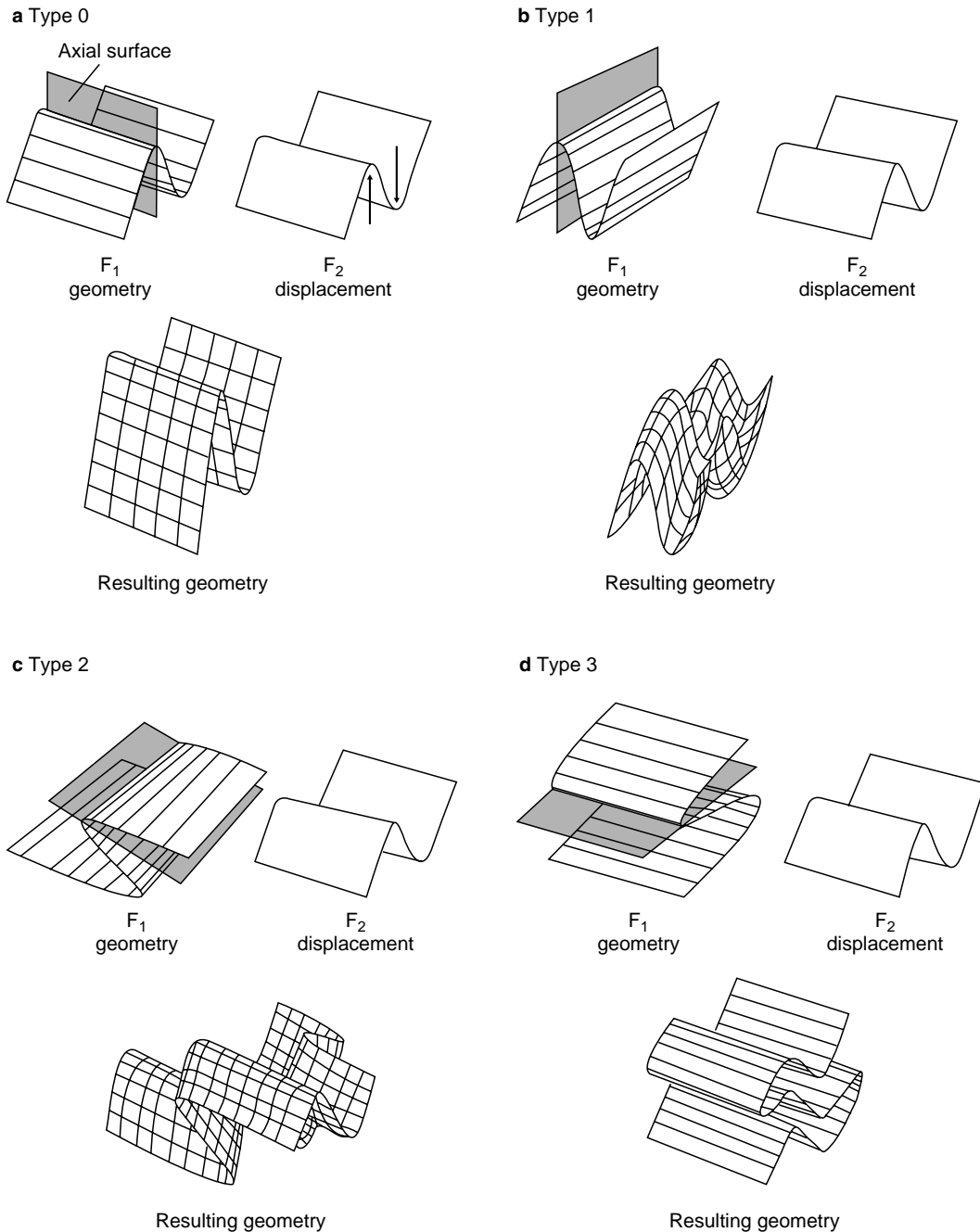
**Fig. 8.7** Superposition of folding (map view). (a) First generation of folding ( $F_1$ ).  $S_1$  is the axial-surface trace of the  $F_1$  folds; the symbols show the  $F_1$  parasitic folds. (b) Map pattern after two generations of folding ( $F_1$  and  $F_2$ ).  $S_2$  is the axial-surface trace of the  $F_2$  folds, and double-headed arrows denote  $F_2$  parasitic folds.

surfaces,  $S_1$ , developed before the north–south axial surfaces,  $S_2$ , because the  $S_1$  traces have been folded while the  $S_2$  traces are straight.

Various fold interference patterns can occur, depending on the initial orientation of the  $F_1$  fold hinge and its axial surface relative to the  $F_2$  fold. Figure 8.8 shows the four basic patterns that result from fold superposition. In each case the  $F_2$  fold has a vertical axial surface and a horizontal hinge line. In a type 0 interference pattern (Fig. 8.8a), both fold generations have parallel hinge lines and axial surfaces. Type 0 is so named because this type of superposed folding does not produce a recognizable interference pattern in the field; from the fold geometry alone, you would not know that two episodes of folding had occurred. Type 1 involves two sets of upright folds; the  $F_1$  hinge lines and axial surfaces are perpendicular to the  $F_2$  hinge lines and axial surfaces, resulting in a dome-and-basin (sometimes called “egg-carton”) interference pattern (Fig. 8.8b). In type 2 interference folding, the  $F_1$  folds have subhorizontal axial

surfaces (recumbent folds); the  $F_2$  hinge lines are oriented perpendicular to the  $F_1$  hinge lines. This type of fold superposition results in complex mushroom-shaped and boomerang-shaped map

patterns (Fig. 8.8c). In type 3 interference folding, the  $F_1$  folds are also recumbent; however, in this case the  $F_2$  hinge lines are parallel to the  $F_1$  hinge lines (Fig. 8.8d).



**Fig. 8.8** Four basic patterns resulting from the superposition of folds. In each case the orientation of the  $F_2$  fold is the same, superimposed on variously oriented  $F_1$  folds. After Ramsey (1967).

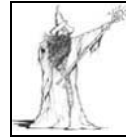
**Problem 8.4**

Figure G-24 is a photograph of a slabbed rock that experienced two generations of folding. Compare this photograph with the patterns shown in Fig. 8.8; indicate which type of interference pattern is present in the space provided. Place a sheet of tracing paper over the photograph, lightly outline the slab, and then draw and label the  $S_1$  and  $S_2$  axial-surface traces.

**Problem 8.5**

In the southeastern fault block of the Bree Creek Quadrangle, Paleozoic rocks have experienced two episodes of folding,  $F_1$  and  $F_2$ . The foliations shown on the Bree Creek map are axial planar.  $F_1$  parasitic folds are indicated by the symbol with a single-headed arrow, and  $F_2$  parasitic folds are indicated by the symbol with a double-headed arrow.

- 1 On your Bree Creek Quadrangle map draw the axial-surface traces,  $S_1$  and  $S_2$ , for both generations of folds, as is done in Fig. 8.7, using the parasitic folds to help you locate them. Use appropriate symbols to indicate synclines and anticlines.
- 2 Draw structure sections C–C' and D–D', using the axial-planar foliations to help you determine the attitudes of the axial planes of the folds.



**Wizard hint: Structure section D–D' is simpler than C–C'; draw the simpler one first.**

Because structure sections C–C' and D–D' are intersecting vertical planes, they have a common vertical line. Draw this vertical line on both structure sections and label it "Intersection of C–C' and D–D'." The depth from the surface to the top and bottom of each rock unit must be the same along this vertical line on both structure sections, as if you had cored down at this spot on your Bree Creek map and shown the data from the core on both structure sections. After you have drawn structure section D–D', the depth and thickness of each rock unit on this line of intersection can be transferred to your C–C' topographic profile, thereby providing stratigraphic control for your C–C' structure section.

- 3 Completely and succinctly describe each generation of folding. Include attitudes of the fold axes, attitudes of the axial surfaces, interlimb angles, symmetry, fold class (see Chapter 6), age of folding, and type of interference pattern.





### Objectives

- Measure slip.
- Measure rotational slip.
- Describe geometry, sense of slip, and age of faults.
- Reconstruct the history of faulting from outcrop patterns on a geologic map.

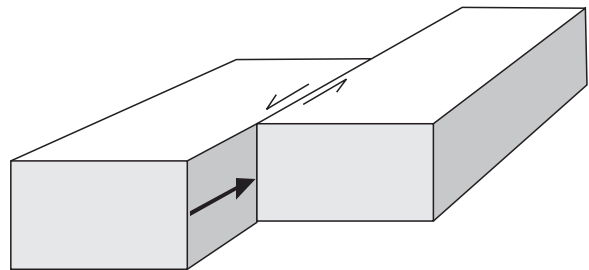
A fault is a fracture along which movement has occurred parallel to the fracture surface. Sometimes there is a single discrete fault surface, or *fault plane*, but often movements take place on numerous sub-parallel surfaces resulting in a *fault zone* of fractured rock. The San Andreas fault in California, for example, in most places has a single, recently-active fault plane lying within a highly sheared fault zone that is tens to hundreds of meters wide.

Some faults are only a few centimeters long, while others are hundreds of kilometers long. On geologic maps it is usually impossible to show every fault. Only those faults that affect the outcrop pattern of two or more map units are usually shown. The scale of the map determines which faults can be shown.

Below are some terms used to describe faults and their movements.

**Slip vector** The displacement of originally adjacent points, called *piercing points*, on opposite sides of the fault.

**Strike-slip fault** A fault in which movement is parallel to the strike of the fault plane (Fig. 9.1). Strike-slip faults are sometimes called



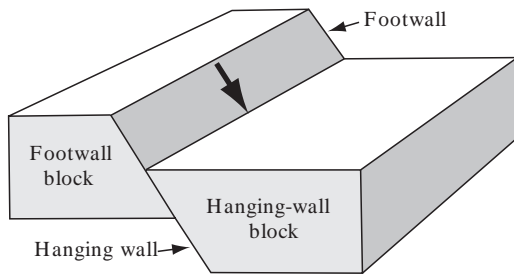
**Fig. 9.1** Block diagram showing a left-lateral strike-slip fault. The bold arrow shows the slip vector.

*wrench* faults, *tear* faults, or *transcurrent* faults.

A right-lateral (dextral) strike-slip fault is one in which the rocks on one fault block appear to have moved to the right when viewed from the other fault block. A left-lateral (sinistral) strike-slip fault, shown in Fig. 9.1, displays the opposite sense of displacement.

**Dip-slip fault** A fault in which movement is parallel to the dip of the fault plane (Fig. 9.2).

**Oblique-slip fault** A fault in which movement is parallel to neither the dip nor the strike of the fault plane.



**Fig. 9.2** Block diagram showing a dip-slip fault. This is a normal fault because the hanging-wall block has moved down relative to the footwall block. The bold arrow shows the slip vector.

**Hanging-wall block** The fault block that overlies an inclined fault (Fig. 9.2).

**Footwall block** The fault block that underlies an inclined fault (Fig. 9.2).

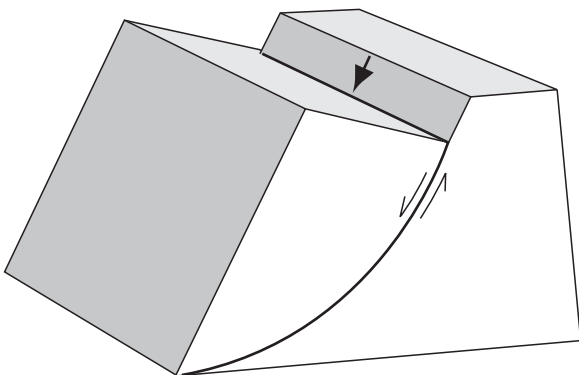
**Normal fault** A dip-slip fault in which the hanging wall has moved down relative to the footwall (Fig. 9.2).

**Reverse fault** A dip-slip fault in which the hanging wall has moved up relative to the footwall.

**Thrust fault** A low-angle reverse fault, typically dipping less than  $30^\circ$ .

**Décollement or detachment fault** A regionally extensive, low-angle or subhorizontal fault that typically separates upper- and lower-plate rocks with different structural characteristics. Both terms imply decoupling between the upper and lower plates. The term *detachment fault* is commonly, but not exclusively, applied to major low-angle normal faults.

**Listric fault** A fault shaped like a snow-shovel blade, steeply dipping in its upper portions and becoming progressively less steep with depth (Fig. 9.3).



**Fig. 9.3** Block diagram showing a listric fault. The bold arrow shows the slip vector.

**Translational fault** One in which no rotation occurs during movement, so that originally parallel planes on opposite sides of the fault remain parallel (Figs 9.1 and 9.2).

**Rotational fault** One in which one fault block rotates relative to the other (Fig. 9.4).

**Scissor fault** A fault in which one fault block rotates relative to the other along a rotational axis that is perpendicular to the fault surface. The sense of displacement is reversed across a point of zero slip, and the amount of displacement increases away from this point (Fig. 9.4).

**Slickensides** A thin film of polished mineralized material that develops on some fault planes. Slickensides contain striations parallel to the direction of latest movement. Often it is not possible to tell from slickenside lineations alone in which of two possible directions movement actually occurred.

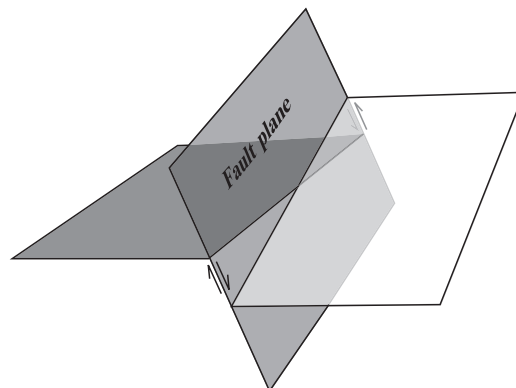
**Slickenlines** Slickenside lineations (see above).

**Fault trace** Exposure of the fault plane on the earth's surface.

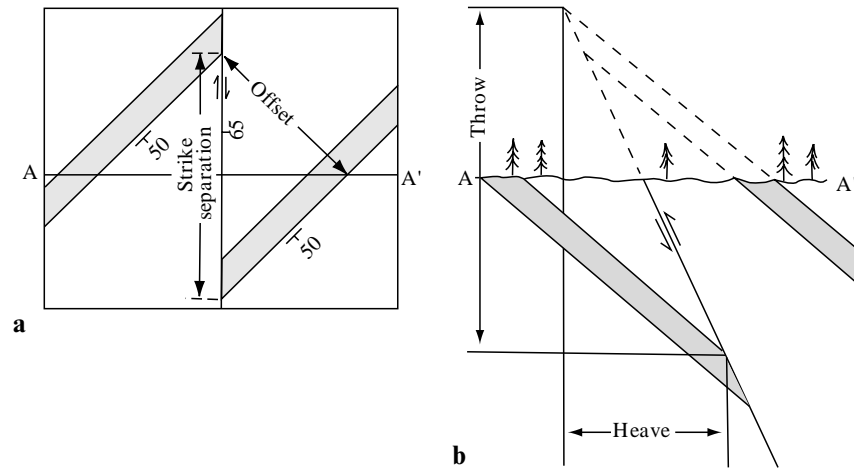
**Offset** Horizontal separation of a stratigraphic horizon measured perpendicular to the strike of the horizon (Fig. 9.5a).

**Strike separation** Horizontal distance parallel to the strike of the fault between a stratigraphic horizon on one side of the fault and the same horizon on the other side. Strike separation may be described as having either a right-lateral (dextral) or left-lateral (sinistral) sense of displacement (Fig. 9.5a).

**Dip separation** Horizontal (heave) and vertical (throw) distance between a stratigraphic horizon on one side of the fault and the same horizon on the other side as seen in a vertical cross section drawn perpendicular to the fault plane



**Fig. 9.4** Block diagram showing a rotational fault. This is a scissor fault because there is a reversed sense of displacement across a point of zero slip.



**Fig. 9.5** (a) Geologic map showing the difference between offset and strike separation. (b) Vertical structure section showing the heave and throw components of dip separation.

(Fig. 9.5b). Dip separation has either a normal or reverse sense of displacement.

Notice that the term separation is concerned with the *apparent* displacement of some reference horizon, and the terms right-lateral, left-lateral, normal, and reverse are used to describe the separation, whether or not the actual direction of movement is known. Similarly, arrows are often drawn along faults on geologic maps to indicate the sense of strike separation, even on faults with no history of strike-slip movement. More often than not, the actual slip path of a fault cannot be determined. When describing faults it is important to distinguish clearly between separation and slip.

### Measuring slip

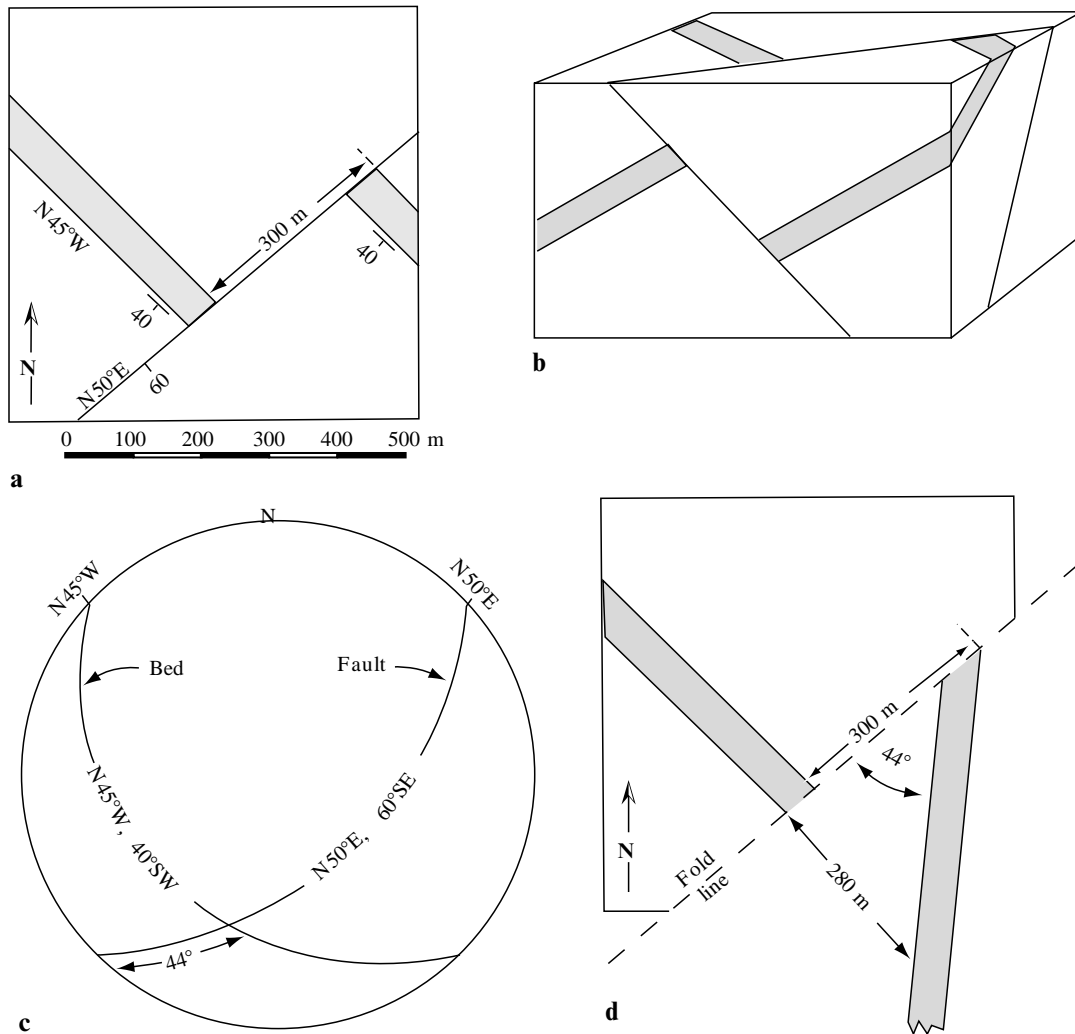
Of fundamental importance in the study of faults is the distance that two originally contiguous points have been separated. This displacement is called *slip*. Slip is a vector, having both magnitude and direction. To measure slip on a fault, the geologist must either: (1) determine the slip direction, or (2) identify two originally contiguous points that have been displaced by movement on the fault. In the ideal situation, two intersecting planes, such as a dike and a bed, are located on both fault blocks. The points of intersection on the hanging wall and footwall serve as piercing points. Unfortunately, one rarely finds such a happy situation in the field. More commonly, the structural geologist must use a single distinctive bed,

together with slickenside lineations, to estimate slip. The danger here is that the slickenside lineations may indicate the orientation of only the latest movement. Some faults have complex slip paths that cannot be reconstructed from slickenside lineations.

Figure 9.6a is a geologic map showing the trace of a fault plane (N50°E, 60°SE) and a bed (N45°W, 40°SW) with 300 m of strike separation. Figure 9.6b is a block diagram of the situation. Without further information it is impossible to know if this fault is a left-lateral strike-slip fault, a normal fault, or an oblique-slip fault. It would also be impossible to determine the slip. The relative sense of offset may be easily visualized by the down-plunge viewing method described in Chapter 6. Orient Fig. 9.6a so that your line of sight is directly down the plunge of the line of intersection of the fault and the layers on one of the fault blocks. In this orientation, the left or east block (hanging wall) can be seen to have moved down relative to the right or west block (footwall), but this does not reveal the actual slip path.

Let us assume that the fault in Fig. 9.6a is a normal fault, as indicated by slickenside lineations on the fault plane. The slip is determined as follows:

- 1 On an equal-area net, draw the great circles that represent the fault plane and the plane that is offset (Fig. 9.6c).
- 2 Find the pitch of the offset plane in the fault plane (Fig. 9.6c). In this example the pitch is 44°.
- 3 Place a piece of tracing paper over the map. Draw the fault trace on the map view, and draw the offset layer on the *upthrown* block.



**Fig. 9.6** Diagrams showing the solution of a slip problem. (a) Geologic map. (b) Block diagram. (c) Equal-area plot of the fault plane and bedding plane. (d) Orthographic projection of the fault plane showing the pitch of bedding. The slip is 280 m in the same direction as the dip (direction indicated by slickenside lineations).

Mark the place where the offset layer on the downthrown block intersects the fault, but do not draw it in (Fig. 9.6d).

- 4 The fault trace on your tracing paper is now considered to be a fold line, and the fault plane is imagined to be folded up into the horizontal plane. We know that the pitch of the offset bed in the fault plane is  $44^\circ$ . With the fault plane now horizontal, we can draw this  $44^\circ$  angle on the tracing paper, showing what the offset layer looks like in the fault plane (Fig. 9.6d).
- 5 If we know the pitch of the slip direction within the fault plane we can now measure the amount of slip. Because we know that this is a normal

fault, the slip direction is  $90^\circ$  from the fault trace in the fault plane, that is, directly down-dip. The amount of slip in this example is 280 m (Fig. 9.6d). The direction of slip is the same as the dip of the fault plane,  $60^\circ$ ,  $S40^\circ E$ .

**Problem 9.1**

Figure 9.7 shows the trace of a fault ( $330^\circ$ ,  $50^\circ SW$ ) and a dike ( $040^\circ$ ,  $35^\circ SE$ ) with 450 m of strike separation. Assume that this is a normal fault. What is the amount of slip?

### Problem 9.2

Measure the slip in Problem 9.1 if slickenside lineations trend northwest and have a pitch of  $60^\circ$ .

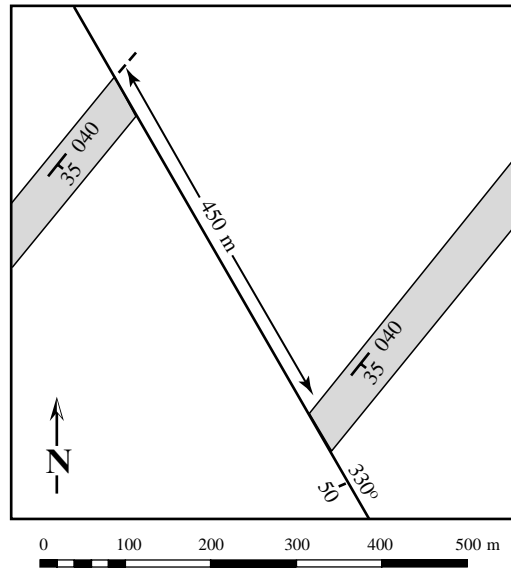


Fig. 9.7 Geologic map for use in Problem 9.1.

### Rotational (scissor) faulting

In Fig. 9.7 the beds on opposite sides of the fault have identical attitudes, indicating that all of the movement was translational. Fault movement often has a rotational component as well, which can be measured. We consider here only the case of planar bedding and the type of rotational faulting in which the rotational axis is oriented perpendicular to the fault plane. Look at the example in Fig. 9.8a. Obviously some rotation has occurred on the fault because the beds have different attitudes on the two fault blocks. The hanging wall has rotated counterclockwise relative to the footwall. (The sense of movement on rotational faults, as on strike-slip faults, is determined by imagining yourself on one fault block looking across the fault at the other fault block.)

Before we determine how much rotation has occurred in this example it will be instructive to

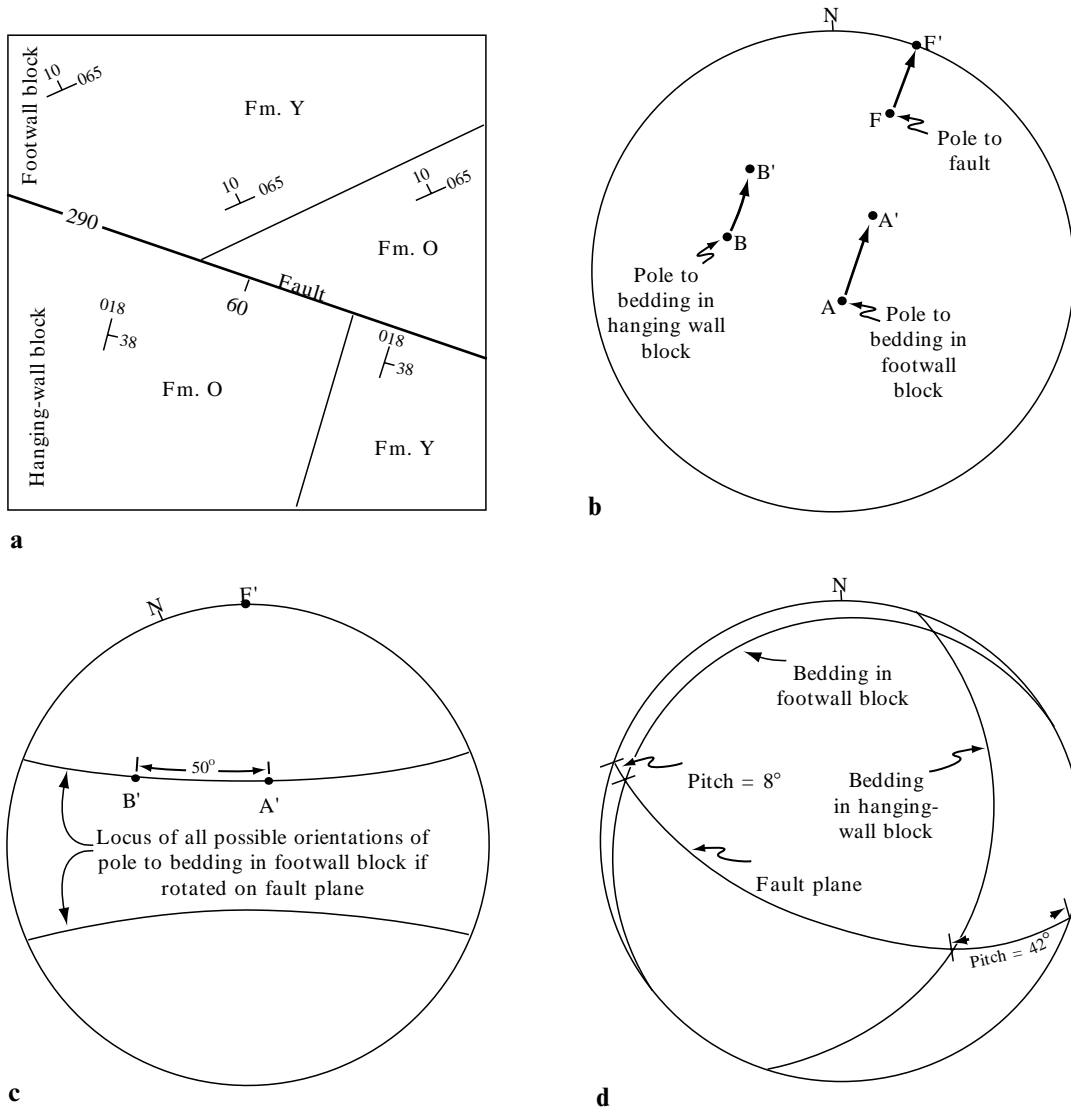
examine the range of possible attitudes that rotation on this fault could produce. This can be done as follows:

- 1 Plot the pole of the fault (point F) and the poles of the bedding in the footwall block (point A) and in the hanging-wall block (point B) on the equal-area net (Fig. 9.8b).
- 2 We now need to orient the fault so that it is vertical, so we move point F  $30^\circ$  to point F' on the primitive circle. Points A and B move  $30^\circ$  to points A' and B' (Fig. 9.8b). (You may want to review the procedure for rotating lines on the equal-area net in Chapter 5.)
- 3 During rotational faulting the axis of rotation is perpendicular to the fault plane. Look at the geologic map (Fig. 9.8a) again and imagine rotating the fault from its  $60^\circ$ S dip into a vertical position. Use your left hand to represent the fault and your right hand to represent the bedding in the footwall. Stick a pencil through the fingers of your right hand to represent the pole to bedding. Now, keeping your left hand vertical, rotate your hands  $180^\circ$  and observe the relationship between the vertical fault plane and the pole to the bedding. This relationship can be plotted on the equal-area net by turning the tracing paper to put the pole of the fault (point F') at the north (or south) pole of the net. The small circle on which A' now lies, together with its mirror image across the equator, defines the locus of all possible pole-to-bedding orientations if the footwall block is rotated about an axis perpendicular to the fault (Fig. 9.8c).

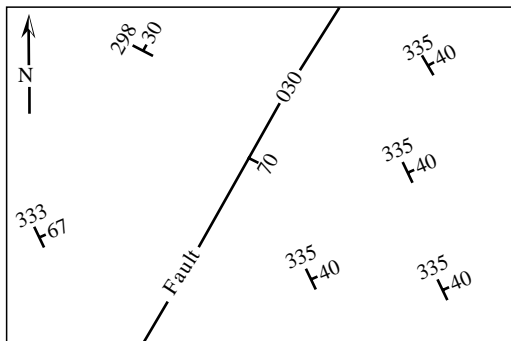
Having plotted the range of possible attitudes that rotation on this fault could produce, we can confirm that B' is included within this set. Rotation on this fault is equal to the angle between A' and B', which is  $50^\circ$  (Fig. 9.8c).

An alternative approach to measuring the rotation on faults involves determining the pitch of each apparent dip in the fault plane. Because the pitch on the footwall and hanging wall were identical prior to rotation, the difference in pitch equals the amount of rotation. In this problem the apparent dips are in opposite directions so the pitches are added together. The pitch on the hanging wall in the fault plane is  $42^\circ$  and the pitch on the footwall is  $8^\circ$  (Fig. 9.8d), indicating  $50^\circ$  of rotation.

Solve Problem 9.3.



**Fig. 9.8** Diagrams showing the solution to a rotational-slip problem. (a) Geologic map. (b) Equal-area net plot of the pole to fault plane (point F') and the poles to bedding in each fault block. (c) Small circles that define the locus of possible poles to bedding in the footwall block if rotated on the fault plane. (d) Measuring rotation by the pitch of bedding on each wall of the fault.



**Fig. 9.9** Geologic map for use in Problem 9.3.

**Problem 9.3**

Figure 9.9 is a geologic map showing a fault. On the east side of the fault the beds all have an attitude of  $335^{\circ}$ ,  $40^{\circ}\text{E}$ . West of the fault the rocks are poorly exposed, with only two outcrops, which have different attitudes.

- 1 Plot the attitude in the hanging wall on the equal-area net, and also plot the range of possible attitudes in the footwall that could result from rotation on this fault. Determine whether either of the two attitudes west of the fault could be the result of rotation on the fault.
- 2 If so, determine direction and amount of rotation.

### Tilting of fault blocks

Layers that were deposited horizontally and then tilted provide an opportunity for measuring the rotation of fault blocks. Tilting occurred after the deposition of the youngest tilted beds and before the deposition of the oldest horizontal beds within the fault block. Review, for example, Problem 5.11, in which you determined the amount of post-Rohan Tuff/pre-Helm's Deep Sandstone tilting within the northeastern fault block of the Bree Creek Quadrangle.

#### Problem 9.4

By stereographic projection, using the attitudes determined in Problem 3.1, determine the amount (in degrees) and direction of Neogene tilting on the fault blocks of the Bree Creek Quadrangle that contain Tertiary rocks.

	Post-Rohan Tuff/pre-Helm's Deep Sandstone tilting	Post-Helm's Deep Sandstone tilting
Northeastern fault block	_____	_____
Central fault block	_____	_____
Western fault block	_____	_____

### Map patterns of faults

The map pattern of faults and strata can provide insight to the types of faults present in an area if the deformational history is relatively simple. For example, the approximate attitude of a fault surface can commonly be determined by its trace across the topography. Steeply dipping (more than  $\sim 75^\circ$ ) faults appear as nearly straight lines across rugged topography on geologic maps, whereas gently dipping faults, such as thrusts and low-angle normal faults, will be deflected following the rules of "Vs" (see Figs 2.1–2.7). The relative offset of strata across faults may allow one to distinguish between normal, reverse, and strike-

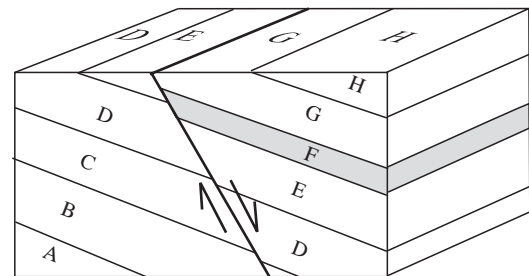
slip faults. The discussions below assume that the original stratigraphic order has not been disrupted by a previous deformational event.

### Normal faults

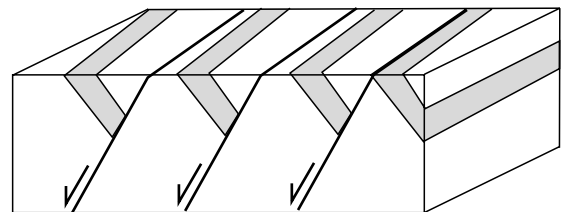
Normal faults can dip at any angle. High-angle normal faults generally dip between  $50^\circ$  and  $70^\circ$ , and they show relatively straight traces across topography. However, detachment faults (a special class of low-angle normal faults) may dip less than  $30^\circ$  and conform closely to topographic contours. Normal faults typically place young rocks in the hanging wall against older rocks in the footwall; that is, the fault dips *toward the younger rocks* (Fig. 9.10). Depending on the angular relationship between the fault and the bedding, normal faults may result in the omission of strata across the fault (such as layer F in Fig. 9.10) or the repetition of strata across the fault (Fig. 9.11).

### Reverse and thrust faults

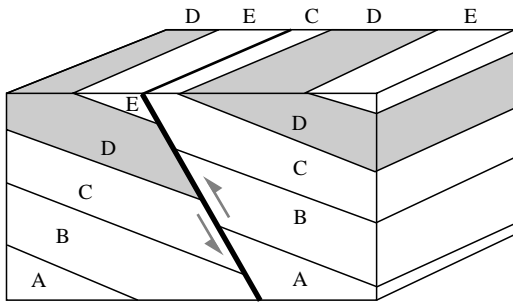
Reverse faulting causes older rocks to be placed on top of younger rocks; that is, the fault dips *toward*



**Fig. 9.10** Block diagram showing the omission of strata (as exposed on the earth's surface) across a normal fault.



**Fig. 9.11** Block diagram showing domino-style normal block faulting, resulting in a repetition of strata on adjacent fault blocks.



**Fig. 9.12** Block diagram showing the repetition of strata (as exposed on the earth's surface) across a reverse fault.

the older rocks (Fig. 9.12). This results in a repetition of strata across individual faults.

Thrust faults (reverse faults that dip at angles less than  $30^\circ$ ) may transport relatively thin sheets of rock over distances measured in tens of kilometers. Sometimes one portion of a thrust sheet moves farther than an adjacent portion, resulting in the development of a *tear fault*. Tear faults are strike-slip faults that are confined to the upper plate (hanging wall) of the thrust; they

strike parallel to the movement direction (Fig. 9.13).

Erosion can significantly modify the original extent of a thrust sheet, sometimes creating erosional windows (*fensters*) and isolated outliers (*klippen*) (Fig. 9.13).

The structural style of thrust faults is explored in greater detail in Chapter 15.

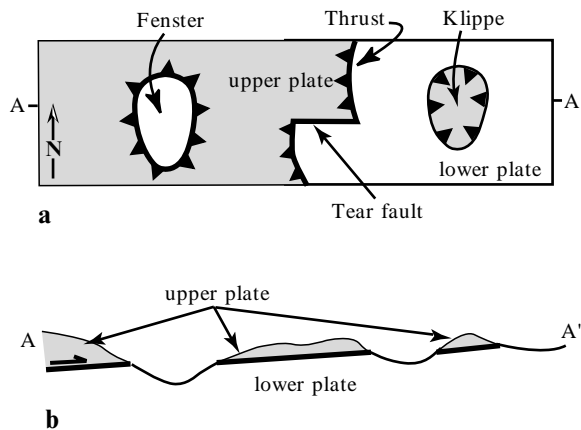
### Strike-slip faults

Strike-slip faults are characterized by horizontal slip vectors. Strike-slip faults commonly, but not always, show dips greater than about  $70^\circ$ . Because there is no differential vertical motion across a pure strike-slip fault, no predictable age relationships exist between rocks on the opposite sides of these faults. Note that strike-slip faulting in an area of horizontal strata will produce no offset in map view. If old and young rocks occur in a non-systematic manner on both sides of a high-angle fault, one should consider the possibility of either strike-slip faulting or a complex, multiphase deformational history.

### Timing of faults

An important goal of structural analysis in complexly deformed terranes is to determine the timing of movement along faults. This is generally accomplished through the study of cross-cutting relationships; any geologic feature (e.g., fault, sedimentary layer, pluton) must be younger than another feature that it cuts or truncates. However, application of this principle is complicated in the case of a growth fault, in which sediments accumulated simultaneously with the faulting. In such cases, only a portion of the motion must be younger than the strata cut. In fact, a significant percentage of the total displacement along a fault could be older than the strata cut.

The age of faulting commonly cannot be precisely determined, even in areas unaffected by growth faulting. Typically the timing of movement along a fault is *bracketed* between the *youngest* rock unit or feature that the fault cuts and the *oldest* unit or feature that cuts the fault.



**Fig. 9.13** (a) Map and (b) cross-section showing typical elements of a thrust belt. The sawtooth pattern indicates the upper-plate (hanging-wall) rocks. See text for discussion.



**Problem 9.5**

Answer the following questions regarding features on the geologic map shown in Figure G-25 (Appendix G). Use the spaces provided on Fig. G-25. This exercise will require you to integrate information from previous chapters as well as this one.

- 1** For each fault (A, B, C, D, and E) determine the type of faulting that has occurred and bracket the age of faulting as precisely as possible.
- 2** Identify the following features indicated by circled, lower-case letters on the map.
  - (a) Type of contacts at localities a, b, c, and d.
  - (b) Specific geologic structure present at localities e, f, g, and h.
- 3** The strike and dip directions that are shown are correct; however, three of the dips are actually overturned. Correct these directly on the map by substituting the correct symbol for overturned beds.
- 4** Is the unit on the east side of the map labeled "Tm" older or younger than the other Miocene rocks on the map? Give a reason for your answer.
- 5** Determine the *minimum* amount of displacement on fault C.
- 6** Write a one-paragraph geologic history of the map area. Include all episodes of deposition, erosion, and plutonism. Also indicate when specific deformational styles (folding and faulting) occurred.

**Problem 9.6**

Using the geologic map, your structure sections, and your work in this chapter, write a succinct, complete description of each fault in the Bree Creek Quadrangle. Use complete sentences, but avoid them being long and rambling. Include the following information for each fault:

- 1** Type of fault (normal, reverse, strike-slip). (If you cannot determine the sense of movement with certainty, describe the possible senses of movement and the evidence for each.)
- 2** Attitude of the fault plane (including geographic variation).
- 3** Strike separation and dip separation (heave and throw) as the data allow (sometimes only a minimum amount of separation may be determined).
- 4** Age of movement as specifically as the evidence permits.

## Dynamic and Kinematic Analysis of Faults

### Objectives

- **Determine the orientation of the stress ellipsoid responsible for a given population of faults.**
- **Reconstruct the history of change in the orientation of the stress ellipsoid for a given area from the distribution of various types of faults in time and space.**
- **Use kinematic analysis of faults to determine the direction of extension (or shortening) for which a given population of faults is responsible.**
- **Use kinematic analysis of faults to test for kinematic compatibility within a population of faults.**

Structural geologists use fault analyses to glean as much information as possible about the structural history of a region, and also to better understand deformation processes within the earth's crust. In this chapter we explore two types of fault analysis—dynamic analysis and kinematic analysis. This chapter also begins our exploration of *stress* in structural geology. Stress is measured in units of force per unit area.

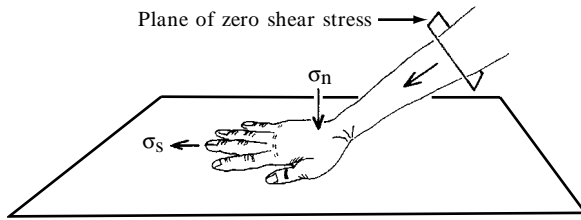
### Dynamic analysis

Dynamic analysis seeks to reconstruct the orientation and magnitude of the stress field that produced a particular fault or a population of faults. In this chapter we examine the relationship between stress *orientation* and faulting, while the relationship between stress *magnitude* and faulting is the subject of Chapter 13.

### Three principal stresses

Imagine a hand pushing diagonally on a table top (Fig. 10.1). The stress acting on the table top can be resolved into two components: *normal stress* acting perpendicular to the surface, and *shear stress* acting parallel to the surface. We use the Greek letter  $\sigma$  (sigma) to symbolize stress:  $\sigma_n$  represents normal stress, and  $\sigma_s$  represents shear stress. [The Greek letter  $\tau$  (tau) is sometimes used to represent shear stress.]

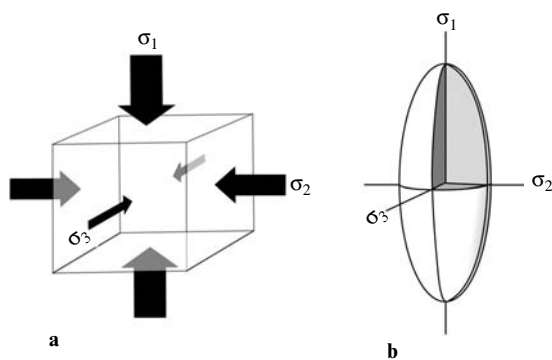
Although both normal and shear stresses are acting on the table top in Fig. 10.1, we can easily imagine a plane perpendicular to the arm in which the shear stress is zero. Within a body under stress from all directions there are always three planes of zero shear stress; these are called the *principal planes of stress*. The three normal stresses that act on these planes are called the *principal stresses*.



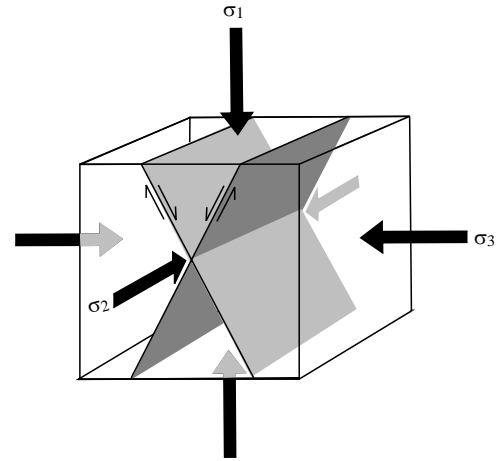
**Fig. 10.1** The diagonal force of a hand pushing on a table top resolved into a normal stress ( $\sigma_n$ ) acting perpendicular to the surface and a shear stress ( $\sigma_s$ ) acting parallel to the surface. The plane of zero shear stress experiences only normal stress.

By convention, the three principal stresses are named  $\sigma_1$ ,  $\sigma_2$ , and  $\sigma_3$  in order of magnitude, where  $\sigma_1 \geq \sigma_2 \geq \sigma_3$  (Fig. 10.2a). Together the three principal stresses define the *stress ellipsoid* (Fig. 10.2b). The normal stress acting on any plane within a stressed body cannot exceed  $\sigma_1$  nor be less than  $\sigma_3$ . Even in situations where the crust is being extended, such as in rift valleys, all three principal stresses may be compressive.

Laboratory studies of rock fracturing have shown that when an isotropic body fractures under applied stress, the fracture surfaces have a predictable orientation with respect to the stress ellipsoid. As shown in Fig. 10.3, there are two predicted fracture surfaces, or *conjugate shear surfaces*, which are both perpendicular to the  $\sigma_1$ – $\sigma_3$  plane. These shear fractures form an acute angle in the  $\sigma_1$  direction and an obtuse angle in the  $\sigma_3$  direction. The angle between  $\sigma_1$  and each of the shear fractures is variable, depending on the difference in magnitude between  $\sigma_1$ ,  $\sigma_2$ , and  $\sigma_3$ , and also on the material properties of the rock, but it is always less than  $45^\circ$ .



**Fig. 10.2** (a) The three principal stresses and the three planes of zero shear stress on which they act. (b) The stress ellipsoid, defined by the three principal stresses.



**Fig. 10.3** Relationship between the three principal stresses and conjugate shear surfaces.

### Problem 10.1

Figure G-26 (Appendix G) shows three pairs of conjugate shear surfaces. Sketch the arrows representing the three principal stress directions on each pair of conjugate shear surfaces, as was done on Fig. 10.3.

### Fault attitudes and orientation of the stress ellipsoid

Modern ideas about the relationship between faults and the stress ellipsoid began with the work of British geologist E. M. Anderson (1942). Anderson reasoned that because the earth's surface is an air–rock interface it must be a surface of zero shear stress and therefore a principal plane of stress. In the shallow crust, therefore, one principal stress can be assumed to be vertical and the other two must be horizontal. As a first approximation, this assumption has proved to be valid for many faults. Some exceptions are discussed below.

Anderson's assumption that one principal stress is always vertical explains the occurrence of three classes of fault: normal faults ( $\sigma_1$  vertical), strike-slip faults ( $\sigma_2$  vertical), and thrust faults ( $\sigma_3$  vertical) (Fig. 10.4). This assumption also allows us to reconstruct the orientation of the stress ellipsoid responsible for a given population of faults. Figure 10.4 also shows stereograms of typical populations of faults of each type. These stereograms are based on field observations and measurements. Points on the fault-plane great circles indicate the pitch of slickenside lineations. For normal and thrust faults,

arrows on the great circles point in the direction of hanging-wall motion. Notice that on stereograms of normal faults the pitch of the lineations is at a high angle, and the arrows point toward the perimeter of the net (Fig. 10.4a). Stereograms of reverse faults also show the pitch of the lineations at a high angle, but the arrows point toward the center of the net (Fig. 10.4c). On stereograms of strike-slip faults, the lineations have a very low-angle pitch, and pairs of arrows are used to indicate the sense of offset of each fault (Fig. 10.4b).

The population of normal faults (Fig. 10.4a) occurs as two subpopulations; the faults in each subpopulation dip steeply in a direction opposite to those in the other subpopulation. The population of thrust faults displays parallel strikes, and the faults dip gently in opposite directions (Fig. 10.4c). And the strike-slip fault population consists of two subpopulations with different strikes (Fig. 10.4b). Note that in each case  $\sigma_1$  bisects the acute angle between the faults. The two subpopulations in each case represent the conjugate set of shear surfaces analogous to those observed in experimental studies (see Fig. 10.3).

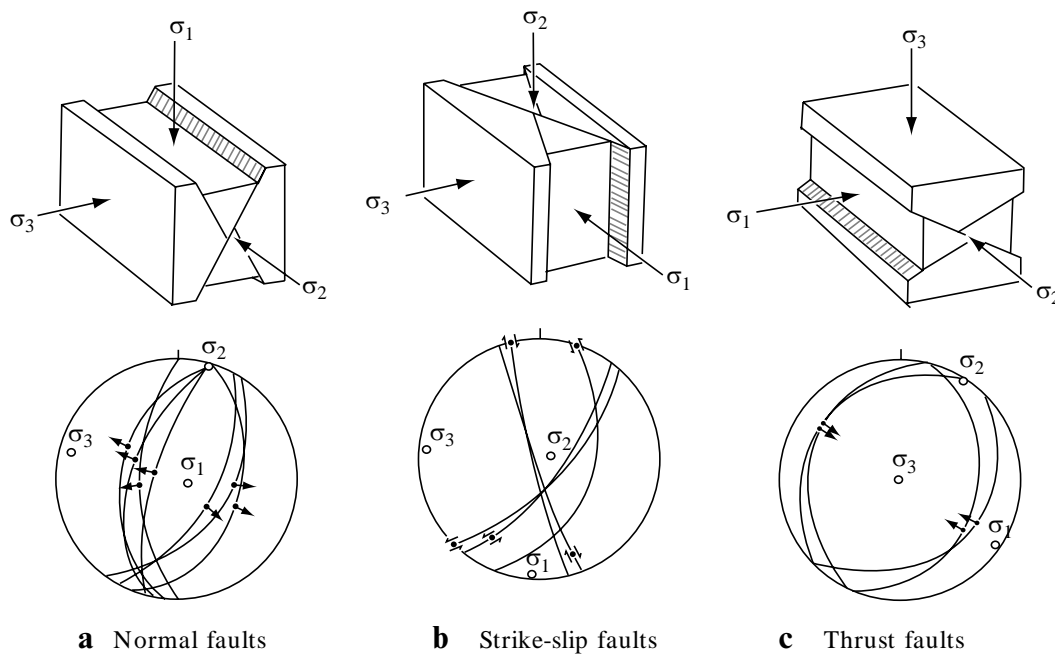
In order for two discrete subpopulations of faults to develop in isotropic rocks as shown in Fig. 10.4, there must be a distinct quantitative difference between  $\sigma_1$ ,  $\sigma_2$ , and  $\sigma_3$ . If two of the principal stresses are approximately equal in value, the resulting faults would not occur in two well-defined

sub-populations. For example, if  $\sigma_1$  is vertical, and  $\sigma_2$  and  $\sigma_3$  are of approximately the same magnitude, the resultant fault population would consist of normal faults with no preferred strike.

To reconstruct the orientation of the stress ellipsoid from a population of faults, draw the fault-plane great circles on the equal-area net along with any available data on the sense of slip and the orientation of slickenlines (as in Fig. 10.4). One principal stress is assumed to be vertical and the other two horizontal. The line of intersection between the two fault sets gives the orientation of  $\sigma_2$ . The bisector of the acute angle between the fault sets is  $\sigma_1$ , and the bisector of the obtuse angle between the fault sets is  $\sigma_3$ .

### Complications due to preexisting planes of weakness

All of the foregoing discussion assumes that the rocks being studied have no intrinsic preferred directions of shear. Of course, this assumption is very often incorrect. Planes of weakness, such as bedding or cleavage planes, joints, or preexisting faults will serve as preferred shear surfaces and will cause faults to have different attitudes than they otherwise would have had. Old faults that formed in response to one stress system are often reactivated by new stresses.



**Fig. 10.4** Block diagrams and equal-area plots of three classes of faults predicted by E. M. Anderson. The equal-area stereograms show typical fault and slickenline orientation data for a set of faults within each class. For normal faults and thrust faults, the arrows on the great circles of the stereograms point in the direction of the hanging-wall motion. For strike-slip faults, the arrows on the great circles indicate the sense of shear. After Angelier (1979) in Suppe (1985).

Movement on such preexisting planes of weakness is typically oblique-slip. The orientation of the stress ellipsoid cannot be determined in such cases unless there is a population of variously oriented faults with slickenlines. If such faults do occur, the theoretically preferred fault plane is the great circle defined by the stereographically projected slickenlines that occur on the preexisting planes of weakness.

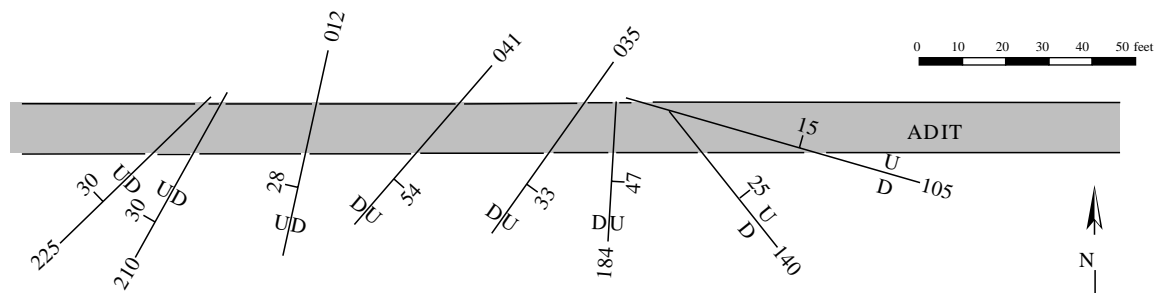
### Problem 10.2

The table below lists measurements from 10 normal faults in a small area on the island of Crete (Angelier, 1979). Plot the data on an equal-area net and determine the orientation of the principal stresses. (In reality, 10 faults are not enough to reliably determine the orientation of the stress ellipsoid; ideally, about 40 should be used.)

Fault number	Strike of fault	Dip of fault	Pitch of slickenlines
1	045°	61°S	80°E
2	036°	59°S	80°W
3	090°	80°N	58°W
4	052°	68°N	78°W
5	045°	63°N	78°W
6	110°	88°N	59°W
7	074°	78°N	65°W
8	046°	60°S	80°W
9	077°	61°N	86°E
10	067°	56°S	88°E

### Problem 10.3

Figure 10.5 shows a map of a mine adit and a series of minor faults that occur in a homogeneous rock unit. Plot the fault planes on the equal-area net and determine the orientation of the stress ellipsoid.



**Fig. 10.5** Map view of a mine adit, showing the attitude and sense of motion on eight faults. For use in Problem 10.3. D, down; U, up.

### Problem 10.4

Figure G-27 is a geologic map and structure section from the Inyo Range of eastern California. Using complete sentences, describe the history of principal stress orientations in this area. What can you say about the specific time periods that the variously oriented stresses were in effect? Is there any evidence that shear surfaces were controlled by anything other than the orientation of the principal stresses? Explain.

### Problem 10.5

In one succinct paragraph, describe the history of the principal stress orientations in the Bree Creek Quadrangle. Be as specific as possible about the time intervals during which variously oriented stress ellipsoids were in effect. Cite specific evidence to support your conclusions.

### Nonuniform stress fields

Although Anderson's assumptions about faulting and the stress ellipsoid have proved to be extremely useful, we now know that they are not always valid. For example, instead of the two sets of conjugate faults predicted by Anderson, sometimes a rhombohedral network of four fault sets forms in isotropic rock (Aydin & Reches, 1982). In the cases of thrust faults and strike-slip faults, usually only one of the predicted two sets of faults actually develops. In addition, Anderson's theory does not explain the formation of low-angle normal faults or high-angle reverse faults. Despite these limitations, Anderson's theory of faulting remains the basis for all dynamic analysis.

Anderson also assumed that the orientation of the stress ellipsoid does not change with depth and that the stress field causing deformation in the shallow

crust is uniform over a large area. Implicit in these assumptions was the expectation that a single fault type would characterize a region, and that multiple fault types require multiple deformation episodes. This expectation has turned out to be wrong. We will examine two examples of nonuniform stress fields occurring during a single tectonic episode. The first (Problems 10.6 and 10.7) is from an extensional tectonic regime, the Basin-and-Range province of the western United States, in which the stress system has been nonuniform through time, and the second (Problem 10.8) is from a compressive regime, the Himalayan–Tibetan region of Asia, in which the stress system is highly variable in space.

### Problem 10.6

Figure G-28 is a generalized map of a portion of the southwestern United States showing the Basin-and-Range geologic province and bordering regions. The Basin-and-Range province derives its name from the north–south-trending basins and ranges that occur there. Two late Cenozoic deformational fields are recognizable in this area (Wright, 1976).

- 1 Examine Field I on the map. This field, which includes central and northern Nevada and western Utah, is characterized by listric normal faults. What are the two *horizontal* principal stresses in this field, and how are they oriented? Draw your answer in the space provided below the map.
- 2 Examine Field II, which includes southern and westernmost Nevada and eastern California. Notice that this field contains a combination of normal and strike-slip faults. These faults have all been active during the same general time interval, but not necessarily exactly synchronously. Focusing first on the normal faults, in the space provided below the map, draw the orientation of the horizontal principal stresses indicated by the normal faults in Field II.
- 3 Notice that the strike-slip faults in Field II include both dextral and sinistral faults. What horizontal principal stresses, and in what orientations, are indicated by these strike-slip faults? Draw your answer in the space provided below the map.



**Wizard hint:** Carefully examine the relationship between the horizontal principal stresses and dextral and sinistral strike-slip faults in the block diagram in Fig. 10.4b, and compare these to the strike-slip faults in Field II.

- 4 You should now recognize that your answers have revealed a stress-orientation paradox in Field II. In the space provided near the bottom of Fig. G-28, use one or two succinct sentences to state what this paradox is, including a description of the orientation of the stress ellipsoid responsible for each type of fault. Finally, think of at least one hypothesis to explain this paradox, and write your hypothesis in the space provided. If you can think of more than one hypothesis, all the better.

### Problem 10.7

Let us look more closely at the fault history within Field II of Fig. G-28. We will examine the detailed fault pattern of one small area at Hoover Dam on the Arizona–Nevada border, a highly controversial area within the Basin-and-Range province. The faults at Hoover Dam were studied by Angelier *et al.* (1985); Fig. G-29 is a schematic summary of their results. Although not all workers in the area would agree, Angelier *et al.* (1985) recognized four faulting episodes at Hoover Dam — two episodes of normal faulting and two episodes of strike-slip faulting. The first faulting episode (early normal faulting) is depicted in Fig. G-29a, and the second (early strike-slip faulting) is depicted in Fig. G-29b.

- 1 Draw the three principal stresses on Fig. G-29a and b that would account for each of these first two stages of faulting.
- 2 The early strike-slip stage was followed by a late normal-faulting stage, which was then followed by a late strike-slip stage. The end result is schematically shown in Fig. G-29c. Draw the three principal stresses on Fig. G-29c that would account for this late strike-slip stage of faulting.
- 3 Notice that in Fig. G-29b one of the strike-slip faults is left-lateral and the other is right-lateral. Notice also that one segment of the left-lateral fault is reactivated in Fig. G-29c with right-lateral motion. All of the faulting depicted in Fig. G-29 took place during Miocene regional extension, when the Basin-and-Range province developed in the Hoover Dam region. In the space provided near the bottom of Fig. G-29, explain how a strike-slip fault can change from sinistral to dextral during one tectonic episode.



**Wizard hint:** Examine the block diagram in Fig. 10.4b again, and imagine slowly rotating the stress ellipsoid about a vertical axis.

- 4 The authors of this study attributed the alternation of normal and strike-slip faulting depicted in Fig. G-29 to “permutations of  $\sigma_1$  and  $\sigma_2$  [which] represent stress oscillations in time and space” (Angelier *et al.*, 1985, p. 361). Bearing in mind that the Miocene was a time of active volcanism, crustal thinning, and high denudation rates in the Hoover Dam region, in the space provided at the bottom of Fig. G-29, speculate about the geologic factors that might have caused the vertical principal stress to increase and decrease in magnitude relative to the horizontal principal stresses.

- 2 Place a sheet of tracing paper over the three drawings of Fig. G-31. On Fig. G-31c locate the faults that correspond to the seven faults listed above. Draw these faults on the overlay, and transfer the stress orientations from Fig. G-30.
- 3 On the overlays of Fig. G-31a and b, draw the major faults and indicate the orientation of the horizontal principal stresses along each of these.
- 4 In one succinct paragraph describe the evolution of regional stresses during the India–Asia collision. Use the space provided on Fig. G-30.

### Problem 10.8

Asia contains a complex array of active fault types. As shown in Fig. G-30, for example, there is a major system of thrust faults in the Himalaya (Himalayan Frontal Thrust), major left-lateral strike-slip faults in China (e.g., Kunlun and Altyn Tagh Faults), major right-lateral strike-slip faults in Central Asia (e.g., Talasso-Fergana Fault) and also in Indochina (e.g., Red River Fault), and normal fault systems in Siberia (Baikal Rift System) and also in China (Shansi Graben System). Obviously, no single stress ellipsoid orientation can account for this tectonic nightmare, yet all of these faults probably owe their existence to the collision and continued compression between India and Asia, which began in the Eocene (Molnar & Tapponnier, 1975).

The India–Asia collision has been experimentally reconstructed with plasticene, producing insightful results (Tapponnier *et al.*, 1982). Figure G-31 shows drawings made from photographs taken during one of the plasticene experiments. The upper and lower surfaces of the plasticene were confined between two plates, preventing the development of dip-slip faults, but in spite of this limitation there is a remarkable similarity between the features in Fig. G-31c and the fault map of Asia (Fig. G-30).

- 1 On the basis of fault type and orientation, on Fig. G-30 draw the orientations of the two horizontal principal stresses acting on each of the seven faults listed below. (Refer to Fig. 10.4 for help with this.)
- Himalayan Frontal Thrust.
  - Quetta-Chaman Fault.
  - Talasso-Fergana Fault.
  - Altyn Tagh Fault.
  - Baikal Rift System.
  - Shansi Graben System.
  - Kang Ting Fault.

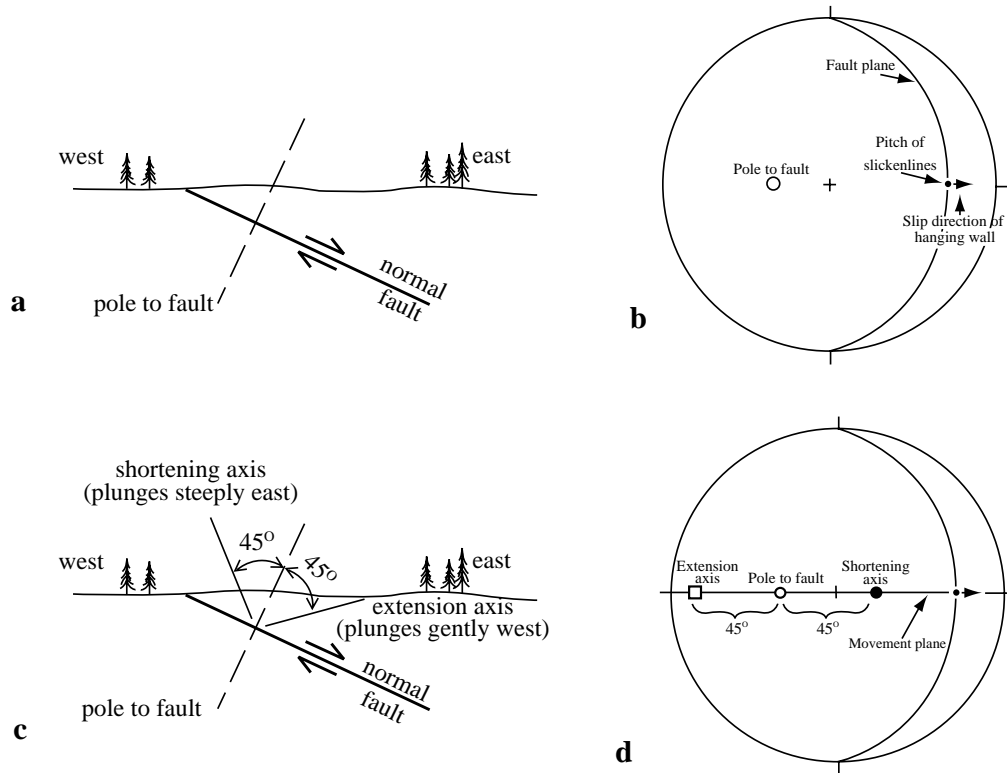
### Kinematic analysis

Kinematic analysis is a graphical technique for analyzing fault data (Marrett & Allmendinger, 1990). It allows the structural geologist to quantitatively characterize the overall deformation or movement pattern resulting from cumulative fault motions in a region and to determine the direction of bulk shortening or extension (i.e., strain). Unlike dynamic analysis, kinematic analysis does not seek to determine the orientation and magnitude of the stresses responsible for deformation.

As with dynamic analysis, the basic data necessary for kinematic analysis of faults are: (1) the strike and dip of the fault surface, (2) the pitch of slickenlines within the fault plane, and (3) the sense of movement on the fault. Sense of movement is most commonly determined by using stratigraphic separation in combination with the orientation of slickenlines. [For a discussion of various additional brittle sense-of-shear indicators see Petit (1987).]

As an example of the first steps needed for a kinematic analysis of faults, consider a fault striking north–south and dipping  $30^\circ$  east (Fig. 10.6a). We know from field observations that this is a normal fault, and that the slickenlines have a pitch of  $90^\circ$  within the fault plane, indicating that all of the motion is dip-slip. Here is how this information should be plotted:

- The fault plane and its pole are plotted on tracing paper superimposed on the equal-area net, and the pitch of the slickenlines is plotted as a point on the same great circle (Fig. 10.6b).
- From this slickenline-pitch point draw a small arrow to indicate the direction of motion of the hanging-wall block (Fig. 10.6b). Be sure that the slickenline-pitch point is positioned over the east–west or north–south axis of the stereonet when you draw your small arrow.



**Fig. 10.6** (a) Cross-section diagram of a normal fault dipping  $30^\circ$  to the east. (b) Equal-area projection, showing the pole to the fault,  $90^\circ$  pitch of slickenlines, and corresponding slip-direction arrow. (c) Cross-section diagram showing the shortening and extension axes, which are perpendicular to one another and  $45^\circ$  from the pole to the fault. (d) Equal-area projection showing the movement plane and projection of the shortening and extension axes. The movement plane lies on the great circle defined by the pole to the fault and the pitch of the slickenlines. The slip-direction arrow points toward the extension axis and away from the shortening axis.

- 3 The slickenline-pitch point and the pole to the fault lie in a plane called the *movement plane*. To locate this plane, rotate the tracing paper so that the pole to the fault and the slickenline-pitch point lie on a common great circle. This great circle is the movement plane. In the example shown in Fig. 10.6, the slickenline pitch is  $90^\circ$ , so the movement plane is vertical; in the more general case the movement plane is inclined and is represented on the stereonet as a curved great circle.
- 4 We are now ready to plot the shortening axis and the extension axis of the fault. Both of these axes are defined for each fault, regardless of what type of fault it happens to be. These axes lie within the movement plane, they are oriented  $90^\circ$  from one another, and each is  $45^\circ$  from the pole to the fault (Fig. 10.6c). On the stereonet plot, the two axes are plotted on the line that represents the movement plane; *the slip-direction arrow always points toward the extension axis and away from the shortening axis* (Fig. 10.6d). It

is important to use different symbols for the extension and shortening axes, such as a square for the extension axis and a dot for the shortening axis, as in Fig. 10.6d.

### Quantifying the direction of shortening or extension

Suppose you have mapped a population of faults. You want to test the hypothesis that these faults were all produced as part of a single deformational episode, and you also want to determine the direction of extension (or shortening).

Figure 10.7 shows the plots of five reverse faults, their slip-direction arrows, and their extension and shortening axes. This stereogram tells us that these faults represent a regional shortening in the direction of approximately  $110^\circ$ . In order to characterize quantitatively a large number of plots, the points should be contoured, using the technique described in Chapter 7.



**Problem 10.9**

The data tabulated below were collected within the Basin-and-Range province, from faults in southern Nevada, and from north of Hoover Dam in the Lake Mead area. Although local exceptions exist, the overall extension direction in the Basin-and-Range province during the Tertiary was east–west. Construct one plot showing the orientations of faults, pitch of slickenlines, and slip directions (as in Fig. 10.6b). Construct a second plot that shows the extension and shortening axes (as in Fig. 10.6d). There are not enough data to contour, so visually determine the “best fit” extension axis direction (or directions, if there are more than one).

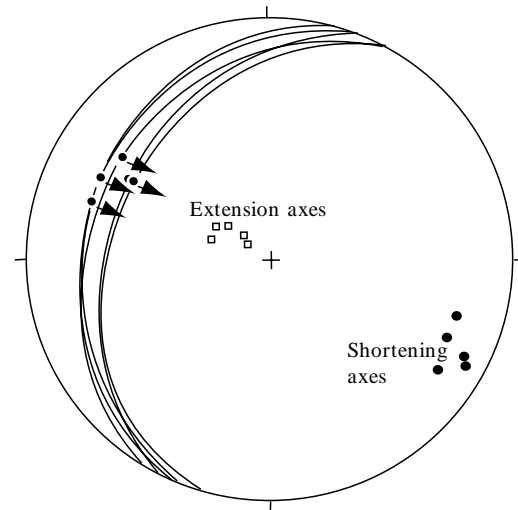
Strike of fault	Dip of fault	Pitch of slickenlines	Dominant slip sense
195°	65°W	85°N	Normal
358°	62°E	84°N	Normal
349°	59°E	77°N	Normal
355°	76°E	75°N	Normal
202°	72°W	76°N	Normal
346°	60°E	85°N	Normal
208°	65°W	78°N	Normal
155°	58°W	80°N	Normal
025°	70°E	82°N	Normal
190°	68°W	79°N	Normal

Are these data from the Lake Mead area consistent with the regional extension direction in the Basin-and-Range province as a whole? (In reality, many more data points would be needed to rigorously address this question.)

**Kinematic compatibility**

Kinematic analysis is useful, not only for characterizing the overall strain pattern in an area, but also for testing the *kinematic compatibility* of fault sets. Kinematic compatibility is a complex topic, and our brief discussion below is designed to only introduce you to the basic principle.

In some regions, faults of different orientations and movement sense, such as strike-slip and normal faults, may act in concert to accommodate regional extension. These faults are said to be kinematically compatible. Kinematic analysis of such fault sets should yield a single extension or shortening axis. If kinematic analysis shows two or more distinct extension and shortening axes, the faults are



**Fig. 10.7** Equal-area plot of five reverse faults, showing the pitch of slickenlines, slip-direction arrows, extension axes, and shortening axes. The faults dip 20° to 30° to the northwest. The direction of tectonic transport is east-southeast. Consistent with this transport direction, the shortening axes trend east-southeast and are subhorizontal; the extension axes are nearly vertical.

probably not kinematically compatible and may represent different deformational events.

Here is an example of the kinematic compatibility test applied to a population of faults. Consider the following data set collected from 10 faults in a particular area:

Strike of fault	Dip of fault	Pitch of slickenlines	Dominant slip sense
345°	34°W	82°NW	Normal
078°	70°N	35°SW	Left-oblique
329°	32°W	78°NW	Normal
090°	51°N	25°W	Left-oblique
084°	62°N	21°SW	Left-oblique
066°	90°	32°SW	Left-oblique
071°	54°N	42°SW	Left-oblique
335°	29°W	75°NW	Normal
088°	40°N	26°SW	Left-oblique
321°	35°W	68°NW	Normal

Do these 10 faults represent a single, kinematically compatible population, or do they represent two or more separate, kinematically incompatible sets?

These fault data are plotted in Fig. 10.8. The faults, slickenline pitches, and slip-direction arrows are plotted on the equal-area net in Fig. 10.8a. Despite the variability in fault surface attitude, the slip direction arrows show a consistent

westerly slip direction. Figure 10.8b is a contoured plot of the extension axes, and Fig. 10.8c is a contoured plot of the shortening axes. (One would not usually contour 10 data points; these contour diagrams are shown here as an example of the procedure.) The contoured plots indicate generally uniform extension and shortening directions for the fault data. This analysis allows us to conclude that these 10 faults *could have* operated in a kinematically compatible fashion.

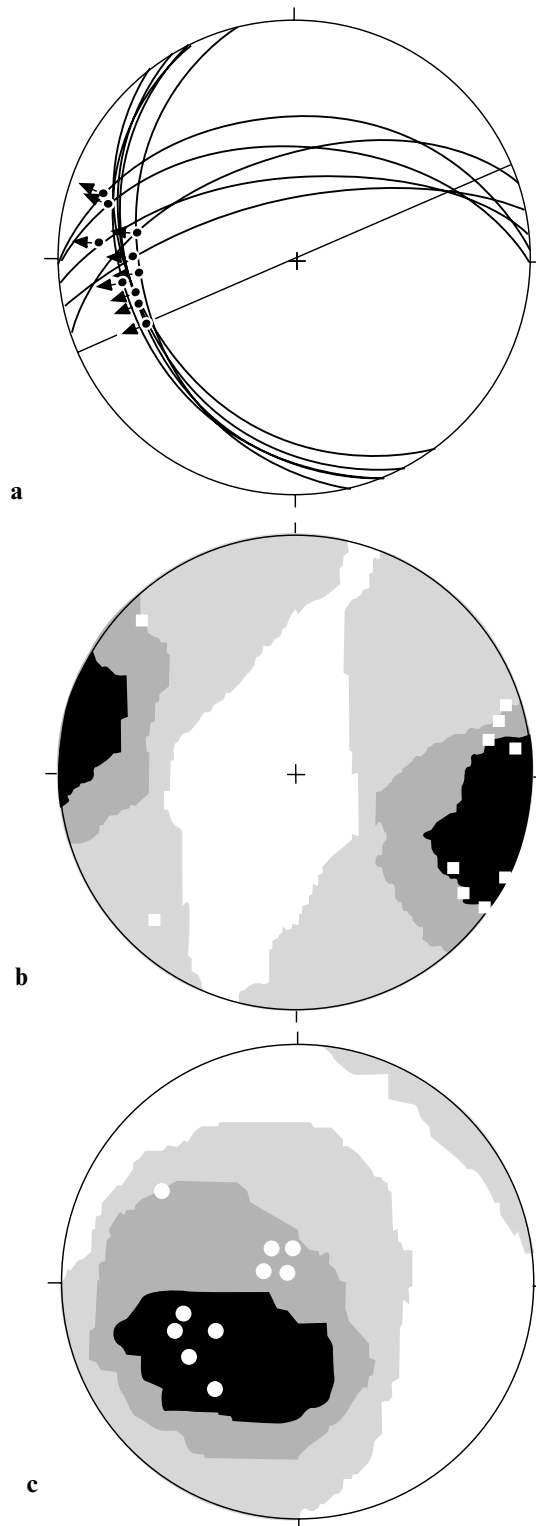
**Problem 10.10 Part A: Testing a dead geologist's hypothesis**

A geologist studying thrust faults in a Proterozoic shear zone in southern Wyoming developed the hypothesis that all of the thrust faults formed during a regional north–northwest/south–southeast shortening event. Unfortunately, before she was able to analyze her data she was killed by a grizzly bear. Fortunately, her field notebook survived the attack. With her last breath, the dying geologist whispered to her field assistant: “Please, do a kinematic analysis of the fault data and find out whether they support or falsify my hypothesis.”

Use the data from her notebook, tabulated below, to fulfill her dying wish. First construct a plot showing the orientations of the faults, pitch of slickenlines, and slip direction (as in Fig. 10.6b). Then, construct a second plot that shows the extension and shortening axes (as in Fig. 10.6d). There are not enough data to contour, so visually determine the “best fit” shortening axis direction.

In one succinct sentence, explain what your analysis tells you about the dead geologist's hypothesis.

Strike of fault	Dip of fault	Pitch of slickenlines	Dominant slip sense
075°	65°S	76°E	Thrust
075°	40°S	90°	Thrust
241°	32°N	88°W	Thrust
234°	37°N	86°W	Thrust
061°	51°S	83°E	Thrust
062°	45°S	82°E	Thrust
094°	30°S	75°E	Thrust
263°	22°N	73°W	Thrust
055°	22°S	80°E	Thrust



**Fig. 10.8** (a) Equal-area plot of 10 faults, including the fault plane, pitch of slickenlines, and slip direction. (b) Contour diagram of the extension axes; the squares indicate individual extension axes. (c) Contour diagram of the shortening axes; the dots indicate individual shortening axes. Contouring was done following the method of Kamb (1959).

**Problem 10.10 Part B: Testing the hypothesis of her precocious field assistant**

Near the shear zone discussed in Part A, above, is a region characterized by faults with a dominantly strike-slip sense of slip. There is a controversy as to whether or not these strike-slip faults are kinematically related to the thrust faults. While continuing the work of her deceased boss, the precocious field assistant developed the hypothesis that the strike-slip faults are tear faults (cf. Fig. 9.13) that formed during the same episode of thrusting as the faults examined in Part A. Tabulated below are her data on six faults. Test this hypothesis by constructing two plots, as before, one plot of the faults and slickenlines, and the second plot of the extension and shortening axes for the faults tabulated below. Succinctly discuss the kinematic compatibility or lack of compatibility of the strike-slip and thrust faults.

Strike of fault	Dip of fault	Pitch of slickenlines	Sense of shear
100°	85°S	6°E	Right lateral
352°	85°W	8°S	Left lateral
282°	78°N	7°W	Right lateral
107°	77°S	10°E	Right lateral
348°	85°W	4°S	Left lateral
000°	90°	3°S	Left lateral

## A Structural Synthesis

### Objective

- Write a professional-quality structural history of the Bree Creek Quadrangle.

The ultimate objective of analyzing the structures of an area is to reconstruct the area's structural history. Even when the impetus is purely economic, a great deal of time and money is often spent on sorting out generations of deformation and compiling a detailed geologic history. Such knowledge is not just academic; it may be crucial for the successful discovery of ore bodies and petroleum reservoirs.

### Structural synthesis of the Bree Creek Quadrangle

From your work on the Bree Creek Quadrangle map you have the data to reconstruct a detailed structural history of that area. The task in this chapter is to do just that. Below is a review of the problems in this book that deal with the Bree Creek Quadrangle.

- |                    |  |                     |  |
|--------------------|--|---------------------|--|
| <b>Problem 2.2</b> | Draw structure contours on the upper surface of the Bree Conglomerate in the northeastern corner of the Bree Creek Quadrangle. | <b>Problem 3.2</b>  | Determine the thicknesses of the Paleogene units.  |
| <b>Problem 3.1</b> | Determine the attitudes of the Neogene units.  | <b>Problem 3.3</b>  | Determine the approximate thicknesses of the Neogene units.  |
|                    |  | <b>Problem 3.5</b>  | Construct a stratigraphic column for the Cenozoic and Mesozoic units.  |
|                    |  | <b>Problem 4.4</b>  | Draw structure sections for A–A' and B–B'.   |
|                    |  | <b>Problem 5.11</b> | Determine the amount of post-Rohan, pre-Helm's Deep tilting of the northeast fault block.  |
|                    |  | <b>Problem 7.2</b>  | Construct contoured $\pi$ -diagrams, profile views, dip isogons, and summary diagrams of the folds; as well as describing the folds. |
|                    |  | <b>Problem 8.5</b>  | Draw axial-surface traces of the superposed folds; draw structure sections C–C' and D–D'; and describe the superposed folds.         |
|                    |  | <b>Problem 9.4</b>  | Determine the amount and direction of Neogene tilting on the fault blocks.   |
|                    |  | <b>Problem 9.6</b>  | Describe the faults.   |
|                    |  | <b>Problem 10.5</b> | Describe the history of the principal stress orientations.   |

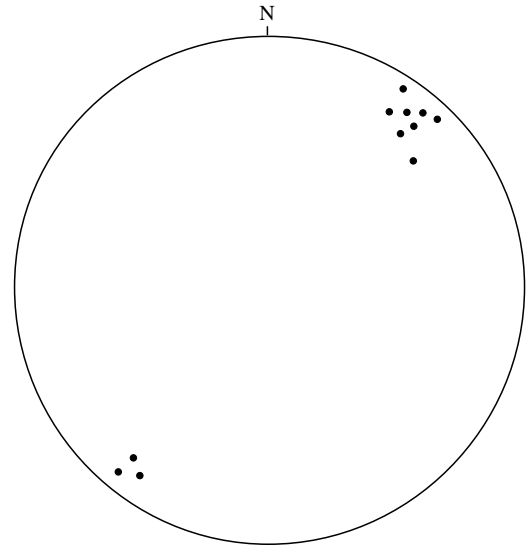
Synthesize as many of these tasks as you have completed into a cohesive summary of the structural history of the Bree Creek Quadrangle. This synthesis should consist of the following.

- 1 Geologic map (in an envelope at the back of the report).
- 2 Structure sections A–A', B–B', C–C', and D–D', neatly drawn, inked, and colored (in an envelope with the map).
- 3 Text (to include the following, with a *sub-heading* for each section):
  - (a) Title.
  - (b) Abstract. Write this *last*, but put it at the front of your report on a separate page. An abstract is a concise but comprehensive summary. It *is* the report, condensed and packed with concentrated information and significant results.
  - (c) Table of contents.
  - (d) Introduction. Briefly introduce the terrain and the structures. Since you did not actually do the fieldwork yourself, your introduction in this case should be one succinct paragraph.
  - (e) Stratigraphy. Add the Paleozoic rocks to the stratigraphic column you drew in Problem 3.5, and include this complete column in your report. The approximate thicknesses of the Paleozoic units can be measured directly off your structure sections C–C' or D–D'. Irregular plutonic units, such as the Dark Tower Granodiorite, are not assigned a thickness.

Briefly describe the stratigraphy, paying special attention to unconformities; they often have structural significance. If you had mapped the Bree Creek Quadrangle yourself, you would include detailed rock descriptions here as well.

- (f) Folds. Combine your work from Problems 7.2 and 8.5 into a detailed but readable description of the folds. Use your cross-section diagrams, contoured diagrams, and profile views to support and illustrate your descriptions. For descriptive purposes the Bree Creek Quadrangle can be conveniently divided into four subareas, each of which is a separate fault block. To allow a quick comparison of the folding in each subarea, include the page-sized reference map used in Problem 7.2 (Fig. G-20, Appendix G).

Prepare a *synoptic diagram* that shows the variation in the orientation of the fold axes of the folded Tertiary rocks. A synoptic diagram shows data from different subareas



**Fig. 11.1** Synoptic  $\beta$ -axis diagram prepared from 11 subareas. Each point represents a different subarea. After Weiss (1954).

- plotted together. Figure 11.1 is an example of such a diagram.
- (g) Faults. As specifically as possible, describe the age of each fault, the orientation of the fault surface, the sense of movement, and the amount of offset.
  - (h) Orientation of principal stresses. Review the orientation of the principal stresses at various times, citing *specific* structural features to support your statements.
  - (i) Discussion. Discuss how faulting, folding, and stratigraphy relate to one another. Did faulting precede folding or follow folding or both? Have the folded sections been rotated by faulting? Can sedimentation, erosion, intrusion, or metamorphism be related to structural events? Specifically how? Has the stress orientation of the area changed? When and in what way? Support your statements with references to the map, cross sections, and other diagrams.
  - (j) Summary of structural history. Succinctly summarize the structural history that you have just discussed in detail. Begin with the oldest events and work forward. Be very specific about the period or epoch in which an event occurred. This is your chance to tie everything together into a neat package.
  - (k) References cited. Give credit to your sources of information by citing references. Many students seem to have trouble

learning when and how to cite references. It is worth the trouble to look at any geologic journal and to pay close attention to the reference citations.

Generally speaking, any time you use someone else's observations or conclusions you need to cite the reference. This is done by providing the author and date of the publication in either of the following two ways:

Example no. 1: *Although it had generally been thought that the Mt Doom volcanic center is no longer active, Baggins and Gamgee (2005) showed that this is not the case.*

Example no. 2: *Although it had generally been thought that the Mt Doom volcanic center is no longer active, recent observations have shown that this is not the case (Baggins & Gamgee, 2005).*

The complete bibliographic reference is then provided in the References Cited section of the report.

If a reference has two authors it is normal practice to list both of them in the text of the paper, as in the examples given above. With three or more authors, the citation is commonly written like this: "(Baggins and others, 2005)" or "(Baggins *et al.*, 2005)." "*Et al.*" literally means "and others;" a period must be placed after "*al.*" because it is an abbreviation of *alii* (masculine others) or *aliae* (feminine others) or *alia* (mixed gender or neuter others). The names of all of the authors must be listed in the References Cited section of the report.

Regarding the precise method of listing references in the References Cited section, different scientific journals follow different nit-picky conventions. Here is the style used by publications of the Geological Society of America:

Baggins, F. and Gamgee, S., 2005, Reconnaissance survey of Mt. Doom Volcano: *Journal of Middle Earth Field Studies*, v. 27, p. 116–125.

Do *not* list any references in your References Cited section that are not cited in the text of the report. Conversely, all citations in the text of the report *must* be listed in the References Cited section. Citation of internet resources requires special attention; consult your local reference librarian.

## Writing style

Write with a specific reader in mind. This should be a geologist who has never seen the area you are describing. You do *not* need to explain basic geologic concepts and terms (e.g., anticlines are folds with the oldest rocks in their cores), but you *do* need to explain things that are known only to geologists familiar with the local area (e.g., the Bree Creek fault strikes north–south and dips 50° to the west).

Explain your data and conclusions in clear, simple prose. Aim for short sentences. Try reading aloud what you have written; if it does not flow smoothly it needs to be rewritten. Here is an example of a sentence that makes the reader struggle: "It should be noted that a clast of indurated crustal material perpetually rotating on its axis along the modern air–lithosphere interface is somewhat unlikely to accumulate an accretion of bryophytic vegetation."

Do not put all of your diagrams at the back of the report, where they are difficult for the reader to find. In this report, the map and cross sections must be separated from the text, but in general it is desirable to place figures on the page following the first reference to them in the text. Label your diagrams "Figure 1," "Figure 2," etc., and be sure each figure has a caption that explains its significance, even though this will duplicate some of the explanation in the text. At appropriate places within the text of your report, refer your reader to the figure she should be looking at.

Within reason, avoid using passive-voice and third-person constructions, such as: "The Bree Creek Quadrangle was studied by the author in 2005." This style is very common in the older literature, but today most editors consider the convention of always referring to yourself in the third person to be clumsy and stiff. It is much more direct to write: "I studied the Bree Creek Quadrangle in 2005." Furthermore, when you use third person/passive voice construction you convey a sense that you are trying to distance yourself from your work, as if you do not want to be responsible if it is not quite correct.

Beware of vague qualifiers such as "rather," "somewhat," and "fairly." Also, avoid "weasel words" such as "seems" and "might." In rare instances these words are appropriate, but people often use them by reflex and then do not think through what they are saying. For example, a geologist might write: "The principal axis of extension seems to rotate clockwise during the

Tertiary by a rather small amount.” If the evidence is not conclusive, it is better to write: “The data suggest that the principal axis of extension rotated clockwise approximately  $10^\circ$  during the Tertiary, but more fault orientations must be measured to confirm the rotation.”

### Common errors in geologic reports

Here are a few errors that repeatedly appear in the reports of geology students.

- 1 The most commonly misspelled word in student reports is “occurred,” which, like “occurring” and “occurrence,” has two “r”s.
- 2 The most commonly misspelled geologic period is the Ordovician, with the Cretaceous a close second. Do not confuse Paleocene with Paleogene.
- 3 In scientific usage, the word “data” is the plural form of the word “datum.” Therefore, use “these data show that ...” rather than “this data shows that ...”
- 4 When you are describing rocks that you personally examined, use the present tense. Students often write such things as “the Tapeats Sandstone *was* a coarse-grained quartz sandstone,” because that *was* what they saw. If the rocks still exist, use the present tense to describe them.
- 5 Many geologists make a distinction between Upper and Late, and between Lower and Early. For them, Upper and Lower refer to rocks, while Late and Early refer to time: the Upper Cambrian Nopah Formation was deposited during the Late Cambrian Epoch. However, due to the evolution of stratigraphic methods and nomenclature, some prominent stratigraphers now advocate the use of the terms *Early* and *Late* for both strata and time (Gradstein *et al.*, 2004; Zalasiewicz *et al.*, 2004). Ask your instructor what he or she prefers.

## Rheologic Models

### Objective

- **Acquire a qualitative understanding of rheologic models as analogs of rock deformation.**

### Equipment required for this chapter

- Rubber bands and springs
- Plastic disposable syringe (available from any medical facility)
- String
- Silly Putty® (available at toy stores)
- Standard masses
- Spring scale (or fish scale)
- Laboratory stands
- Bars and clamps
- Meter stick

Rocks respond in complex ways to stress. A layer of rocks that will fold under one set of conditions will fracture under another set. Adjacent layers may behave differently under the same conditions. Various aspects of stress and strain are examined in Chapters 10, 13, and 14. In this chapter we will investigate idealized relationships between stress, strain, and strain rate, and try to achieve a more intuitive understanding of why rocks deform the way they do.

Stress, symbolized by the Greek letter  $\sigma$  (sigma), is the force intensity experienced by a body; it is measured in units of *force per unit area*. Strain, symbolized by the Greek letter  $\epsilon$  (epsilon), is the resulting *change in shape or volume* caused by stress. Strain can be measured in various ways (see Chapter 14).

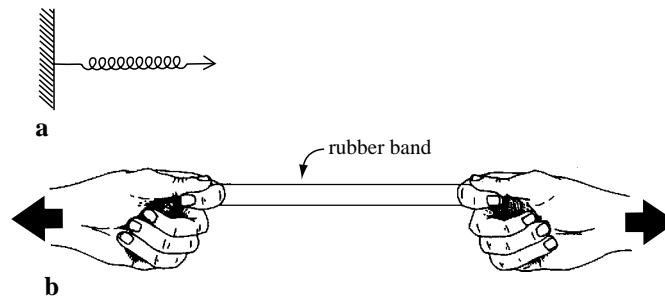
In addition to stress and strain, *time* is an important element in the study of deformation. The study of the relationships between stress, strain, and time is called *rheology*, from the Greek work *rheos*, which means a flow or current. A rheologic model is a characteristic relationship between stress, strain, and time, exhibited by an object being deformed.

In order to gain a qualitative understanding of stress and strain, it will be useful to examine three rheologic models: elastic deformation, viscous deformation, and plastic deformation. We will examine these separately and in combination.

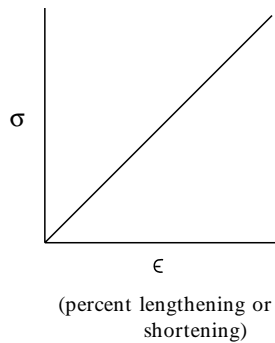
### **Elastic deformation: instantaneous, recoverable strain**

Elastic deformation is exhibited by a rubber band or a coiled spring (Fig. 12.1). With a perfectly elastic body the strain is strictly a function of





**Fig. 12.1** Elastic deformation. (a) Schematically represented as a coiled spring. (b) Simulated with a rubber band.



**Fig. 12.2** Stress/strain graph of elastic deformation. The slope of line varies with the elasticity (Young's modulus) of the material.

stress, and stress graphed against strain is a straight line (Fig. 12.2). Elastic deformation is described by Hooke's law,  $\sigma = E\epsilon$ , where  $E$  is the elasticity (Young's modulus) of the material. Objects that display perfect elastic behavior are called *Hookean bodies*. Rocks behave as Hookean bodies during earthquakes, when they transmit seismic waves.

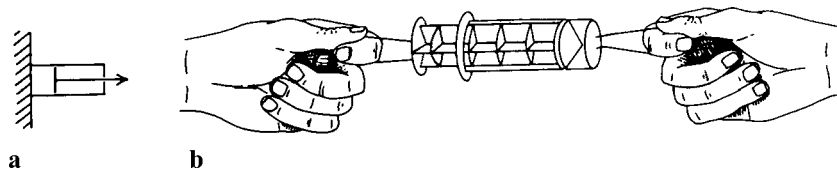
Unlike other types of deformation, elastic deformation occurs very quickly in the earth; for our purposes it will be assumed to be instantaneous. Another unique characteristic of elastic deformation is that the strain is recovered when the stress is removed, providing that the elastic limit of the material has not been exceeded.

To summarize the key features of elastic deformation: strain is directly proportional to stress, strain is (for our purposes) instantaneous, and strain is completely recovered when the stress is removed (unless the elastic limit has been exceeded).

### Viscous deformation: continuous strain under any stress

Viscosity is the measurable resistance of a fluid to flow. The viscosity of water is low, while the viscosity of honey is relatively higher. There are two categories of viscous deformation: Newtonian and non-Newtonian. The viscosity of water, and many other fluids, can be altered only by changing the temperature of the fluid. As long as the temperature remains constant, there is a linear relationship between stress and strain rate. Materials that behave this way are called *Newtonian fluids*. The lower crust may behave like a Newtonian fluid (Wang *et al.*, 1994).

In this chapter the viscous deformation that we model will assume Newtonian behavior, in which the strain rate is proportional to stress. The schematic analog of Newtonian viscous deformation is a porous piston in a fluid-filled cylinder, together called a dashpot (Fig. 12.3a). A suitable dashpot for our experimentation is a plastic, disposable syringe, common in hospitals (Fig. 12.3b).



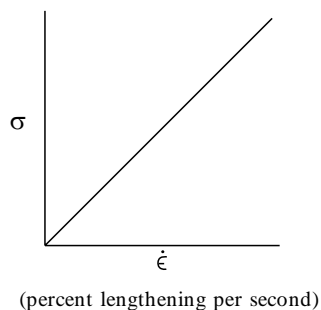
**Fig. 12.3** Viscous deformation. (a) Schematically represented as a leaky piston in a fluid-filled cylinder (together called a dashpot). (b) Simulated with a disposable syringe.

Another class of fluids — called *non-Newtonian fluids* — behave differently. In non-Newtonian fluids, the viscosity can be altered by means other than temperature, such as by shearing the fluid. A geologic example of a shear-thickening fluid is quicksand. Quicksand occurs where sand is suspended in water that is under pressure due to a slow influx of water below the surface, such as at the orifice of a spring. If you rapidly shear the quicksand, such as by stepping into it, its viscosity increases, and you may be unable to extricate your foot. The more you struggle, the more you shear the quicksand, and the greater the viscosity becomes. The trick is to move slowly. If necessary, lie down backward with your arms spread, and slowly free your legs.

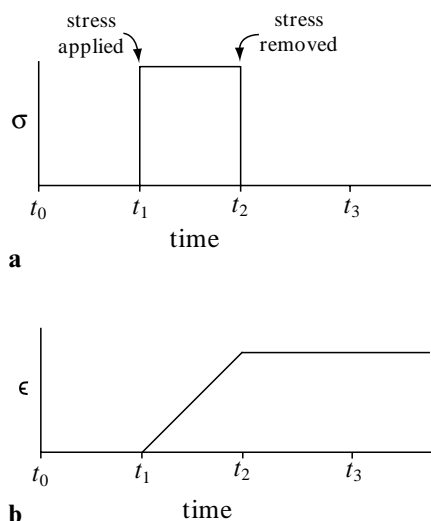
An example of a shear-thinning non-Newtonian fluid is ink in a ballpoint pen. As the ball turns, the ink is sheared and becomes less viscous, allowing it to flow freely as you write. Non-Newtonian viscous behavior is fairly common in the earth, but it does not lend itself to the simple modeling used in this chapter, so we will not be incorporating it into the following experiments.

Notice that, because viscous deformation is continuous at any stress, it is meaningless to graph stress against strain as in Fig. 12.2. Here it is the strain *rate* rather than absolute strain that is significant. Strain rate is symbolized  $\dot{\epsilon}$  (the first time derivative of  $\epsilon$ ). The strain rate of a Newtonian fluid is a function of stress and viscosity:  $\sigma = \eta\dot{\epsilon}$ , where  $\eta$  (eta) is the coefficient of viscosity of the material. The greater the stress, the faster the deformation. Figure 12.4 shows  $\sigma$  graphed against  $\dot{\epsilon}$  for a given material. Unlike elastic deformation, viscous deformation is permanent.

Because the total strain is partly a function of time, it is instructive to graph stress and strain separately against time, as in Fig. 12.5. Examine the two graphs in Fig. 12.5 carefully, and be sure



**Fig. 12.4** Stress/strain rate graph of viscous deformation. The slope of the line varies with the viscosity of the material.



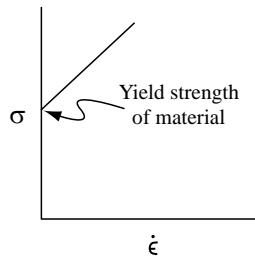
**Fig. 12.5** Viscous deformation experiment in which time is simultaneously graphed against stress (a) and strain (b).

that you understand how they relate to each other. We will be using such pairs of graphs throughout the rest of this chapter. In Fig. 12.5a stress is shown first applied at  $t_1$  and removed at  $t_2$ . In Fig. 12.5b it can be seen that strain is continuous from  $t_1$  to  $t_2$ , after which no more strain occurs.

Strain is commonly measured in percent lengthening or shortening per second, because seconds are convenient units of time for laboratory experiments. For example, if an object under stress were shortened from 10 cm to 9 cm in 100 s the strain rate would be:  $-10\%/100\text{ s} = -0.1/100\text{ s} = -0.001/\text{s} = -1 \times 10^{-3}/\text{s}$ . By convention, shortening is considered to be negative strain, while lengthening is considered to be positive. Strain rates in the earth's crust, of course, are many orders of magnitude slower. For example, by measuring the change in distance between points on opposite sides of the San Andreas fault, a strain rate of  $1.5 \times 10^{-13}/\text{s}$  has been determined.

#### Plastic deformation: continuous strain above a yield stress

Plastic deformation is similar to viscous deformation, except that flow does not begin until a threshold stress, or yield stress ( $\sigma_y$ ), is achieved. Yogurt, for example, will not flow off a horizontal table if you dump it out of the carton. It has a yield

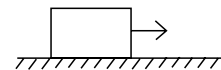


**Fig. 12.6** Stress/strain rate graph of plastic deformation. Once the yield strength of the material has been exceeded, behavior is viscous.

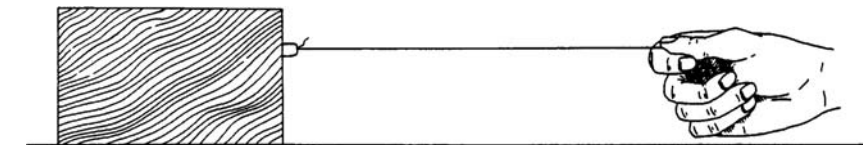
stress of about  $800 \text{ dynes/cm}^2$ , which is greater than the gravitational force acting on it. If you place a dish on top of the yogurt it will flow because the yield strength of the yogurt has been exceeded. Above the yield stress, stress graphed against strain rate is like viscous deformation (Fig. 12.6). Materials that behave in this manner are called *Bingham plastics*.

To simulate plastic deformation we will use a block on a flat surface (Fig. 12.7). Small amounts of stress may be applied with no movement at all. There exists a yield stress  $\sigma_y$ , however, that will overcome the frictional force on the stationary block. Once the yield stress is applied, the frictional force is overcome, the block begins to move, and it continues to move. A block on a table is not really a case of plastic deformation; a key difference is that while the block is not deformed, a plastic body is deformed. However, the similarity in the relationships between stress, strain, and time allows us to use the block as an analog of plastic deformation.

Notice that after the yield stress is applied, the amount of strain is a function of time. In Fig. 12.8, stress and strain are separately graphed against time. Stress is first applied at  $t_1$  and gradually increased until the yield stress is reached at  $t_2$ .

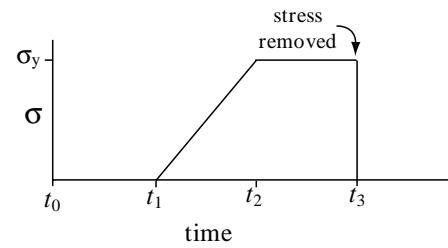


**a**

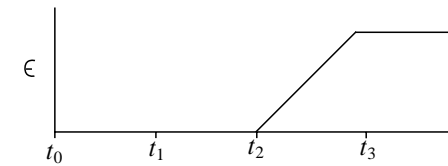


**b**

**Fig. 12.7** Plastic deformation. (a) Schematically represented as a block on a flat surface. (b) Simulated by pulling a wooden block with a string.



**a**



**b**

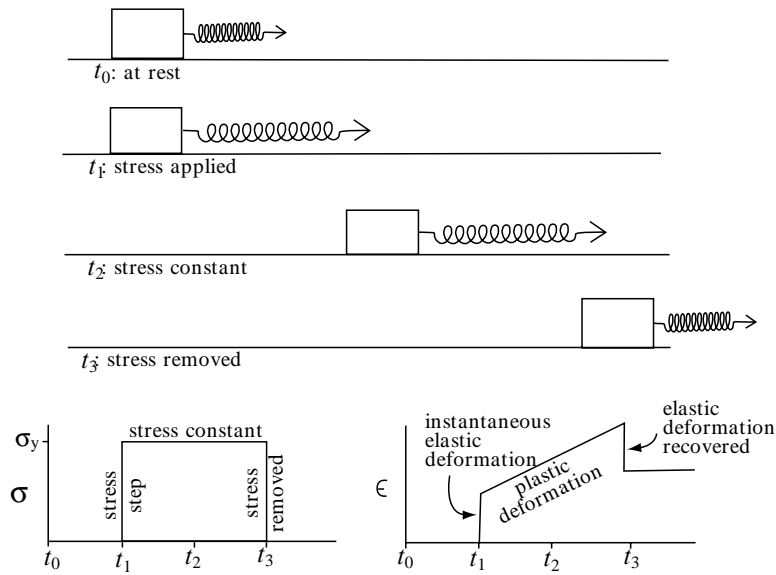
**Fig. 12.8** Plastic deformation experiment in which time is simultaneously graphed against stress (a) and strain (b).

### Elasticoplastic deformation

Most materials display complex rheologic characteristics that can be simulated with some combination of elastic, plastic, and viscous deformation. Attach a rubber band to a wooden block and conduct the experiment shown in Fig. 12.9. Consider the behavior of the rubber band and block as a unit, and carefully examine how this behavior is reflected in the  $\sigma/\text{time}$  and  $\epsilon/\text{time}$  graph pair in the figure. Notice that the rubber band provides an elastic component and causes the strain to begin at  $t_1$ , even before the yield stress is reached. When the stress is removed at  $t_3$ , however, the elastic deformation is recovered and the permanent deformation is a result of the plastic component.

### Elasticoviscous deformation

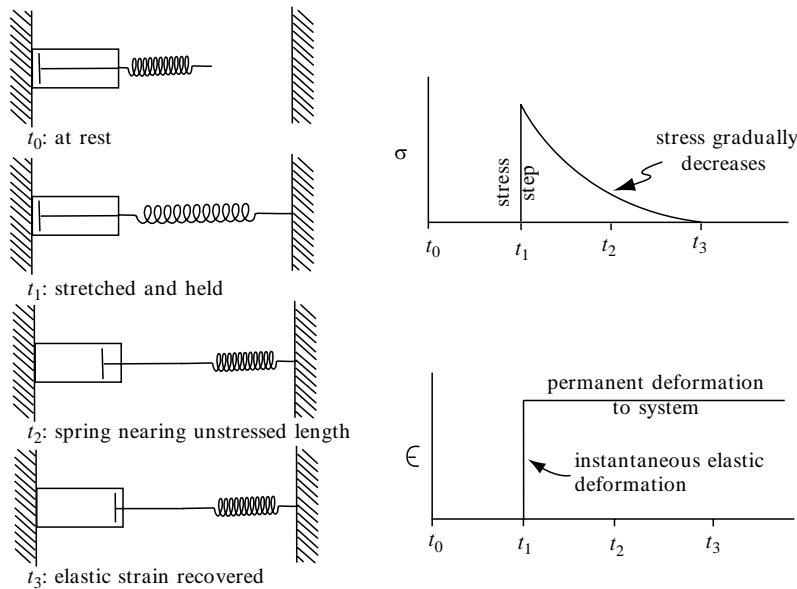
Attach a rubber band to a syringe (as shown with string in Fig. 12.3b) and experiment with the



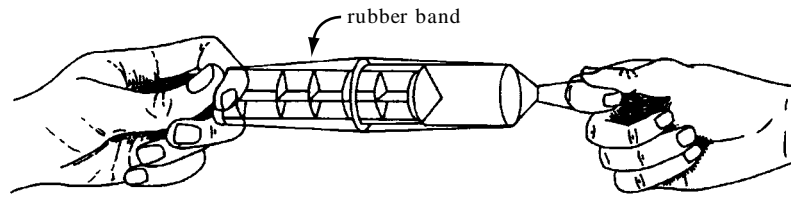
**Fig. 12.9** Elasticoplastic behavior.

behavior of this unit. This apparatus behaves just like the elasticoplastic body except that there is no yield stress that must be overcome before permanent strain begins. An object that behaves this way is called a *Maxwell body*.

In the experiment shown in Fig. 12.10 the rubber band is stretched and fixed, giving the body instantaneous permanent strain. In the two graphs, notice that although the strain is instantaneous and permanent, the stress is greatest at  $t_1$



**Fig. 12.10** Elasticoviscous behavior.



**Fig. 12.11** Firmoviscous behavior simulated with a rubber band and syringe.

and gradually decreases until the elastic strain is completely recovered.

### Firmoviscous deformation

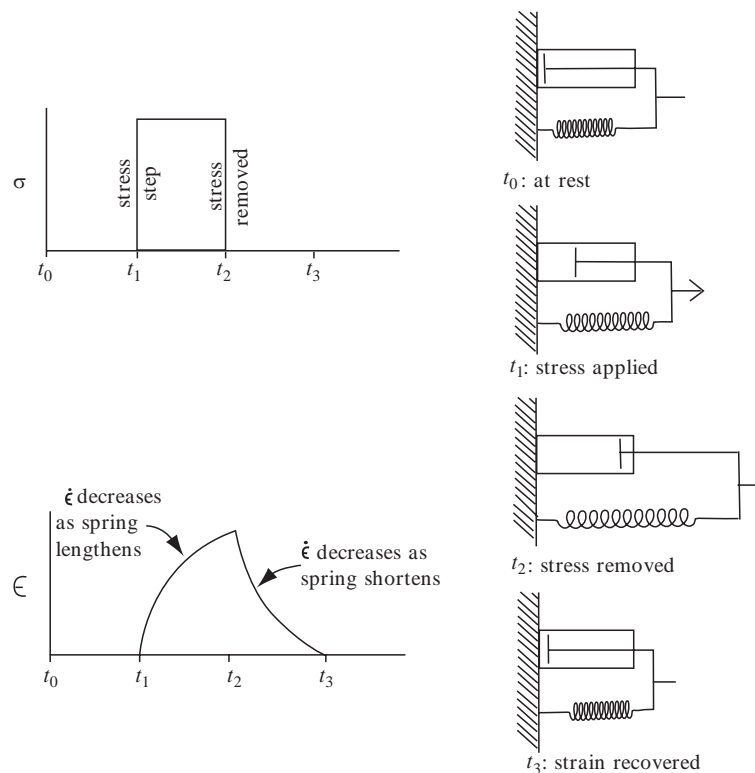
Combine a rubber band and a syringe as shown in Fig. 12.11. Neither the elastic nor the viscous component can move without the other. Examine the stress and strain graphs of Fig. 12.12 and note that even though the stress is constant, the strain rate decreases with time as the rubber band lengthens. When the stress is removed at  $t_2$  the strain rate jumps and then gradually decreases until all of the strain is recovered. An object that behaves this way is called a *Kelvin body*.

The earth can be thought of as a self-gravitating firmoviscous sphere. For example, when the weight

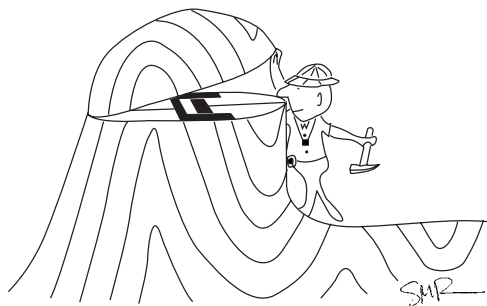
of glacial ice was removed at the end of the Pleistocene, northern portions of Europe and North America responded by isostatically rebounding. This rebound is still occurring, but at a steadily decreasing rate.

### Within every rock is a little dashpot

Under conditions of low temperatures, low pressures, and high strain rates, rocks deform by brittle deformation mechanisms. (The conditions under which rocks fracture are explored in Chapter 13; deformation mechanisms are discussed in Chapter 16.) However, deeper within the earth's crust, where temperatures and pressures are high, rock deformation occurs by plastic deformation



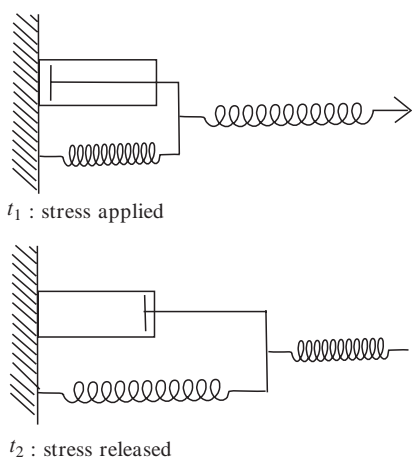
**Fig. 12.12** Firmoviscous behavior.



**Fig. 12.13** Within every rock is a little dashpot.

mechanisms. The boundary between shallow-crust brittleness and deeper-crust plasticity is a zone called the *brittle-plastic transition*.

Even within the brittle upper crust, however, at low strain rates rocks may deform in such a manner that they appear to flow at the mesoscopic scale. Such behavior is called *ductile behavior*, and it can involve brittle or plastic deformation mechanisms. Over very long time intervals, rocks are unable to resist any differential stress at all. On a large planet with a strong gravitational field and no active tectonism there would be no mountains. The rocks would flow like Silly Putty®. An analogous situation exists on Europa, one of the satellites of Jupiter. Europa has an ice crust that is pockmarked with very few impact craters; it is



**Fig. 12.14** Rheologic model called a standard linear solid.

the smoothest known body in the solar system. The mass of Europa and the rheologic properties of the ice conspire to erase craters soon after they form. Within every rock is a little dashpot (Fig. 12.13).

Many real solids behave like the rheologic model shown in Fig. 12.14. If stress is applied and immediately released, the strain is elastic and is immediately recovered. But if stress is applied and held for a while, the firmoviscous component (dashpot and spring) becomes important. This combination of a Kelvin body and an elastic body is called a *standard linear solid*. Such behavior can be seen in an old rubber band that has been wrapped around a newspaper for several weeks and is finally taken off; the limp rubber band slowly recovers some of its strain.

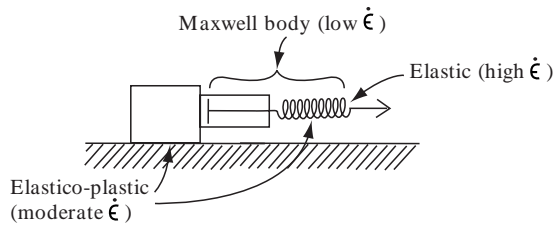
### Problem 12.1

On the  $\epsilon/\text{time}$  graph in Fig. G-32a (Appendix G) show the strain history of a standard linear solid that would correspond to the stress history in the  $\sigma/\text{time}$  graph.

### Problem 12.2

The rheologic model shown in Fig. 12.15 behaves differently at different strain rates. At high strain rates it behaves elastically (“bounces”). At moderate strain rates it behaves elasticoplastically (the dashpot does not have time to work unless the strain rate is low). And at low strain rates it behaves elasticoviscously. Experiment with Silly Putty®, and notice that it shares some of the properties just described but is not exactly the same as the model drawn in Fig. 12.15. Silly Putty® exhibits the following behavior: it bounces at high strain rates, stretches with slow *partial* recovery at moderate strain rates, and flows under gravitational force (low strain rates).

Draw a rheologic model for Silly Putty® that satisfies all of these requirements, and indicate on your drawing which parts behave in which ways.



**Fig. 12.15** Rheologic model for use in Problem 12.2.

### Problem 12.3

Figure G-32b is a sketch of a folded rock layer. The limbs of the folds deformed without fracturing, while fracturing occurred in the hinge zones. In terms of rheologic models, explain why the same material under the same conditions of temperature and pressure might behave differently in different places.

### Problem 12.4

In this problem you will quantitatively explore some rheologic models.

- 1** Using a spring scale and meter stick, graph stress against strain for several rubber bands and springs. Are these perfect Hookean bodies? Explain your answer.
- 2** Using a syringe and a rubber band, construct a Kelvin body (see Fig. 12.11). Suspend your Kelvin body from a horizontal bar. Using different masses, graph strain against time.
- 3** Place a stick of chalk horizontally across the jaws of a clamp. Suspend different masses from the chalk. Does it display elastic deformation? Determine the *breaking strength* of the chalk (the maximum stress it can support).

## Brittle Failure

## Objective

- Predict the principal stress magnitudes that will cause a given material to fracture.

## Equipment required for this chapter

- Graph paper
- Drawing compass
- Protractor

Chapter 10 was partly devoted to an examination of the orientation of the stress ellipsoid, especially with regard to faulting. Here we will investigate how the magnitude of the principal stresses influences brittle deformation. The chief objective is to be able to determine the differential stress at which a particular brittle failure will occur. We emphasize that, strictly speaking, the following discussion applies only to isotropic, homogeneous materials. Real-world geologic situations are usually more complicated. The material in this chapter lies at the heart of engineering geology because it concerns the conditions under which rock breaks.

## Quantifying two-dimensional stress

Experimental rock fracturing has shown that the difference in magnitude between  $\sigma_1$  and  $\sigma_3$  – called the *differential stress* – is the most

important factor in causing rocks to fracture. The magnitude of  $\sigma_2$  does not play a major role in the initiation of the fracture. For this reason we may profitably examine stress in two dimensions, in the  $\sigma_1$ – $\sigma_3$  plane.

If we know the orientations and magnitudes of  $\sigma_1$  and  $\sigma_3$ , then we can determine the normal and shear stresses acting across any plane perpendicular to the  $\sigma_1$ – $\sigma_3$  plane. Consider the plane in Fig. 13.1a. We want to determine the normal and shear stresses acting on that plane. To simplify the situation we will isolate the plane, along with two adjacent surfaces that are perpendicular to  $\sigma_1$  and  $\sigma_3$  (Fig. 13.1b). Viewed in the  $\sigma_1$ – $\sigma_3$  plane, we will call these surfaces A and B, and we will define angle  $\theta$  as the angle between the plane and the  $\sigma_3$  direction (Fig. 13.1c). This is equivalent to the angle between  $\sigma_1$  and the normal to the plane (Fig. 13.1d).

If our triangle in Fig. 13.1c is not moving, then it must be in equilibrium. This means that the normal stress ( $\sigma_n$ ) and shear stress ( $\sigma_s$ ) acting on the plane must be equal to  $\sigma_1$  and  $\sigma_3$  acting on surfaces A and B. We will now use this equilibrium relationship to define  $\sigma_n$  and  $\sigma_s$  in terms of  $\sigma_1$ ,  $\sigma_3$ , and angle  $\theta$ .

Figure 13.1d shows  $\sigma_1$  and  $\sigma_3$  acting on the plane, and it also shows the horizontal and vertical



components of  $\sigma_1$  and  $\sigma_3$ . The length of the line that represents the plane is:

$$\frac{A}{\cos \theta} \text{ or } \frac{B}{\sin \theta}$$

The vertical and horizontal forces acting on this line are indicated in Figure 13.1d. The equations of equilibrium for this plane are as follows:

$$\sigma_1 A = \frac{A}{\cos \theta} (\sigma_n \cos \theta + \sigma_s \sin \theta) \quad (13.1)$$

$$\sigma_3 B = \frac{B}{\sin \theta} (\sigma_n \sin \theta - \sigma_s \cos \theta) \quad (13.2)$$

Solving these equations simultaneously for  $\sigma_n$  and  $\sigma_s$  in terms of  $\sigma_1$ ,  $\sigma_3$ , and  $\theta$ , we derive the following equations:

$$\sigma_n = \sigma_1 \cos^2 \theta + \sigma_3 \sin^2 \theta \quad (13.3)$$

$$\sigma_s = (\sigma_1 - \sigma_3) \sin \theta \cos \theta \quad (13.4)$$

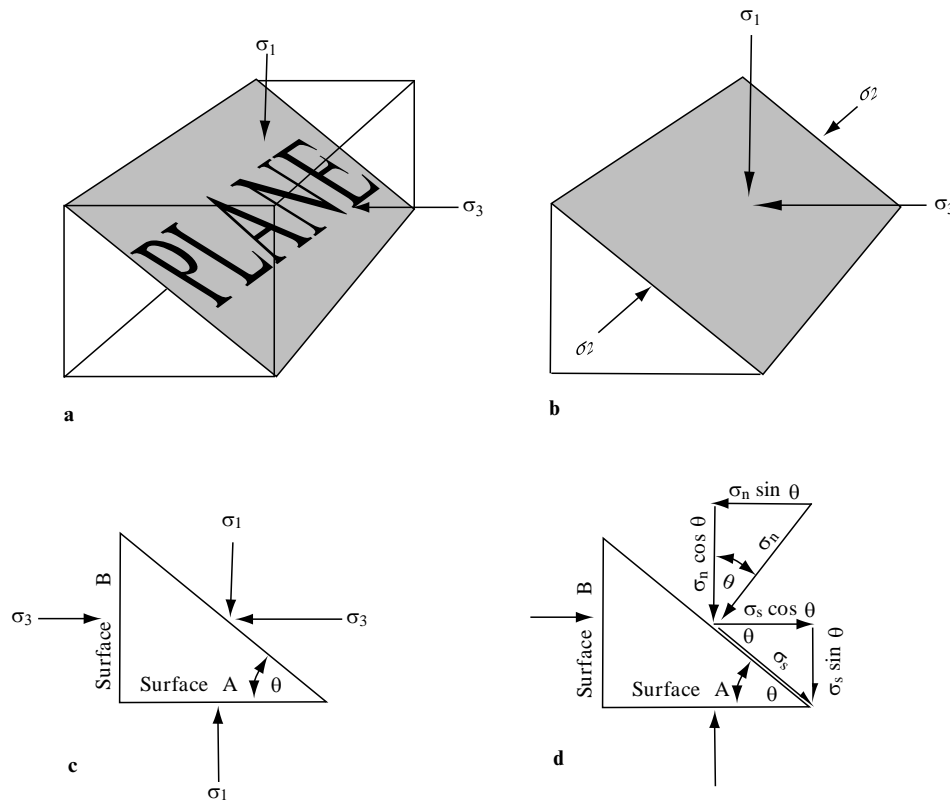
In order to reconstitute these equations into a more useful form we can substitute the following trigonometric identities:  $\sin 2\theta = 2 \sin \theta \cos \theta$ ,  $\cos^2 \theta = 1/2(1 + \cos 2\theta)$ , and  $\sin^2 \theta = 1/2(1 - \cos 2\theta)$ . The result is the following two equations:

$$\sigma_n = \left( \frac{\sigma_1 + \sigma_3}{2} \right) + \left( \frac{\sigma_1 - \sigma_3}{2} \right) \cos 2\theta \quad (13.5)$$

$$\sigma_s = \left( \frac{\sigma_1 - \sigma_3}{2} \right) \sin 2\theta \quad (13.6)$$

Stress is measured in units of force per unit area, for which the basic unit is the *pascal* (1 Pa = 1 newton per square meter);  $10^5$  Pa equals 1 bar, which is approximately equal to atmospheric pressure at sea level. The most convenient unit for most geologic applications is the megapascal (MPa), which is equal to  $10^6$  Pa or 10 bars. Stress within the earth's crust ranges up to about  $10^3$  MPa.

Using equations 13.5 and 13.6, we can now determine the normal and shear stress acting



**Fig. 13.1** Two-dimensional relationship between a plane and its state of stress. See text for explanation.

across a plane if we know the orientations and magnitudes of  $\sigma_1$  and  $\sigma_3$ . Suppose, for example, that in Fig. 13.1,  $\sigma_1 = 100$  MPa,  $\sigma_3 = 20$  MPa, and  $\theta = 40^\circ$ . Using equation 13.5, the normal stress is determined as follows:

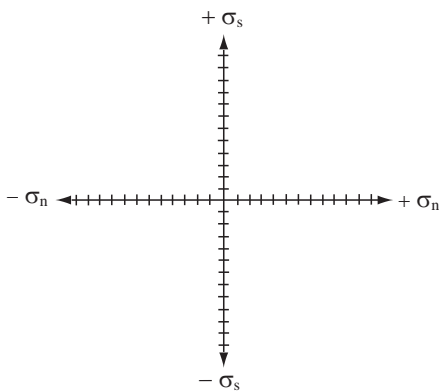
$$\begin{aligned} \sigma_n &= \left(\frac{\sigma_1 + \sigma_3}{2}\right) + \left(\frac{\sigma_1 - \sigma_3}{2}\right) \cos 2\theta \\ &= (60 \text{ MPa}) + (40 \text{ MPa})(0.17) \\ &= 67 \text{ MPa} \end{aligned}$$

Similarly, equation 13.6 can be used to determine the shear stress acting on the plane:

$$\begin{aligned} \sigma_s &= \left(\frac{\sigma_1 - \sigma_3}{2}\right) \sin 2\theta \\ &= (40 \text{ MPa})(0.98) \\ &= 39 \text{ MPa} \end{aligned}$$

**Problem 13.1**

Given the principal stresses of  $\sigma_1 = 100$  MPa (vertical) and  $\sigma_3 = 20$  MPa (horizontal), determine the normal and shear stresses on a fault plane that strikes parallel to  $\sigma_2$  and dips  $32^\circ$  (Plane I in Fig. G-33a, Appendix G).



**Fig. 13.2** Mohr diagram for graphing the state of stress of a plane. Within a stress field consisting of a particular combination of  $\sigma_1$  and  $\sigma_3$ , planes with different dips will experience different magnitudes of  $\sigma_n$  and  $\sigma_s$  and will therefore plot at different points on the Mohr diagram.

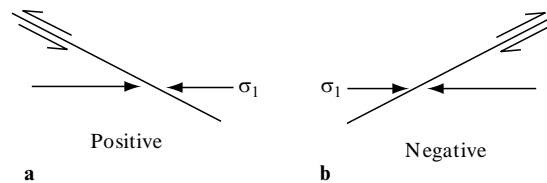
**The Mohr diagram**

In 1882, a German engineer named Otto Mohr developed a very useful technique for graphing the state of stress of differently oriented planes in the same stress field. The stress ( $\sigma_n$  and  $\sigma_s$ ) on a plane plots as a single point, with  $\sigma_n$  measured on the horizontal axis and  $\sigma_s$  on the vertical axis (Fig. 13.2). Such a graph is called a *Mohr diagram*. Most stresses in the earth are compressive, so geologists, by convention, consider compression to be positive. (Engineers, as a rule, are more tightly strung than geologists, so in engineering, tension is considered positive.) As a practical matter in structural geology,  $\sigma_n$  in the earth's crust is always positive and will therefore always plot on the positive (right) side of the vertical axis of the Mohr diagram.

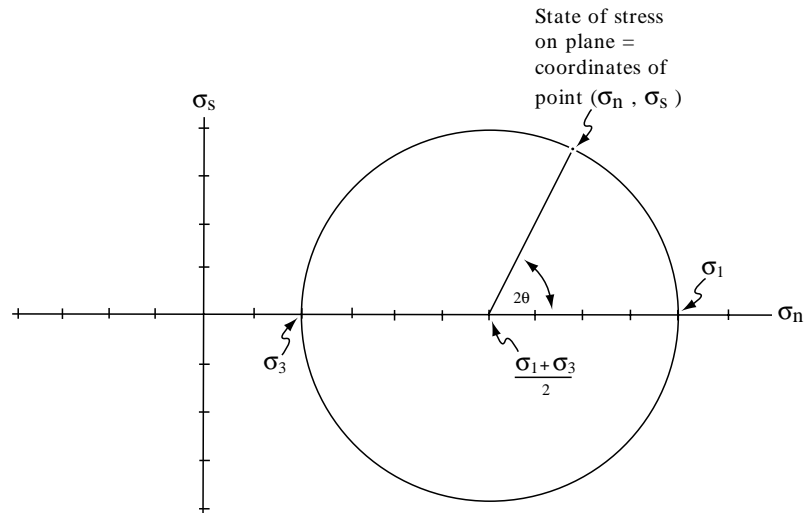
The vertical axis of the Mohr diagram, like the horizontal axis, has a positive and a negative direction. Shearing stresses that have a sinistral (counterclockwise) sense (Fig. 13.3a) are, by convention, considered positive and are plotted above the origin. Dextral (clockwise) shearing stresses (Fig. 13.3b) are plotted on the lower, negative half of the diagram.

**Problem 13.2**

Plane I in Fig. G-33a has been plotted on the Mohr diagram in Fig. G-33b. Determine the normal and shear stresses on planes 2 through 5 and plot them on the Mohr diagram. (Recall that trigonometric functions of angles in the second and fourth quadrants are negative, e.g.,  $\cos 180^\circ = -1.0$ .)



**Fig. 13.3** Conventional signs assigned to shearing stresses for the purpose of plotting on the Mohr diagram. Sinistral shearing (a) is considered positive; dextral shearing (b) is considered negative.



**Fig. 13.4** Main features of the Mohr circle of stress. The Mohr circle is the set of states of stress on all possible planes in a two-dimensional stress field. The position on the circle of a given plane is determined by finding angle  $\theta$  (the angle between the plane and  $\sigma_3$ ) and plotting  $2\theta$  on the Mohr circle. Planes with sinistral shear are plotted in the upper hemisphere; planes with dextral shear are plotted in the lower hemisphere.  $2\theta$  is always measured (up or down) from the  $\sigma_1$  intercept.

### The Mohr circle of stress

The five points you have plotted on Fig. G-33 in Appendix G (see Problem 13.2) should lie on a circle. A key feature of the Mohr diagram is that for a given set of principal stresses the points representing the states of stress on all possible planes perpendicular to the  $\sigma_1$ - $\sigma_3$  plane graph as a circle. This is called the *Mohr circle*. As seen in Fig. 13.4, the Mohr circle intersects the  $\sigma_n$  axis at values equal to  $\sigma_3$  and  $\sigma_1$ . The radius is  $(\sigma_1 - \sigma_3)/2$  and the center is at  $(\sigma_1 + \sigma_3)/2$ . Note how these expressions relate to equations 13.5 and 13.6.

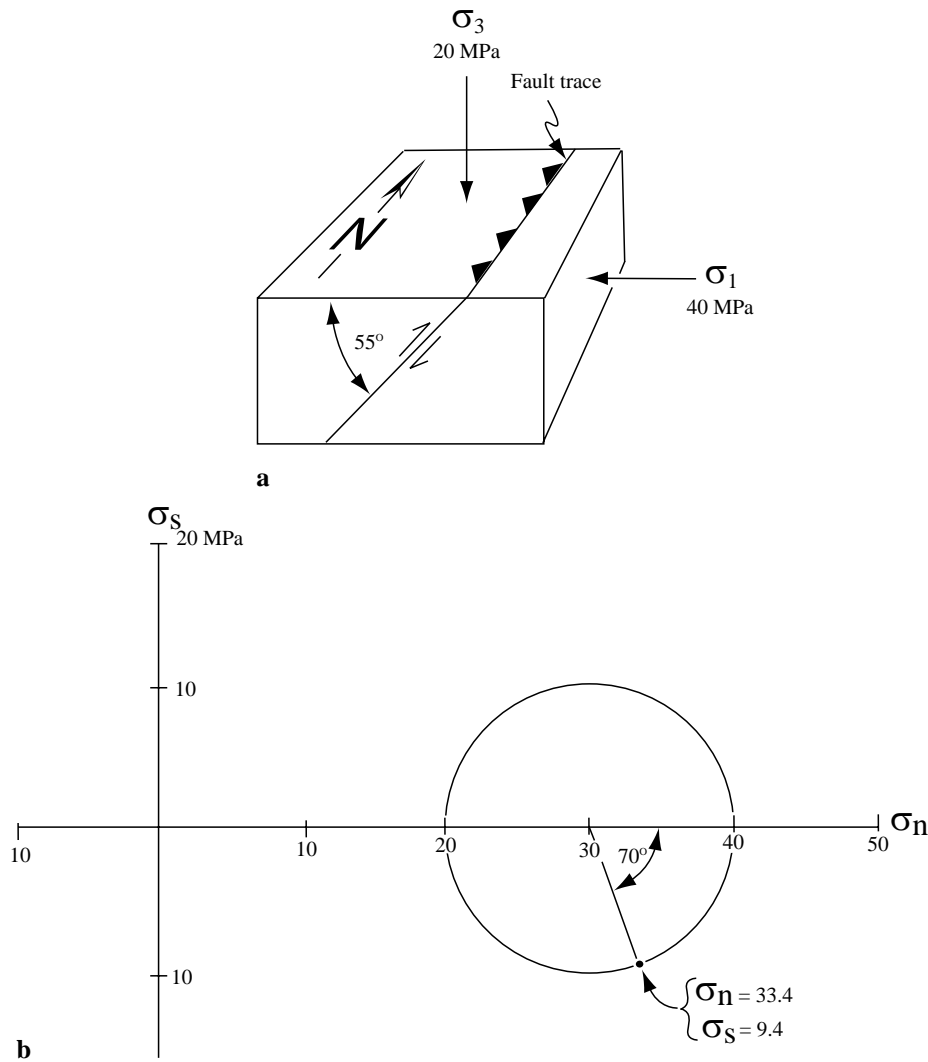
It is important to understand that the axes of the Mohr diagram have no geographic orientation. They merely allow the magnitudes of stresses on variously oriented planes to be plotted together. Planes perpendicular to either  $\sigma_1$  or  $\sigma_3$  (planes 3 and 5 of Fig. G-33) have no shear stress acting on them, so they plot directly on the  $\sigma_n$  axis. Shear stress is maximum on planes oriented  $45^\circ$  to the principal stress directions ( $\theta = 45^\circ$ ); the points representing these planes plot at the top and bottom of the Mohr circle.

Values of  $2\theta$  can be measured directly off the Mohr circle as shown in Fig. 13.4. The  $2\theta$  angles corresponding to planes with positive (sinistral) shearing lie in the upper hemisphere of the Mohr circle, while those corresponding to planes with

negative (dextral) shearing stresses lie in the lower hemisphere. In either case the angle  $2\theta$  is measured from the right-hand end of the  $\sigma_n$  axis.

The chief value of the Mohr circle of stress is that it permits a rapid, graphical determination of stresses on a plane of any desired orientation. Suppose, for example, that  $\sigma_1$  is oriented east-west, horizontal, and equal to 40 MPa, while  $\sigma_3$  is vertical and equal to 20 MPa. We want to find the normal and shear stresses on a fault plane striking north-south and dipping  $55^\circ$  west. The solution is as follows.

- 1 Figure 13.5a shows the geologic relationships. Before being concerned with the fault plane, construct a Mohr circle of stress for the given values of  $\sigma_1$  and  $\sigma_3$  (Fig. 13.5b).
- 2 Next determine the value and sign of angle  $2\theta$  for the fault plane. Angle  $\theta$  is the angle between the fault plane and  $\sigma_3$ , which in this case is  $35^\circ$ . So  $2\theta$  is  $70^\circ$ . Shearing stresses on this fault have a dextral or negative sense, so angle  $2\theta$  is located in the lower hemisphere of the Mohr circle (Fig. 13.5b).
- 3 The normal and shear stress coordinates corresponding to the points thus located on the Mohr circle are read directly off the horizontal and vertical axes of the graph. In this example  $\sigma_n$  is 33.4 MPa and  $\sigma_s$  is 9.4 MPa.



**Fig. 13.5** Mohr circle solution to a sample problem requiring the determination of  $\sigma_n$  and  $\sigma_s$  on a particular plane. (a) Block diagram. (b) Mohr circle solution.

**Problem 13.3**

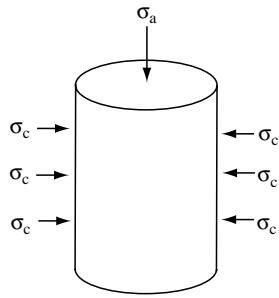
If  $\sigma_1$  is vertical and equal to 50 MPa, and  $\sigma_3$  is horizontal, east–west, and equal to 22 MPa, using a Mohr circle construction determine the normal and shear stresses on a fault striking north–south and dipping  $60^\circ$  east.

**The failure envelope**

Up to this point in this chapter we have examined the stresses acting on variously oriented planes. The main objective of all of this is to understand

or predict the orientation and magnitude of stresses that will cause a particular rock to fracture or “fail.” To begin our examination of brittle failure we will imagine an experiment in which a cylinder of rock is axially compressed (Fig. 13.6). Suppose that the radially applied *confining pressure*,  $\sigma_c$ , is kept constant at 40 MPa, while the *axial load*,  $\sigma_a$ , begins at 40 MPa and is gradually increased until the rock fails when the axial load reaches 540 MPa. The magnitudes of  $\sigma_a$  at several stages of this experiment are recorded in Table 13.1, and the corresponding Mohr circles are drawn in Fig. 13.7. In this type of experiment  $\sigma_a$  is analogous to  $\sigma_1$ , and  $\sigma_c$  is analogous to  $\sigma_3$ .

As shown in Fig. 13.7, a fracture experiment with constant confining pressure results in a series of progressively larger Mohr circles, all of which

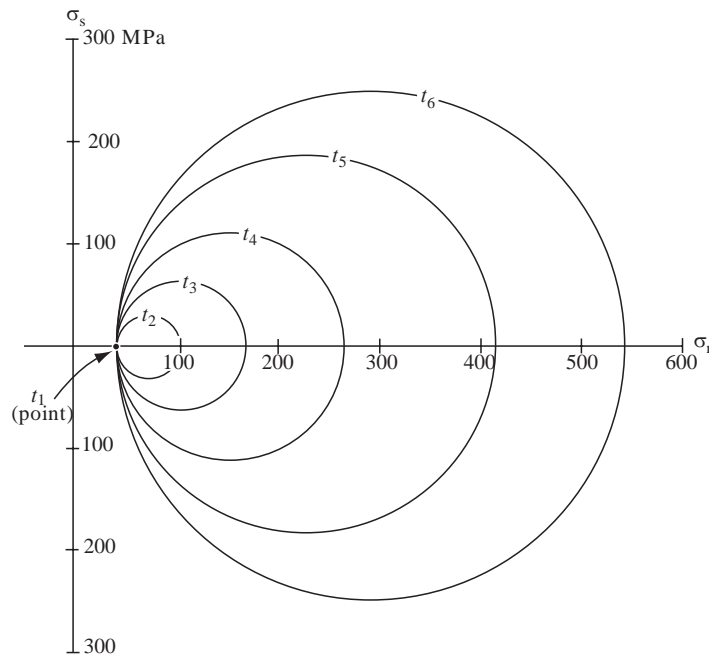


**Fig. 13.6** Schematic diagram of a rock-fracture experiment in which a cylinder of rock is axially compressed. The axial load ( $\sigma_a$ ) is steadily increased while the confining pressure ( $\sigma_c$ ) is kept constant.

**Table 13.1** Data from a hypothetical rock fracture experiment. Mohr circles corresponding to each recorded stage are drawn in Fig. 13.7.

Time	$\sigma_a$ (MPa)	$\sigma_c$ (MPa)	$\sigma_a - \sigma_c$ (MPa)
$t_1$	40	40	0
$t_2$	100	40	60
$t_3$	165	40	125
$t_4$	265	40	225
$t_5$	413	40	373
$t_6$	540	40	500 Failure

intersect the  $\sigma_n$  axis at  $\sigma_c$ . The *fracture strength* is the diameter of the Mohr circle ( $\sigma_a - \sigma_c$ ) when the rock fractures. In the experiment shown in



**Fig. 13.7** Mohr circles representing successive stages of the rock-fracture experiment recorded in Table 13.1.

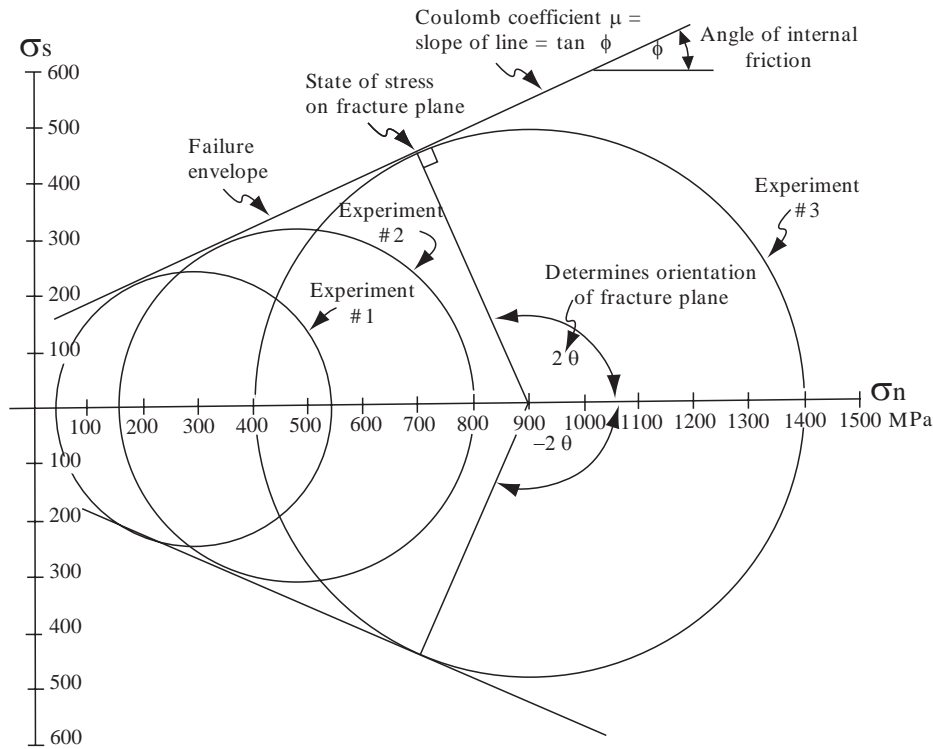
**Table 13.2** Data from three fracture experiments on identical rock samples. The Mohr circles at failure are drawn in Fig. 13.8.

Experiment no.	$\sigma_c$ (MPa)	$\sigma_a$ at failure (MPa)	$\sigma_a - \sigma_c$ (MPa)
1	40	540	500
2	150	800	650
3	400	1400	1000

Fig. 13.7 the fracture strength was determined to be 500 MPa at a confining pressure of 40 MPa.

Now, suppose we performed a series of three experiments on identical samples, but at different confining pressures. We would find that the fracture strength of the rock increases with confining pressure. Table 13.2 lists the results of our hypothetical series of experiments, with Experiment 1 being the one discussed above and graphed in Fig. 13.7. In Experiment 2 the confining pressure was raised to 150 MPa, and in Experiment 3 to 400 MPa. In Fig. 13.8 the three resulting Mohr circles are drawn. Because each experiment in this series has a higher confining pressure than the previous one, the Mohr circles at failure become progressively larger.

The Mohr circles at failure under different confining pressures together define a boundary called the *failure envelope* for a particular rock



**Fig. 13.8** Main characteristics of a failure envelope. The envelope is defined by Mohr circles at failure of identical rock samples under different confining pressures. The data for these three envelopes are recorded in Table 13.2.

(Fig. 13.8). The failure envelope is an empirically derived characteristic that expresses the combination of  $\sigma_1$  and  $\sigma_3$  magnitudes that will cause a particular rock (or manmade material such as concrete) to fracture. If the Mohr circle representing a particular combination of  $\sigma_1$  and  $\sigma_3$  intersects the material's failure envelope, then the material will fracture; if the Mohr circle does not intersect the failure envelope the material will not fracture.

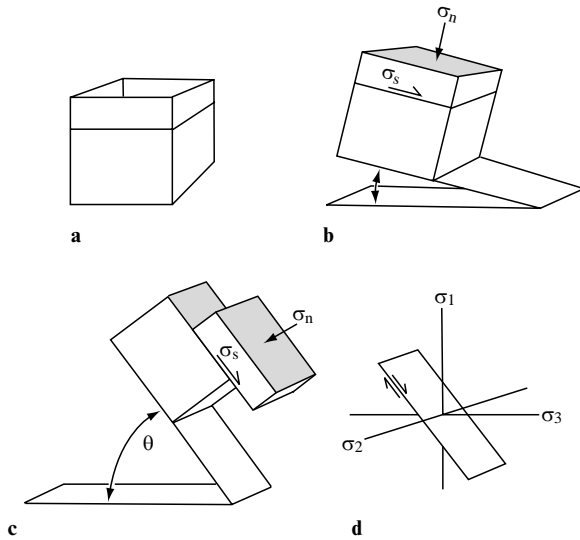
The failure envelope also allows us to predict the orientation of the macroscopic fracture plane that will form when the rock fails. In an isotropic rock this will be the plane that has a state of stress represented by the point on the Mohr circle that lies on the failure envelope (Fig. 13.8). The angle between this plane and the  $\sigma_3$  direction (angle  $\theta$ ) can be determined by measuring angle  $2\theta$  directly off the Mohr diagram. In the example shown in Fig. 13.8, angle  $2\theta = 114^\circ$ , so the fracture plane will be oriented  $57^\circ$  from  $\sigma_3$ .

At intermediate confining pressures the fracture strength usually increases linearly with increasing confining pressure, producing a failure envelope with straight lines, as in Fig. 13.8. The angle between these lines and the horizontal axis is called the *angle*

*of internal friction*,  $\phi$  (phi), and the slope of the envelope is called the *Coulomb coefficient*,  $\mu$  (mu):

$$\mu = \tan \phi \quad (13.7)$$

It is helpful to develop a familiarity with the Coulomb coefficient. This is a measurable property of the rock, like specific gravity, and indicates its fracture behavior at intermediate confining pressures within the earth's crust. The Coulomb coefficient is analogous to the coefficient of friction resisting the sliding of one block over another. Consider a bottomless box sitting on top of another box (Fig. 13.9a). If the two boxes are filled with dry sand, it would be possible, by pushing sideways on the upper box, for a shear surface to develop between the sand in the upper box and that in the lower box. With respect to this potential shear surface,  $\sigma_n$  can be imagined as the force keeping the sand together, and  $\sigma_s$  as the force trying to make the sand in the upper box slide (Fig. 13.9b). If the boxes are tilted, eventually an angle  $\theta$  is reached, at which point movement occurs on the shear surface (Fig. 13.9c). This is analogous to the angle  $\theta$  that we have been using for the angle between the shear plane and the  $\sigma_3$



**Fig. 13.9** Sandbox experiment for determining the cohesion properties of sand. (a) A bottomless box is placed over another box. (b) Both boxes are filled with sand and tilted. (c) Eventually an angle  $\theta$  is reached at which the upper box slides. In the experiment depicted here the material in the boxes is cohesionless dry sand, analogous to a Coulomb coefficient of zero and  $\theta = 45^\circ$ . (d) Orientation of the shear plane with respect to the principal stresses.

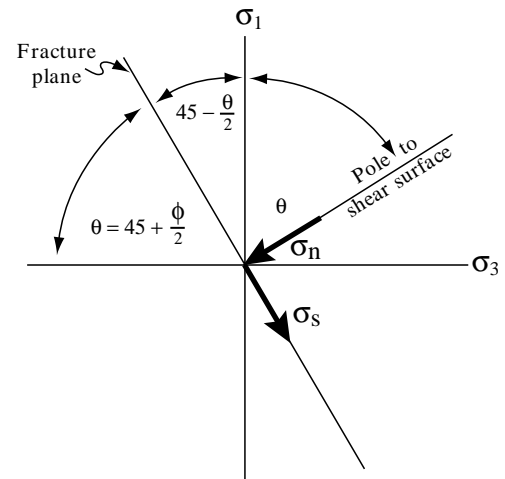
direction (Fig. 13.9d). The Coulomb coefficient is, in fact, sometimes called the *coefficient of internal friction*. The greater the Coulomb coefficient, the greater the resistance to fracture.

If the failure envelope plots as straight lines, which is typical of brittle materials at low confining pressures, then the Coulomb coefficient can be determined from a single fracture experiment, such as any of the three plotted in Fig. 13.8. Conversely, if the Coulomb coefficient of a rock is known, the orientation of the shear surfaces relative to  $\sigma_1$  and  $\sigma_3$  can be predicted. It can be seen on Fig. 13.8 that  $2\theta = 90 + \phi$ , or:

$$\theta = 45 + \phi/2 \quad (13.8)$$

Figure 13.10 summarizes the relationships between  $\sigma_1$ ,  $\sigma_3$ ,  $\theta$ ,  $\phi$ ,  $\sigma_n$ ,  $\sigma_s$ , and the fracture plane.

A material having a Coulomb coefficient  $\mu$  equal to zero would have an angle of internal friction  $\phi$  equal to zero, and  $\theta = 45^\circ$ . Plastic materials (see Chapter 12) behave this way. As the value of  $\mu$  increases, angle  $\theta$  also increases. Measured values of  $\mu$  for nine rock units are listed in Table 13.3.



**Fig. 13.10** Generalized relationships between the principal stresses and angles  $\theta$  and  $\phi$ .

**Table 13.3** Coulomb coefficient  $\mu$  of nine rock units (from Suppe, 1985).

Formation	Coulomb coefficient
Cheshire Quartzite	0.9
Westerly Granite	1.4
Frederick Diabase	0.8
Gosford Sandstone	0.5
Carrara Marble	0.7
Blair Dolomite	0.9
Weatuck Dolomite	0.5
Bowral Trachyte	1.0
Witwatersrand Quartzite	1.0

### Problem 13.4

The results of four fracture experiments on samples of Rohan Tuff are recorded in the table below.

Experiment no.	$\sigma_c$	$\sigma_a$ at failure
1	14 MPa	87 MPa
2	42 MPa	164 MPa
3	70 MPa	242 MPa
4	99 MPa	321 MPa

- 1 Draw Mohr circles for each experiment, and draw the failure envelope.
- 2 Determine the Coulomb coefficient of the Rohan Tuff.
- 3 Determine the angle  $\theta$  that the fracture plane is predicted to form with the  $\sigma_3$  direction when a sample of Rohan Tuff fractures.

**Problem 13.5**

Suppose you are an engineering geologist designing a nuclear waste repository in the Rohan Tuff (see Problem 13.4). Figure 13.11 shows the general plan of the repository. It will be a large room, the ceiling of which is to be 20 m deep within the tuff. During excavation of the repository, cylindrical pillars of tuff 5 m in diameter will be left in place to support the 20 m of overburden. Determine the maximum spacing of pillars (center to center) sufficient to support the overlying tuff. The density of the tuff is 2.0 g/cm<sup>3</sup>. Assume that the confining pressure on the pillars is atmospheric pressure, 0.1 MPa. Clearly show how you got your answer.

**Wizard hint:** One way to approach this problem is to first use your failure envelope from Problem 13.4 to find the value of  $\sigma_1$  at failure when  $\sigma_3$  is 0.1 MPa. Convert this compressive strength to kg/m<sup>2</sup> (see Appendix E). Next, determine the weight per square meter of the overburden and the area of overburden that each pillar can support. Finally, determine the maximum allowable spacing of pillars.

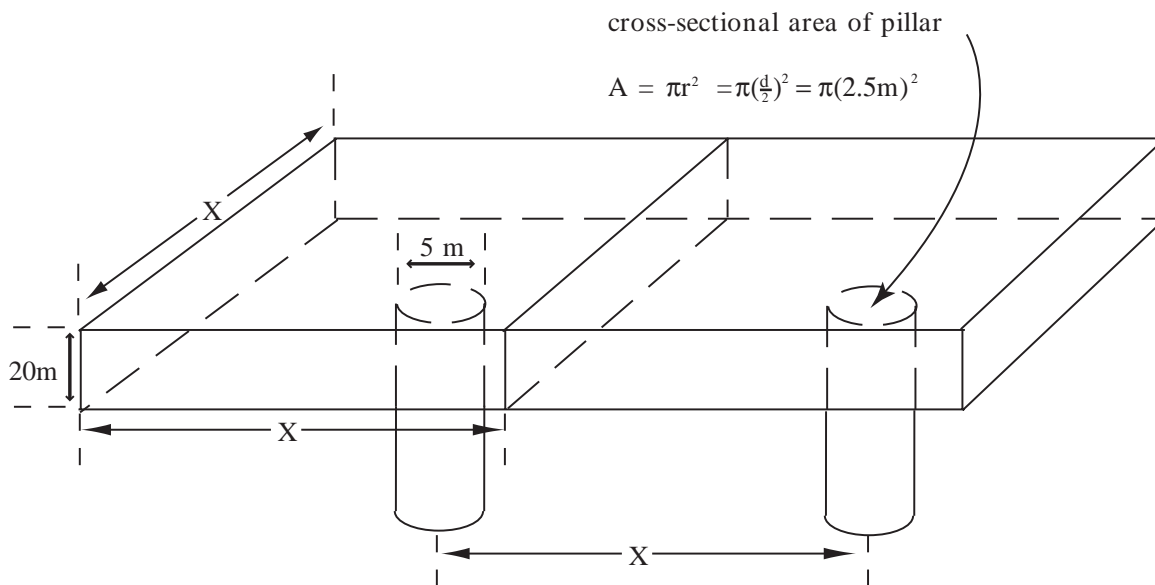


**Problem 13.6**

Figure G-34 shows a block of fine-grained limestone that was experimentally shortened by about 1% at room temperature. Four sets of fractures developed. Fractures of sets “a” and “b” are conjugate shear surfaces (the angular relationship between which can be measured directly on the diagram). Fractures of set “c” are extension fractures that formed during loading. Fractures of set “d” are extension fractures that formed during unloading when the orientation of  $\sigma_3$  became vertical in the rock-squeezing apparatus. Determine the Coulomb coefficient  $\mu$  for this rock.

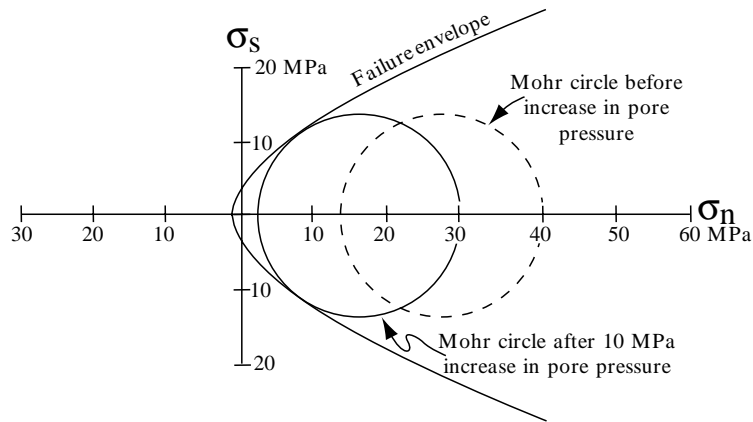
**The importance of pore pressure**

Many rocks contain a significant amount of pore space filled with fluids. These fluids support some of the load that would otherwise be supported by the rock matrix. Consider Fig. 13.12, which shows the failure envelope of a porous sandstone. This sandstone is subject to the following principal stresses:  $\sigma_1 = 40$  MPa and  $\sigma_3 = 13$  MPa. The dashed Mohr circle in Fig. 13.12 represents this state of stress. Now, suppose we add 10 MPa of pore pressure to the rock. This has the effect of lowering the principal stresses by 10 MPa. Fluid pressure is hydrostatic (equal in all directions), so



**Fig. 13.11** Schematic diagram for use in Problem 13.5.





**Fig. 13.12** Effect of pore pressure on brittle failure. The dashed Mohr circle is based on measured principal stresses. Pore pressure effectively translates the Mohr circle to the left, as indicated by the solid Mohr circle of effective stress.

all principal stresses are affected equally, but shear stress is unaffected. The Mohr circle remains the same size; it merely moves to the left on the horizontal axis a distance equal to the increase in pore pressure (Fig. 13.12).

The reduction of principal stresses by pore pressure is expressed through the term *effective stress*. The effective stress acting on the rock is the total (regional) stress minus the pore pressure.

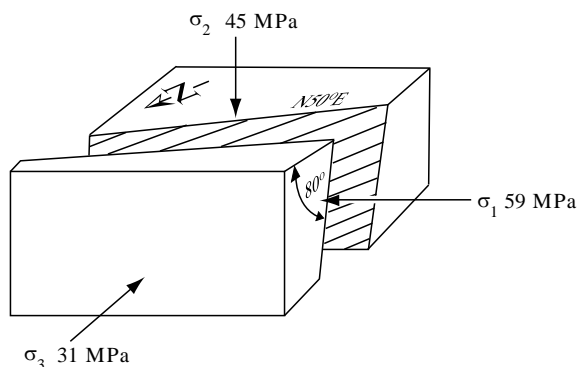
Notice that in Fig. 13.12 the solid Mohr circle (representing effective stress) intersects the failure envelope. The increase in pore pressure caused this rock to fracture. This phenomenon, called *hydraulic fracturing*, is routinely used to create

fractures in low-permeability rocks, thereby increasing the flow of water, oil, or gas.

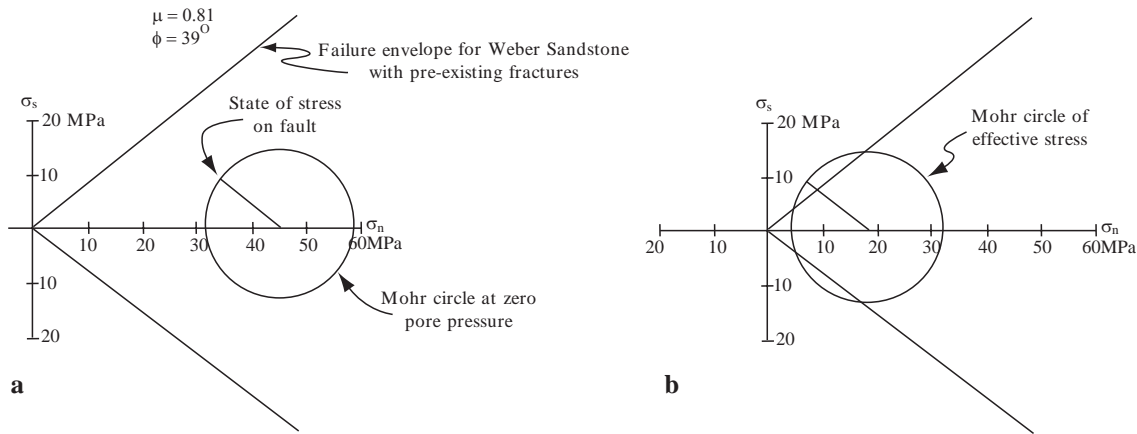
In addition to triggering the formation of new fractures, fluid pressure can be used to control movement and earthquakes on preexisting faults. This was first demonstrated in the 1960s when the US Army accidentally triggered some earthquakes near Denver by injecting wastewater into the ground. A controlled experiment was subsequently conducted by the US Geological Survey at Rangely, Colorado (Raleigh *et al.*, 1972). The geologic setting and principal stresses of this experiment are schematically depicted in Fig. 13.13. A preexisting oblique-slip fault in the Weber Sandstone was successfully activated when water was injected into the ground. Pore pressure was experimentally raised and lowered while seismicity was monitored.

Mohr circles for the Rangely experiment are shown in Fig. 13.14. Because movement was occurring on a preexisting fault in this case, the failure envelope is different from the normal envelope for intact rock. The failure envelope in Fig. 13.12 was derived from experiments with unfractured Weber Sandstone; the failure envelope in Fig. 13.14 was derived from experiments with previously cut samples.

In order to determine the state of stress on the fault shown in Fig. 13.13, the principal stress magnitudes ( $\sigma_1 = 59$  MPa,  $\sigma_3 = 31$  MPa) were resolved onto the fault plane in the direction of slip, yielding a normal stress of 35 MPa and a shear stress of 8 MPa. This state of stress is indicated on the Mohr circle in Fig. 13.14a. The injection of water into the rock created a pore pressure of 27 MPa, thereby reducing  $\sigma_1$  and  $\sigma_3$



**Fig. 13.13** Block diagram showing an oblique-slip fault that was experimentally activated at Rangely, Colorado, by increasing the pore pressure within the rocks. The principal stress magnitudes were determined from fluid-pressure measurements made during hydraulic fracturing. The fault plane is subject to a normal stress of 35 MPa and a shear stress of 8 MPa. After Raleigh and others (1972).



**Fig. 13.14** Mohr circles and failure envelope for Weber Sandstone at Rangely, Colorado. (a) Assuming zero pore pressure. (b) Mohr circle of effective stress after the injection of 27 MPa of fluid pressure, which triggered a series of earthquakes. The earthquakes ceased when the Mohr circle of effective stress was moved 3.5 MPa to the right.

to effective stresses of 32 and 4 MPa, respectively. The Mohr circle of effective stress, shown in Fig. 13.14b, is 27 MPa to the left of the pre-injection Mohr circle.

Notice in Fig. 13.14b that the point on the Mohr circle that represents the state of stress on the fault plane has crossed the failure envelope. Movement on the fault did indeed occur at this level of pore pressure. When the pressure was reduced by 3.5 MPa the earthquakes stopped. This is in impressive agreement with Fig. 13.14b, which indicates that if the Mohr circle is translated 3.5 MPa to the right, the state of stress of the fault lies directly on the failure envelope.

**Problem 13.7**

Figure G-35a shows the failure envelope of a “tight” (low-permeability) sandstone, which is a petroleum reservoir rock. If  $\sigma_1 = 72$  MPa and  $\sigma_3 = 42$  MPa, determine the amount of pore pressure that would be necessary to fracture this reservoir hydraulically.

**Problem 13.8**

Figure G-35b is a map showing the Johnson Valley Fault in southern California. This is a right-lateral strike-slip fault that lies a short distance to the north of the San Andreas Fault zone. On June 28, 1992, one of the largest earthquakes in recent decades occurred on the Johnson Valley Fault, a magnitude 7.5 event named the “Landers earthquake”. This large earthquake presumably released shear stress that had accumulated over a long period of time on the Johnson Valley Fault.

Some geologists have suggested that such an accumulation of shear stress on faults can be prevented by injecting water into the fault zone. By increasing the pore pressure, blocks on opposite sides of the fault are permitted to slip continuously past one another, rather than lurching episodically.

Determine the pore pressure required for a fault slip to occur on the Johnson Valley Fault. Regional  $\sigma_1$  in this area is oriented  $007^\circ$ , and estimated to be 10 MPa;  $\mu$  is 0.4 (Stein *et al.*, 1992). Assume  $\sigma_3$  to be 6 MPa. (Because the rocks are already fractured, draw your failure envelope with straight lines that meet at the origin of the graph, as in Fig. 13.14.)

## Strain Measurement

### Objectives

- Measure longitudinal and shear strain from deformed objects.
- Determine the orientation and relative dimensions of the strain ellipse from deformed objects.
- Determine in which of three strain fields a particular structure developed.

### Equipment needed for this chapter

- Play dough\*
- Card stock (such as 3 × 5 inch cards; exact dimensions are not critical; you will need a stack of cards about 5 cm thick)
- Protractor
- Metric ruler

Strain is a change of shape or volume, or both. One fundamental aspect of structural geology is the study of how rocks deform under different stresses. Our observations, however, are limited to the end product of rock deformation long after the stresses have disappeared. We never can really measure stress directly; all “stress determinations” are really

\* *Recipe for play dough: Mix together 1 cup flour, 1 cup water, 1 tablespoon cooking oil, 1/2 cup salt, 1 teaspoon cream of tartar, and food coloring as desired. Cook over medium heat until mixture pulls away from sides of pan and becomes doughlike. Knead until cool. Keeps about 3 months unrefrigerated.*

inferences based on strain. It is very important to thoroughly measure and characterize strain if we are to understand the deformational history of a particular region. In this chapter we will measure strain several different ways, starting with changes in the lengths of lines (longitudinal strain) and changes in the angles between intersecting lines (shear strain). We will also examine how it may be possible to distinguish between the two end-member strains — coaxial and noncoaxial strain.

### Longitudinal strain

If the original length of a line is known, then a comparison may be made between the original length ( $l_0$ ) and the deformed length ( $l_1$ ). This value is called the *extension* ( $e$ ) of the line. It is the proportional change in unit length:

$$e = \frac{l_1 - l_0}{l_0}$$

Notice that if  $l_1$  is greater than  $l_0$  then  $e$  will be positive, and if  $l_1$  is less than  $l_0$  then  $e$  will be

negative. For a line that is stretched to twice its original length,  $e = 1.0$  (100% has been added). For a line that is contracted to half its original length,  $e = -0.5$  (50% has been eliminated). Throughout this chapter it will be assumed that undeformed lines have a length of 1 unit. After extension their length may be defined as  $1 + e$ . This parameter is defined as the stretch,  $S$ .

### Shear strain

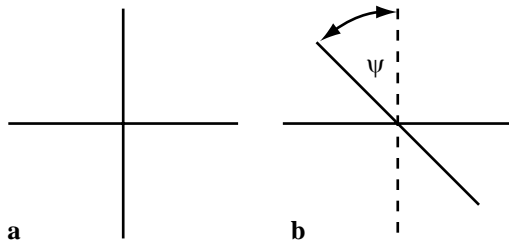
If the original shape of a deformed object is known, then changes in angular relationships can be measured. *Angular shear*, symbolized by the Greek letter  $\Psi$  (psi), is the angular change after deformation of two lines that were originally perpendicular (Fig. 14.1). *Shear strain*, symbolized by the Greek letter  $\gamma$  (gamma), is the tangent of angular shear:

$$\gamma = \tan \Psi$$

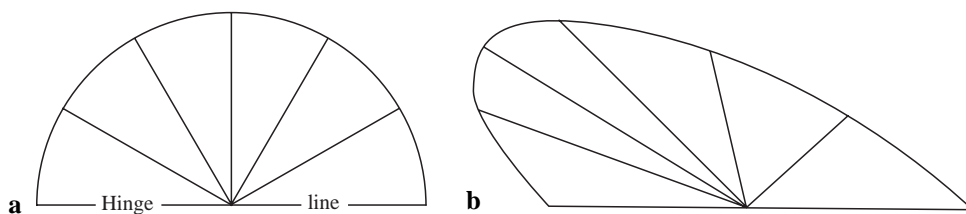
#### Problem 14.1

Figure 14.2 shows a diagrammatic brachiopod shell before deformation (Fig. 14.2a) and after deformation (Fig. 14.2b).

- 1 Determine the extension  $e$  of the hinge line.
- 2 Determine the angular shear  $\Psi$  and the shear strain  $\gamma$  of the shell.



**Fig. 14.1** Shear strain measured as angular shear ( $\Psi$ ). (a) Before deformation. (b) After deformation.



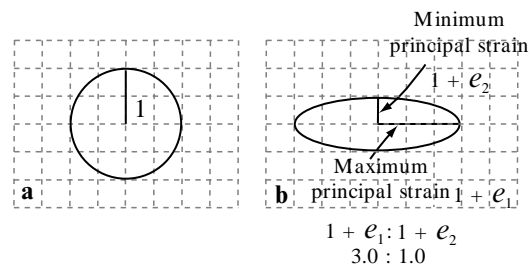
**Fig. 14.2** Schematic brachiopod. (a) Undeformed. (b) Deformed. For use in Problem 14.1.

### The strain ellipse

Deformation in rocks is described in terms of the change in shape or size of an imaginary sphere. During homogeneous deformation the imaginary sphere within the rock becomes an ellipsoid. Before considering three-dimensional deformation, however, it is instructive to examine deformation in two dimensions.

Imagine a plane containing a circle. Upon deformation, the circle becomes an ellipse (Fig. 14.3). This ellipse is called a *strain ellipse*, and its orientation and dimensions characterize the deformation of the plane in which it lies. Figure 14.3a contains a circle from which the strain ellipse develops; it is always, by convention, given a radius of 1 arbitrary unit. Figure 14.3b contains the strain ellipse representing the deformed circle.

The strain ellipse is described in terms of the two *principal strains*, which correspond to the semi-major and semi-minor axes of the strain ellipse. The lengths of the maximum and minimum principal strains are  $1 + e_1$  and  $1 + e_2$ , respectively. The shape of the ellipse is described by the ratio of the principal strains, which in this example is 3 : 1.



**Fig. 14.3** The strain ellipse. Beginning with a circle with a radius of 1 unit (a), the strain ellipse develops with maximum and minimum principal strain axes (b).

### Problem 14.2

Figure G-36 (Appendix G) contains four photographs of slabs of a breccia from the Alps. The sample in photograph G-36a is undeformed; Fig. G-36b-d show slabs of this same breccia from nearby localities where it has been deformed. The scale is the same in all photographs.

On each of the three photographs of the deformed breccia, measure the long and short axis of at least five clasts. Calculate the mean for each axis to determine the  $1 + e_1 : 1 + e_2$  ratio of the strain ellipse. Write the ratio in the space provided below each photograph.

Next to each photograph is a square. A circle has been drawn in the square adjacent to the undeformed sample. Within each of the other three squares sketch a properly proportioned strain ellipse for the rock sample.

### Three strain fields

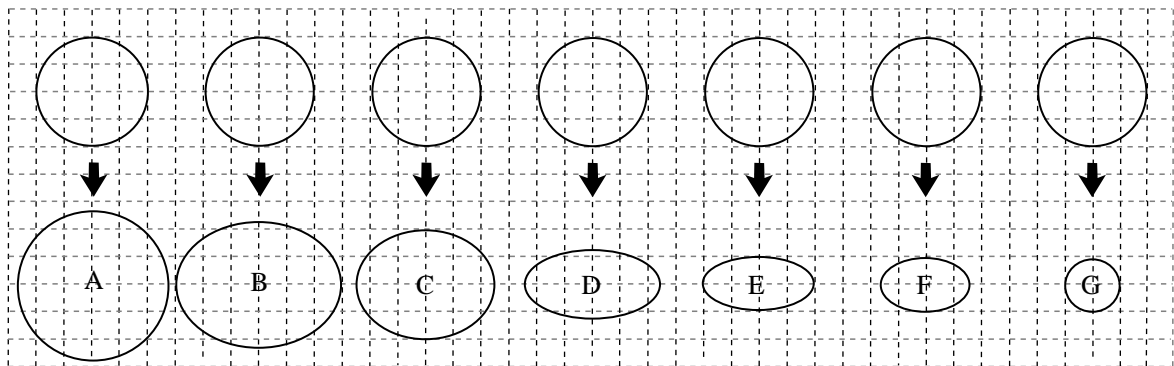
Strain ellipses may occur in a variety of shapes. In Fig. 14.4 there are seven circles of radius 1, and the strain ellipse that has developed from each. In Fig. 14.5 is a graph in which  $1 + e_2$  is plotted against  $1 + e_1$ . The undeformed circle is shown at  $1 + e_2 = 1.0$  and  $1 + e_1 = 1.0$ . Before reading further, plot the letter of each of the seven strain ellipses of Fig. 14.4 onto its appropriate position on Fig. 14.5. You will probably have difficulty understanding the following discussion if you do not take the time to do this.

The seven strain ellipses that you have plotted on Fig. 14.5 represent seven generalized classes. Notice that no ellipse can ever be plotted above the diagonal line on the graph, because  $1 + e_1$  is always greater than or equal to  $1 + e_2$ . The diagonal line is the locus of all strain ellipses that are not ellipses at all; they are circles. "Ellipse" A, which exhibits equal elongation in all directions, and "ellipse" G, which exhibits equal contraction in all directions, both plot on this line.

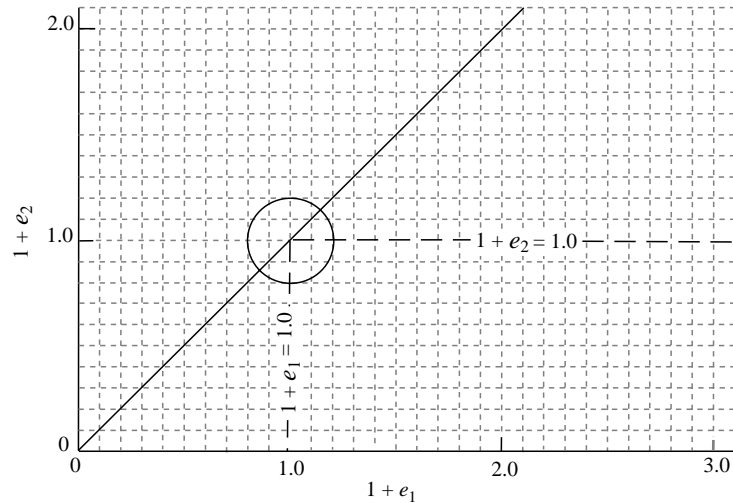
The graph of Fig. 14.5 can be divided into three fields with the  $e_1 = 0$  and  $e_2 = 0$  lines acting as dividers. Field 1 includes all ellipses in which both principal strains have positive extensions, such as ellipse B in Fig. 14.4. Field 2 includes ellipses in which  $e_1$  is positive and  $e_2$  is negative, such as ellipse D in Fig. 14.4. And field 3 includes ellipses in which both  $e_1$  and  $e_2$  are negative, such as ellipse F in Fig. 14.4. Figure 14.6 summarizes the characteristics of each of the three fields.

Layered rocks may develop structures that are useful for determining the characteristics of the strain ellipse and the field in which it developed. Some layers have a higher viscosity than other layers and are therefore less inclined to flow. When elongated, such stiff layers break up or are stretched into clumps, while the less viscous layers flow around them. The result is the formation of sausage-shaped structures called *boudins* of the stiff layers surrounded by the lower viscosity material. This process is called *boudinage*. Figure 14.7 is a photograph of boudins in cross section.

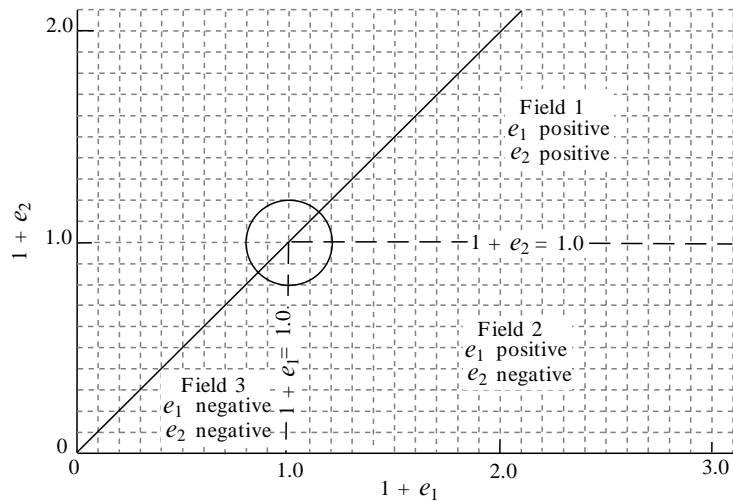
If the viscosity of a rock does not allow it to deform in a ductile manner, then fractures commonly develop during elongation. Such fractures will be oriented perpendicular to the maximum principal strain. Boudinage, fractures, fold geometry, and other products of deformation can often be used to determine the strain field in which a



**Fig. 14.4** Seven circles and their corresponding strain ellipses. The seven strain ellipses should be plotted on the graph in Fig. 14.5.



**Fig. 14.5** Graph on which  $1 + e_2$  is plotted against  $1 + e_1$  for a given strain ellipse.



**Fig. 14.6** Graph on which  $1 + e_2$  is plotted against  $1 + e_1$ , showing three fields.

deformed rock lies. Figure 14.8 shows the types of structures that develop in each of the three strain fields. Study this diagram carefully, and make sure that you understand why each structure exists where it is shown.

### Problem 14.3

For each of the three photographs in Fig. G-37 do the following:

- 1 Decide which field the strain ellipse lies in, and give your reasons. Refer to Fig. 14.8 for assistance.
- 2 The circle next to each photograph represents the strain ellipse prior to deformation. Superimpose an approximation of each rock's post-deformation strain ellipse on the circle.

### The coaxial deformation path

Up to this point we have viewed strain ellipses as the final products of deformation. It is important to see how the strain ellipse develops as deformation proceeds. We will limit our examination to strain ellipses that lie in field 2, because these are the most common. Even with this restriction, however, strain ellipses may develop in an infinite number of ways. We will examine in some detail only the two simplest.

#### Experiment 14.1: Coaxial strain in play dough

The simplest possible strain ellipse forms by compressing a circle. An ellipse made this way in play dough is convenient for study. Record the results of this experiment on the table provided in the



**Fig. 14.7** Boudinage in cross section. From the collection of O. T. Tobisch.

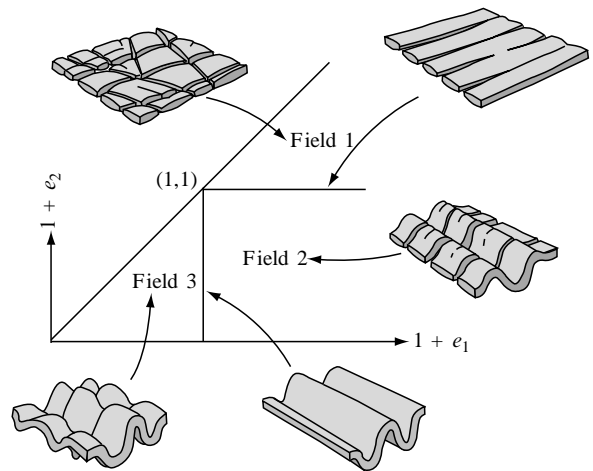
upper part of Fig. G-38 (Appendix G). (This experiment may also be simulated by using graphics software that permits you to deform objects. One useful example of such a program is *StrainSim*, available on the website of Cornell University geology professor Richard Allmendinger who has graciously made it available to the geological community: <http://geo.cornell.edu/geology/faculty/RWA/maintext.html>.)

Flatten a slab of play dough and impress into it a circle several centimeters in diameter. A jar lid or drinking glass can be used as a circle press. With a straightedge, inscribe two perpendicular lines through the center of the circle, as in Fig. 14.9. These two perpendicular lines are to be the lines of principal strain as the strain ellipse develops. Measure and record the radius of the circle. This measurement is  $l_0$  for both axes of the strain ellipse. You need to know  $l_0$  to compute  $e$ , but the radius of the circle is arbitrarily given a length of 1.0.

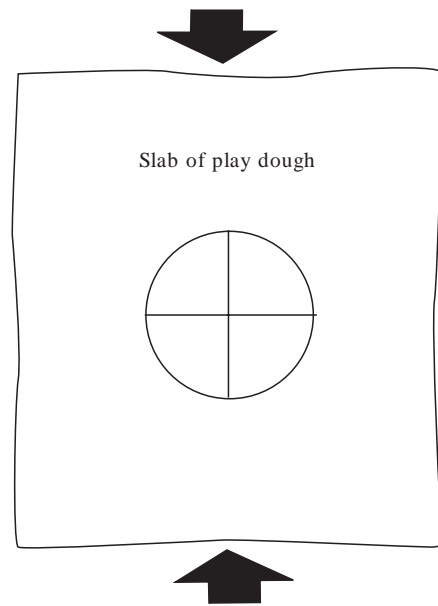
Compress the slab a small but measurable amount parallel to one of the two lines. Measure the lengths of the semi-major axis and semi-minor axis of the resultant ellipse and determine  $e_1$  and  $e_2$ . Proceed to fill in the table as you deform the play dough in small increments. After measuring the dimensions of six such ellipses, graph the strain path on the graph below the table.

The strain exhibited by the play-dough strain ellipse is called *coaxial strain* because the principal axes of strain do not change their orientation with respect to the material being deformed. In contrast, during *noncoaxial strain* the principal axes rotate with respect to the material being deformed. We will examine an example of noncoaxial strain later in the chapter.

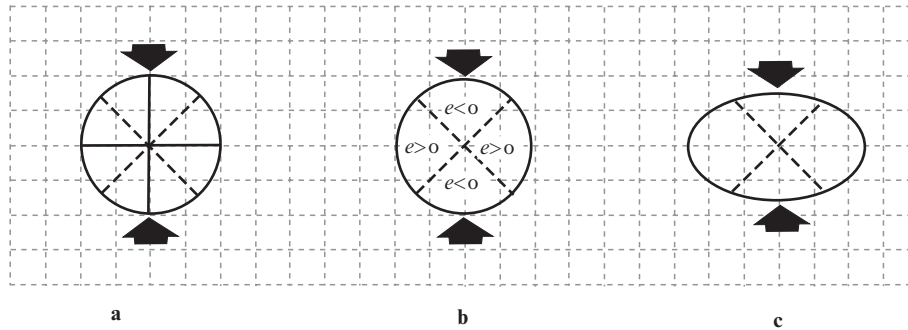
The type of deformation path you observed in Experiment 14.1 is sometimes referred to as *pure shear*, which is defined as coaxial strain with no change in volume, although some authors consider the constant-volume requirement unnecessarily restrictive. You could check to see if your play-dough ellipse maintained its surface area by comparing the area of the undeformed circle with that of the ellipse.



**Fig. 14.8** The three strain fields, as in Fig. 14.6, showing the types of structures predicted to occur in each strain field. After Ramsay (1967).



**Fig. 14.9** Circle and lines impressed into play dough at the beginning of Experiment 14.1.



**Fig. 14.10** Coaxial strain, in which the principal strain axes do not rotate during deformation. (a) The solid lines are the strain axes. (b) The dashed lines represent both material lines impressed into the play dough and geometric lines that separate the zone of compression from the zone of extension. (c) During deformation the geometric-zone boundaries (dashed lines) do not move, while the material lines (not shown) rotate into the zone of extension.

Now that you have graphed a coaxial deformation path, we will take a closer look at other properties of coaxial strain. For the purpose of discussing the evolution of the strain ellipse, it will be useful to distinguish between *material* lines, such as the lines you pressed into the play dough, and *geometric* lines, such as the boundaries between the zone of shortening and the zone of elongation.

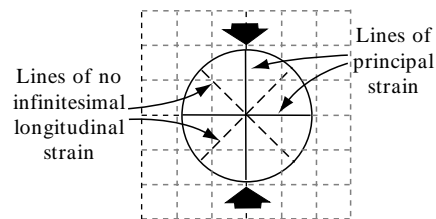
#### **Experiment 14.2: Lines of no infinitesimal longitudinal strain**

Re-form your play-dough slab, and impress a circle into it once again. As before, impress on the circle two perpendicular lines that will be the axes of principal strain. Now impress two more perpendicular lines on the circle so that they make  $45^\circ$  angles with the first pair, as shown in Fig. 14.10a. Deform the play dough as in Experiment 14.1, and pay close attention to the fate of the second pair of lines.

At the onset of deformation the second pair of perpendicular lines divide the circle into zones of shortening and elongation (Fig. 14.10b). These material lines rotate into the zone of elongation during deformation, but the zone boundaries themselves do not move during the evolution of the strain ellipse. As shown in Fig. 14.10c, the percentage of the ellipse's area in the elongation zone increases at the expense of the percentage in the shortening zone, but the boundaries of the two zones remain perpendicular to one another and at  $45^\circ$  to the principal strain axes.

The development of the strain ellipse in any single deformational event is a continuous process, but it may be analyzed in small increments called *incremental strain ellipses* or *infinitesimal strain*

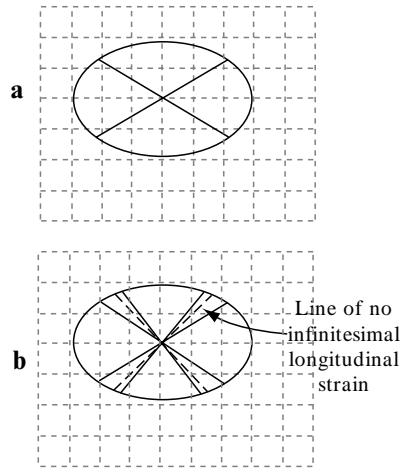
*ellipses*. The geometric lines that separate the zone of elongation from the zone of shortening are called *lines of no infinitesimal longitudinal strain* (Fig. 14.11) because, for all infinitesimal strain ellipses,  $e = 0$  along these two lines. As the ellipse progressively develops, the material lines that occupy the lines of no infinitesimal longitudinal strain in one infinitesimal strain ellipse pass into the zone of elongation in the next increment.



**Fig. 14.11** Infinitesimal strain ellipse.

Your play-dough ellipse should now look something like the one in Fig. 14.12a. Impress two new lines onto your strain ellipse at the positions of no infinitesimal longitudinal strain, then impress two more lines across the center of the ellipse close to these lines but in the zone of shortening, as shown in Fig. 14.12b. This last pair of lines has, up until now, experienced only shortening. As you further deform your play dough, however, notice that these shortened lines become lines of no infinitesimal longitudinal strain for an instant, and then they begin to elongate. During deformation, some lines undergo continuous elongation, some shorten and then elongate, and some shorten continuously. Such behavior explains many features seen in deformed rocks.



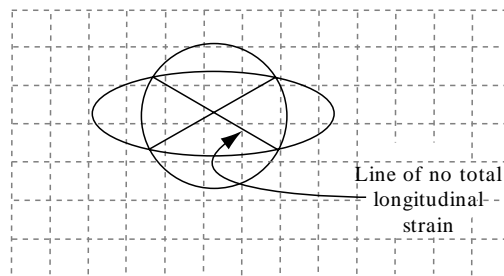


**Fig. 14.12** Shortening and lengthening of material lines. (a) Deformed play-dough ellipse with two sets of originally perpendicular material lines. (b) Same ellipse with two new sets of material lines.

### The coaxial total strain ellipse

Once deformation has ceased, we can call the strain ellipse a *total* or *finite strain ellipse*. Imagine impressing a unit circle into play dough and deforming it into an ellipse. Now imagine superimposing another unit circle on top of the ellipse, as in Fig. 14.13. Notice that two axes of the ellipse are also diameters of the circle. Regardless of how these lines might have shortened and elongated during the development of the strain ellipse, the net result is that they are the same length that they were before deformation began. These are called *lines of no total (or finite) longitudinal strain*. All axes of the strain ellipse that fall within the unit circle have undergone net shortening, while all of those that extend beyond the circle have undergone net elongation.

Now we can divide our coaxial total strain ellipse into four zones that characterize the deformation



**Fig. 14.13** Total strain ellipse with lines of no total longitudinal strain.

history of lines. Figure 14.14 shows these four zones on the coaxial strain ellipse, and Table 14.1 lists the structures that are predicted to form in each. Zone 1a, which includes lines that have only elongated, produces boudinage in competent beds. Zones 1b and 2 include lines that underwent early shortening followed by elongation; those in zone 1b ended up long; while those in zone 2 ended up short. In these two zones, folds that formed during the shortening stage become disrupted or unfolded during the elongation stage. Zone 3 includes lines that have been only shortened, producing folds with large amplitude and short wavelengths. Figure 14.15 shows a fold containing structures from all four zones.

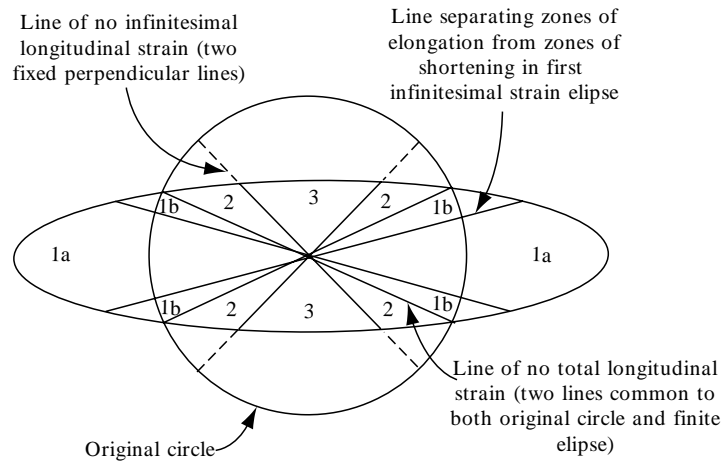
### Experiment 14.3: Superimposed total strain ellipses

Before setting the play dough aside, one more observation needs to be made. Impress a circle on a smooth slab of play dough and deform the circle into a distinct ellipse as before. Now squeeze the slab from a different direction. You will see that the total strain ellipse from the first strain regime becomes deformed into a different-shaped ellipse under a differently oriented strain field. Any strain ellipse, therefore, may be the product of any number of strain episodes of varying orientations. The possibility of multiple phases of deformation must always be considered in finite strain analysis.

### Problem 14.4

Figure G-39 shows a dike and sill complex in which a competent rock, colored black, has intruded into a schist. The horizontal lines represent cleavage in the schist. Consider the cleavage planes to be perpendicular to the minimum principal strain axis. Assume that all structures formed during the same deformational event.

- 1 What has been the approximate extension  $e$  perpendicular to the cleavage?
- 2 What has been the approximate extension  $e$  parallel to the cleavage?
- 3 Using the two extensions just determined and the structures seen in the dikes and sills, draw a properly proportioned and properly oriented strain ellipse for this rock. Label the zones within the strain ellipse, and give the  $1 + e_1 : 1 + e_2$  ratio.
- 4 Indicate the zone of the strain ellipse into which each of the two diagonal dike segments falls, and discuss briefly the strain history implied for each.



**Fig. 14.14** Coaxial total strain ellipse with four zones, each of which has a different deformation history. After Ramsay (1967).

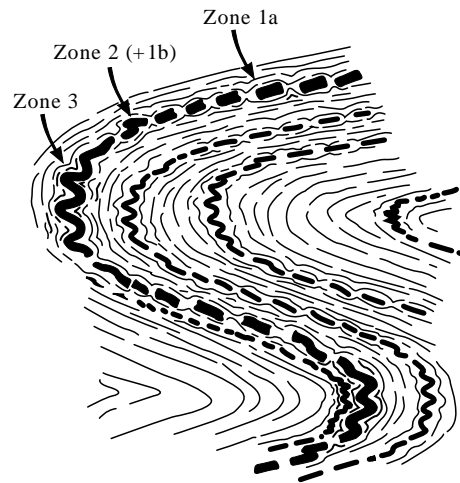
**Table 14.1** Coaxial total strain ellipse with four zones, each of which has a different deformation history. After Ramsay (1967).

Zone	Strain history	Structures in competent beds
1a	Lines that have been elongated only	Boudinage
1b	Lines that underwent early shortening followed by elongation (net lengthening)	Remnants of disrupted folds and isolated fold hinges
2	Lines that underwent early shortening followed by elongation (net shortening)	Folds that are becoming unfolded and boudinaged
3	Lines that have been shortened only	Folds with large amplitude and short wavelengths

### Noncoaxial strain

#### Experiment 14.4: The card-deck strain ellipse

Noncoaxial strain, in which the principal axes of strain change their orientation with respect to material lines, is easily demonstrated with a stack of cards about 5 cm or more in thickness. Ideally, a wooden box such as the one shown in Fig. 14.16

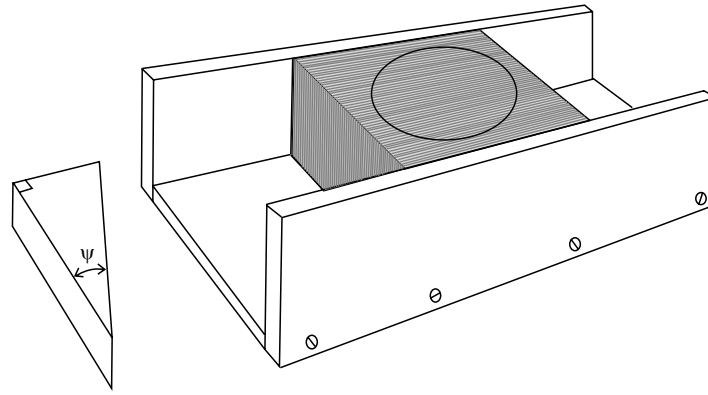


**Fig. 14.15** Fold developed by coaxial strain showing the structures in each zone. The maximum principal strain axis is vertical. From Ramsay (1967).

should be constructed to hold the cards during the experiment. This can also be done using the “skew” function of many graphics programs.

First, draw a circle on the edge of the cards. Using a straightedge, produce a uniform shear in one direction, thereby deforming the circle into an ellipse (Fig. 14.17). Deck-of-cards-type deformation is referred to as *simple shear*. Simple shear is noncoaxial, constant volume, two-dimensional deformation with no flattening perpendicular to the plane of slip. Notice that the ellipses produced by shearing the cards must all be of equal area because the component chords that lie on each card are of constant length.

An important aspect of simple shear, and noncoaxial strain in general, is the angle of shear of



**Fig. 14.16** Wooden-box apparatus to hold cards during noncoaxial strain experiments. After Ramsay and Huber (1983).

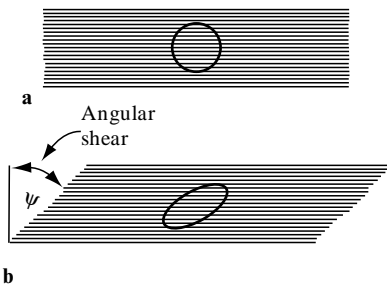
reference lines in the deforming rock. In this experiment you will measure the angular shear  $\Psi$ , as shown in Fig. 14.17b.

Deform the deck in small increments of  $\Psi = 10^\circ$ , and record the pertinent data on the table provided in the lower half of Fig. G-38. Then graph the deformation path of the ellipse on the graph below the table, as you did with the coaxial ellipse.

Compare the simple-shear strain path of the card-deck ellipse with the strain path of the play-dough ellipse. In fact, there should be very little difference between the two strain paths. The two processes are, however, quite different. As summarized in Fig. 14.18, the principal strain axes rotate within the stress field during noncoaxial strain; in coaxial strain they do not rotate.

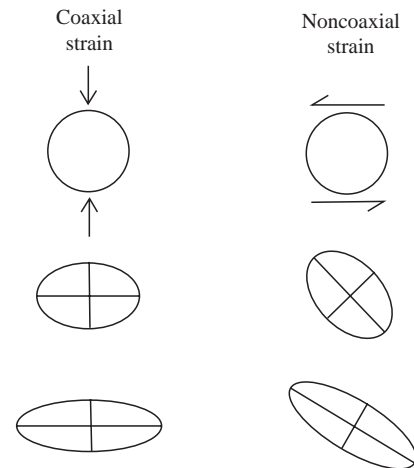
### The noncoaxial total strain ellipse

We will now examine some details of noncoaxial strain. As with the coaxial ellipse, this ellipse has two fixed, perpendicular boundaries between the zones of shortening and elongation. These are

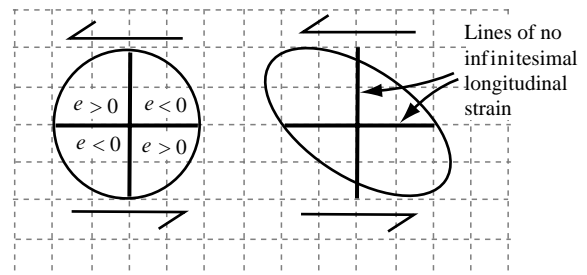


**Fig. 14.17** Noncoaxial strain demonstrated with a stack of cards. (a) Before deformation. (b) After deformation, showing angular shear.

the lines of no infinitesimal longitudinal strain, and they are parallel and perpendicular to the edges of the cards. Recall that these are geometric and not material lines. As with coaxial deform-



**Fig. 14.18** Comparison of coaxial and noncoaxial strain.



**Fig. 14.19** Noncoaxial-strain ellipse showing zones of shortening and elongation, and the lines of no infinitesimal longitudinal strain. Left, before deformation; right, after deformation.

ation, as the ellipse deforms, the area of the ellipse in the zone of elongation increases, while the area in the zone of shortening decreases (Fig. 14.19).

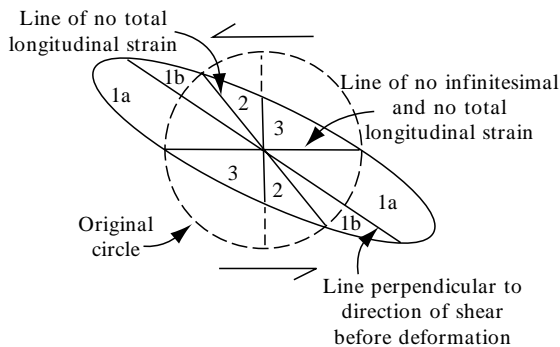
#### Experiment 14.5: The asymmetrically zoned noncoaxial ellipse

Square up your card deck and draw the lines of no infinitesimal longitudinal strain on the undeformed circle (Fig. 14.19). Deform the circle into a distinct ellipse, and draw a circle equal in diameter to the original circle symmetrically on the ellipse. Finally, draw in the lines of no infinitesimal longitudinal strain once again and also the lines of no total longitudinal strain, as in Fig. 14.14.

As summarized in Fig. 14.20, the noncoaxial ellipse can be divided into four zones based on the behavior of the lines. These zones correspond to those shown in Fig. 14.14 for the coaxial ellipse. Notice, however, the asymmetric arrangement of the zones on the noncoaxial ellipse. Because lines that are parallel to the shear direction are lines of no infinitesimal *and* no total longitudinal strain, zones 1b and 2 occur only on one side of zone 1a in the noncoaxial ellipse. This phenomenon is useful in attempting to determine whether or not rotation has been involved in the development of certain structures.

#### Problem 14.5

Figure 14.15 shows some folds and associated structures produced by coaxial strain. Sketch a similar drawing of structures produced by noncoaxial strain. You may find it useful to use two or three differently oriented planar surfaces.



**Fig. 14.20** Noncoaxial total strain ellipse showing four zones. Notice the asymmetric arrangement of the zones compared with those in the coaxial ellipse (Fig. 14.14). After Ramsay (1967).

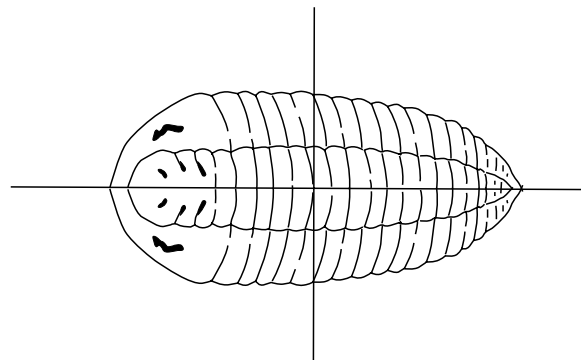
#### Deformed fossils as strain indicators

Many rocks are lithologically homogeneous and do not contain structures such as folds and boudins that reveal the strain. In such rocks, fossils or other objects with known starting shapes (e.g., ooids), can sometimes be used as strain indicators. If the undeformed size and shape of a fossil is precisely known, then the problem is merely one of measuring extensions and angular shear in different directions, as in Problem 14.1. Usually, however, it is impossible to reliably determine what the lengths of lines were before deformation. This problem can be partially overcome when several variously oriented individuals are present.

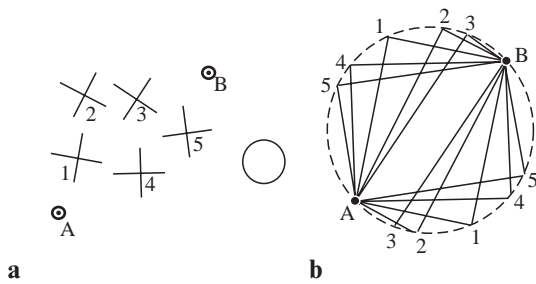
Fossils that are especially suitable for strain measurement are bilaterally symmetric ones such as brachiopods and trilobites. Trilobites, for example, have a central axis that divides the animal into mirror-image right and left sides (Fig. 14.21).

A technique developed by Wellman (1962) provides an elegant approach to the use of such fossils in strain analysis. Imagine five randomly oriented, undeformed trilobites on a slab of mudstone. These are represented by five sets of perpendicular lines in Fig. 14.22a. Points A and B are arbitrarily located points on the slab. Without changing the orientation of the lines, imagine translating each set of perpendicular lines to points A and B and lengthening the lines until they meet to form a rectangle. If this is done for all five sets of lines, the corners of the five rectangles lie on a common circle (Fig. 14.22b). This circle represents the strain ellipse prior to deformation.

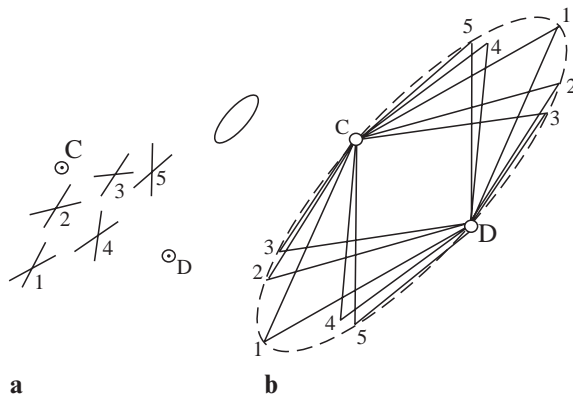
Now imagine five deformed trilobites on a slab, represented by five pairs of nonperpendicular lines (Fig. 14.23a). Points C and D are arbitrarily



**Fig. 14.21** Undeformed trilobite.



**Fig. 14.22** Wellman technique for determining strain ellipse. In this example the rock is not deformed, and the fossils are represented by perpendicular lines, as in Fig. 14.21. (a) Perpendicular lines representing five fossils. Points A and B are arbitrary points located on the rock slab. (b) The strain ellipse (dashed line) passes through the corners of the squares formed by extending perpendicular sets from points A and B. Because the rock is not deformed, the strain ellipse is a circle.



**Fig. 14.23** Using the Wellman technique on deformed fossils. (a) Five non perpendicular lines representing deformed fossils, with points C and D. (b) Strain ellipse (dashed line) drawn through the corners of the parallelograms.

located on the slab, and each pair of lines is translated to each point and extended, resulting in five parallelograms. The corners of the parallelograms define the strain ellipse (Fig. 14.23b).

To determine the axial ratio and orientation of the strain ellipse from a group of deformed fossils, follow these steps:

- 1 Draw two lines on each fossil. These lines represent perpendicular lines prior to deformation.
- 2 Place two points several centimeters apart on the photograph or drawing. The line between these two points should not be parallel to any of the lines you have drawn on the fossils.
- 3 Place tracing paper over the photograph, transfer the two points to the tracing paper,

and proceed to transfer the pairs of lines to the two points without rotating the tracing paper with respect to the photograph.

- 4 Sketch the ellipse that most closely fits the corners of the parallelograms.

### Problem 14.6

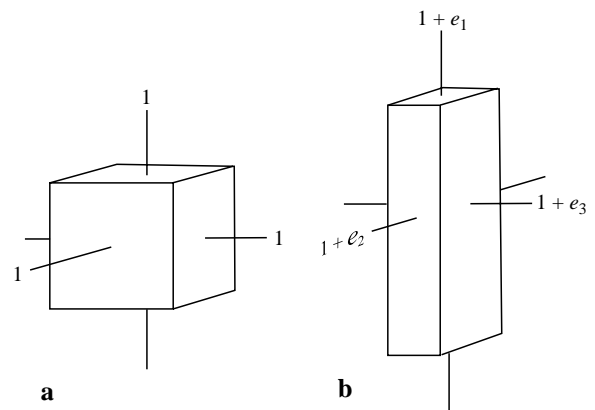
Figure G-40 is a photograph of an exposed bedding plane containing deformed portions of several trilobites.

- 1 Determine the strain ellipse for this rock.
- 2 Determine the  $1 + e_1 : 1 + e_2$  ratio and the orientation of the maximum principal strain with respect to north.

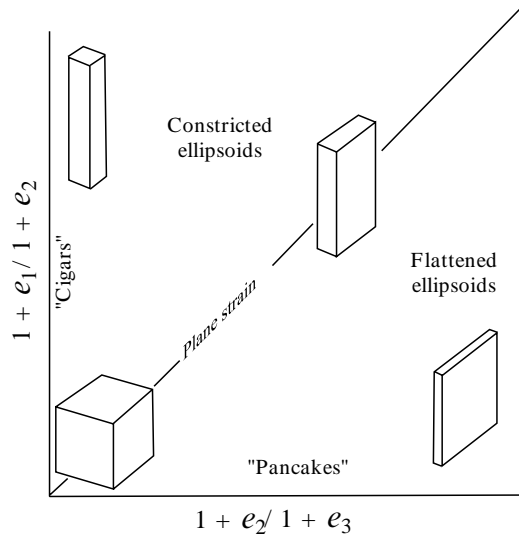
### Strain in three dimensions

Because rocks are three-dimensional objects, consideration must be made for the third dimension in describing and measuring strain. Undeformed rocks are imagined to contain a sphere that becomes an ellipsoid during homogeneous deformation. This is the *strain ellipsoid*, and its dimensions and orientation describe the strain in the rock.

The strain ellipsoid has three principal axes, the maximum, intermediate, and minimum principal strain axes. Their lengths are  $1 + e_1 \geq 1 + e_2 \geq 1 + e_3$ , respectively, with the original sphere having a radius of 1. Figure 14.24a shows an equidimensional, undeformed block. Figure 14.24b shows the same block after deformation, showing the principal strain axes. The graph in Fig. 14.25, in which  $(1 + e_1)/(1 + e_2)$  is graphed against  $(1 + e_2)/(1 + e_3)$ , displays the range of



**Fig. 14.24** The three principal strain axes. (a) Undeformed. (b) After deformation.



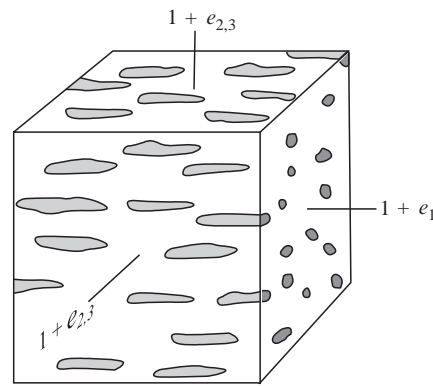
**Fig. 14.25** Flinn diagram. Two strain fields are divided by a plane-strain line along which  $e_2 = 0$  and volume is preserved. Constant volume pure shear and simple shear both fall on the plane-strain line.

strain ellipsoids. This graph, called a *Flinn diagram*, is divided into two fields by the plane strain line. *Plane strain* is deformation in which extension is zero on the intermediate principal strain axis. Above the plane strain line the ellipsoids are constricted, the ultimate being cigar-shaped ellipsoids in which  $1 + e_1 > 1 + e_2 = 1 + e_3$ . Below the plane strain line the ellipsoids are flattened, the ultimate being pancake-shaped ellipsoids in which  $1 + e_1 = 1 + e_2 > 1 + e_3$ .

The fabrics of deformed rocks may often be used to diagnose the orientation and shape of the strain ellipsoid. The rock depicted in Fig. 14.26, for example, contains pebbles that have been elongated during deformation. The strain ellipsoid is cigar-shaped in which  $1 + e_1 > 1 + e_2 = 1 + e_3$ . The principal strain axes are shown on the drawing.

#### Problem 14.7

On the four drawings of deformed rocks in Fig. G-41, indicate the orientations of the principal strain axes. Below each drawing indicate the relative lengths of the axes (e.g.,  $1 + e_1 > 1 + e_2 = 1 + e_3$ ).



**Fig. 14.26** Deformed conglomerate containing elongated pebbles. The consistent lineation in this rock indicates the orientation of the maximum principal strain axis. The equidimensional nature of the pebbles on the right-hand face indicates that  $1 + e_2 = 1 + e_3$ .

#### Quantifying the strain ellipsoid

Several techniques have been devised for quantifying strain. Most are beyond the scope of an introductory course. Ramsay and Huber (1983) is the source to be consulted for a more complete discussion of this topic. One technique that is, in principle, very simple involves the measurement of deformed objects in the rock. Pebbles in deformed conglomerate, for example, may be used this way, but a lack of original sphericity complicates the measurements.

A rock type that is particularly well suited to strain measurement is oolite, a limestone composed of spherical, sand-sized grains called ooids. Upon deformation, the spherical ooids become ellipsoidal and can be measured directly.

#### Problem 14.8

Figure G-42a is a sketch of a hand specimen of oolite. The orientations of the principal strain axes have been determined in the field on the basis of lineations, cleavages, and the shapes of the ooids. Two thin-sections have been cut perpendicular to two of the principal strain axes, and Fig. G-42b contains sketches of photomicrographs of each of the two thin-sections.

- 1 Measure the dimensions of several ooids and determine the arithmetic mean ( $\bar{x}$ ) of the semi-major and semi-minor axes in each field of view. Indicate the semi-major to semi-minor axes ratio for each field of view, and combine these ratios to find the  $1 + e_1 : 1 + e_2 : 1 + e_3$  ratio for the strain ellipsoid.
- 2 Plot the strain ellipsoid on the Flinn diagram in Fig. G-42c.



## Construction of Balanced Cross Sections

### Objectives

- Determine the relationship between the shapes of folds exposed at the earth's surface and the types of faults in the subsurface that produced these folds.
- Evaluate existing cross sections for balance.
- Construct retrodeformable, balanced cross sections in fold-thrust belts.

A geologic cross section depicts subsurface geology along a vertical profile. Cross sections are constructed from geologic maps, well data, seismic lines, and other geophysical data. Typically, a geologist can draw different cross sections that satisfy the available, and usually limited, data. This chapter introduces you to the construction of balanced, or restorable, cross sections. These techniques will help you draw cross sections that are geologically reasonable, and they will also help you evaluate published cross sections. Our discussion is limited to thrust belts, where the concepts of balanced cross sections were first developed and where the structural style is well understood. A different set of techniques is needed to balance cross sections in regions of extension.

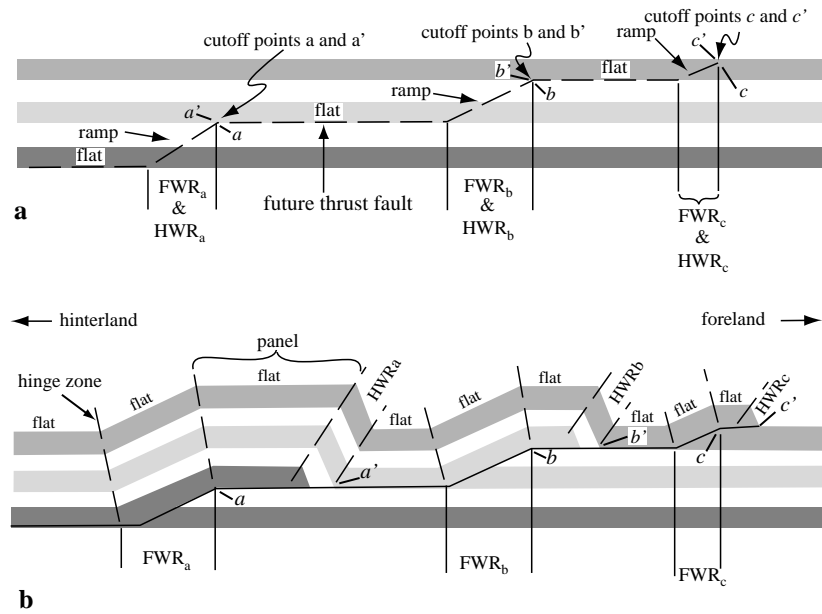
### Thrust-belt “rules”

Research in many thrust belts has revealed several recurring characteristics that can be synthesized into the following set of “rules” regarding the geometry and orientation of thrust faults. As with most rules in geology, there are notable

exceptions and variations; hence, these “rules” should be treated as guidelines only.

- Rule 1** Thrust faults follow a staircase trajectory marked by *flats* and *ramps*. Flats occur where a fault lies at a specific stratigraphic horizon for a great distance. Ramps occur where a fault cuts across stratigraphic contacts over a short distance (Fig. 15.1a); they usually dip at angles of less than 30°.
- Rule 2** Thrusts cut up section, most commonly in the direction of tectonic transport (left to right in Fig. 15.1b).
- Rule 3** The conditions that promote thrust faulting often result in the creation of multiple thrusts. The thrust system commonly propagates in the direction of slip; that is, new thrusts tend to form “in front of” or toward the *foreland* of existing thrusts. For this reason, thrusts tend to be progressively younger in the direction of tectonic transport (toward the foreland). However, “out-of-sequence” thrusts (younger faults that developed behind earlier





**Fig. 15.1** Schematic cross section showing typical elements of thrust terranes. (a) Pre-deformation cross section showing ramp-and-flat geometry of future thrust fault (dashed line). Letters *a*, *b*, and *c* show the positions of future footwall cutoffs at the tops of footwall ramps; *a'*, *b'*, and *c'* show the positions of future hanging-wall cutoffs at the tops of hanging-wall ramps. (b) Deformed-state cross section showing the relation of folds to thrust ramps and the new positions of hanging-wall cutoffs. Dashed lines are fold axial traces; FWR, footwall ramp; HWR, hanging-wall ramp. Notice that for each hanging-wall cutoff there is a corresponding footwall cutoff.

formed thrusts) have been recognized in many thrust belts and often play an important role in the evolution and movement history of thrust belts.

**Rule 4** Net slip along a thrust cannot increase upward. But it can decrease upward, provided that shortening is accommodated by folding or imbricate faulting.

**Rule 5** Thrusts may terminate upward, without reaching the earth's surface. Such faults are called *blind thrusts*, and they terminate in asymmetric folds. Thrusts that reach the surface are referred to as *emergent thrusts*.

### Recognizing ramps and flats

Thrust sheets are typically characterized by kink folds, which consist of “panels” and “hinges.” A panel is a portion of the hanging wall in which the bedding attitude is more or less constant over a large area. A hinge, or hinge zone, is the narrow zone between adjacent panels (Fig. 15.1b).

Carefully examine Fig. 15.1a and b; note the geometry of the thrust, paying particular attention to the geometry of the folds in the upper plate (hanging wall). Find point *a* on both diagrams. It

is the point in the footwall where the upper surface of the lower white bed has been cut by the thrust. Such a point is called a *cutoff point*. In three dimensions a cutoff point is a line, called a *cutoff line*.

Now find point *a'* on Fig. 15.1a and b. Prior to faulting, cutoff points *a* and *a'* lay adjacent to one another. Cutoff points *a*, *b*, and *c* all lie in the footwall, and each has a corresponding displaced point, *a'*, *b'*, and *c'*, in the hanging wall.

Notice in Fig. 15.1 that this thrust has three footwall ramps, labeled FWR<sub>a</sub>, FWR<sub>b</sub>, and FWR<sub>c</sub>. Footwall ramps are recognizable as portions of the lower plate (footwall) containing strata that have been diagonally truncated. Each footwall ramp must have a corresponding ramp in the hanging wall of the thrust.

Hanging-wall ramps and flats are defined by their positions *relative to bedding*. Ramps occur where the thrust fault cuts across bedding; flats are present where the thrust is parallel to bedding. For example, hanging-wall ramp HWR<sub>a</sub>, which corresponds to FWR<sub>a</sub>, is recognizable as the panel in the hanging wall in which the same strata that are diagonally truncated in FWR<sub>a</sub> are truncated in the direction of tectonic transport. Strata in hanging-wall-ramp panels typically dip in the direction of tectonic transport (toward the *foreland*). Examine

Fig. 15.1b, and be sure you understand why  $HWR_a$  is identifiable as the portion of the hanging wall that lay adjacent to  $FWR_a$  prior to faulting.

Flats are the panels between ramp panels. They do not contain truncated strata, either in the hanging wall or in the footwall. Displacement along the thrust fault may result in a hanging-wall flat coming to lie either parallel to bedding in the footwall or at an angle to bedding in the footwall. In the latter case, the bedding in the hanging wall typically dips in the direction opposite to the direction of tectonic transport (toward the *hinterland*) (Fig. 15.1b). It is important to remember that hanging-wall flats do not have to be horizontal, but they do not contain truncated strata. In Fig. 15.1b, all of the panels in the hanging wall that lie between hanging-wall-ramp panels are flats.

For each footwall flat there must be a corresponding hanging-wall flat, and both flats must be the same length. However, due to deformation of the hanging wall, a particular footwall segment may correspond to two or more adjacent panels in the hanging wall. Similarly, each hanging-wall ramp must have a corresponding footwall ramp of equal length. This is known as the “template” constraint.

The most important feature is the relationship between the fault and stratigraphy. If the fault stays at the same stratigraphic horizon in either the footwall or the hanging wall, then that portion of the footwall or hanging wall is a flat. If the fault cuts stratigraphically upward, then that portion of the hanging wall or footwall in which this occurs is a ramp.

### Problem 15.1

For each lettered panel on the cross section in Fig. G-43 (Appendix G), determine whether the panel in the hanging wall and the footwall directly below is a ramp or a flat. Write the term “ramp” or “flat” in the table provided; the first one has been completed for you. Next, determine which hanging-wall panel corresponds to each footwall segment. Do this by dropping a short line segment downward from the edge of each footwall ramp and flat; below each footwall segment, write the letter of the corresponding hanging-wall panel.  $A'$  has already been written below the leftmost footwall ramp on Fig. G-43, because that footwall segment corresponds to panel  $A$  in the hanging wall. Follow this format for panels B

through J. Be careful; there may be more than one hanging-wall panel for each footwall segment. Note that there are no footwall panels that correspond to hanging-wall panels K through O; their corresponding portions of the footwall lie to the right of the cross section.

### Relations between folds and thrusts

Research in thrust belts has shown that most folds are ultimately generated by fault movement at depth. There is a systematic and predictable geometric relation between a fold and the thrust that generated it. Thus, we can use the geometry of an exposed fold to infer the position and geometry of a fault at depth. The kink-like character of folds in thrust belts can be generalized in cross-section construction by use of the “kink-fold” method, which is described below. This method, developed in the early 1980s by John Suppe of Princeton University, assumes that the folds are produced by a flexure-slip mechanism so that bed thickness does not change. This assumption of constant bed thickness will be taken for granted throughout this chapter, but it must be established for each individual geologic situation.

Another assumption of the kink-fold method is that the footwall remains undeformed during the formation of folds in the hanging wall. This assumption is a necessary simplification of the real world; the relatively common occurrence of footwall synclines in thrust belts indicates that it is not exactly correct. If footwall folds are present in an area, they must be shown on the cross section, but they can be added after the kink-fold method has been applied.

Many folds in thrust belts are associated with underlying thrust ramps. Two types of ramp-related folds are the most common. These are *fault-bend folds* and *fault-propagation folds*, each of which is described below.

### Fault-bend folds

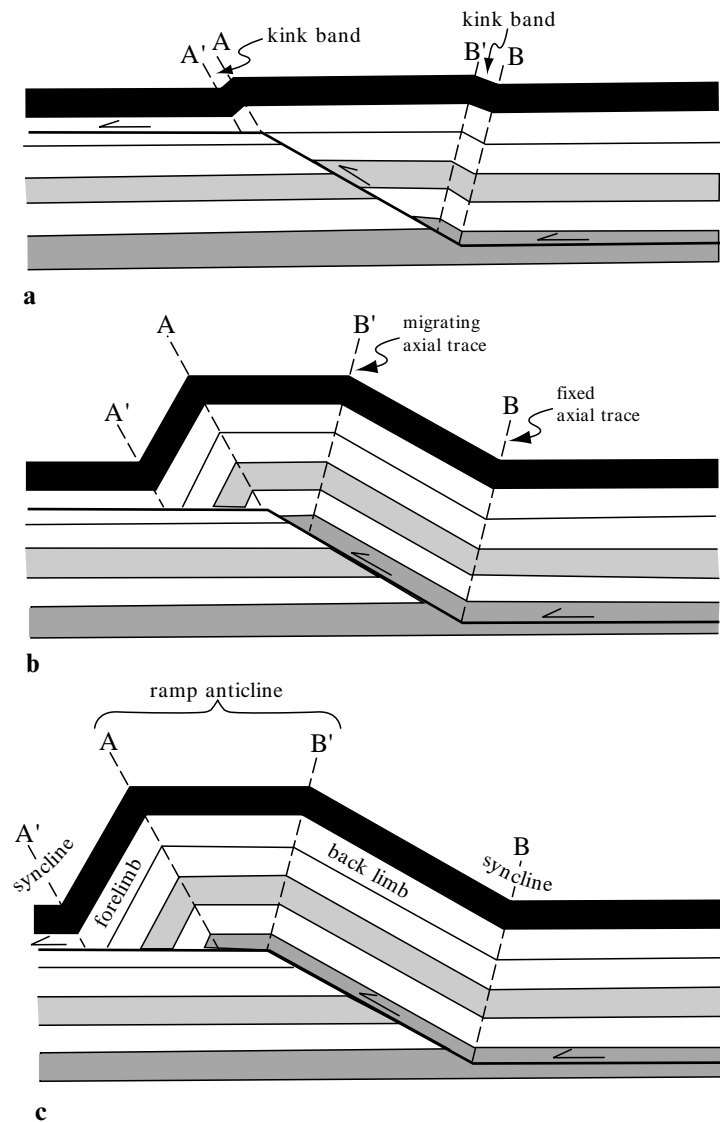
Fault-bend folds occur where a thrust fault steps up from a structurally lower flat to a higher flat. The folds in the hanging wall of Fig. 15.1b are all fault-bend folds. Figure G-44 (Appendix G) contains a series of drawings that can be cut up and compiled into a flipbook, permitting you to observe the evolution of a fault-bend fold and compare it with a fault-propagation fold.

Figure 15.2 shows the evolution of a fault-bend fold. Initially, two kink bands form in the hanging wall, one above the base of the ramp, and the

other above the top of the ramp (Fig. 15.2a). With continued slip on the fault, these two kink bands grow in width (Fig. 15.2b). As the truncated hanging wall moves up the ramp, and the two kink bands widen, an anticline forms at the top of the ramp. This anticline terminates downward into the upper flat (Fig. 15.2c). The ramp anticline grows in amplitude as the kink bands grow in width. Meanwhile, one syncline develops at the base of the ramp, and another develops on the foreland-side of the anticline (Fig. 15.2c). Note that the ramp height determines the amplitude of the fold, which, in turn, determines the structural relief.

Notice that throughout the development of a fault-bend fold, axial traces A and B coincide with the top and bottom of the ramp, respectively, and the hanging wall “rolls” through these hinges as it traverses the ramp. The other two axial traces (A' and B') migrate along the fault, but they are fixed with respect to the rocks in the hanging wall.

When the cutoff point of the lowest stratigraphic unit in the upper plate reaches the upper flat (Fig. 15.2c), the fold ceases to grow in amplitude, but the distance between the axial traces of the ramp anticline (A and B' in Fig. 15.2c) increases with increasing displacement. In a fully developed fault-bend fold, axial traces A and A'



**Fig. 15.2** Progressive development of a fault-bend fold as the thrust sheet moves over a ramp in a decollement (after Suppe, 1983). Letters A, A', B, and B' denote the axial traces.

are fixed with respect to the hanging-wall rocks, and they move along the flat with movement on the fault. Note that all fold axial traces bisect the interlimb angle of the fold, i.e., the angle between adjacent panels. Use the flipbook (Fig. G-44) to confirm these features of fault-bend folds.

Look at Fig. 15.2c again and note the following important relations between an exposed fault-bend fold and the associated thrust. These relations allow us to infer subsurface fault geometry from known fold shape.

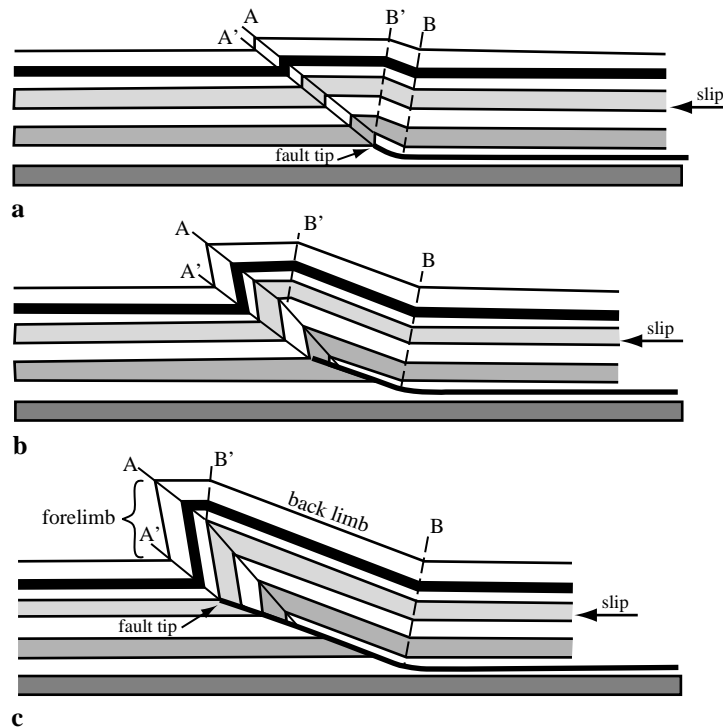
- 1 In originally horizontal or gently dipping strata, the backlimb of the hanging-wall anticline always dips more gently than the forelimb.
- 2 The dip of the backlimb is equal to the dip of the ramp in all stages of fold growth.
- 3 The axial trace of the hanging-wall syncline (axial trace B) terminates at the base of the ramp.
- 4 In a fully developed fault-bend fold, the axial trace that separates the backlimb from the upper flat (axial trace B') terminates at the top of the ramp.

- 5 For every hanging-wall cutoff there must be a corresponding footwall cutoff of equal stratigraphic thickness. This is the template constraint, discussed above.
- 6 For every hanging-wall flat there must be a corresponding footwall flat of equal length.

### Fault-propagation folds

In a fault-propagation fold, rather than stepping from one flat to another, the fault simply dies out upward, into the axial surface of a syncline (Fig. 15.3). A fault-propagation fold is the surface expression of a blind thrust. Shortening above the fault terminus, or *fault tip*, is accommodated by folding. Use your flipbook (Fig. G-44) to compare the development of a fault-propagation fold with that of a fault-bend fold.

As is the case with fault-bend folds, there are several important relations between the exposed fault-propagation folds and the associated thrusts that allow us to infer fault geometry at depth. Note that in both types of folds the axial trace bisects the interlimb angle of the fold. This is the geometry required to preserve constant bed thickness.



**Fig. 15.3** Progressive development of a fault-propagation fold at the tip of a thrust, as the thrust sheet moves over a ramp in a decollement (from Suppe, 1983). Letters A, A', B, and B' denote the axial surfaces. Note that the fault tip coincides with the hinge of an asymmetric syncline.

- 1 In cases where the fault cuts originally horizontal (or gently dipping) strata (as in Fig. 15.3), the backlimb dips more gently than the forelimb. In general, fault-propagation folds are more strongly asymmetric than are fault-bend folds, and the forelimb of a fault-propagation fold is typically very steep to overturned (Fig. 15.3c). This characteristic alone is an important clue about the type of fold you are dealing with, especially in the absence of other information.
- 2 The dip of the backlimb is equal to the ramp angle.
- 3 The axial trace of the syncline that forms on the hinterland-side of the fold (axial trace B in Fig. 15.3) terminates at the base of the ramp.
- 4 The thrust terminates in an asymmetric syncline that forms on the foreland side of the structure. The fault tip lies at the intersection of the synclinal axial surface and the thrust ramp (Fig. 15.3c).
- 5 The fault-propagation model of fold formation explains why box folds commonly reduce to simple chevron folds in their cores. The two axial traces of a box-like fold (A and B' of Fig. 15.3c) bound a flat panel that separates the backlimb from the forelimb of the anticline. The stratigraphic horizon at which the fault terminates is the same stratigraphic horizon at which the two axial traces merge to form a single axial trace (Fig. 15.3c). This single axial trace bisects the angle between the fold forelimb and fold backlimb (Fig. 15.3c). Cool, isn't it!

### Requirements of a balanced cross section

For a cross section to be valid, certain assumptions inherent in its construction must be valid. A fundamental assumption is that rock *volume* (displayed as area in a two-dimensional cross section) is conserved during deformation; that is, deformation approximates *plane strain* and simply redistributes rock volume in the two-dimensional cross-section profile. This assumption will not be justified if volume loss has occurred (e.g., due to pressure solution accompanying cleavage development) or if there is movement of material in or out of the cross section. This latter situation can occur if oblique slip occurs along the thrust faults, if strike-slip faults intersect the cross-section line, or if the line of section is oblique to the principal

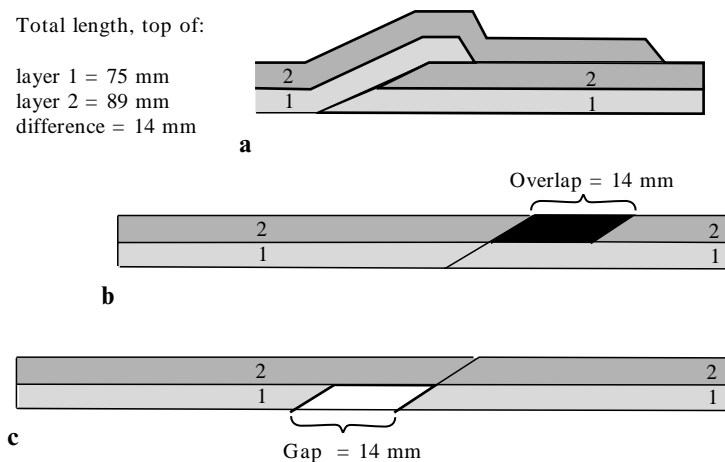
movement direction. In order for the techniques described in this chapter to be applicable in a particular situation, the validity of the conservation-of-volume assumption must be demonstrated. The methodologies for testing this assumption are beyond the scope of this book; references are provided at the end of the book.

Within any given region, specific types of structures, and associations of structures, are characteristic. A geologically reasonable cross section must honor the structural style of the region. For example, uniformly verging asymmetric folds are characteristic of thrust belts. A cross section that honors this constraint is said to be *admissible* (Elliott, 1983). In addition, the cross section must be restorable, or *retrodeformable*. This means that if all of the shortening represented by the faults and folds is removed, the layers should restore to a reasonable predeformational configuration, without large gaps or overlaps in strata. A cross section that can be restored to a reasonable predeformational configuration is said to be *viable*. A *balanced cross section* must be both admissible and viable. Note that there may be several viable solutions to a given data set. Just because a cross section is balanced does not mean it is correct. However, if it is not balanced, it cannot be correct, assuming plane strain and no volume change.

Examine Fig. 15.4a, which is a simple example of a cross section that is *not* balanced. If this cross section represents a portion of a thrust belt, with tectonic transport from left to right, it is an admissible cross section. But is it restorable (and therefore viable)? To test this, imagine sliding the hanging wall back down the thrust fault until layer 1 in the hanging wall connects with layer 1 in the footwall. As shown in Fig. 15.4b, when we do that, there is an overlap of layer 2. If the hanging wall is slid back to the point at which layer 2 in the hanging wall connects with layer 2 in the footwall, there is a gap in layer 1 (Fig. 15.4c). Therefore, this is not a viable cross section; it is not balanced.

### Problem 15.2

Redraw the cross section in Fig. 15.4a to make it balanced. Assume that the footwall geometry is correct.



**Fig. 15.4** Unbalanced cross section. (a) Deformed-state cross section. (b) The removal of the slip along a thrust to restore bed 1 to its predeformational configuration does not produce a reasonable predeformational restoration of bed 2, but results in an “excess” or overlap of bed 2. (c) The restoration of bed 2 to a reasonable configuration results in a “deficiency” of bed 1, creating a gap. Thus, the deformed-state cross section is not viable.

### Constructing a restored cross section

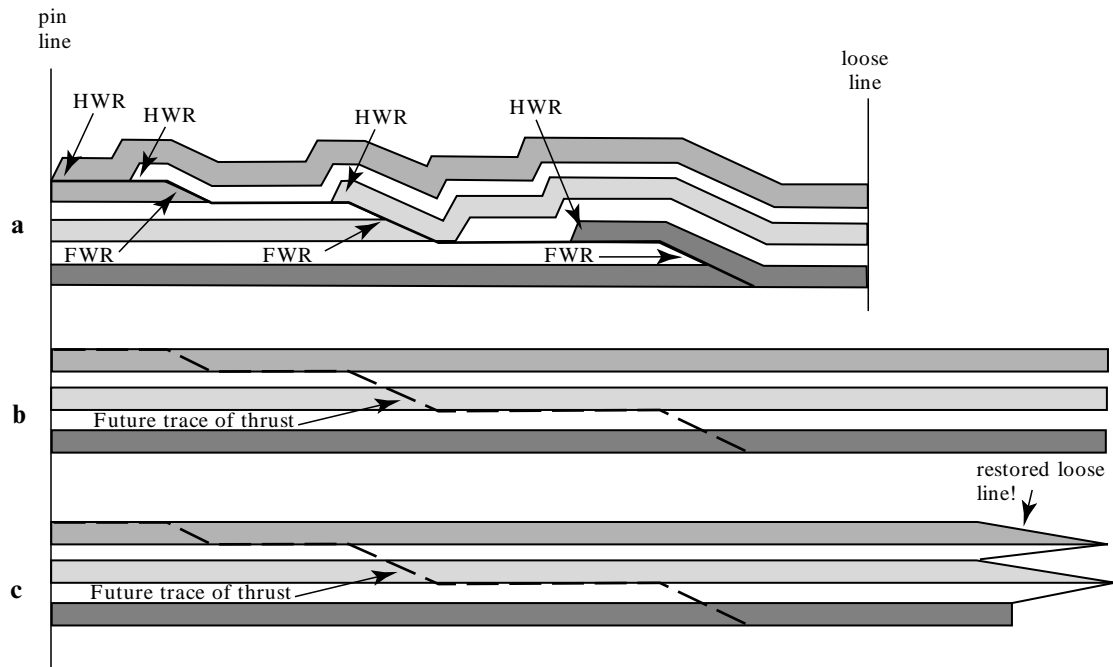
If the assumptions discussed above are valid, then a deformed cross section should restore to an undeformed section of equivalent area. A cross section can be tested for balance by measuring areas in both the deformed and restored states. Where map units show consistent thicknesses over the distance of the cross section, the *bed length* will be proportional to the area (i.e., area = bed length  $\times$  thickness; if thickness is constant, area is proportional to bed length). Therefore, in regions of constant unit thickness we can simply measure bed lengths in deformed and restored (undeformed) cross sections. If the cross section is balanced, the bed lengths will be equal, or nearly so. We will focus exclusively on bed-length balancing in this chapter.

Here are the steps for evaluating whether a cross section is balanced:

- 1 Draw a regional *pin line* on the deformed cross section (Fig. 15.5a). This is a vertical line drawn on the foreland side of the cross section that will serve as a reference marker from which the bed lengths will be measured. Typically, a regional pin line is chosen in an area of no interbed slip such as a point beyond the limits of thrusting or in a fixed fold hinge. In Fig. 15.5a the pin line is drawn to the left of the leftmost thrust.
- 2 Draw another line, called the *loose line*, perpendicular to bedding on the hinterland side of the deformed cross section (Fig. 15.5a).

- 3 Begin the construction of the restored cross section by drawing a series of horizontal, parallel lines representing the regional stratigraphic sequence, as in Fig. 15.5b. The spacing between the lines must be proportional to the thicknesses of the units. This regional stratigraphic sequence will serve as the template for the restored cross section.
- 4 On the deformed cross section (Fig. 15.5a), measure the length of each stratigraphic unit, from the pin line to the loose line. Measure the top and bottom (or center) of each unit, and record the length within each panel. Determine the total length of each bed, and also the distance from the pin line to each cutoff point, where a bed has been truncated by the fault.
- 5 Transfer the bed-length measurements from the deformed section to the restored section. Use the bed lengths from the pin line to each cutoff point to determine where to draw the fault on the restored section.
- 6 On the restored section, connect the cutoff points with a dashed line to indicate the prethrusting configuration of the fault (Fig. 15.5b).

If the cross section is balanced, all of the bed lengths in the restored sections will be equal within 5–10% of each other, depending upon the complexities of geology and the validity of the assumptions discussed above for that particular cross section. Figure 15.5c is an example of a restored cross section in which the bed lengths



**Fig. 15.5** (a) Deformed-state cross section. (b) Stratigraphic “template.” (c) Undeformed-state cross section restored by measuring the bed lengths at the top and bottom of each unit. Note that the bed lengths are not consistent, hence the section does not balance. Notice also that the section does not obey the template constraint. FWR, footwall ramp; HWR, hanging-wall ramp.

are not equal; the corresponding deformed cross section, therefore, is not balanced.

Several features can also be used to inspect a cross section for problems without actually measuring each bed length. For example, the cross section shown in Fig. 15.5a contains several serious errors that indicate, at a glance, that it cannot be balanced. Specifically, there are four hanging-wall ramps (labeled HWR), but only three footwall ramps (FWR). Thus, the section violates the template constraint. Another problem is that the hanging-wall flats are not the same length as the footwall flats. Recall that each hanging-wall ramp or flat must have a corresponding footwall ramp or flat. Although application of these principles may seem overwhelming at first, a bit of practice will train your eye to recognize inconsistencies such as those just described; they occur in many published cross sections.

Once a restored cross section is constructed, the amount of net shortening can be determined by the equation:

$$[(l_d - l_u)/l_u] \times 100\%$$

where  $l_u$  is the bed length in the undeformed state, and  $l_d$  is the bed length in the deformed state. For

thrust belts, this equation will yield a negative number, which indicates percent shortening.

### Constructing a balanced cross section

Having learned to critique cross sections drawn by others, you are now ready to draw your own. When deciding the best place on a geologic map to draw a cross section, remember that it must be drawn parallel to the tectonic transport direction. Cross-section lines that are oriented more than 5–10° from parallel to the tectonic transport direction may not restore to a reasonable predeformational configuration. In thrust belts, one should choose a line of section that is perpendicular to the regional strike of the major thrust faults and also perpendicular to the trend of the major fold axes. Avoid lateral ramps (those that are approximately parallel to the transport direction) or areas near tear faults.

After you have: (1) constructed the topographic profile along the line of section, (2) transferred the strikes and dips from the geological maps, and (3) incorporated any well-log data onto the cross section, the chances are you will still be confronted with a lot of “blank space” on your cross-section

diagram where you have no data to guide you. It is your task to infer the structure at depth to fill up the blank paper. This is where you earn the big bucks that the oil company is paying you. Fortunately, a few simple rules and techniques can help you in this effort. Recall that in thrust belts, folds bear systematic and predictable geometric relations to the thrusts that generate them. Therefore, you can use the shapes of folds to infer fault position and orientation at depth, as indicated in the following procedure.

- 1 Define panels of constant dip. Project all contacts into the “air” and into the subsurface. But do not project faults to depth just yet!
- 2 Determine the orientations of axial traces of folds. This is done by constructing bisectors of adjacent dip panels. The axial surface of a concentric fold bisects the interlimb angle. For example, if the interlimb angle of a fold is  $150^\circ$ , in a cross-section diagram the axial trace would be shown as a dashed line that lies at  $75^\circ$  to each fold limb or panel.
- 3 Project folds to depth, or into the “air” where eroded. Where two axial traces merge downward, as in a box fold, the result is a single hinge that bisects the chevron fold (recall that box folds reduce to chevron folds in their cores, as in Fig. 15.3). Construct a new axial trace that bisects the limbs of the chevron fold.
- 4 Determine which of the two types of ramp-related folds is probably present (fault bend or fault propagation). If there is evidence that the fault ramps up from a lower to an upper flat, then the fold is a fault-bend fold. If the evidence suggests that the fault dies out into an asymmetric syncline, a fault-propagation fold is indicated. The presence of an overturned limb is evidence of a fault-propagation fold. If data are insufficient to choose between the two possibilities, you may have to construct both fold types and select the solution that best honors the available geologic data.
- 5 When you are working on the exercises at the end of this chapter, refer freely to Figs 15.2 and 15.3 and the discussions of fold characteristics that accompany those figures.

### Problem 15.3

Use the bed-length technique to restore the cross section in Fig. G-45 and evaluate whether or not it balances. That is, draw the stratigraphic template for the restored cross section below the deformed cross section. Then measure the bed lengths of each unit from the pin line, and determine the positions of the ramps and flats of the future fault on the stratigraphic template. Be sure to measure both the top and bottom of each of the three layers; you will have six measurements in all. If the cross section does not balance, state *specifically* what is wrong with it and key your comments to the deformed-state cross section. Identify every error; it is not sufficient to say “bed length too long.”

### Problem 15.4

Balance the cross section that you evaluated in Problem 15.3. Use the footwall template provided in Fig. G-46. Assume that the footwall structure (i.e., position of ramps and flats) is correct. Use the same dip for the forelimbs of all of the folds (follow the example of the fold in the Permian bed). Remember to keep the footwall and hanging-wall flats the same length. Your section should balance by line length, but will not conserve slip on the fault because some shortening is accommodated by folding. Explain *in detail* why your section is superior to the one given in Fig. G-45. Calculate the amount of shortening represented by the section using an average of the lengths of the Permian/Triassic contact and the Triassic/Jurassic contact.



**Problem 15.5**

Figure G-47 contains a geologic map and topographic profile. Two wells have been drilled in the area, as indicated on the map. Well number 1 encountered a thrust decollement at 1500 m. Well number 2 encountered the following units:

Depth to top of unit (m)	Unit encountered
350	Jurassic rocks below an interval of fault gouge
900	Triassic rocks
1680	Permian rocks
2150	Proterozoic crystalline rocks

Regional mapping indicates that the thickness of Cretaceous rocks is 700 m.

Use the map, together with stratigraphic thicknesses from the well log and regional mapping, to construct a cross section on the topographic profile. Be sure to show the eroded layers above the level of the present exposure. Determine: (1) the type of fold present, and (2) the amount of shortening.

**Problem 15.6**

You have been hired by an oil company, and your first assignment is to take over a project from another employee. Figure G-48 contains a geologic map and topographic profile of an area that your company has leased. The oil-bearing unit in the region is an Eocene sandstone that is not exposed in the map area. It is overlain by unit To (Tertiary, Oligocene shale).

As indicated on the map and profile, an exploratory well has been drilled. Some drill bits produce a solid core of rock for the geologist to examine, but that type of drilling is very slow and expensive. Usually, oil companies use a drill bit that chews up the rock into little chips. It is more difficult to recognize and interpret the rocks in the well, but it is much cheaper and faster. Such a drill bit was used for this well. Your predecessor was the on-site geologist who logged the well. Unfortunately, she was unable to identify the rock units within the well, nor was she able to determine their attitudes. She did record the depth at which the drill bit encountered different lithologies. These are indicated by the three short horizontal lines on the vertical line that represents the well. These indicate the depth of each lithologic contact within the well, but not the attitude of each contact. You will have to determine which rock units occur above and below these contacts in the subsurface. The heavy line lower in the well indicates the position of a major fault.

Complete the cross section. Start by projecting the dips and contacts onto the topographic profile. Then determine the orientations of the axial surfaces of the folds (remember, axial surfaces bisect adjacent fold limbs or panels). Be sure to complete the geology in the footwall of the thrust, as well as in the hanging wall. Follow the rules for fold construction.

After completing the cross section, do the following:

- 1** Determine what type of fold is present.
- 2** Calculate the amount of shortening accommodated by the fold.
- 3** On both the map and cross section, indicate where you recommend drilling a production oil well. In one or two succinct sentences, explain why this is the best place to drill for oil.

## Deformation Mechanisms and Microstructures

### Objectives

- **Recognize microstructures produced by different deformation mechanisms.**
- **Identify rocks produced by faulting under different crustal conditions.**
- **Use kinematic indicators to determine sense of shear in mylonites.**

Most of this book concerns geologic structures on the scale of maps, outcrops, and hand samples. In this chapter, we examine grain-scale structures (microstructures) and the mechanisms that produce them. The manner in which rocks and minerals deform at the grain scale is a function of several parameters, including mineralogy, temperature, pressure, stress magnitude, presence or absence of pore fluids, and strain rate. An understanding of deformation mechanisms and recognition of the microstructures they produce can therefore provide important information regarding environmental conditions during deformation.

### Deformation mechanisms

Deformation mechanisms that produce readily observable microstructures can be grouped into four categories: fracture processes (cataclasis), diffusive mass transfer, intracrystalline deformation, and recrystallization. These mechanisms are not mutually exclusive; all can operate simultaneously in a rock. For example, under certain temperature conditions, quartz may deform plastically while an adjacent feldspar deforms brittlely. However, for

a given mineral in a rock, one mechanism usually predominates over the others and imparts its characteristic microstructures to the rock.

#### ***Fracture processes (cataclasis)***

At relatively low temperature and low confining pressure (or high fluid pressures), most minerals deform by fracturing or cataclasis. Fracturing involves loss of cohesion at the grain scale. However, under moderate confining pressures, rocks can fracture pervasively and deform without losing cohesion at the outcrop scale. Fractures may be filled with mineral material, commonly iron oxides and hydroxides, carbonates, or silica, producing a hard, cemented rock. Fracturing does not generally cause the grains in a deformed rock to have a preferred orientation; however, subsequent frictional sliding of grains can result in crude banding or “cataclastic foliation.”

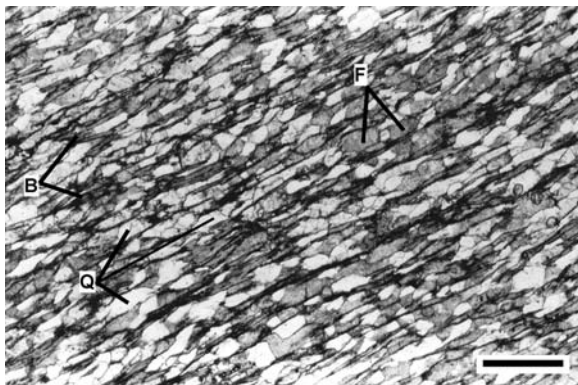
#### ***Diffusive mass transfer***

Diffusive mass transfer accommodates deformation by moving material from zones of high normal stress to regions of lower normal stress. The

process can result in significant volume loss if the dissolved material is transported out of the system. Diffusive mass transfer processes include ionic diffusion within grains (Nabarro–Herring creep), and along grain boundaries in the absence (Coble creep), or presence, of a fluid phase (pressure solution). With the exception of pressure solution, diffusive mass-transport processes do not result in well-developed microstructures. For this reason, we restrict our discussion to pressure solution and the resulting fabrics.

Pressure solution refers to the transfer of dissolved material in the presence of an intergranular fluid film, generally water. Dissolved material may be precipitated in nearby low-stress sites or be transported completely out of the system. Pressure solution may be the dominant deformation mechanism at temperatures and confining pressures intermediate between those that favor fracture mechanisms and those that favor crystal plasticity, and it appears to be the dominant process in the development of metamorphic cleavage.

Several features and microstructures evident in thin section suggest that material may be dissolved and reprecipitated during deformation. For example, fossils may be strongly dissolved along margins parallel to rock cleavage but unaffected along other interfaces. Grains that are normally equidimensional, such as quartz and feldspar, may show an elongate morphology and straight grain boundaries due to dissolution at cleavage-parallel interfaces (Fig. 16.1). Adjacent grains may show straight or interpenetrating grain boundaries resulting in a “fitted” texture that clearly does not

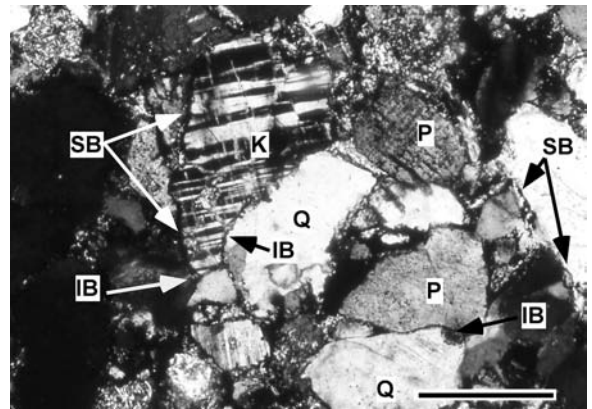


**Fig. 16.1** Straight grain boundaries and the crudely rectangular shape of quartz grains (white) in this metamorphosed siltstone suggest that silica has been dissolved at grain boundaries parallel to the rock cleavage. Cleavage is defined by the alignment of biotite grains, and, to a lesser extent, the grain-shape fabric defined by the quartz and feldspar. B, biotite; F, feldspar; Q, quartz. Plane polarized light. Scale bar is 1 mm.

reflect the original detrital grain shapes (Fig. 16.2). Subparallel concentrations of iron oxides, graphite, or clay minerals are insoluble residues left behind as the more soluble materials were removed from the rock. Stylolites, common in carbonate rocks, provide a familiar example. Dissolved material may reprecipitate as overgrowths on mineral faces perpendicular to cleavage to form pressure shadows. “Mica beards,” or growths of sericite or muscovite on feldspars, are indicative of dissolution and reprecipitation (Fig. 16.3). Abundant vein arrays, particularly those oriented at high angles to the cleavage direction, may represent reprecipitation of formerly dissolved material in extension fractures.

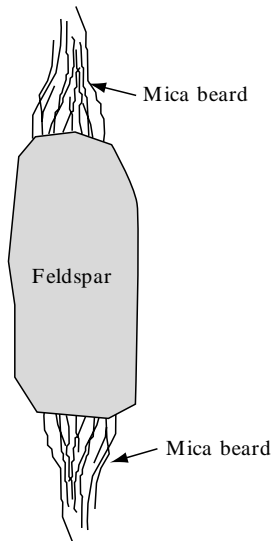
### ***Intracrystalline plastic deformation/crystal plasticity***

The processes discussed above dominate at relatively low temperatures ( $< 300^{\circ}\text{C}$ ) and low to moderate confining pressures. At higher temperatures and confining pressures and/or slower strain rates, individual crystals may deform by the movement of lattice defects, such as dislocations,\* through the crystal. This process results in changes in grain shape, thus altering the overall shape of the rock mass as it undergoes strain. In highly strained rocks, formerly equidimensional quartz grains may be deformed into highly elongate quartz ribbons (Fig. 16.4).

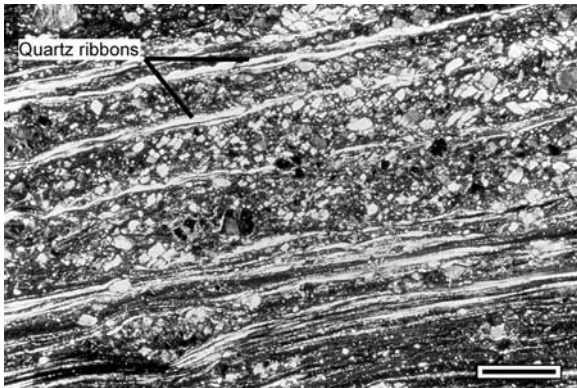


**Fig. 16.2** Photomicrograph of a sandstone that has undergone a high degree of pressure solution. Note the straight and interpenetrating grain boundaries that could not reflect the original detrital grain shapes. IB, interpenetrating boundary; K, potassium feldspar (microcline); P, plagioclase feldspar; Q, quartz; SB, straight boundary. Crossed polars. Scale bar is 1 mm.

\* The term dislocation refers to curvilinear defects in the crystal structure. A discussion of dislocation theory is beyond the scope of this manual; references are included at the end of the book.



**Fig. 16.3** Sketch showing development of “mica beards” in the pressure shadow areas of feldspars. Micas may grow at the expense of feldspars during deformation at low temperatures in the presence of grain-boundary water. Mica beards are typically between 1 and 10 mm long.



**Fig. 16.4** Quartz ribbons in mylonite from southern Nevada. Small angular grains are brittlely deformed feldspars. Crossed polars. Scale bar is 1 mm.

### Twining

In some crystals, strain is accommodated by slip on a discrete crystallographic plane, resulting in mechanical or deformation twins. Such twinning commonly occurs at low temperature in calcite and dolomite, and, to a lesser extent, in feldspars.

### Dislocation glide and climb

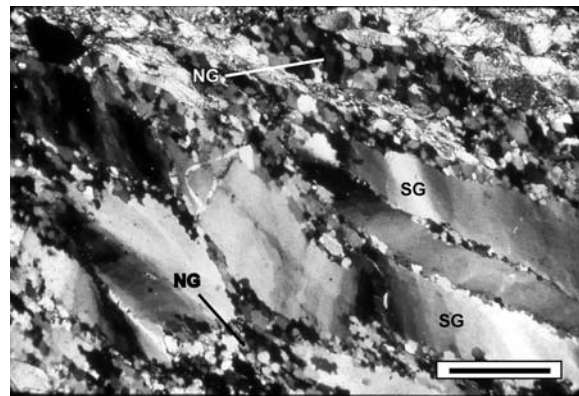
Dislocations may propagate through a crystal lattice by *glide* (motion along a single crystallographic plane) or *climb* (motion in which a

dislocation steps upward or downward to a new glide plane). Lattice distortion due to dislocation glide and climb in a crystal produces several different optical microstructures. At low strains, minerals such as quartz may exhibit *undulose extinction* as a result of dislocation glide. Undulose extinction reflects a nonuniform distribution of dislocations within the crystal. At very high strains, crystals may be drawn into elongate ribbons (Fig. 16.4). When dislocations concentrate in narrow zones within a crystal by a combination of glide and climb processes, the deformed grain begins to show a domainal extinction pattern. These domains are called *subgrains* (Fig. 16.5). Subgrains show low-angle boundaries; that is, the optical misorientations (measured by rotating the microscope stage) between adjacent grains are less than  $10^\circ$ . The development of subgrains is evidence that the grain has experienced a degree of *recovery*; that is, parts of the grains have been swept free of dislocations (which “pile up,” forming the subgrain boundaries).

Dislocation glide and climb becomes an important deformation mechanism in quartz at temperatures of about  $300^\circ\text{C}$ , although factors such as strain rate and the presence of water play a role in determining the brittle-plastic transition in quartz. Feldspars may deform by fracture processes up to about  $450^\circ\text{C}$ .

### Recrystallization

Recrystallization can occur either during deformation (dynamic recrystallization) or in the absence



**Fig. 16.5** Subgrains (SG) and new grains (NG). The subgrains indicate that some recovery has occurred, and the new grains (or neoblasts) record incipient dynamic recrystallization. Shear sense is sinistral. Crossed polars. Scale bar is 1 mm.

of deformation (static recrystallization). The mechanical rotation of subgrains may result in the formation of new grains (*neoblasts*), the lattices of which are no longer continuous with the old grains (Fig. 16.5). Optically, this process of dynamic recrystallization is manifested by grain-boundary angles that exceed  $10^\circ$ , in contrast to subgrains that show very low-angle boundaries with adjacent subgrains. Static recrystallization results in simple, straight grain boundaries that meet at about  $120^\circ$ . This process can occur when heating outlasts deformation in a single deformational event or may be due to later heating of an earlier deformational fabric.

### Problem 16.1

What was the principal deformation mechanism in the quartz in the photomicrograph shown in Fig. G-49 (Appendix G)? What was the principal deformation mechanism in the feldspar? Provide evidence to justify your answers. In what approximate range of temperatures did deformation in this rock occur? Comment on the degree of recovery or recrystallization in the quartz ribbons. Write your answer in well-crafted, lucid, succinct sentences.

### Problem 16.2

What was the principal deformation mechanism operative in the rock shown in Fig. G-50? Being careful to use the correct terminology, list the lines of evidence that support your conclusion. Use labeled arrows to point out an example of each line of evidence you present.

### Problem 16.3

On Fig. G-51, label three examples of subgrains and three examples of new grains.

## Fault rocks

*Faults* are discrete fractures within the earth's crust along which movement has taken place parallel to the fracture surface. A *shear zone* is a zone along which high-magnitude strain has been accommodated without macroscopic loss of cohesion. Shear zones range from plastic to brittle in character, although many geologists restrict the term to

rocks that have accommodated strain by dominantly plastic deformation mechanisms (Fig. 16.6). The general term "fault rocks" applies to rocks deformed in both brittle fault zones and plastic shear zones.

Several classifications for fault rocks have been proposed; Fig. 16.7 shows one that is used widely today. Fault rocks that develop in near-surface fault zones under conditions of low temperature and low confining pressure form by brittle deformation mechanisms (i.e., fracturing). Rocks deformed by brittle processes undergo dilation (volume increase) and loss of cohesion. The resulting fault rock is *fault gouge* or *fault breccia*, depending on the particle size (Fig. 16.7). Fluids circulating through voids and fractures may deposit minerals within fractures, thus producing cemented gouge. The cementing agent usually has a different composition than the host rock.

A *cataclasite* is a fault rock formed dominantly by microfracturing processes (Fig. 16.8). Cataclasites differ from fault breccias in that they undergo



**Fig. 16.6** A centimeter-scale shear zone developed in amphibolite (metagabbro) in Wyoming. Note grain-size reduction and development of strong foliation within the zone of shear. The deflection of foliation adjacent to the shear zone indicates sense of shear, which is dextral in this case. Coin for scale.

	Random Fabric	Foliated Fabric
Noncohesive	Fault gouge (<30% visible fragments)	"Foliated gouge"
	Fault breccia (>30% visible fragments)	
Cohesive	<i>Cataclasite series</i>	<i>Mylonite series</i>
	Protocataclasite    10 - 50% matrix	Protomylonite
	Cataclasite        50 - 90% matrix	Mylonite
	Ultracataclasite    90 - 100% matrix	Ultramylonite

**Fig. 16.7** Fault-rock classification (after Sibson, 1977). The matrix is all material smaller than 50  $\mu\text{m}$  in size.



**Fig. 16.8** Cataclasite from the Whipple detachment fault, California. Note the angular fragments and complete lack of foliation. Pencil for scale.

grain-scale brittle deformation without loss of cohesion at the macroscopic scale. This type of deformation occurs at moderately low temperature but at elevated confining pressure, and most commonly in the presence of fluids. As individual grains are fractured, they seal almost immediately

by dissolution–precipitation processes. No large open spaces are formed and, unlike fault breccia, the material cementing the fractured rock is most commonly derived from the host rock itself. Thin-section examination may be necessary to distinguish fine-grained fault breccia from cataclasite.

Cataclasis typically results in a rock characterized by randomly oriented broken grains; however, a macroscopic planar fabric (“cataclastic foliation”) may form due to fractured grains sliding past one another. Cataclastic foliation should not be confused with the grain-shape foliation that forms as a result of plastic deformation mechanisms. Inspection with a hand lens or in thin-section generally reveals fracturing to be the dominant grain-scale deformation mechanism in cataclasites.

*Mylonites* are rocks in which a dominant mineral, typically quartz, has deformed by crystal-plastic deformation mechanisms (Fig. 16.9). The process usually results in marked grain-size reduction and the development of conspicuous foliation and/or lineation. At high shear strains, the orientations of mylonitic foliation and lineation approximate the shear plane and shear direction, respectively. Mylonites generally form in discrete planar shear zones that range in width from millimeters to kilometers. Many mylonites contain large crystals within a fine-grained matrix. The large minerals, called *porphyroclasts*, are typically stronger than the matrix for a particular set of conditions of deformation. For example, in mylonitized granites, quartz typically exhibits pronounced grain-size reduction due to dynamic recrystallization, whereas feldspars show little or no grain-size reduction, except in the most highly deformed rocks. The relative proportion of porphyroclasts to fine-grained matrix is the basis for the classification of mylonitic rocks into *protomylonites*, *mylonites*, and *ultramylonites* (Figs 16.7 and 16.9).

#### Problem 16.4

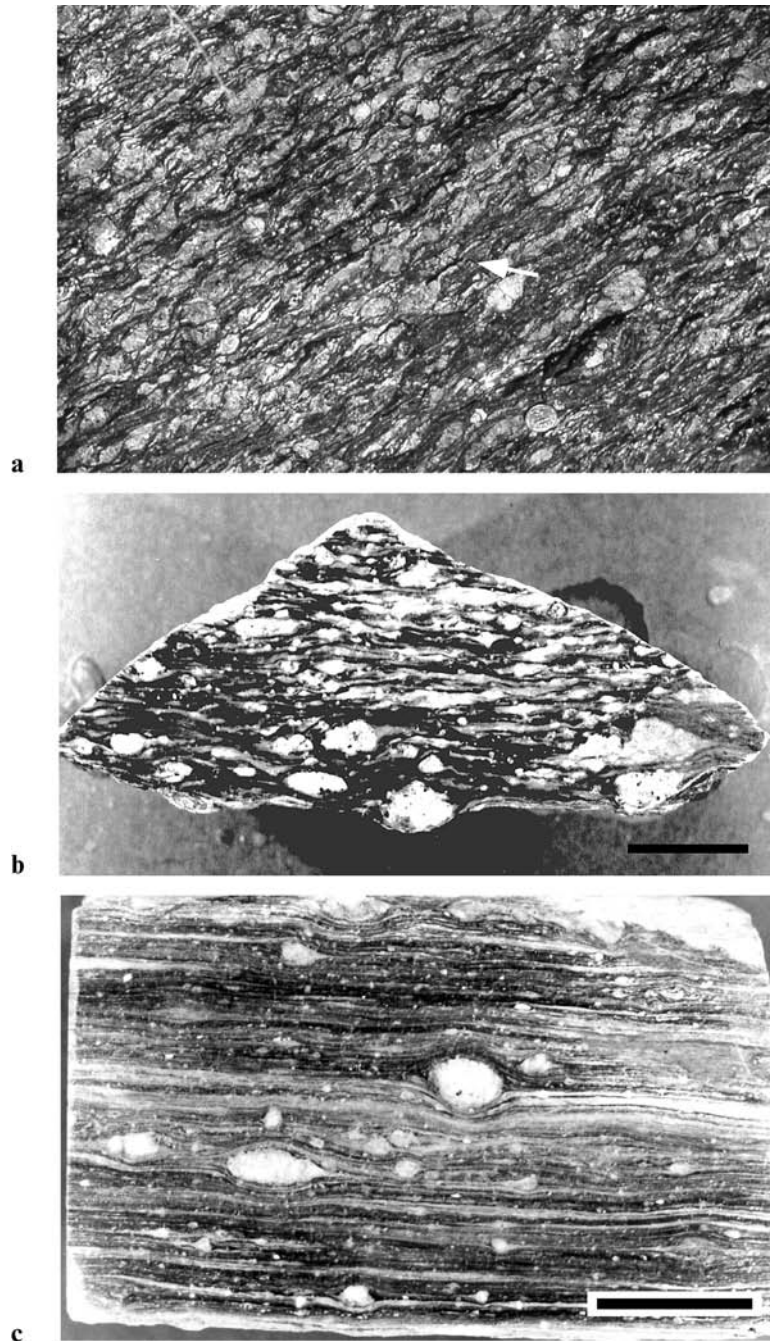
Name the type of fault rock shown in Fig. G-52a, and explain what features you used to identify it. The protolith of this rock was a coarse-grained granite. The irregularly shaped, light-colored masses are lichens growing on the rock.

## Kinematic indicators

**Problem 16.5**

Name the type of fault rock shown in Fig. G-52b, and explain what features you used to identify it. The protolith of this rock was a porphyritic granite.

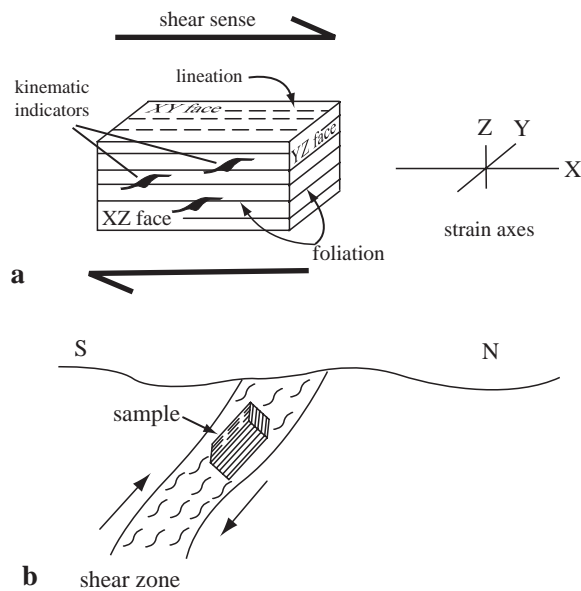
One of the key goals of a geologist studying a shear zone is to determine the direction of movement or *sense of shear*. Rocks that deform plastically at high temperatures commonly lack slickenlines (fault striae) and recognizable strati-



**Fig. 16.9** Mylonitic rocks, showing variation in the relative proportion of porphyroclasts to fine-grained matrix. All surfaces are parallel to the mineral lineation and perpendicular to the foliation. (a) Protomylonite (exhibiting a greater proportion of porphyroclasts than matrix) developed in megacrystic granite, from southern Nevada. Note the stretched feldspar porphyroclasts (arrow points to tails). Coin in lower right is a quarter, 2.4 cm in diameter. (b) Mylonite (exhibiting approximately equal proportions of porphyroclasts and matrix) from southern Nevada. Scale bar is 2 cm. (c) Ultramylonite, in which porphyroclasts constitute less than 10% of the rock, from Wyoming. Scale bar is 2 cm.

graphic markers that can be used to determine sense of shear. Features in the sheared rock, collectively called *kinematic indicators*, must be used instead. A thorough study of kinematic indicators in a shear zone involves recording many kinematic indicators at both the mesoscopic and microscopic scales. Shear-sense indicators must be viewed perpendicular to foliation and parallel to lineation (Fig. 16.10a); that is, on the rock face that corresponds to the XZ plane of the strain ellipsoid. In Chapter 14 we dealt with only two-dimensional strain. In three dimensions, X is the long axis of the strain ellipsoid, Y is the intermediate axis, and Z is the short axis (Fig. 16.10a).

Shear sense in a given sample or outcrop is usually reported as *dextral* (right-lateral or clockwise sense of rotation) or *sinistral* (left-lateral or counterclockwise sense of rotation). One must be careful, however, because two geologists looking at opposite sides of a sample or an outcrop would see opposite shear sense. For that reason, it is necessary to interpret sense-of-shear in the context of the proper geologic or geographic frame of reference (Fig. 16.10b).

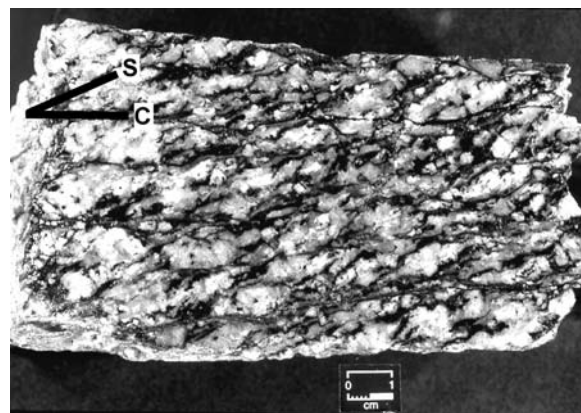


**Fig. 16.10** Relationship between mylonitic fabric and sense of shear. (a) Sketch showing proper orientation for sense-of-shear determination. Field exposure or thin-section must be parallel to lineation and perpendicular to foliation (view in the XZ plane of the strain ellipsoid). (b) True geographic and geologic orientation of a sample for sense-of-shear determination. In this case the dextral shear sense viewed in the hand sample corresponds to south-side up, reverse-sense motion along the shear zone.

## S-C fabrics

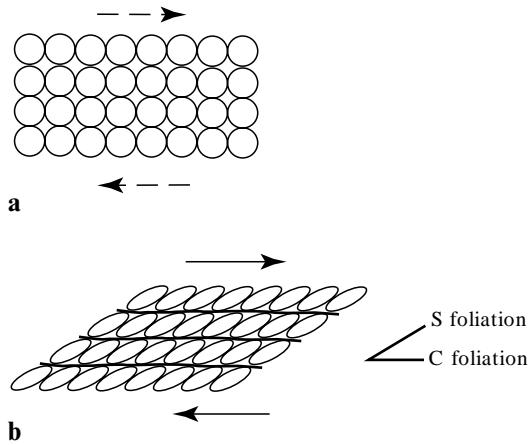
Many rocks in shear zones, particularly granites, possess composite planar fabrics defined by two foliations that are at moderate to low angles to one another (Figs 16.11 and 16.12). Commonly, these foliations weaken and ultimately disappear outside the shear zone, suggesting that the composite fabric was produced as a result of shearing. Close inspection reveals that one of the planar fabrics is clearly a grain-shape fabric; that is, a fabric produced by the parallel alignment of deformed grains. This fabric is generally penetrative at all scales and is commonly called the S surface (for the French word *schistosité*). The second fabric, called C (for the French word *cisaillement*, or shear) consists of a series of spaced surfaces of shear marked by zones of grain-size reduction. C surfaces may be penetrative at the hand-specimen scale but are generally nonpenetrative at the scale of a thin-section. Rocks that possess S and C foliations are termed S-C mylonites, and the angular relation between these fabrics can be used to determine shear sense.

The development of this composite fabric and its use in determining shear sense can be understood in terms of the strain ellipse. Because ideal simple shear is plane strain, we consider only two dimensions (Fig. 16.12). For example, consider an undeformed quartzite with spherical grains (Fig. 16.12a). When subjected to simple shear the grains become slightly elongate into the local finite X direction of the strain ellipse. This produces a grain-shape foliation, S, in the rock (Fig. 16.12b).



**Fig. 16.11** S-C fabric in granite mylonite, from west-central Arizona. C, C surface (*cisaillement*); S, S surface (*schistosité*). The sense of shear is dextral. Sample courtesy of Colin Ferguson.





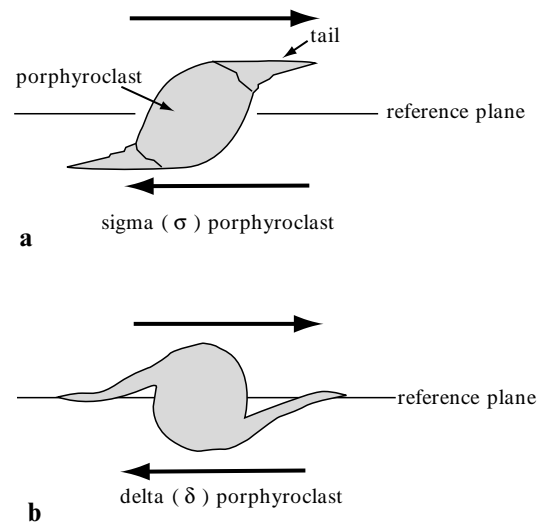
**Fig. 16.12** Schematic diagrams showing the development of S-C fabric. The arrows indicate shear sense. (a) Undeformed specimen; circles represent originally equant grains. (b) Shear strain produces grain-shape foliation (S), represented by ellipses, and also a second foliation (C), parallel to the shear plane. The asymmetry of S and C foliations can be used to determine the sense of shear, which in this case is dextral.

A second foliation, C, forms parallel to the shear plane (Fig. 16.12b). Both fabrics form simultaneously in the deforming rock. The asymmetry of the S foliation relative to the C surface gives the sense of rotation that indicates the shear direction. The sample shown in Fig. 16.11, for example, shows a clockwise (dextral) sense of rotation. When observed in the outcrop, this sense of rotation reveals the shear direction.

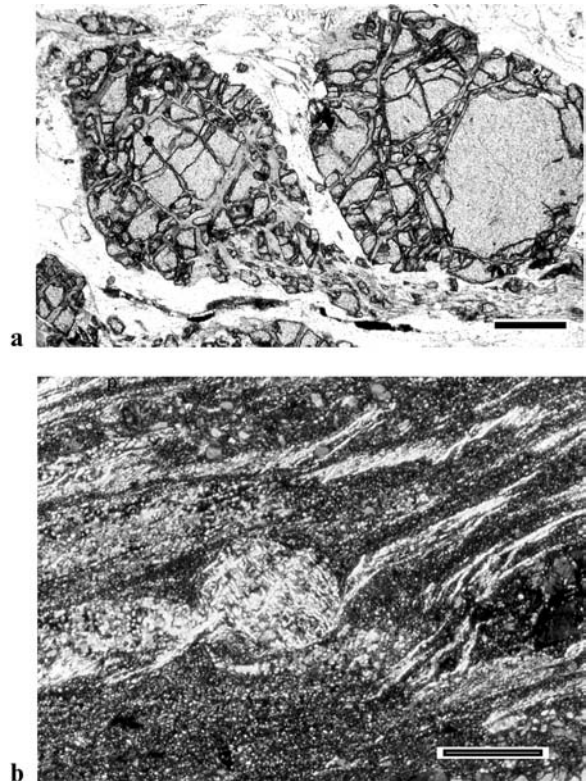
### Asymmetric porphyroclasts

Porphyroclasts (see above) may develop an asymmetric shape as a result of simple shear deformation. As the plastically deforming matrix flows around the more rigid porphyroclasts, the margins of the porphyroclasts may be more highly strained than their interiors. This results in the formation of “tails” of recrystallized or retrograded material at the ends of the porphyroclasts. The sense of asymmetry of the majority of porphyroclasts in a rock gives the sense of the simple shear component of the total strain.

Two types of porphyroclasts have been recognized and are named after Greek letters that approximate their shape (Figs 16.13 and 16.14). Sigma ( $\sigma$ ) porphyroclasts are those with tails that do not extend across an imaginary reference plane drawn through the grain and parallel to the foliation (Figs 16.13a and 16.14a). Delta ( $\delta$ )



**Fig. 16.13** Sketches of two types of asymmetric porphyroclasts. (a) Sigma ( $\sigma$ )-type asymmetric porphyroclast. (b) Delta ( $\delta$ )-type asymmetric porphyroclast. The sense of shear is dextral in both cases.



**Fig. 16.14** Photomicrographs of two types of asymmetric porphyroclasts. (a) Sigma-type porphyroclast (left) is a garnet grain that has been partially retrograded to chlorite. Tails are a mixture of garnet, chlorite, and biotite. The sense of shear is sinistral. Plain polarized light. Scale bar is 0.5 mm. (b) Delta-type porphyroclast; feldspar is highly retrograded to sericite. Sense of shear is dextral. Crossed polars. Scale bar is 0.5 mm.

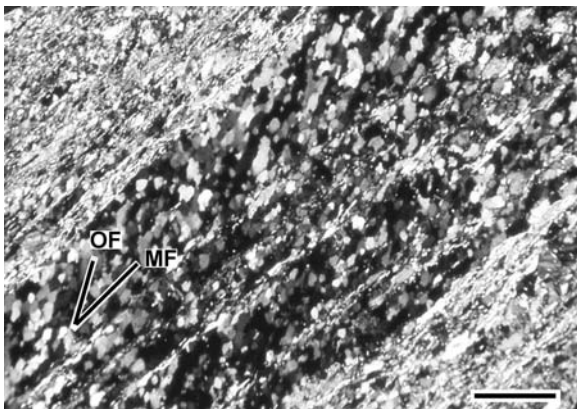
porphyroclasts have tails that do not intersect the reference plane. Delta porphyroclasts form when the rate of rotation of the grain exceeds the rate of recrystallization. In this case, the tail at the lower left of Fig. 16.13a will be dragged upward by (clockwise) grain rotation and will wrap around the grain. Similarly, the tail at the upper right in the same figure will be dragged downward by rotation of the grain. In both cases the tails show a sense of rotation that can be used to infer shear direction (Figs 16.13b and 16.14b). In some cases it is difficult to distinguish between the two types of porphyroclasts, and other kinematic indicators must be used to confirm shear sense.

### Oblique grain shapes in recrystallized quartz aggregates

In quartz-rich rocks, quartz grains may be strained into elongate ribbons. Due to progressive deformation, internal features such as elongate subgrains or new grains may develop a grain-shape alignment that is oblique to the macroscopic foliation. This obliquity is geometrically analogous to S-C fabrics, and it too can be used to infer shear sense (Fig. 16.15).

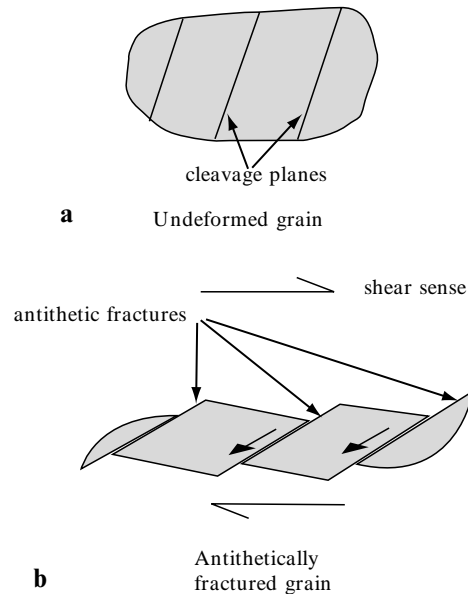
### Antithetic shears

Minerals that possess cleavage and are appropriately oriented with respect to the shear plane may undergo failure along cleavage planes in a sense that is opposite, or antithetic, to that of the shear zone (Figs 16.16 and 16.17). Microfractures in

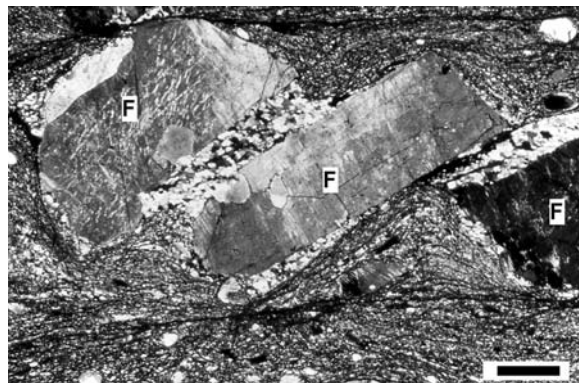


**Fig. 16.15** Oblique foliation in dynamically recrystallized quartz aggregate. MF, mylonitic foliation in rock; OF, oblique foliation in quartz aggregate. The sense of shear is dextral. Crossed polars. Scale bar is 1 mm.

antithetically fractured grains develop in a manner analogous to a sheared stack of cards or dominoes. Grains that have been systematically fractured in this manner may provide supporting evidence for shear sense inferred from other microstructures; however, they must be used with caution.



**Fig. 16.16** (a) Undeformed grain with cleavage planes. (b) Antithetically fractured grain. The long arrows show overall shear direction; the small arrows show the offset on individual antithetic shears.



**Fig. 16.17** Photomicrograph of an antithetically fractured microcline crystal. Note that, in addition to being fractured, the three segments of the original microcline crystal have also been pulled apart. The pull-apart areas have been filled with recrystallized quartz. The overall shear sense is dextral; the displacement between the feldspar fragments (F) is sinistral. Crossed polars. Scale bar is 0.5 mm. Photo courtesy of Colin Ferguson.

**Problem 16.6**

- 1 Examine the photomicrograph in Fig. G-53. Describe the principal microstructures in the quartz and the feldspar, and interpret the deformation mechanisms that led to these microstructures.
- 2 What is the approximate range of temperatures experienced by this rock? How do you know?
- 3 On the photomicrograph, label all of the kinematic indicators you can find. What is the sense of shear recorded by these kinematic indicators?

**Problem 16.7**

- 1 Figure G-54a shows a porphyroclast. What type is it?
- 2 The shear zone that contains this porphyroclast strikes  $050^\circ$  and dips  $70^\circ$  to the southeast. Mineral lineations plunge  $70^\circ$  toward  $140^\circ$  (down dip). The photographer who took this photograph was looking at a vertical cliff face, along the strike of the shear zone (i.e., toward  $050^\circ$ ) so that northwest (NW) is on the left side of the photo and southeast (SE) is on the right. Describe *in detail* the type of movement on this shear zone. (Here is a generic example of a complete description: "normal-sense movement, northeast side down.")

**Problem 16.8**

Figure G-54b is a field photograph of a mylonitic megacrystic (porphyritic) granite from a shear zone that strikes  $330^\circ$  and dips  $20^\circ$ SW. Mineral lineations are down dip. You are looking at a vertical outcrop, parallel to the strike of the shear zone (toward  $330^\circ$ ) so that southwest (SW) is to your left and northeast (NE) is to your right. Describe *in detail* the type of movement on this shear zone. (Here is a generic example of a complete description: "reverse-sense movement, northwest side up.")

**Problem 16.9**

Figure G-55 is a tectonic map of a region that contains three major shear zones that were active at different times. For each shear zone a stereogram is provided that indicates the foliation and lineation orientations within the shear zone. Figure G-56a, b, and c are samples from shear zones A, B, and C, respectively. Use these figures to determine the type of movement in each shear zone. In one succinct paragraph, present the deformational history of the map area, summarizing the timing and style of each deformational event.



## Introduction to Plate Tectonics

### Objectives

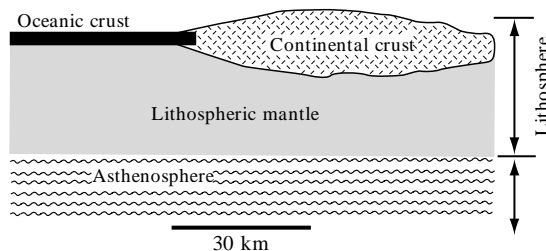
- Determine rates and relative plate motions at triple junctions.
- Use earthquake focal-mechanism solutions to determine type of faulting and type of plate boundary.
- Use ocean-floor magnetic anomalies to determine plate-motion rates.
- Determine latitudinal movement of plates using apparent polar-wander paths.
- Decipher the plate tectonic history of a region (the “plate game”).

A particularly exciting aspect of structural geology during the past few decades has been the integration of fault studies, seismology, and paleomagnetism to better understand plate tectonic processes. The concept of plate tectonics has revolutionized the earth sciences and provides a context for many diverse geologic processes including earthquakes, volcanoes, the construction of mountain belts, and the development of ocean basins. The purpose of this chapter is to introduce a few of the more powerful techniques employed by geologists and geophysicists to decipher both modern-day and ancient plate motions and plate configurations.

Some of the material in this chapter will doubtless already be familiar to many of you from other courses you have taken. However, the details of how seismic patterns, paleomagnetic data, and focal-mechanism solutions can be combined into a powerful tool for reconstructing plate interactions will be new to nearly all of you. The chapter culminates in an exercise in which you will employ all of these techniques to determine the plate tectonic history of a region.

### Fundamental principles

The earth consists of three compositionally distinct, concentric shells: the core, mantle, and crust. Within the upper mantle, a major change in mechanical properties plays an important role in governing plate tectonic processes (Fig. 17.1). The 80–150-km thick lithosphere includes the crust and the upper part of the mantle. The lithosphere behaves rigidly and is reasonably strong. Beneath the lithosphere lies the weak, plastically yielding *asthenosphere*, which is several hundreds

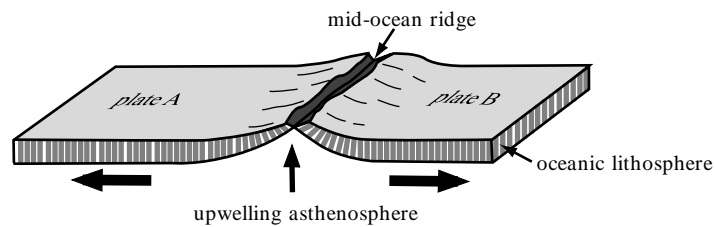


**Fig. 17.1** Structure of the earth's crust and upper mantle.

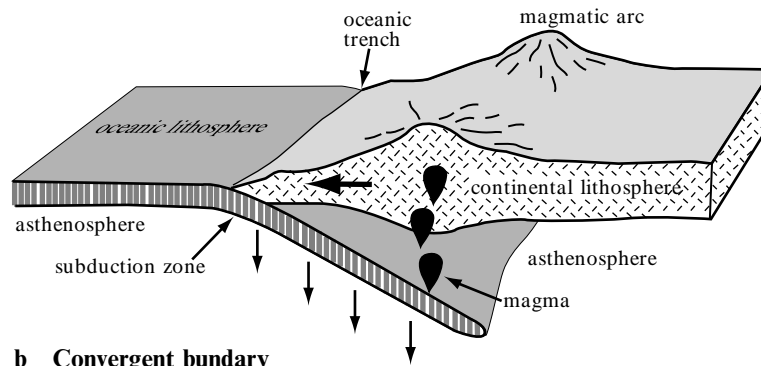
of kilometers thick. The asthenosphere coincides with the depth at which a small fraction of mantle rock begins to melt.

Here are some fundamental principles of plate tectonics:

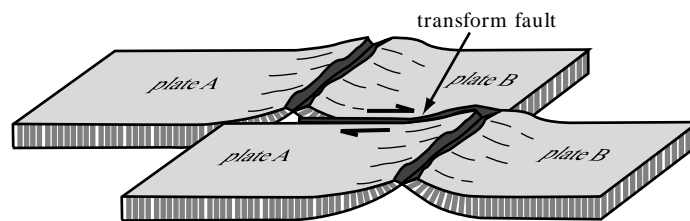
- 1 The lithosphere is broken into six or seven large slabs and about a dozen small ones. These lithospheric slabs are called plates.
- 2 These plates move with respect to one another as they “float” on the underlying asthenosphere.
- 3 Plates mostly interact along their boundaries (although broad areas of intraplate deformation also exist). Boundaries along which plates move away from each other are called *divergent boundaries*; boundaries along which plates move toward one another are called *convergent boundaries*; and boundaries along which plates slide past one another are called *transform boundaries* (Fig. 17.2).
- 4 Plates are internally rigid. Most deformation resulting from plate interaction occurs along plate margins; such regions are called *mobile belts*. Deformation does sometimes occur within the interior of a plate, but such deformation tends to be of lower magnitude and to occur at slower rates than deformation at plate margins.



**a Divergent boundary**



**b Convergent boundary**



**c Transform boundary**

**Fig. 17.2** Plate boundaries. (a) Divergent-plate boundary. (b) Ocean-continent convergent-plate boundary. (c) Transform boundary.

## Plate boundaries

Plates move away from one another at oceanic spreading centers. Basaltic magmatism, induced by partial melting of material within the asthenosphere, erupts at the axis of a ridge, thereby creating new oceanic lithosphere as plates diverge from one another. The mid-ocean ridges are sites of volcanism, extensional faulting, and the creation of new oceanic lithosphere (Fig. 17.2a).

Where an oceanic plate and a continental plate converge, the denser oceanic plate sinks beneath the more buoyant continental plate in a process called subduction (Fig. 17.2b). Subduction causes earthquakes at the interface between the two plates and magmatism in the overriding plate. In this manner oceanic lithosphere is recycled into the asthenosphere. Oceanic trenches are the bathymetric manifestation of the subduction process. Where two continental plates converge, one plate may partially subduct beneath the other. However, this process is not very efficient because the two plates have similar densities. The result of continent–continent convergence is a collisional boundary marked by mountain building, thrust faulting, and limited amounts of granitic magmatism. Where two oceanic plates converge, the older plate is generally subducted beneath the younger one because the older plate is cooler and denser.

Two plates slide past one another at transform boundaries (Fig. 17.2c). Transform boundaries are strike-slip faults that link other types of plate boundaries, most commonly ridge segments. Transform boundaries are sites of earthquakes but little or no volcanic activity. Lithosphere is neither created nor destroyed at these boundaries.

## Triple junctions

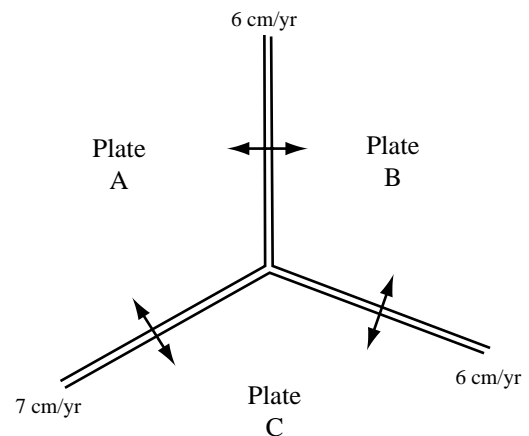
The intersection of three plates is called a triple junction. Consider the simple triple junction in Fig. 17.3a. Each plate is separated from its neighbors by an oceanic ridge, and the three ridges meet at a point. This is a stable and viable plate-boundary configuration. If the rates and directions of relative plate motion across any two boundaries are known, then the rate and direction of motion across the third boundary can be calculated by constructing a velocity triangle, as explained in the two examples below. The construction of velocity triangles can help determine the relative rates and directions of plate motions where other independent means of determining plate motions are not available.

## Example 1

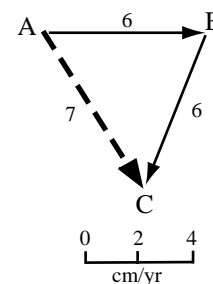
Suppose, as shown in Fig. 17.3a, that the relative rate of spreading between plate A and plate B is 6 cm/yr, and the relative rate of spreading between plate B and plate C is also 6 cm/yr. What is the rate of relative motion between plate A and plate C?

*Solution (Fig. 17.3b)*

- 1 Arbitrarily hold one plate fixed — say, plate A.
- 2 Let a point represent the fixed plate, and plot a vector, in true map orientation, that corresponds to the motion of plate B relative to plate A. The point at the end of the vector represents plate B, and the length of the vector corresponds to the rate of relative plate motion. In Fig. 17.3b the  $A \rightarrow B$  vector points due east and is 6 units long.
- 3 Now, hold plate B fixed, and draw a vector from point B that describes the motion of plate C relative to plate B. The direction of motion between these plates is measured on the map with a protractor.



**a**



**b**

**Fig. 17.3** (a) Ridge–ridge–ridge triple junction. Arrows show relative movement of adjacent plates at the rates indicated. (b) Velocity triangle for plate configuration shown in (a). See text for discussion.

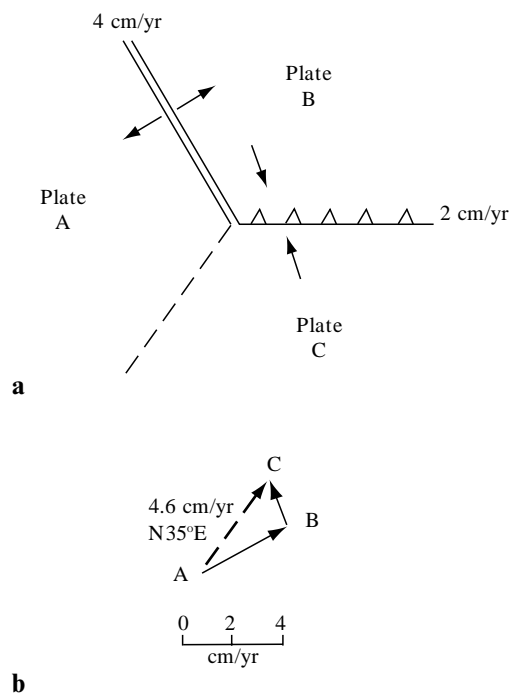
- 4 To complete the velocity triangle, plot the resultant vector from point A to point C. In this example the vector is oriented  $147^\circ$  and is 7 units long, indicating that plate C is moving away from plate A at a rate of 7 cm/yr.

### Example 2

Suppose, as shown in Fig. 17.4, plate B is moving away from plate A at a rate of 4 cm/yr, and plate C is being subducted (somewhat obliquely) beneath plate B at a rate of 2 cm/yr (Fig. 17.4a). What type of plate boundary occurs between plates A and C, and what is the rate of motion between these two plates?

*Solution (Fig. 17.4b)*

- 1 Construct the two sides of the velocity triangle that describe the direction and rate of movement between plates A and B and plates B and C.
- 2 Plot the resultant vector from point A to point C. This vector indicates that plate C is moving 4.6 cm/yr in a direction  $035^\circ$  relative to plate



**Fig. 17.4** Sketch showing the use of a velocity triangle to determine the type of plate boundary. The relative motions of plate A with respect to plate B, and plate B with respect to plate C, are known. But the relative motion of plate A with respect to plate C is unknown. (b) Construction of a velocity triangle indicates that the boundary between plates A and C is a transform fault. See text for discussion.

A. This direction is parallel to the boundary between plates A and C, which tells us that the boundary between plates A and C is a transform fault.

### Problem 17.1

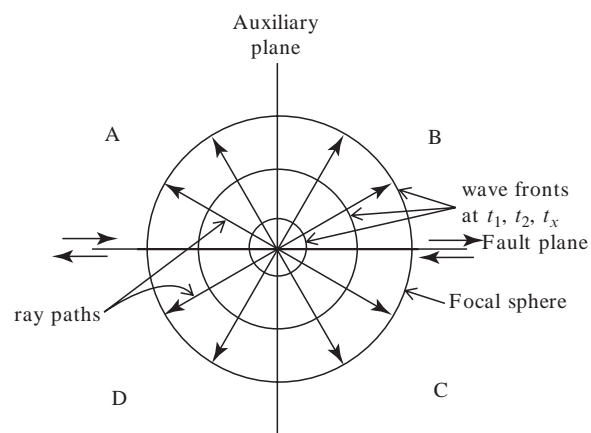
Given the plate tectonic configuration shown in Fig. G-57a (Appendix G), determine the type of plate boundary and the relative rate of motion between plates B and C.

### Problem 17.2

Given the plate configuration shown in Fig. G-57b, determine the type of plate boundary and the relative rate of motion between plates B and C.

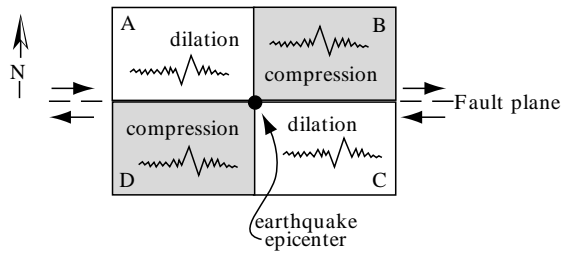
### Focal-mechanism solutions ("beach-ball" diagrams)

During an earthquake, seismic waves are generated at the *hypocenter*, or focus, of the earthquake. These waves radiate in all directions; the wave front travels through the earth and defines an imaginary, expanding spherical surface called the *focal sphere* (Fig. 17.5). The actual seismic ray paths are perpendicular to the wave front. The point on the earth's surface directly above the hypocenter is the *epicenter*.



**Fig. 17.5** Seismic energy released at the hypocenter (center of diagram) releases waves that propagate in all directions. The wave front defines spherical surfaces that increase in radius with time. The ray paths are shown as straight lines perpendicular to the wave front. The focal sphere is the wave front at any time of interest.





**Fig. 17.6** Map view of a right-slip fault showing the quadrants of compression (gray) and dilation (white). Within each quadrant is a schematic representation of the first motion on the needle of a seismograph. Moving from left to right, the first motion is “down” if the seismic station lies within a dilational quadrant; it is “up” if the seismic station lies within a compressional quadrant.

When the wave front arrives at a seismic station on the earth’s surface, a key aspect of the data recorded is the direction — either up or down — of the first motion of the needle of the seismograph. Whether the needle’s first motion is up or down is determined by the nature of the first ground motion experienced at the site. There are two possibilities: a push (compression) or a pull (dilation). If the first ground motion is compressional the first motion of the needle is upward, and if the first ground motion is dilational the first motion of the needle is downward.

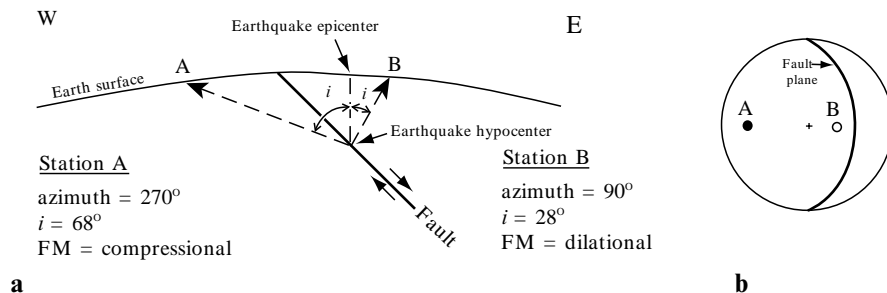
The direction of the first ground motion depends on: (1) the position of the recording station relative to the hypocenter, and (2) the type of faulting that occurred — normal, thrust, or strike-slip. Analysis of earthquake first-motion data from many seismic recording stations provides information about the fault attitude and the direction of slip. Such analyses — called *first-motion studies* — are particularly valuable in the

many cases in which an earthquake does not cause surface rupture. First-motion studies are also used to determine relative motions of lithospheric plates where plate boundaries are not directly observable, such as on the seafloor.

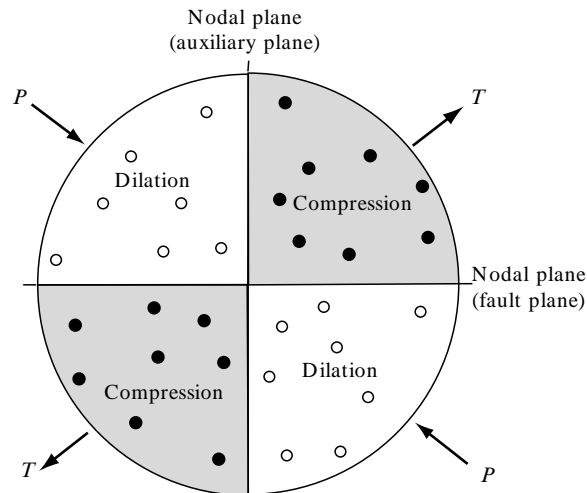
Consider Fig. 17.6, which is a map view of a vertically dipping, right-slip fault. An earthquake has just occurred below the epicenter in the center of the map. The map is divided into four quadrants: A, B, C, and D. Seismic recording stations in quadrants B and D lie “in the direction” of the slip vector and hence experience a *compressional* first ground motion, recorded as an upward first motion on the seismogram. Stations in quadrants A and C, on the other hand, lie “behind” the earthquake; they experience a *dilational* first ground motion, recorded as a downward first motion on the seismogram. Conventional notation for first motion is a closed circle for compression and an open circle for dilation.

In addition to recording first-motion data, a seismic station (along with data from other stations) records its location relative to the hypocenter. The two parameters used to record a station’s location are the *azimuth* of the station relative to the epicenter and the *angle of incidence* ( $i$ ) that the ray vector makes *relative to the vertical* (Fig. 17.7a). These data are plotted on a lower-hemisphere, equal-area projection as shown in Fig. 17.7b.

When first-motion data are recorded at many stations and plotted together, the distribution of points defines four quadrants, two of which are compressional and two dilational (Fig. 17.8). In the case of a large earthquake, these quadrants may extend around the globe (Fig. 17.9). Compressional quadrants are conventionally colored black or gray, while the dilational quadrants are white.



**Fig. 17.7** (a) East–west cross section of a seismically active normal fault. An earthquake at the hypocenter radiates seismic energy in all directions. Seismic waves are recorded at stations A and B. FM, first motion;  $i$ , angle of incidence. (b) Lower-hemisphere plot showing orientation of the fault and the positions of stations A and B relative to the earthquake focus. A seismic station at the epicenter, directly above the hypocenter, would plot at the center of the projection. The solid circle at station A indicates a compressional first motion; the open circle at station B indicates a dilational first motion.



**Fig. 17.8** Focal-mechanism solution, in which each seismic station is plotted on the lower-hemisphere projection according to its location relative to the earthquake focus (see text for discussion). Compressional first motions are indicated by solid circles; dilational first motions are indicated by open circles. Nodal planes are then chosen to separate fields of opposite first motions. Geologic data must be used to determine which of the nodal planes is the fault plane. Note that the  $P$  axis ( $P$  for pressure) bisects the dilational quadrant and the  $T$  axis ( $T$  for tension) bisects the compressional quadrant.

The boundaries between the quadrants are two perpendicular planes called the *nodal planes* (Figs 17.8 and 17.9). These are planes on which the first motion is undefined. One of the nodal planes is always the *fault plane*; the other is termed the *auxiliary plane*. The auxiliary plane is perpendicular to both the fault plane and the slip direction. Occasionally, a station may record a very weak first arrival that is feebly compressional or dilational. This indicates that that particular station coincides with one of the nodal planes. If one or more stations exhibit a nodal first motion, the nodal planes may be plotted directly. If no stations record a nodal first motion, then the seismologist must select nodal planes that best fit the data. The resulting plot is called a *focal-mechanism* (or fault-plane) solution (Fig. 17.8).

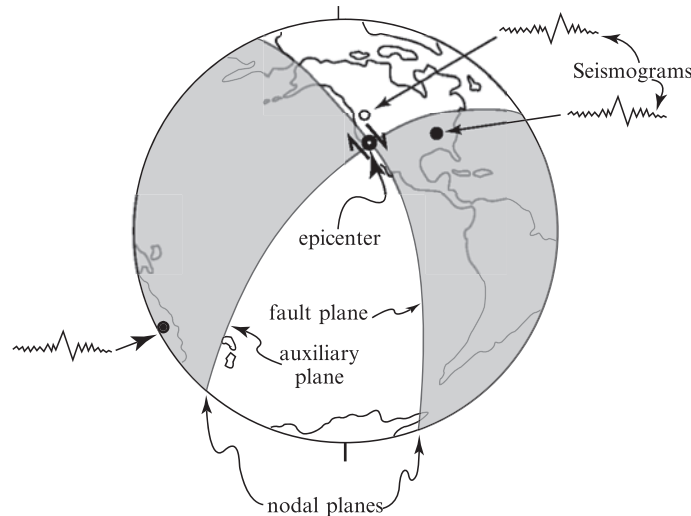
Depending on the orientation of the nodal planes and the location of the earthquake epicenter, the quadrant pattern of a focal-plane solution resembles a beach ball; hence, they are sometimes informally called “beach-ball” diagrams. But it is important to remember that focal-plane solutions are lower-hemisphere, stereonet plots, involving the same techniques discussed in Chapter 5.

Note that a focal-mechanism solution does not distinguish uniquely between the fault plane and the auxiliary plane. The seismologist must take into consideration the geologic setting in which the earthquake occurred, and then select the nodal plane that is most reasonably interpreted

to be the fault plane. Look at Fig. 17.9, for example. This figure is not a lower-hemisphere projection, so it is not a focal-mechanism solution; it is simply a map of a portion of the earth showing compressional and dilational quadrants. The epicenter in this figure is on the San Andreas Fault, which is known to be oriented approximately north–south. This knowledge allows us to pick the north–south nodal plane as the fault plane, leaving the east–west nodal plane as the auxiliary plane.

Focal-mechanism solutions provide additional information about fault movement during an earthquake. By analogy with laboratory tests of rock failure, we may define axes of infinitesimal shortening ( $P$  for pressure) and extension ( $T$  for tension). In each case, the axis lies in a plane perpendicular to the nodal planes; the  $P$  axis bisects the dilational quadrants and the  $T$  axis bisects the compressional quadrants. If this relationship between the  $P$  and  $T$  axes and the quadrants sounds backwards, consider that just prior to rupture, the particles that lie parallel to the  $P$  axis move away from the shortening direction (“dilational” behavior). Particles that lie normal to the  $P$  axis are forced toward one another (“compressional” behavior).

We can also use focal-mechanism solutions to determine the trend and plunge of the slip direction, or *slip line*, of a fault if the attitude of the fault plane is known. The slip line lies within the



**Fig. 17.9** Map of a portion of the earth, showing an earthquake epicenter on the San Andreas Fault in California, and the distribution of compressional and dilational quadrants around the globe. This is not a focal-mechanism solution because it is not a lower-hemisphere projection, but it shows many of the features of a focal-mechanism solution. After Sherburne and Cramer (1984).

fault plane and is the pole of the auxiliary plane. Thus, if the compressional and dilational quadrants are well defined, the slip direction and type of movement along the fault can easily be determined. This type of analysis represents the overlap of seismology and structural geology.

Study the examples in Fig. 17.10, which illustrate how focal-mechanism solutions can be used to interpret fault motion associated with an earthquake. One must always use geologic information to determine which nodal plane is the fault plane and which is the auxiliary plane. For each diagram in Fig. 17.10, try to visualize both possible fault planes. Remember that each diagram is a lower-hemisphere projection and that the  $P$  axis bisects the dilational (white) quadrants.

### Problem 17.3

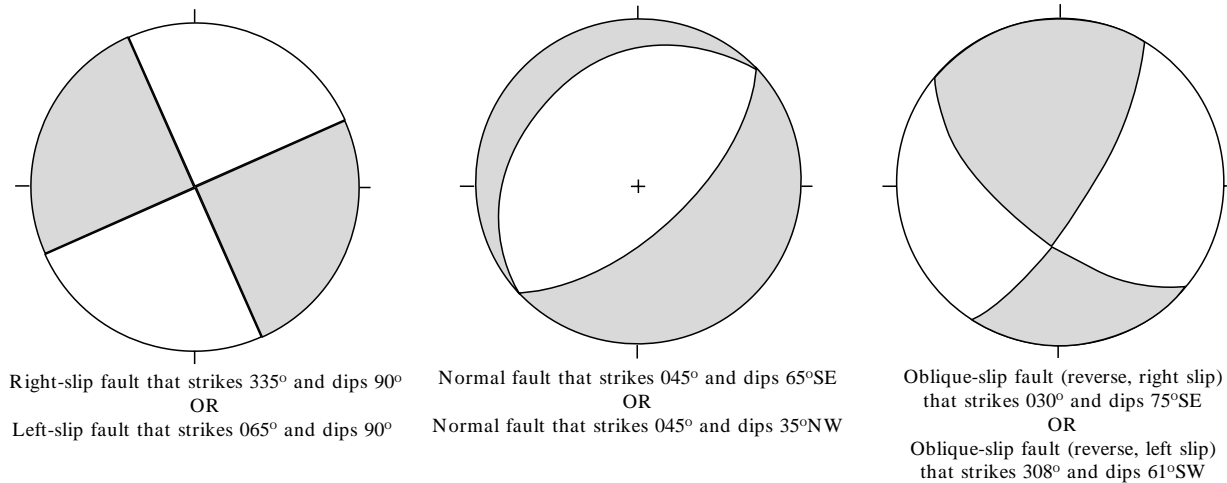
Figure G-58 contains three focal-mechanism solutions. Beneath each diagram write a description of the two possible interpretations for fault orientation and sense of motion (normal, reverse, oblique, etc.), as in the example of Fig. 17.10. Measure the fault strikes precisely with a protractor, but use the template to determine the approximate dip. In the case of oblique movement specify both components of motion, e.g., “left-reverse movement” or “dominantly normal with a component of right slip.”

### Example 3

Suppose you map a seismically active fault that strikes  $030^\circ$  and dips  $60^\circ\text{SE}$ . Slickenlines on the exposed fault surface indicate that the motion on the fault is pure dip slip, but you are unable to determine from field evidence whether it is a normal fault or a reverse fault. An earthquake on the fault is recorded at seismic station “A.” The first motion is compressional, the azimuth from the epicenter to the station is  $175^\circ$ , and the angle of incidence is  $35^\circ$ . Determine whether the motion on the fault is normal or reverse.

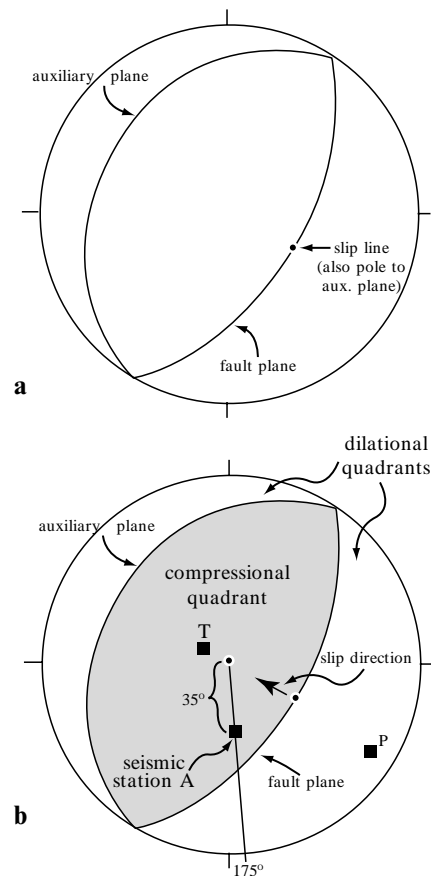
### Solution

- 1 On the stereonet, draw the great circle that represents the fault plane (Fig. 17.11a).
- 2 Draw the point on the fault plane that represents the slip line (determined by the pitch of the slickenlines in the fault plane). In this case, we know that the motion is pure dip slip, so the pitch of the slickenlines is  $90^\circ$ ; thus the slip-line point is plotted at the mid-point of the fault-plane great circle (Fig. 17.11a).
- 3 The slip-line point represents the pole to the auxiliary plane. Use the location of the slip-line point to draw the great circle representing the auxiliary plane (Fig. 17.11a).



**Fig. 17.10** Alternative interpretations for three focal-mechanism solutions. The two possible interpretations for fault orientation and motion are given beneath each plot.

- Plot seismic station “A” on the stereonet, using the azimuth and incidence data. (Refer to the way seismic stations are plotted in Fig. 17.7.) In the present case, the azimuth from the epicenter to the seismic station is 175°, so the station lies somewhere on the line that runs from the center of the net to the 175° point on the perimeter of the net. The angle of incidence is 35°, which tells us the distance from the center of the net to the seismic station (Fig. 17.11b). It turns out that station “A” lies within the quadrant that occupies the middle of the stereonet. We know from the first motion on the station “A” seismogram that it lies within a compressional quadrant, so this quadrant is colored gray on Fig. 17.11b; the adjacent two quadrants are dilational, so they are white.
- Knowing that the central quadrant is a compressional quadrant allows us to now draw a slip direction arrow, which must point into a compressional quadrant (Fig. 17.11b). We can also now plot the axes of maximum shortening (*P*) and extension (*T*), which lie on a plane perpendicular to the nodal planes, each bisecting a quadrant (Fig. 17.11b).
- The slip-direction arrow indicates the slip direction of the hanging wall of the fault. In this example the hanging wall is sliding *up* the fault plane, thus the motion on this fault is reverse. As a general rule, slip-direction arrows of normal faults point toward the perimeter of the net, while slip-direction arrows of reverse faults point toward the center of the net (cf. Fig. 10.4).



**Fig. 17.11** Lower-hemisphere plot showing the solution to Example 3. (a) Plot of fault plane, slip-line point, and auxiliary plane. (b) Completion of Example 3. See text for discussion.

**Problem 17.4**

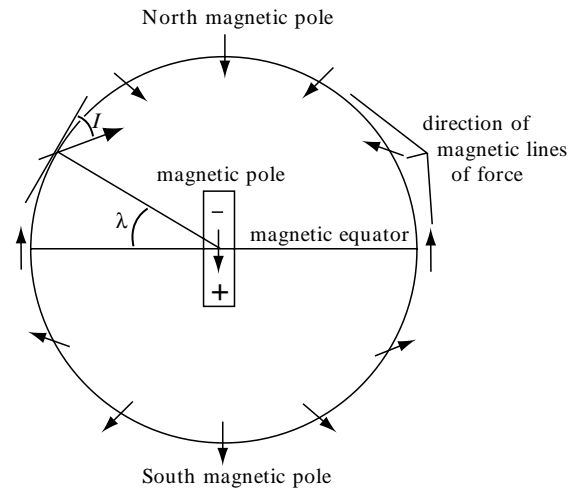
Sketch the focal-mechanism solutions for earthquakes that would be expected to occur at each of the plate boundaries in Problems 17.1 and 17.2 (Fig. G-57). Be sure to label the fault plane, the auxiliary plane, and the *P* and *T* axes.

**Problem 17.5**

Figure G-59 contains a map showing the position of the Mendocino triple junction off the coast of northern California. The Mendocino triple junction is the point of intersection of the Pacific, North American, and Juan de Fuca Plates. Two earthquakes (event A and event B) occurred near the triple junction. They could have been centered on either of two transform boundaries or on the convergent boundary between the Juan de Fuca and North American Plates. The table presents data for the two earthquakes recorded at 25 seismic stations. Using two sheets of tracing paper (one sheet for each event) and your equal-area net (Fig. G-11), do the following: for each earthquake: (1) construct a focal-mechanism plot, (2) determine the plate boundary along which the earthquake occurred, (3) determine the attitude of the fault plane, (4) use arrows to show the slip sense along the fault, and (5) plot the *P* (shortening) and *T* (extension) axes.

**Earth magnetism**

It has long been known that the earth possesses a magnetic field. Although the origin of the magnetic field is controversial, many observations support the hypothesis that it is generated by moving currents in the liquid-metal outer core. The configuration of the earth's magnetic field is the same as one produced by iron shavings around a magnet; that is, it approximates the field that would result if a giant bar magnet were present at the center of the earth. Figure 17.12 shows the lines of force associated with the present-day magnetic field. Note that at the north magnetic pole, the lines of force are directed downward toward the center of the earth and that at the south magnetic pole the lines of force are directed upward, away from the center of the earth. At the equator, the lines of force are horizontal and point toward the north magnetic pole.



**Fig. 17.12** Schematic diagram of the earth showing the orientation of the earth's magnetic field at various latitudes (arrows).  $\lambda$ , magnetic latitude;  $I$ , inclination. See text for discussion.

At any point on its surface, the earth's magnetic field can be expressed in terms of two components: *declination* and *inclination*. Declination is the angle between geographic north and magnetic north. The orientation of the earth's magnetic field (and thus the declination) varies with time. However, the mean magnetic dipole field, averaged over time spans of about 10,000 years, appears to be very close to the geographic pole.

Inclination is simply the angle that the field makes with the horizontal. By convention, a downward inclination is considered positive in sign. Note that there is a systematic relationship between inclination and latitude (Fig. 17.12). Because the earth is nearly spherical, the relationship between latitude and inclination is not linear but is expressed by the equations:

$$I = \tan^{-1} (2 \tan \lambda)$$

$$\lambda = \tan^{-1} [(\tan I)/2]$$

where  $I$  is the magnetic inclination and  $\lambda$  is the latitude relative to the magnetic pole.

Note that in the time-averaged case where the geographic and mean magnetic poles coincide, geographic and "magnetic" latitude will also coincide. There is considerable evidence that the magnetic field of the earth sometimes changes polarity; that is, the north magnetic pole becomes the south magnetic pole and vice versa. These *magnetic reversals* are not sudden, catastrophic events. It appears that the intensity of the magnetic

field progressively weakens in one direction, ultimately reaching zero, then it progressively strengthens in the opposite orientation. Magnetic reversals do not occur with any regularity, but a given polarity interval seems to persist in the order of  $10^4$ – $10^6$  years.

### Problem 17.6

Determine the inclination of the earth's magnetic field at the following latitudes:

20°N

45°S

78°N

10°S.

### Paleomagnetism

In igneous rocks, magnetic minerals acquire a magnetization parallel to the prevailing magnetic field once they cool below the Curie temperature ( $580^\circ\text{C}$  for magnetite). Many sedimentary rocks contain small amounts of magnetite or other magnetic iron oxides. During deposition of fine-grained sediments in quiet water settings, these minerals align themselves parallel to the earth's magnetic field. Thus, under the proper conditions, many rocks preserve a record of the orientation of the earth's magnetic field at the time they formed. The study of ancient or fossil magnetism in rock is called *paleomagnetism*. Paleomagnetic studies were instrumental in leading to the widespread acceptance of plate tectonics, and such studies provide critical data for ancient plate reconstructions as discussed below.

### Magnetic stripes on the ocean floor

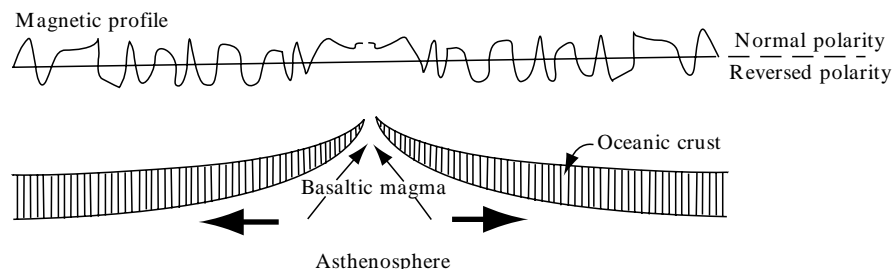
Magnetic surveys of the ocean floor show a magnetic signature that is symmetrically disposed about the mid-ocean ridges. Basaltic crust that forms at the axis of an active oceanic ridge will acquire a magnetization at the time that it cools through the Curie temperature. Because the earth's magnetic field reverses polarity from time to time, the basalt may show either normal or reversed polarity in accord with the magnetic field at the time it cools. Spreading away from the ridge axis is bilateral, so basalts of the same age will lie at equal distances from the ridge and show the same magnetic polarity. The continuous outpouring of basalt at ocean ridges thus serves as a tape recorder, faithfully recording the polarity of the earth's magnetic field through time (Fig. 17.13). Recognition of these magnetic "stripes," or *magnetic anomalies*, of alternating normal and reversed polarity led to widespread acceptance of the concept of "seafloor spreading" in the late 1960s. Recognition and dating of distinct magnetic anomalies on the ocean floor also allow us to determine the rate of movement between diverging plates.

### Example 4

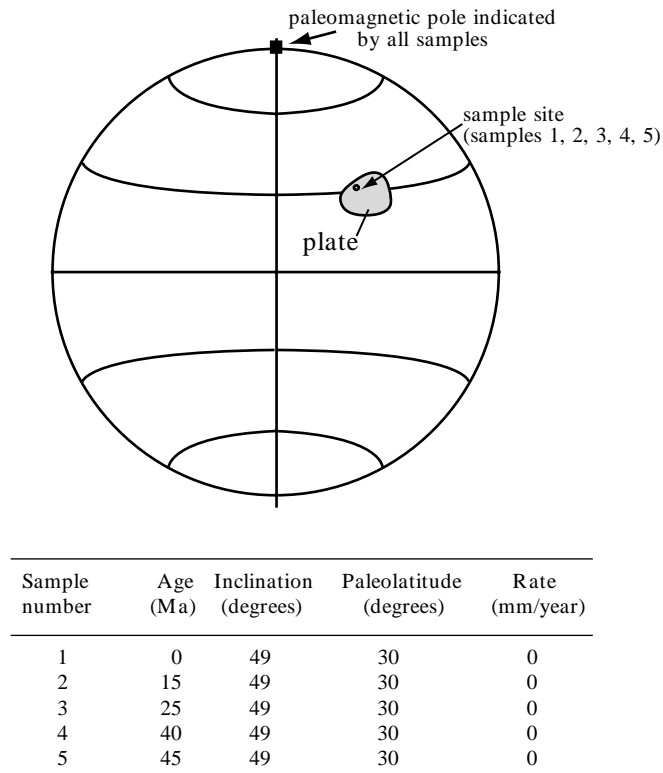
Across a particular ocean ridge, the distance between magnetic anomaly number 25 on one side of the ridge and the same anomaly on the opposite side of the ridge is 3360 km. The rocks are 56 million years old. What is the time-averaged rate of spreading between the two oceanic plates?

### Solution

The rate of relative motion is simply the distance between the anomalies divided by time or  $(3.36 \times 10^3 \text{ km}) / (5.6 \times 10^7 \text{ years}) = 6.0 \times 10^{-5} \text{ km/yr}$  or 6 cm/yr.



**Fig. 17.13** Cross section through a mid-ocean ridge. Note the symmetry of the magnetic profile with respect to the axis of the mid-ocean ridge.



**Fig. 17.14** Sample sites and calculated paleomagnetic poles for a fixed plate. The table provides age and inclination data.

### Apparent polar wander

Because the time-averaged position of the earth's magnetic poles coincides with the geographic poles, we can use paleomagnetic inclination to determine the paleolatitude of a region of interest. Note, however, that paleomagnetic data cannot provide any information regarding paleolongitude. Paleomagnetic studies can therefore document plate motions in a north-south direction (changes in latitude), but not motions in an east-west direction (changes in longitude).

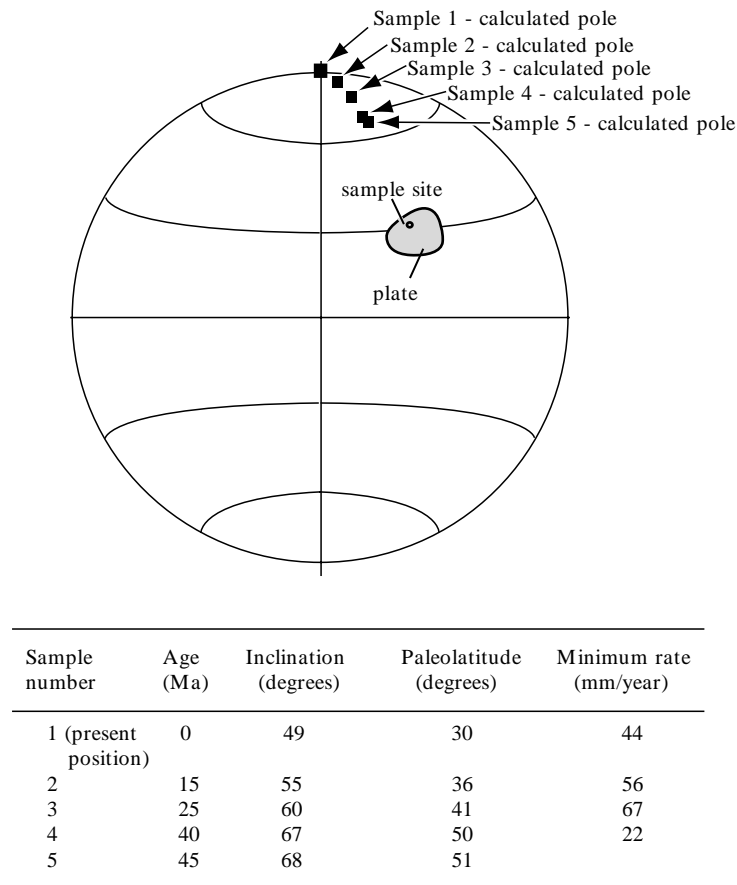
If a plate were to remain fixed in position (latitude), or move only in an east-west direction, rocks of all ages from that plate would show exactly the same magnetic inclination. This is another way of saying that all rock samples would define the same paleomagnetic pole (Fig. 17.14).

If a plate moves from a high-latitude position toward the equator over time, younger rocks will show progressively more gently plunging magnetic inclinations. In this case, from the point of view of a "fixed" plate, the calculated paleomagnetic poles

from progressively younger samples would appear to move "away" from the plate or northward in the northern hemisphere (Fig. 17.15). This apparent movement of paleomagnetic poles is termed *apparent polar wander*. Conversely, if a plate moves poleward from equatorial latitudes with time, younger rocks will show progressively steeper magnetic inclinations. By studying systematic changes in magnetic inclination through time, paleomagnetists can track the north-south motion of a plate.

An important limitation to this technique is that we cannot always be certain whether a given rock was magnetized in a normal or a reverse sense. Therefore the sign of the inclination (positive for northern hemisphere and negative for southern) cannot generally be determined. We can only say that the plate resided at, for example, either 30° north latitude or 30° south latitude at a particular time. Independent data must be used to distinguish between the two possibilities.

By collecting paleomagnetic data from samples with the same range of ages from two plates, we can "track" the motion of the two plates relative to



**Fig. 17.15** Sample sites and calculated paleomagnetic poles for a plate that has moved southward with time. The table provides age and inclination data.

one another. For example, at the beginning of the Cenozoic era, prior to its collision with Asia, India lay about  $30^\circ$  farther south than its present latitude. Paleomagnetic data from rocks that formed early in the Cenozoic era in southern Asia and northern India yield paleomagnetic poles that differ by  $30^\circ$ , reflecting the difference in latitude of the two continents at that time. As India approached Asia throughout the Cenozoic, the difference in latitude decreased, as did the difference in paleomagnetic poles determined from successively younger rocks on the two plates. Very young rocks sampled from the two plates near the suture would show essentially the same pole. In similar fashion, one could paleomagnetically

document a continental rifting event. Rocks on either side of the rift would show equivalent paleomagnetic poles prior to rifting. Rocks that formed after the rifting event would show progressively more divergent paleomagnetic pole positions.

#### Problem 17.7

The distance between magnetic anomalies number 12 (34 Ma) and 23 (52 Ma) on a single oceanic plate is 810 km. What is the time-averaged rate of spreading across the ridge during this interval? (Consider the symmetry of marine magnetic anomalies.)



**Problem 17.8**

Paleomagnetic determinations were conducted on three suites of rocks from the Bree Creek Quadrangle. A sandstone unit within the 60 Ma Edoras Formation yielded average inclinations of  $46^\circ$ ; tuffaceous beds within the 38 Ma Dimrill Dale Diatomite yielded inclinations of  $33^\circ$ ; and the Rohan Tuff (18 Ma) yielded an average inclination of  $25^\circ$ . Independent evidence suggests that the Bree Creek Quadrangle remained north of the equator for its entire history.

- 1** Calculate the starting and ending latitudes for the block of continental crust on which this quadrangle lies for each of the two stages of movement.
- 2** Calculate the minimum rate of movement of the block for each stage of movement.
- 3** Explain why your answer to question 2 is a minimum.
- 4** Use Fig. G-60 to sketch figures showing: (1) apparent motion of the paleomagnetic pole in a “fixed” plate reference frame, and (2) latitudinal motion of the plate with respect to the fixed pole.

**Problem 17.9: The “plate game”**

The map in Fig. G-61 depicts the “present-day” distribution of hypothetical continents and oceans. The map contains geologic information as well as seismicity patterns, focal-mechanism solutions, and paleomagnetic sample sites. The dashed lines show traverses from which marine magnetic anomaly data were acquired, and the marine magnetic anomaly patterns for traverses A–B through K–L are shown adjacent to the map. The table summarizes paleomagnetic data from sites P1–P6. Spreading is parallel to the transform faults and perpendicular to the ocean ridges.

- 1** Outline all the plate boundaries using all available information.
- 2** Name each plate or tectonic feature for use in your discussion. Be creative.
- 3** Fix one plate. Describe all the other plate motions in terms of this “fixed plate” reference frame.
- 4** Write a plate tectonic history of the region shown on this map. *Be succinct but be complete.* Make sure that your history incorporates all of the geologic and geophysical information available to you.

# Appendix A

## Measuring attitudes with a Brunton compass

It is often in their structural geology course that students get their first experience with geologic mapping. This appendix is included to facilitate the inclusion of fieldwork in the structure course. We recommend that students practice measuring the attitudes of planes and lineations in the laboratory before going to the field. One convenient way to do that is with hinged boards that can be set up in the classroom (Rowland, 1978).

In North America the traditional instrument for measuring attitudes is the Brunton compass, which requires the strike and dip to be measured separately. There is an instrument, called the Clar compass, that allows the geologist to measure the dip direction ( $90^\circ$  from strike) and angle of dip in a single operation (see Suppe, 1985, fig. 2.2). The following explanation assumes the use of the Brunton compass. Only the relatively simple cases of measuring strike and dip of an exposed plane and trend and plunge of a lineation on an exposed plane will be considered here. For other aspects of compass craft, refer to a book on field geology (e.g., Compton, 1985).

Strike is measured by placing an *edge* (not a side) of the compass along the plane and leveling the bull's-eye level (Fig. A-1). Either end of the needle may be used to read the strike. It is often useful to place a map board or field book against the plane to flatten out irregularities.

Dip is measured by placing the flat *side* of the Brunton against the plane and rotating the arm on the back of the compass until the tube level is level. The face of the compass *must* be vertical. A common error is failure to make the face vertical. The angle of dip is read on the inner scale of the compass face.

Orientations of lineations in a plane are most easily determined by first measuring the attitude of the plane. Then draw a horizontal line on the plane, and, with a protractor, measure the pitch of the lineation within the plane (Fig. A-2). The trend and plunge of each lineation is then determined with an equal-area net (see Chapter 5, Fig. 5.11). Alternatively, the trend and plunge of a lineation may be measured directly by placing your map board vertically and coplanar with the lineation.

After measuring the attitude of a feature in the field, record it in your field notes and *immediately* plot it on your map. Then orient the map and confirm that it is correct. It is exceedingly easy to incorrectly record the dip to the southeast, for example, when it really dips to the northwest. If you do not double check that it looks right on your map while you are still at the outcrop, you may never realize your error. If you are measuring more than one feature at the same outcrop (e.g., orientations of three joint sets), make a neat sketch in your notebook showing the relationships of the various features and their attitudes.

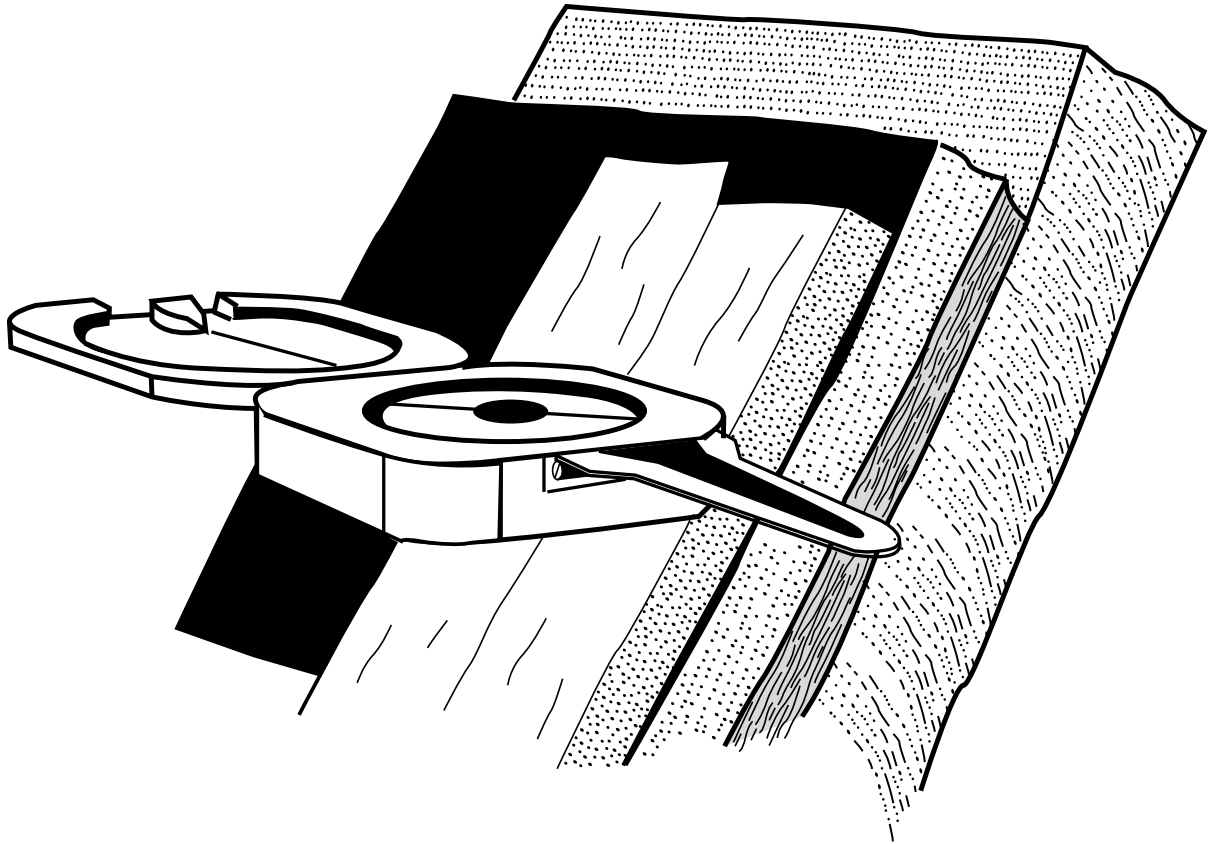


Fig. A-1 Measuring strike with a Brunton compass.

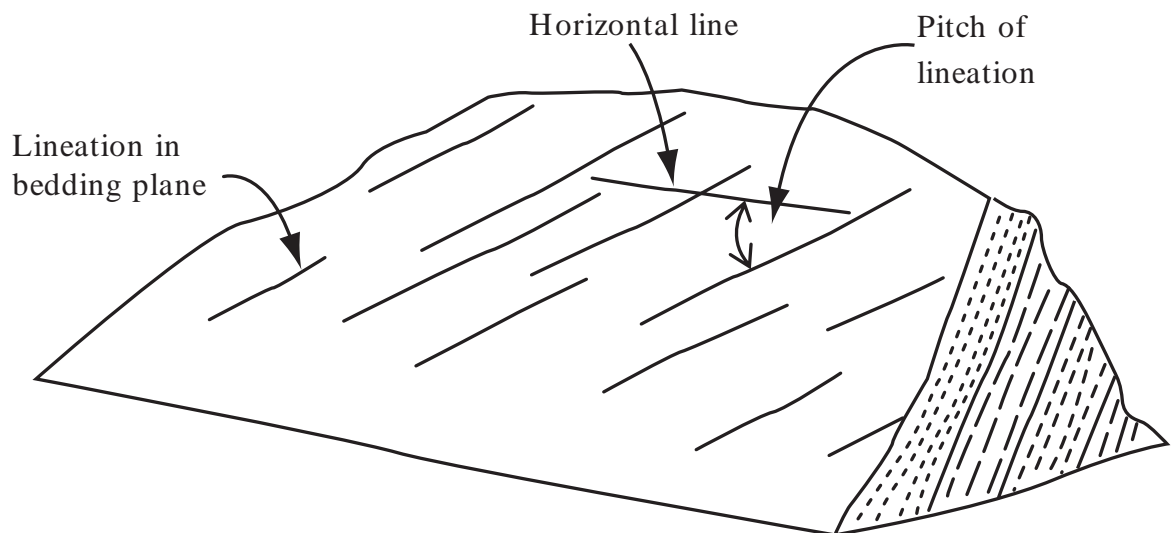
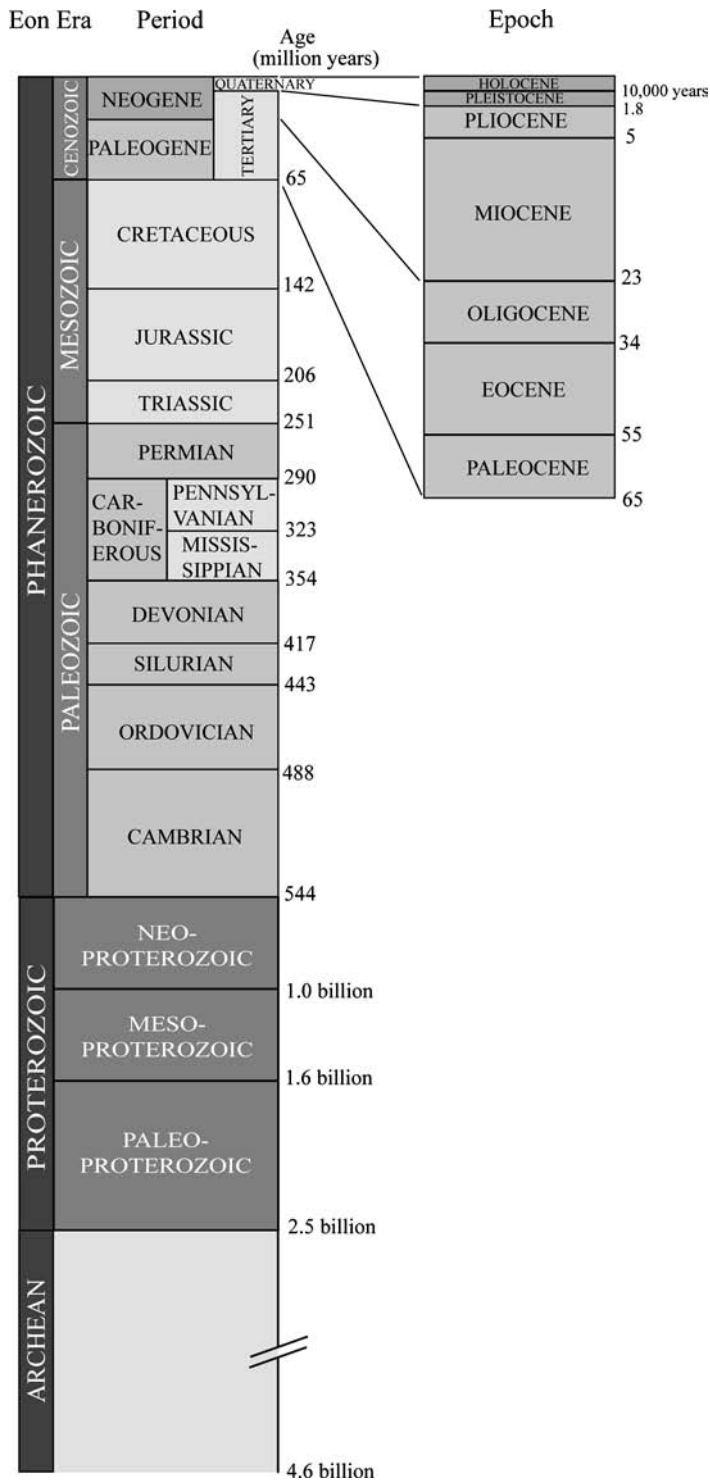


Fig. A-2 Measuring pitch of lineations within a dipping plane.

# Appendix B

## Geologic time scale



# Appendix C

## Greek letters and their use in this book

---

Letter	Use
$\alpha$ (alpha)	Apparent dip (Chapters 1, 2)
$\beta$ (beta)	Angle between the strike of a plane and the trend of an apparent dip (Chapter 1)
$\gamma$ (gamma)	Shear strain (Chapter 14)
$\delta$ (delta)	Plunge of true dip (Chapters 1, 2, 3)
$\varepsilon$ (epsilon)	Strain (Chapter 12)
$\dot{\varepsilon}$	Strain rate (Chapter 12)
$\eta$ (eta)	Coefficient of viscosity (Chapter 12)
$\theta$ (theta)	Trend of apparent dip (Chapters 1, 2)
	Angle between a plane and direction of $\sigma_3$ (Chapter 13)
$\lambda$ (lambda)	Magnetic latitude (Chapter 17)
$\mu$ (mu)	Coulomb coefficient (Chapter 13)
$\pi$ (pi)	Pole of foliation attitude (Chapter 7)
$\sigma$ (sigma)	Stress (Chapters 10, 12)
$\sigma_a$	Axial load (Chapter 13)
$\sigma_c$	Confining pressure (Chapter 13)
$\sigma_n$	Normal stress (Chapter 13)
$\sigma_s$	Shear stress (Chapter 13)
$\sigma_y$	Yield stress (Chapter 12)
$\tau$ (tau)	Same as $\sigma_s$
$\phi$ (phi)	Angle of internal friction (Chapter 13)
$\psi$ (psi)	Angular shear (Chapter 14)

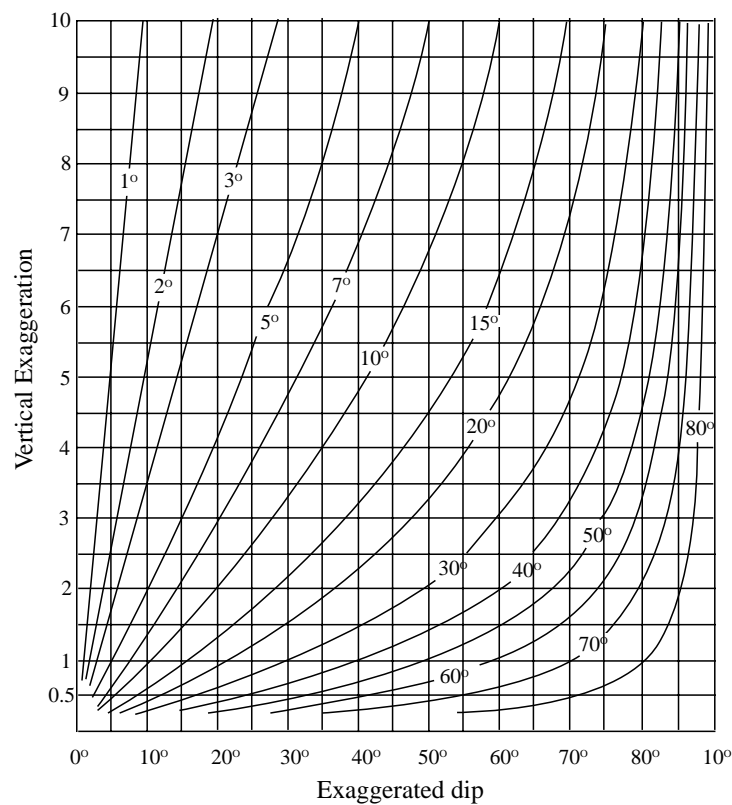
---

# Appendix D

## Graph for determining exaggerated dips on structure sections with vertical exaggeration

Nominal dips are indicated on curved lines. To determine exaggerated dip, carry the vertical exaggeration horizontally across the graph until it intersects with the desired dip. The exaggerated dip lies on the horizontal axis below. For example, on a structure section with 4.0 vertical exagger-

ation, a 20° dip must be drawn at 55° (Dennison, 1968). Alternatively, the exaggerated dip can be calculated trigonometrically using the following relationship:  $\tan \text{exaggerated dip} = (\tan \delta) \times (\text{vertical exaggeration})$ .



# Appendix E

## Conversion factors

### Length

1 inch (in.) = 2.54 cm  
1 cm = 0.3937 in.  
1 m = 39.37 in. = 3.28 ft  
1 foot (ft) = 30.48 cm  
1 mile (mi.) = 1.609 km  
1 km = 0.6214 mi.

### Force

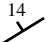
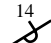


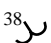

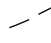
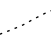




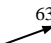
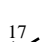
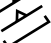

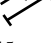



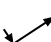


1 newton (N) =  $10^5$  dyne (dn) = 0.1020 kg wt = 0.2248 lb  
1 pound (lb) = 4.448 N = 0.4536 kg wt  
1 kg wt = 2.205 lb = 9.807 N

### Pressure

1 pascal (Pa) =  $1 \text{ N/m}^2 = 9.869 \times 10^{-6} \text{ atm} = 2.089 \times 10^{-2} \text{ lb/ft}^2$   
1 megapascal (MPa) =  $10^6 \text{ Pa} = 10 \text{ bar} = 1.02 \times 10^5 \text{ kg/m}^2$   
1 atmosphere (atm) =  $1.013 \times 10^5 \text{ N/m}^2 = 1.013 \text{ bar}$   
1 bar =  $10^5 \text{ Pa}$

# Appendix F

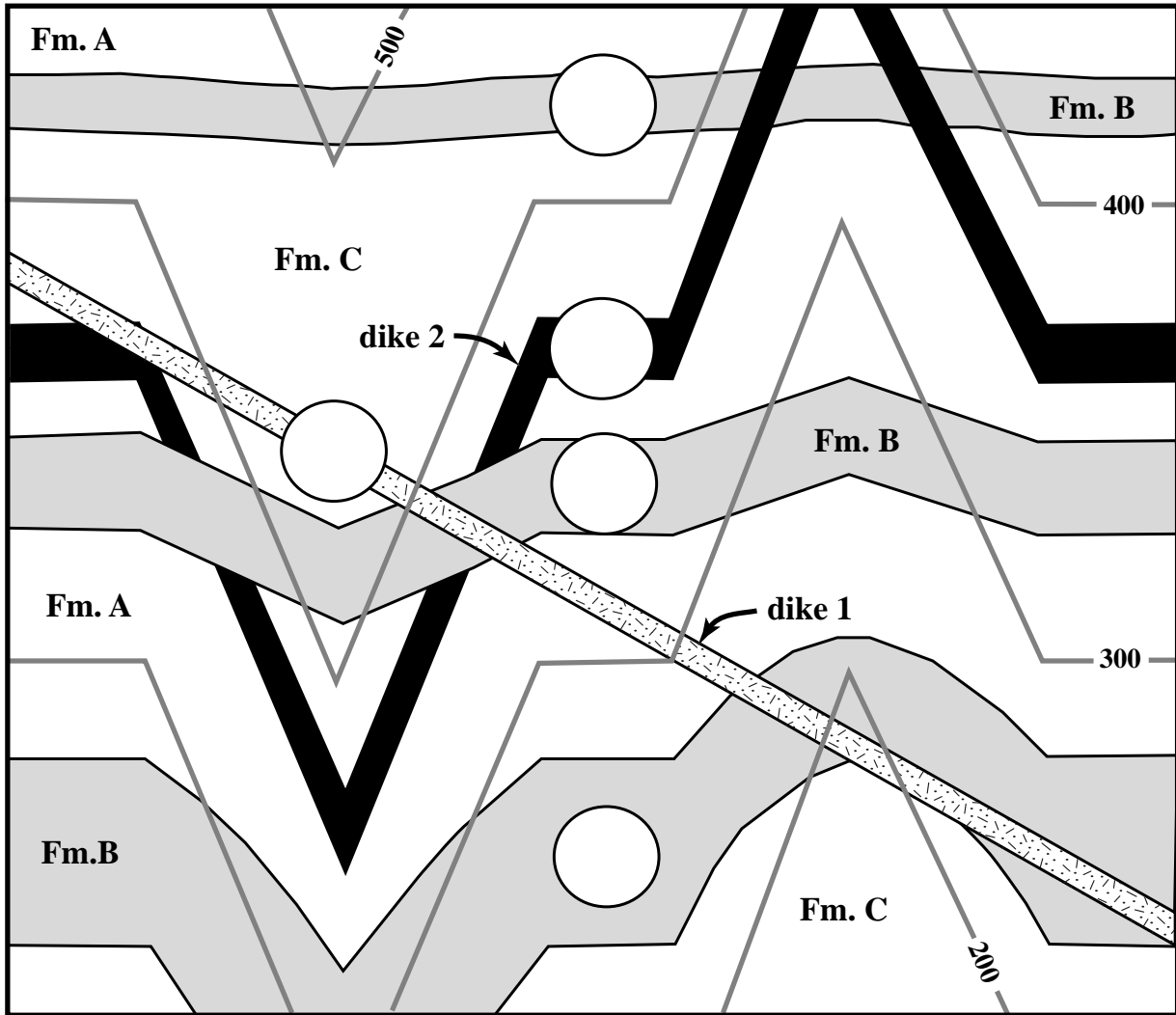
## Common symbols used on geologic maps

	Strike and dip of bedding
	Overtured bedding
	Vertical bedding
	Horizontal bedding
	Crumpled bedding
	Trace of contact
	Less well-located contact
	Covered contact
	Fault contact with dip
	Sense of slip on strike-slip fault
	Sense of slip on dip-slip fault (D = down, U = up)
	Thrust fault, barbs on upper plate
	Bearing and plunge of fold axis or lineation
	Strike and dip of foliation, cleavage, or schistosity
	Vertical foliation, cleavage, or schistosity
	Strike and dip of joints or dikes
	Vertical joints or dikes
	Trace of axial surface or crest of anticline, with plunge
	Trace of axial surface or trough of syncline, with plunge
	Anticline with overturned limb
	Syncline with overturned limb
	Trace of axial surface with bearing and plunge of fold axis
	Overtured anticline with bearing and plunge of fold axis



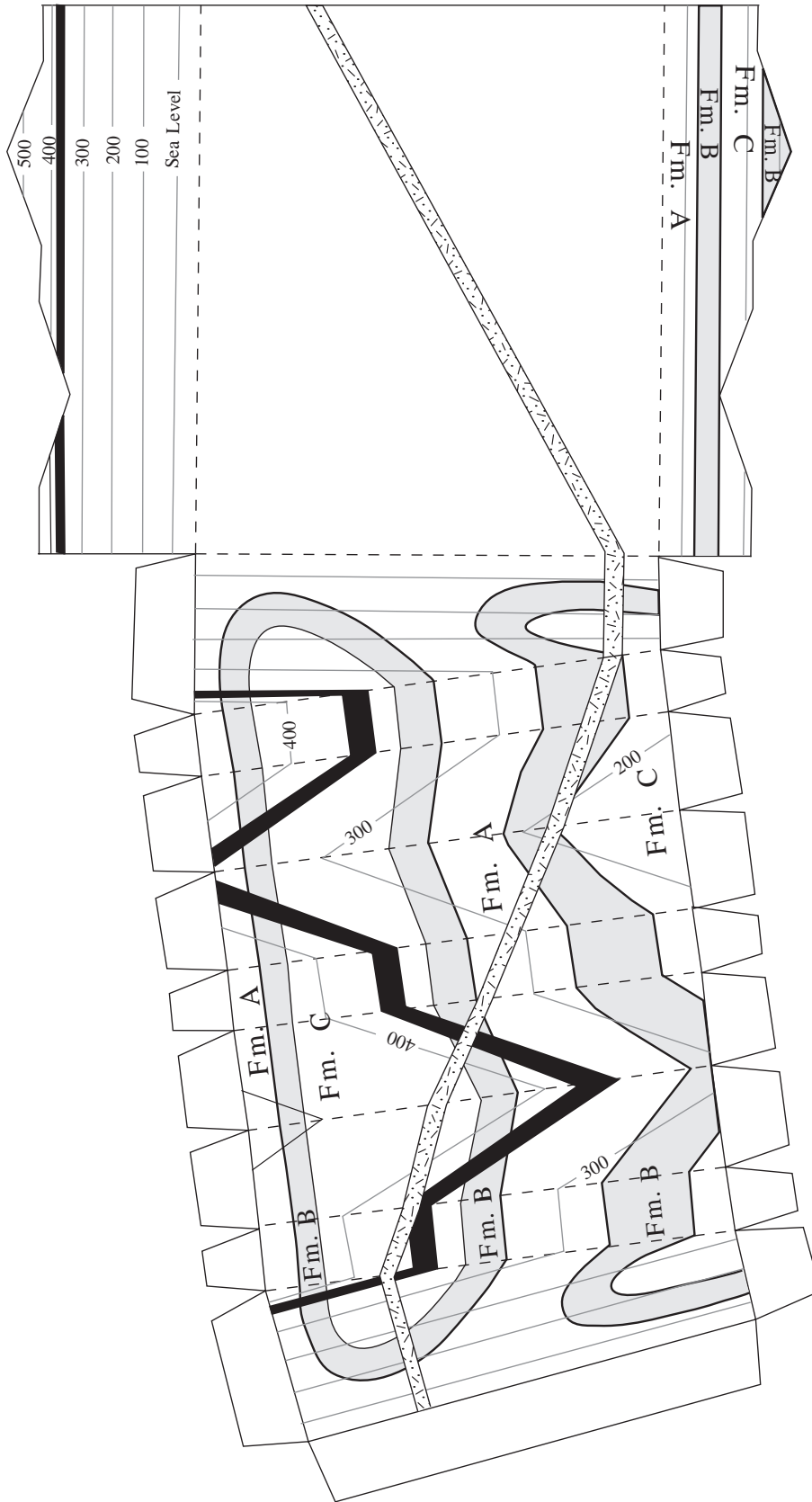
# *Appendix G*

Diagrams for use in problems



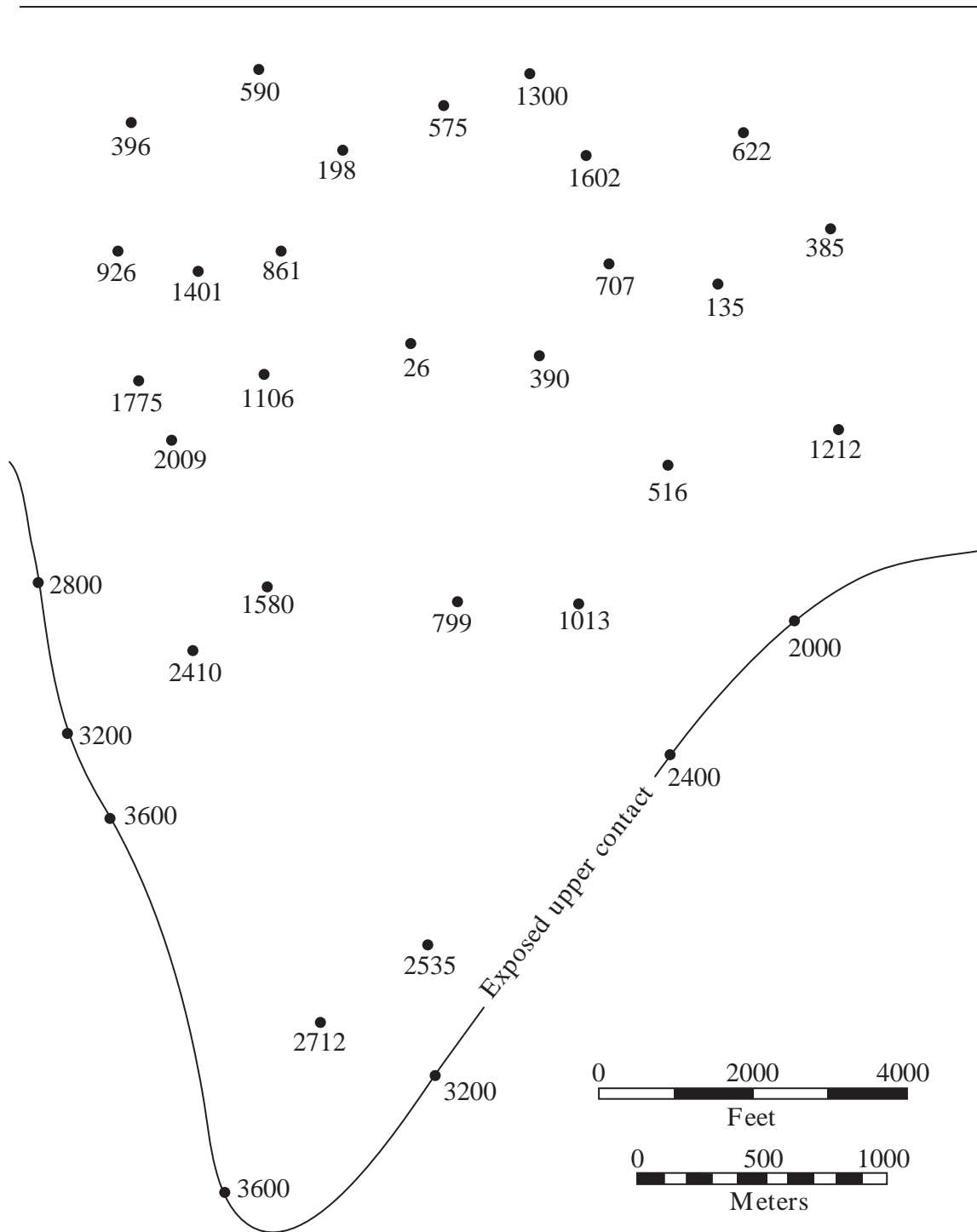
**Fig. G-1** Geologic map for use in Problem 2.1. Formation A is the oldest map unit. Contour interval is 100 m.





**Fig. G-2** Block model to accompany Problem 2.1. Cut out the diagram, fold on the dashed lines, and glue the tabs.

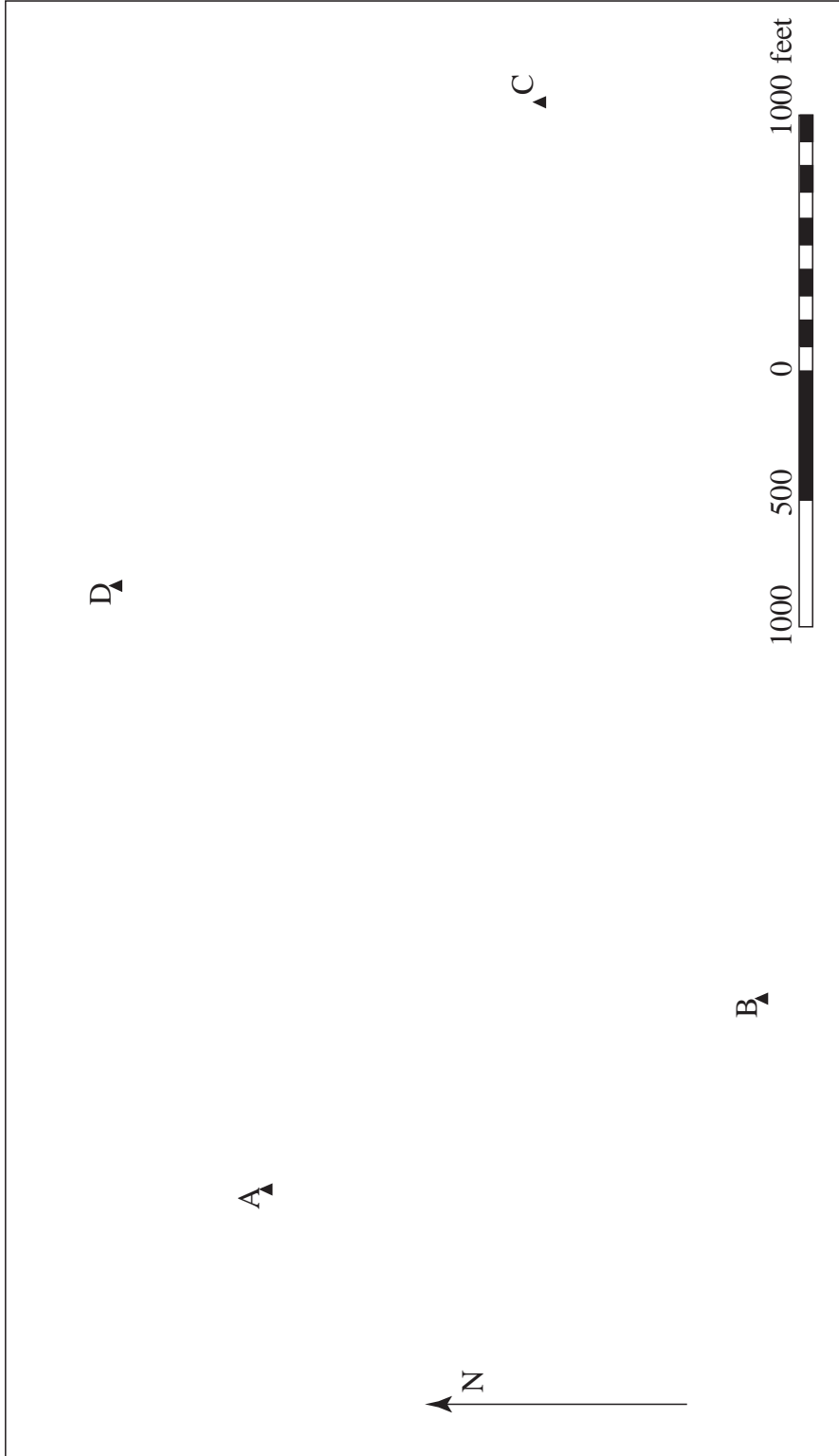




**Fig. G-3** Map to accompany Problem 2.2. This map represents the northeastern corner of the Bree Creek Quadrangle, which is discussed later in this chapter. The numbers on the map represent the elevation in feet of the *upper surface* of the Bree Conglomerate, the outcrop pattern of which is shown. The points that do not lie on the line represent the elevation of the top of the Bree Conglomerate in the subsurface, as measured in drill holes.



Name \_\_\_\_\_



**Fig. G-4** Map for use in Problem 2.3.





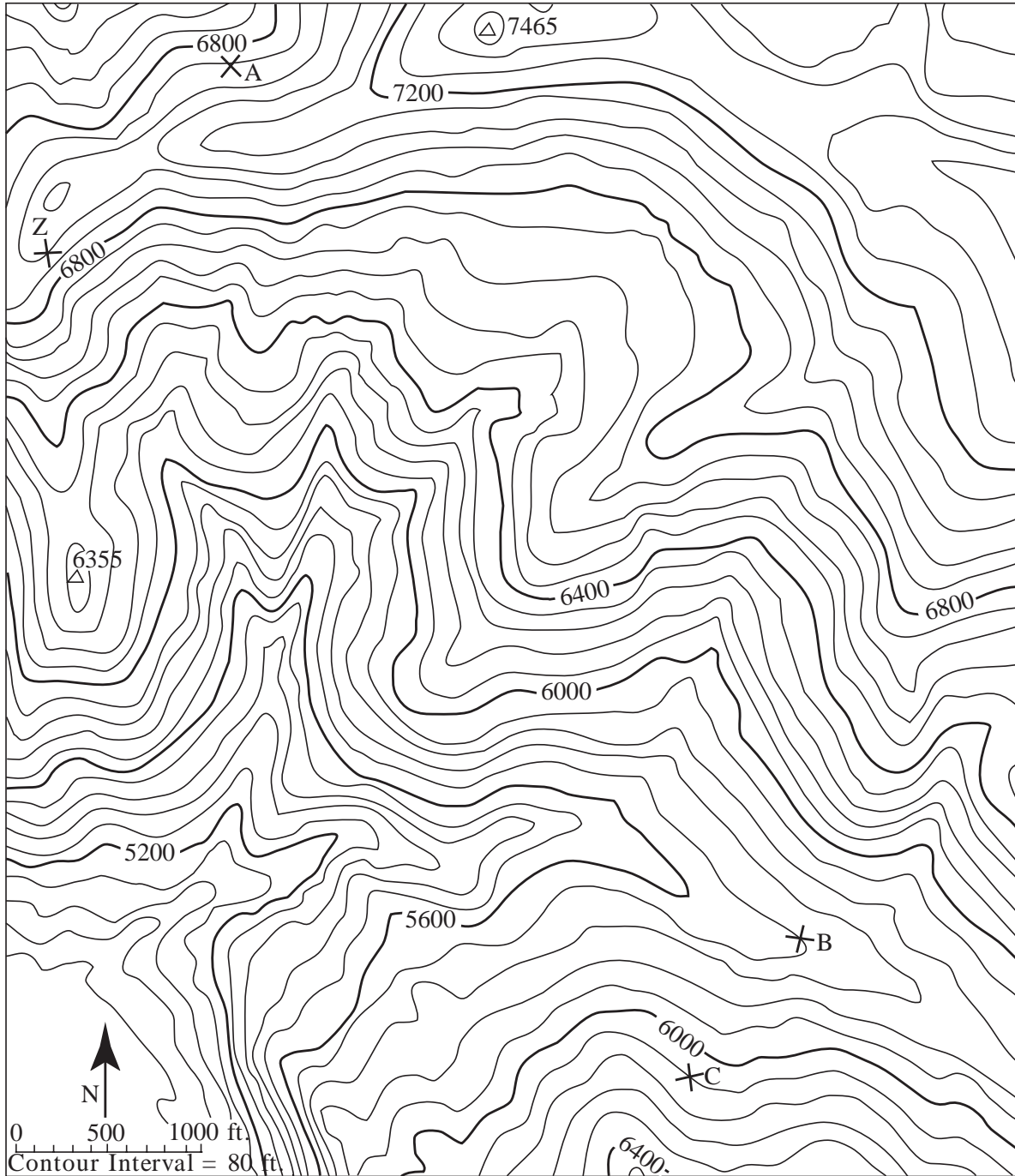


Fig. G-5 Map for use in Problem 2.4.



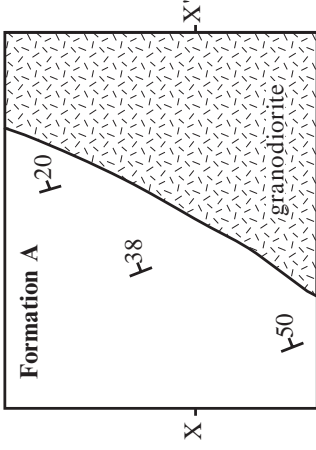
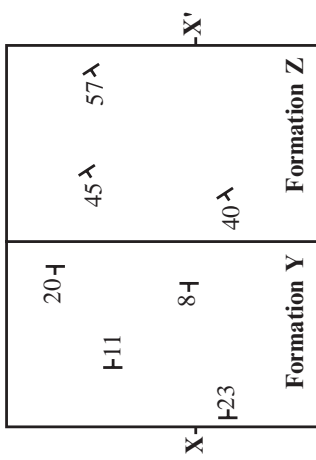
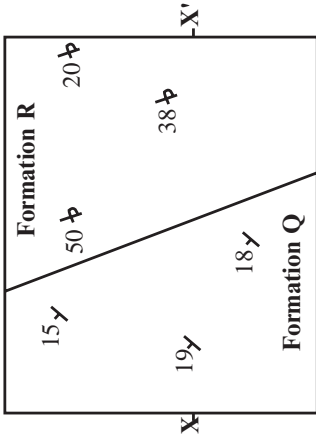
Name \_\_\_\_\_

<b>Problem 3.1</b>	Thd	Tr	Tg
<i>Northeastern fault block</i>			
Northern exposures	_____	_____	_____
Southern exposures		_____	_____
<i>Central fault block</i>			
Northern area		_____	_____
Galadriel's Ridge		_____	_____
Southwestern area		_____	_____
<i>Western fault block</i>			
Gandalf's Knob	_____		
Southern exposures	_____		
<b>Problem 3.2</b>			
Tmm	_____		
Tm	_____		
Tts	_____		
Tb	_____		
Te	_____		
<b>Problem 3.3</b>	Thd	Tr	Tg
Gollum Ridge	_____		
Gandolf's Knob	_____		
Galadriel's Ridge		_____	_____
Mirkwood Creek			_____
N. of Edoras Crk.	_____		

**Fig. G-6** Answer sheet for Problems 3.1–3.3.



Name \_\_\_\_\_



\_\_\_\_\_

\_\_\_\_\_

\_\_\_\_\_

\_\_\_\_\_

\_\_\_\_\_

\_\_\_\_\_

c

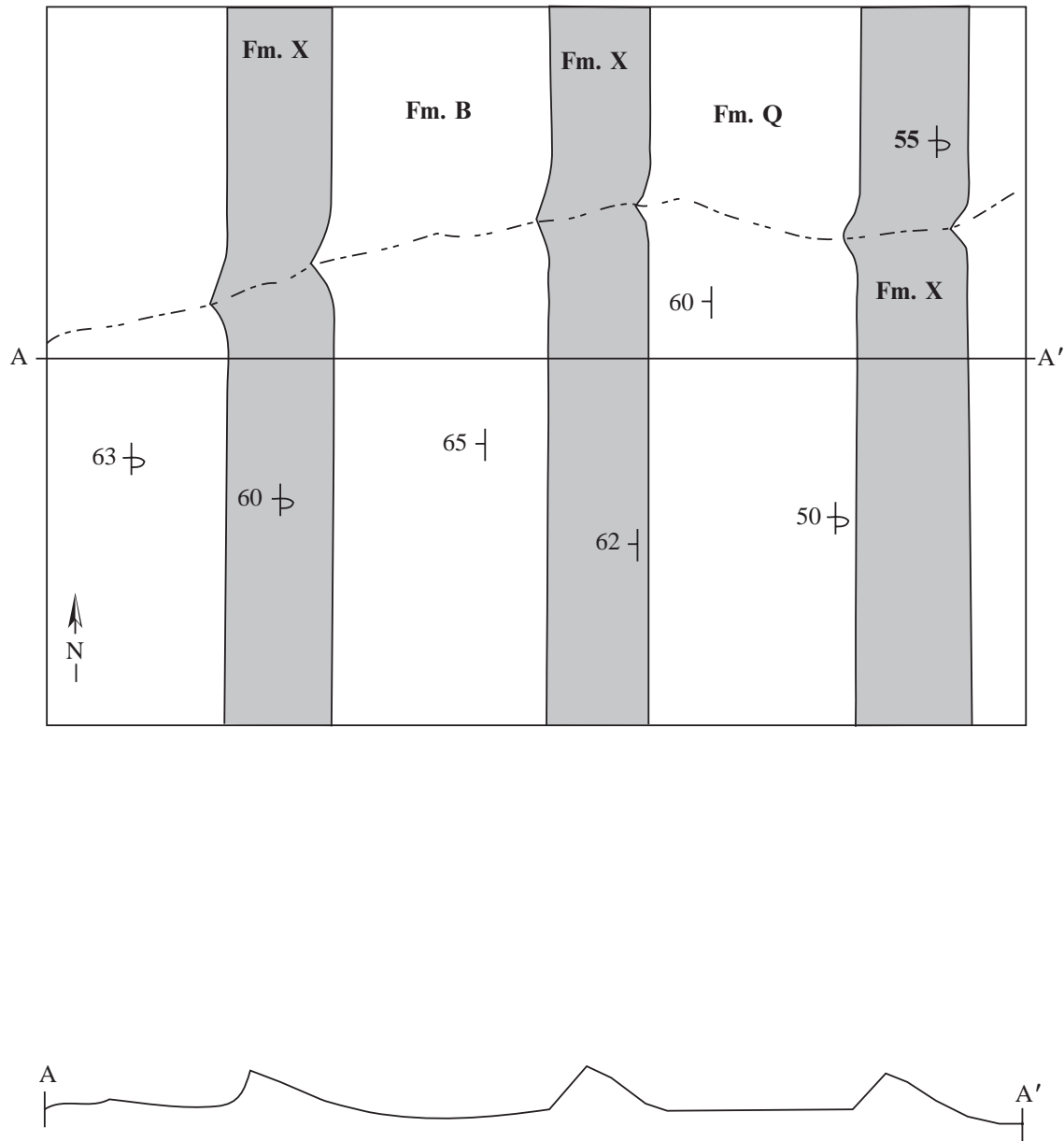
b

a

**Fig. G-7** Three geologic maps, each with two topographic profiles and space to explain which interpretation you consider most likely, and why. For use in Problem 3.4.



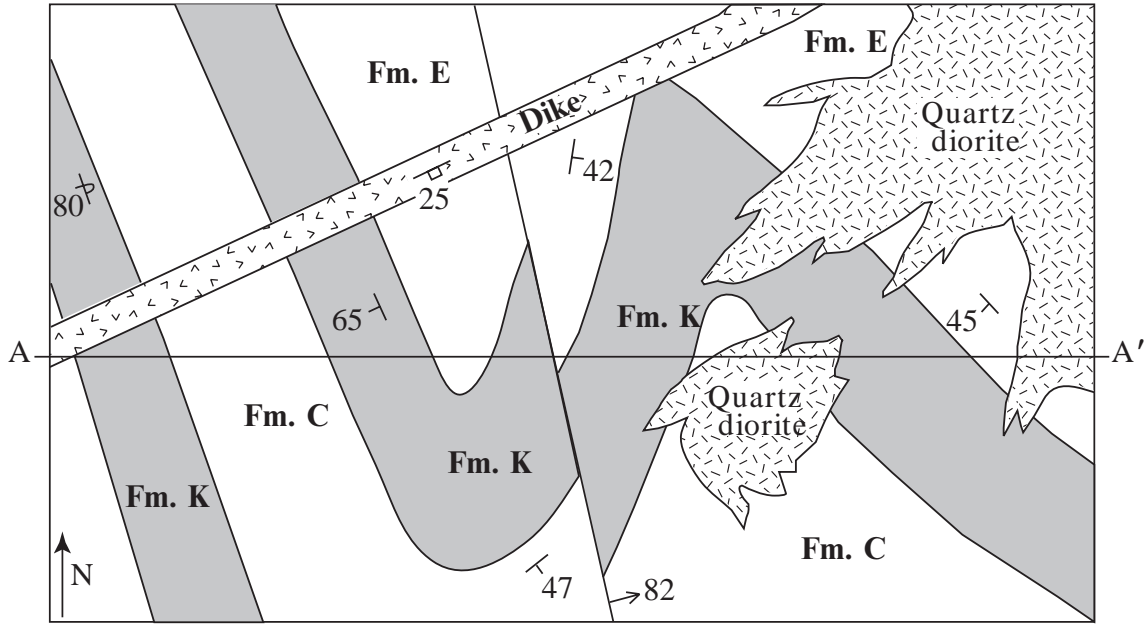
Name \_\_\_\_\_



**Fig. G-8** Map and topographic profile for use in Problem 4.1.







a

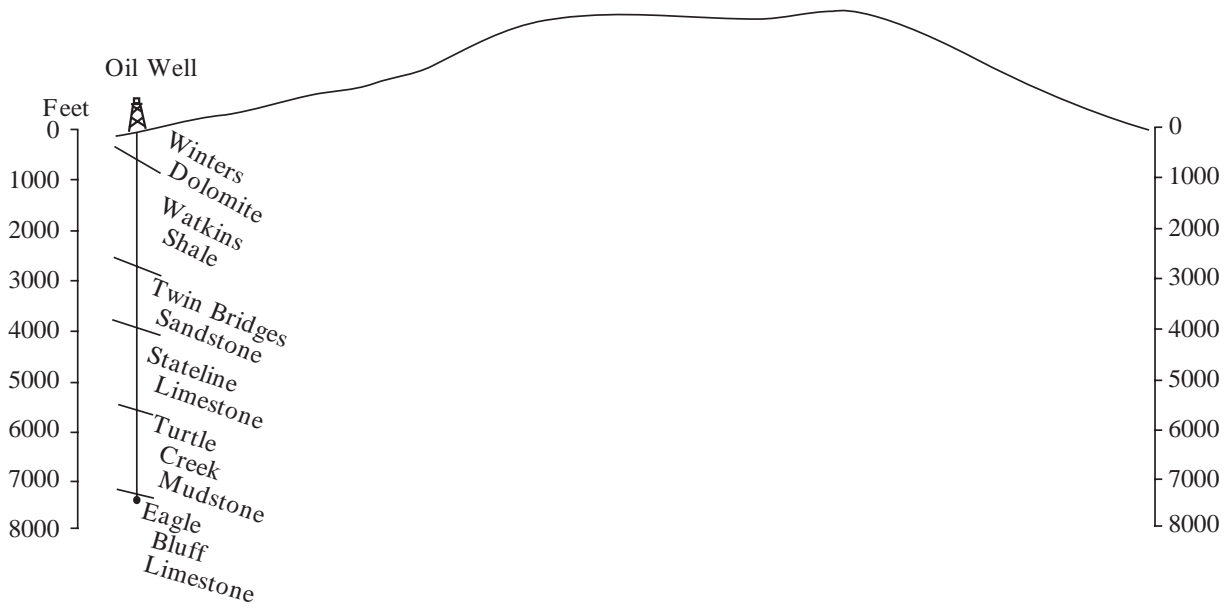
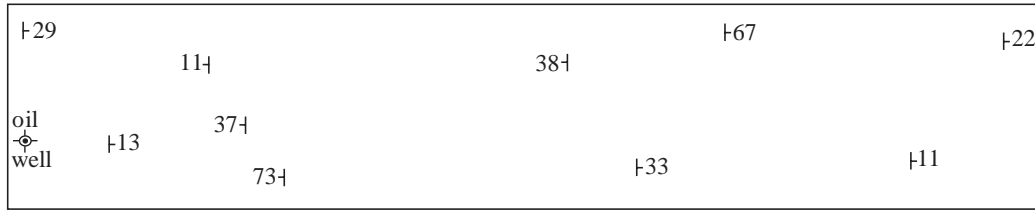


b

Fig. G-9 Map and topographic profile for use in Problem 4.2.

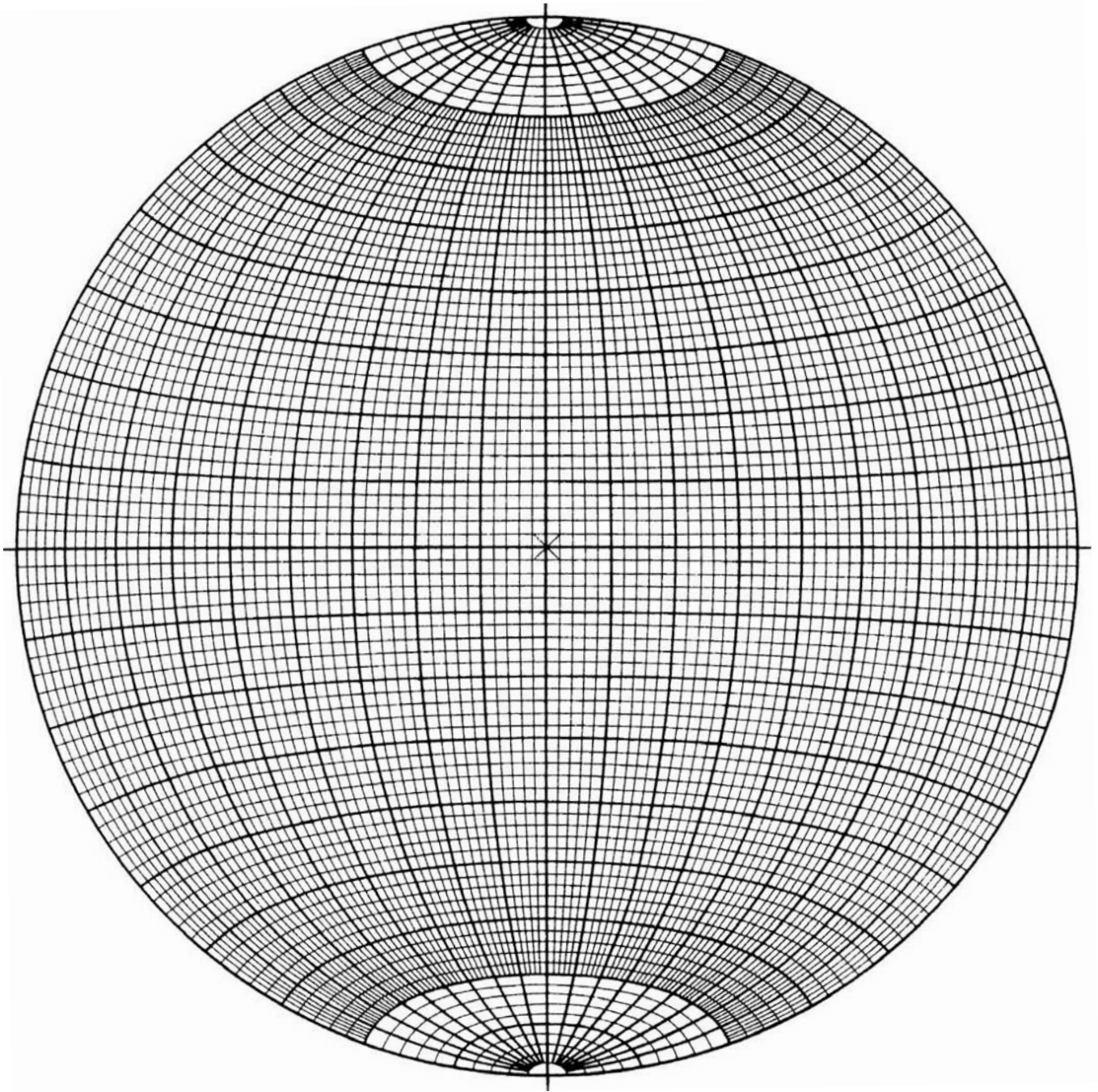


Name \_\_\_\_\_



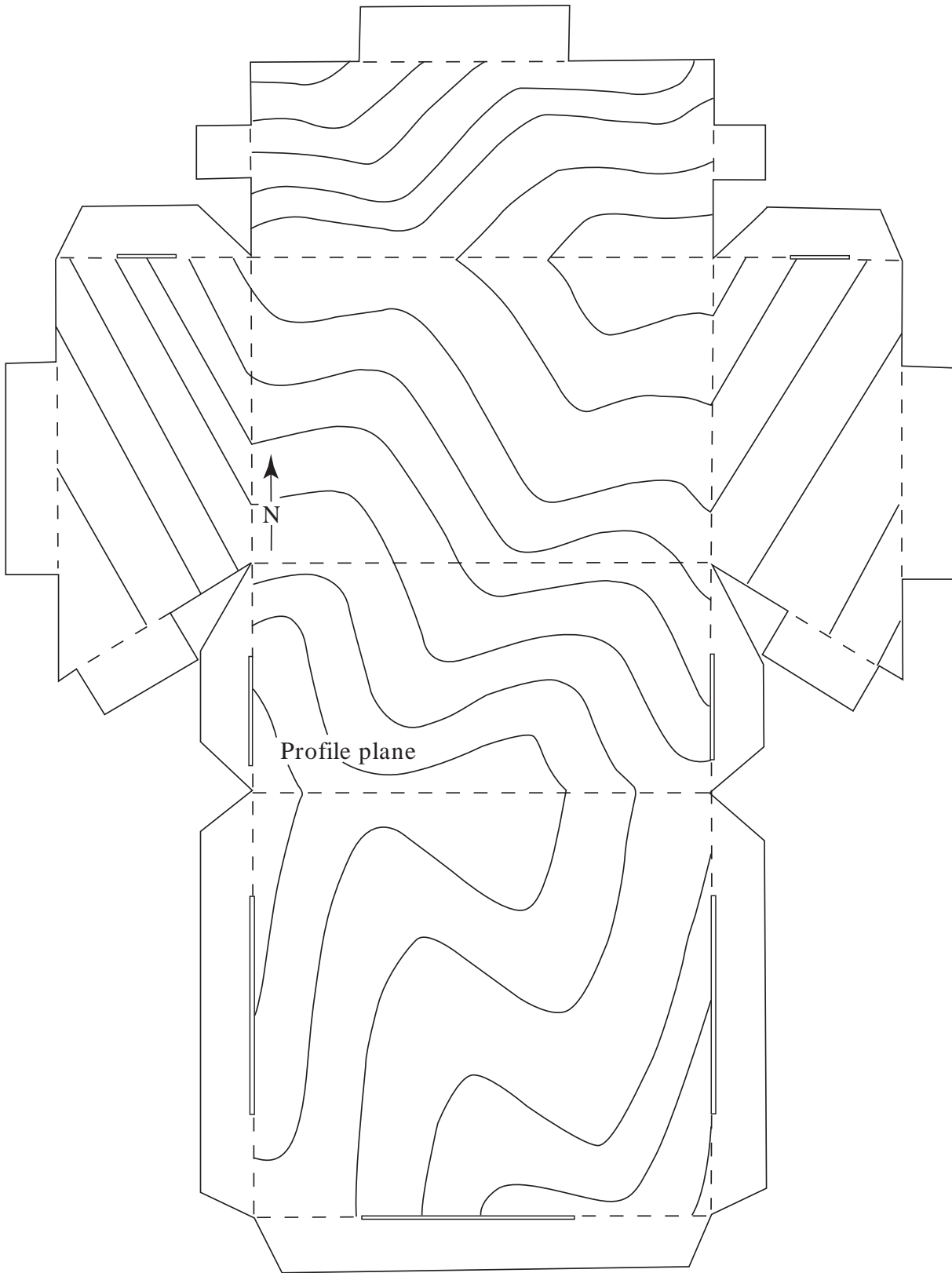
**Fig. G-10** Map, topographic profile, and well log for use in Problem 4.3.





**Fig. G-11** Equal-area net.

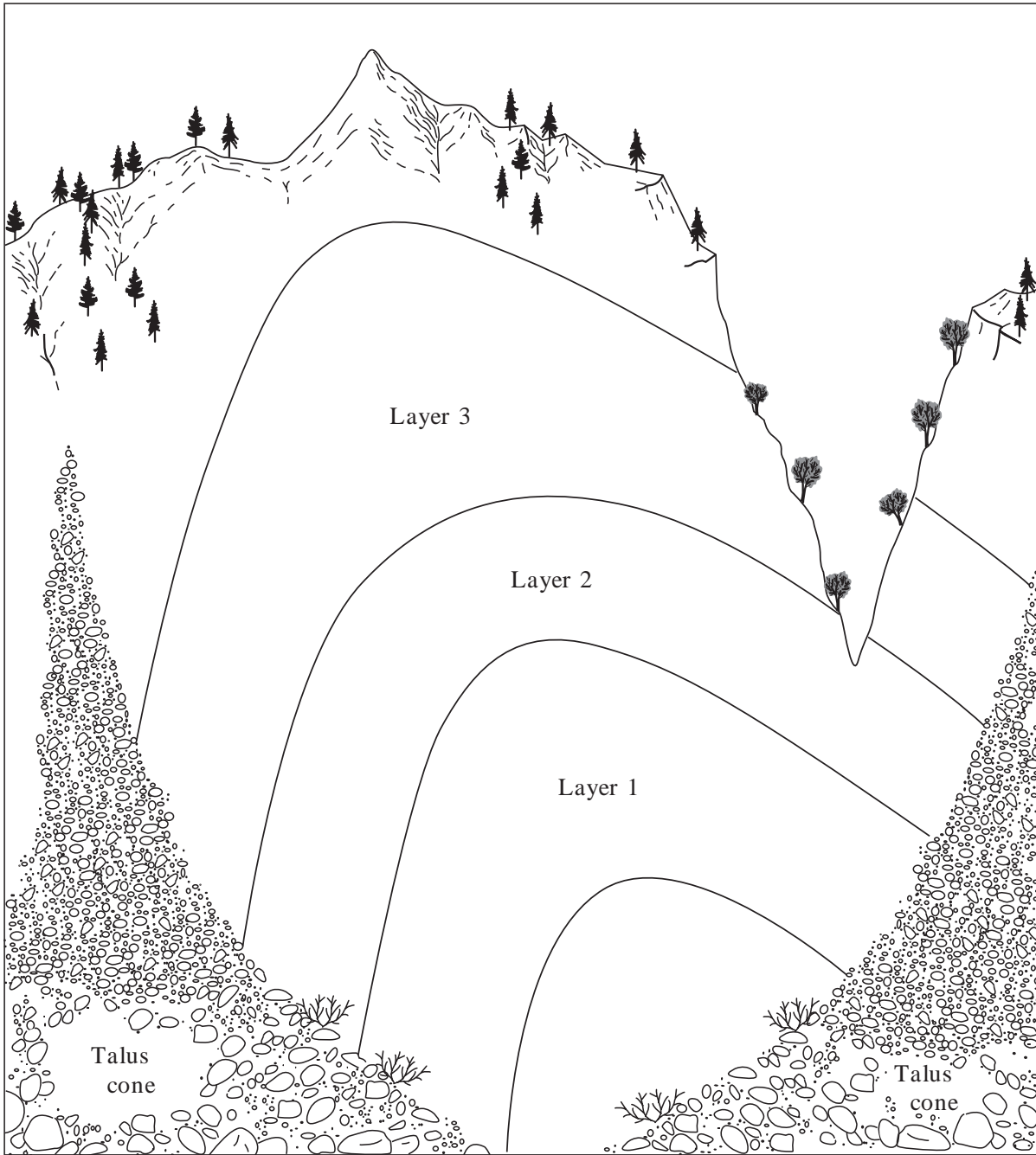




**Fig. G-12** Block model to be cut out and folded for use in Problem 6.1.







**Fig. G-13** Drawing of folds to be used in Problem 6.2. Adapted from *Internal Processes*, Open University Press (1972).



Name \_\_\_\_\_



a

---

---



b

---

---



c

---

---



d

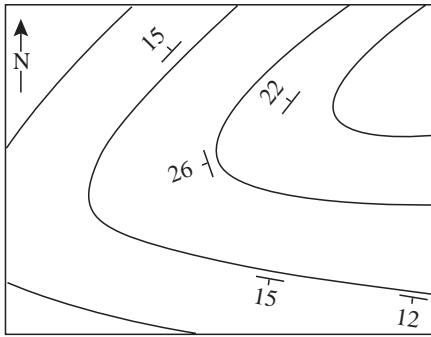
---

---

**Fig. G-14** Slabs of folds for use in Problem 6.3. Photographed from the collection of O.T. Tobisch.

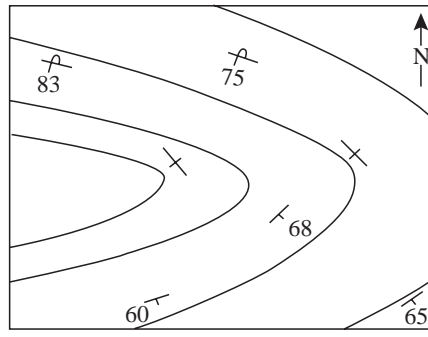


Name \_\_\_\_\_



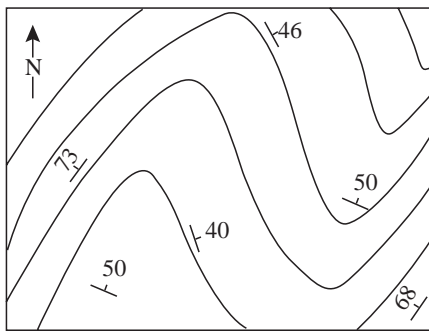
**a**

\_\_\_\_\_



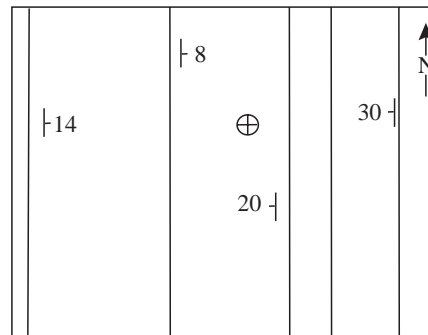
**b**

\_\_\_\_\_



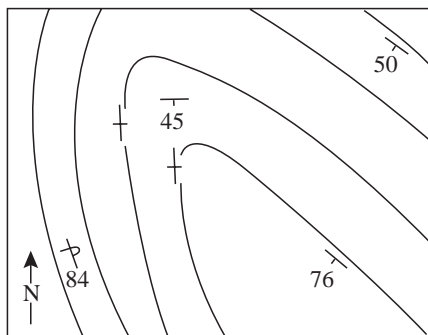
**c**

\_\_\_\_\_



**d**

\_\_\_\_\_

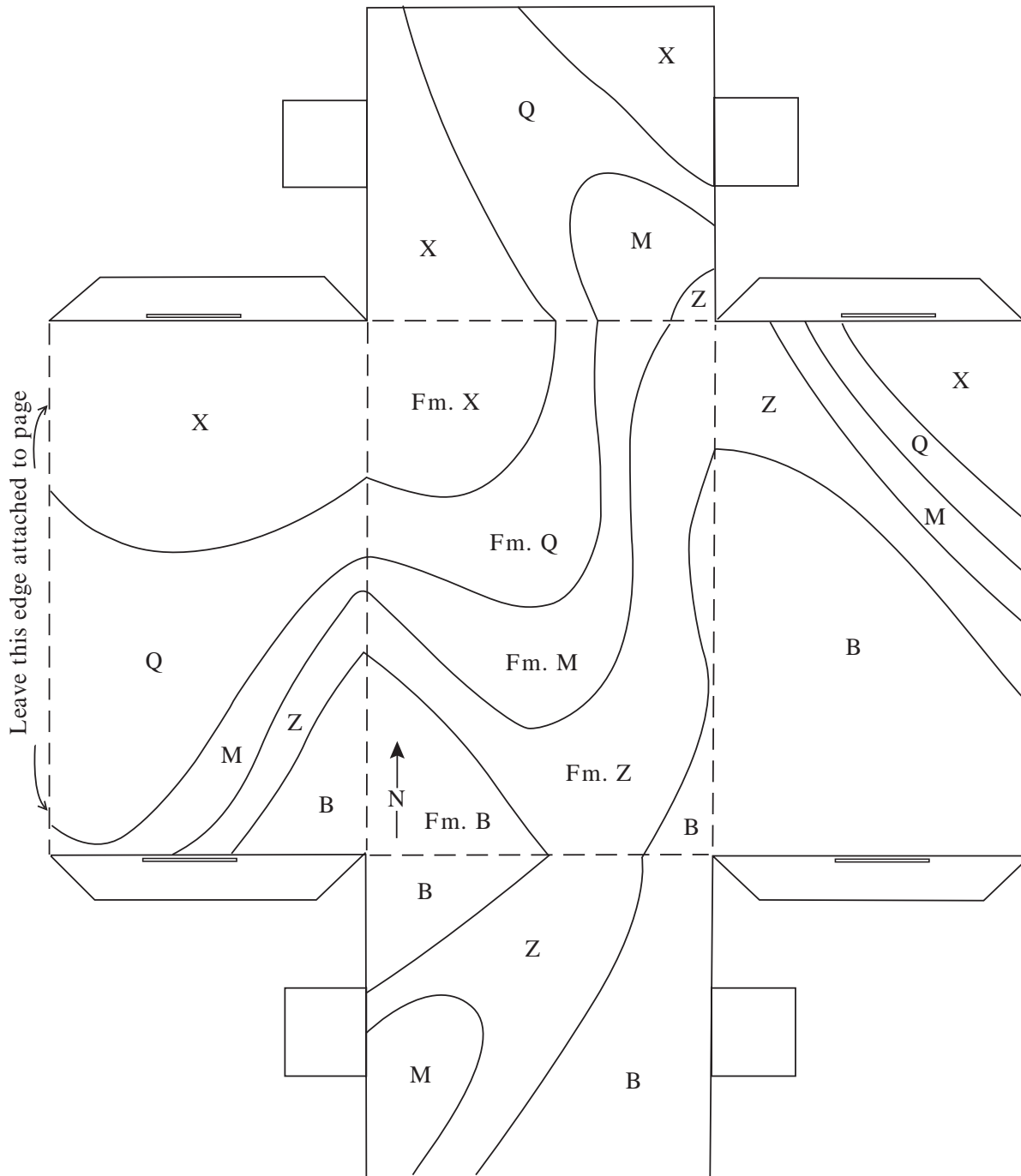


**e**

\_\_\_\_\_

**Fig. G-15** Geologic maps for use in Problem 6.4.



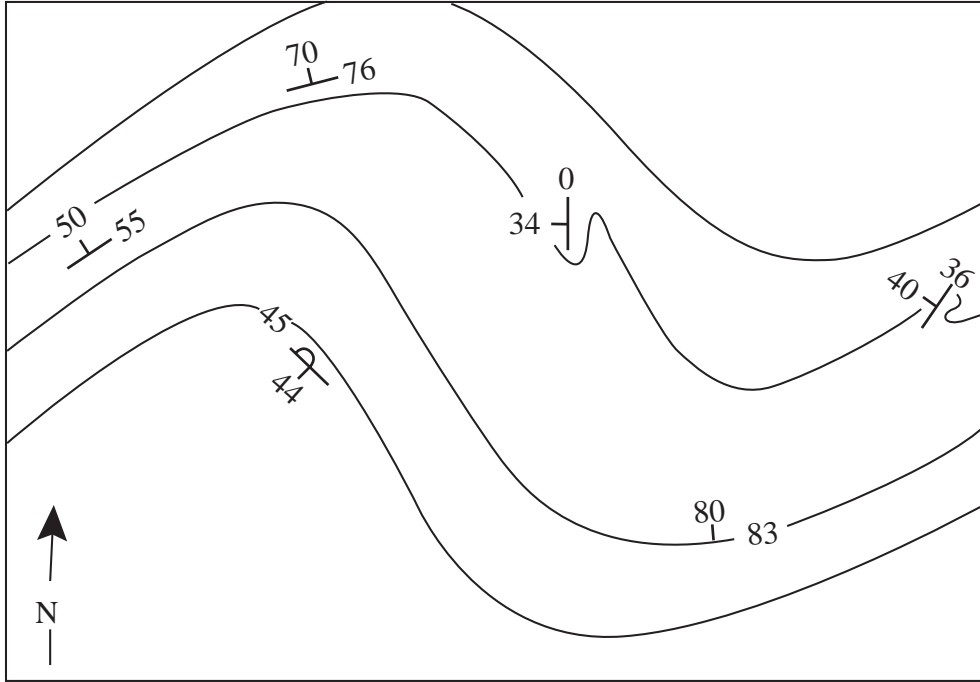


**Fig. G-16** Layout of block diagram to be constructed in Problem 6.5. After Dahlstrom (1954) in Whitten (1966).



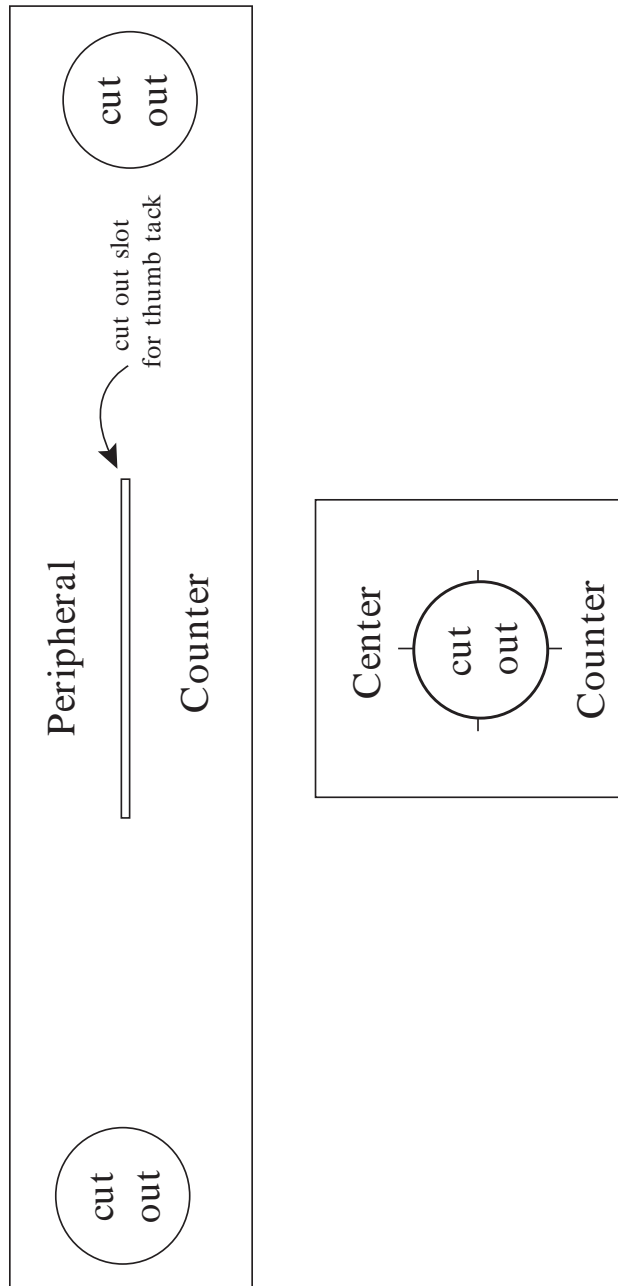


Name \_\_\_\_\_



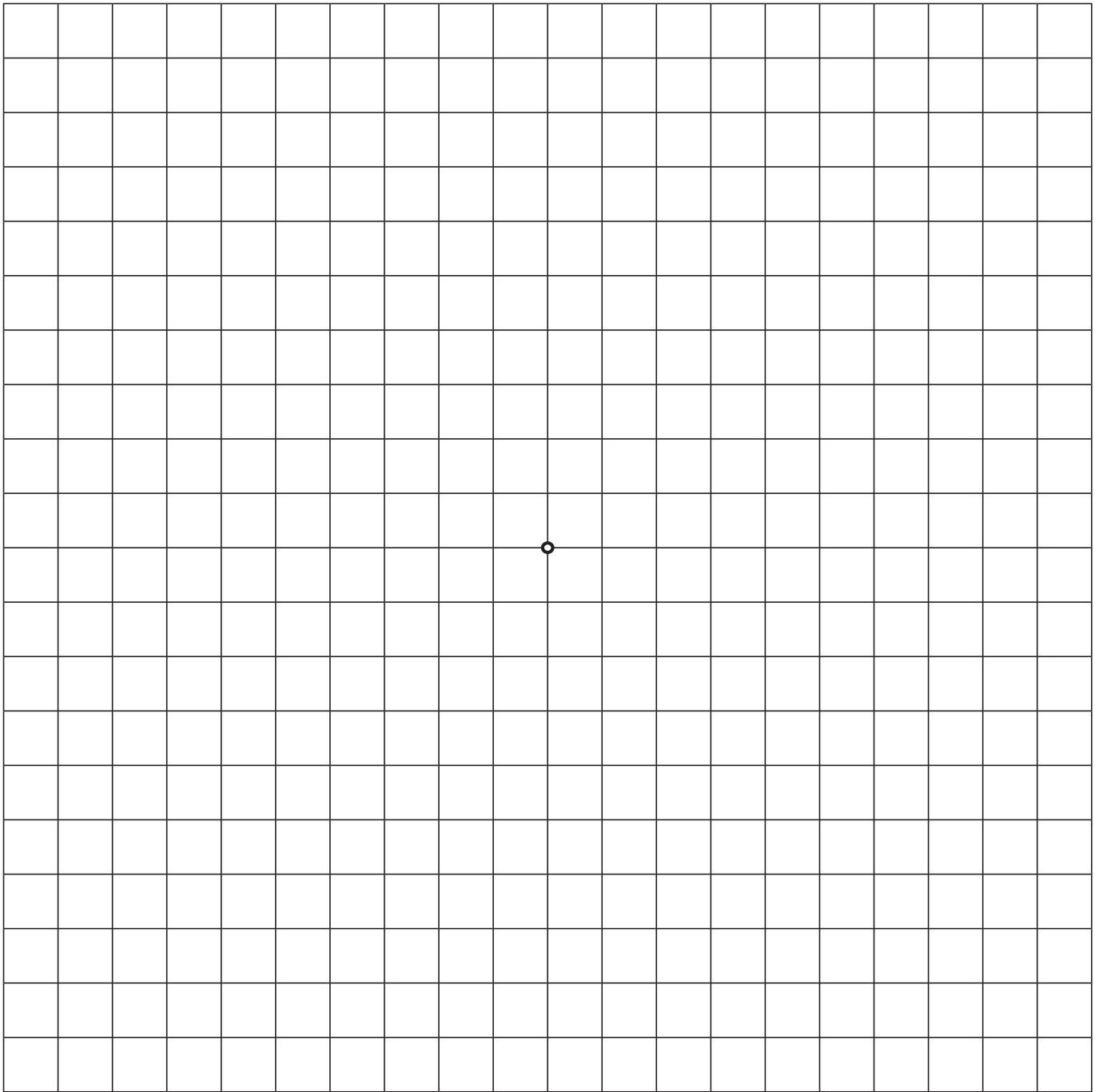
**Fig. G-17** Geologic map for use in Problem 7.1.





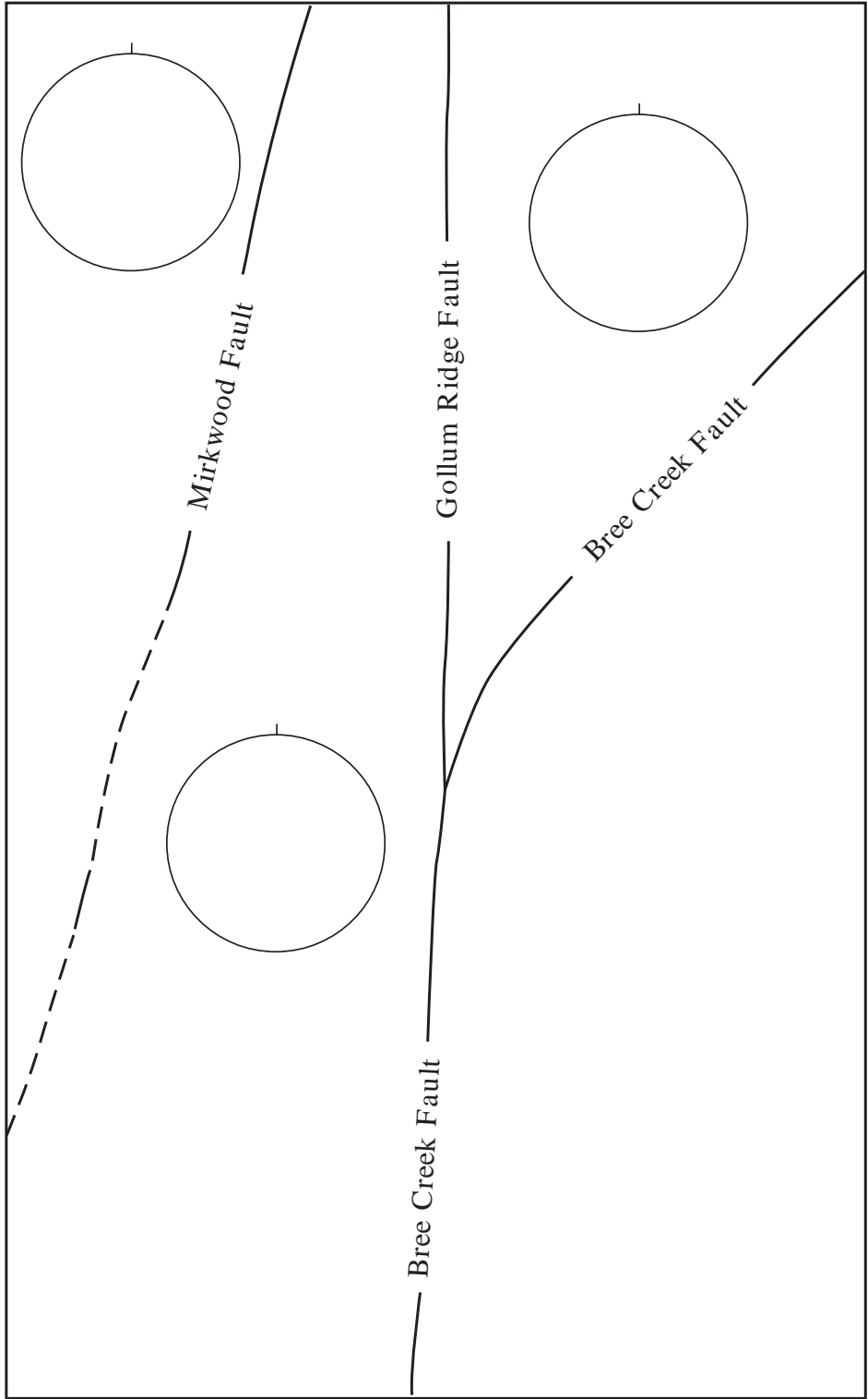
**Fig. G-18** Center counter and peripheral counter to be cut out and used for constructing contour diagrams (Chapter 7).





**Fig. G-19** Grid for use in constructing contour diagrams (Chapter 7).



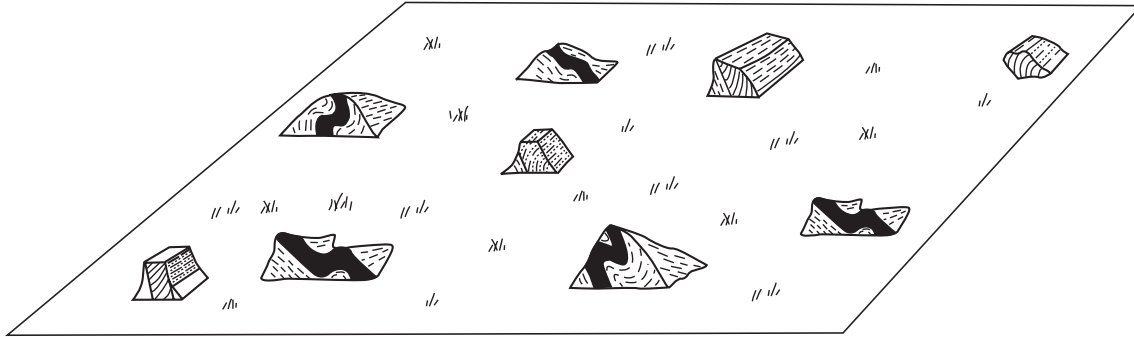


**Fig. G-20** Map of separate fault blocks of the Bree Creek Quadrangle. For use in Problem 7.2.

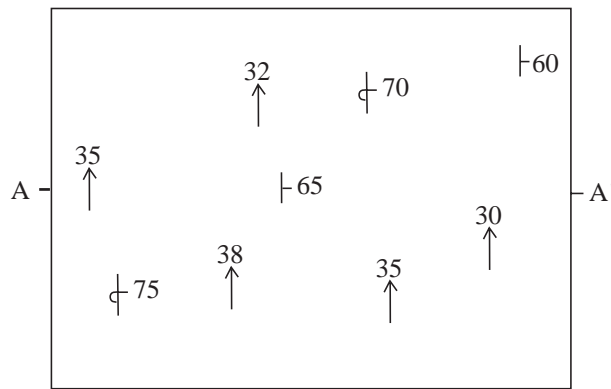




Name \_\_\_\_\_



a



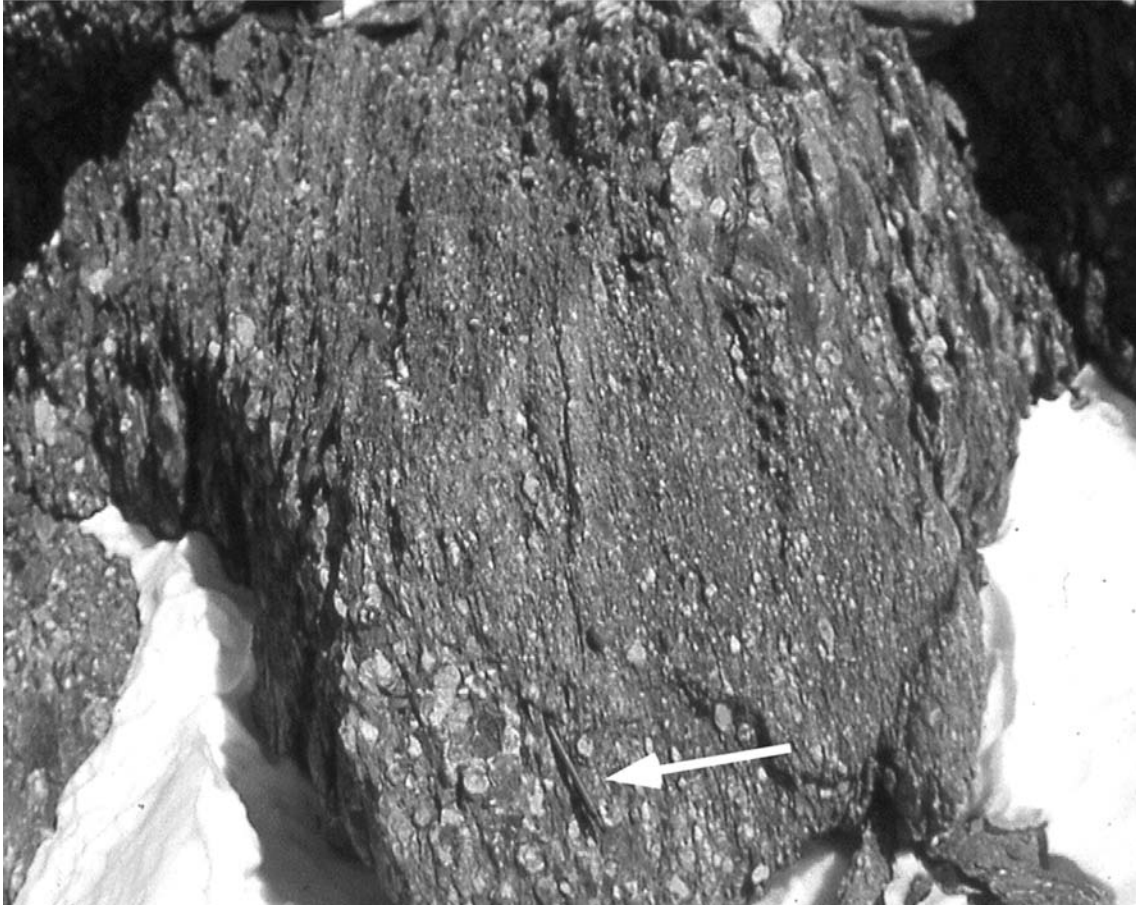
b

c A ————— A'

**Fig. G-21** (a) Oblique view, (b) geologic map, and (c) topographic profile for structure section A-A'. For use in Problem 8.1.



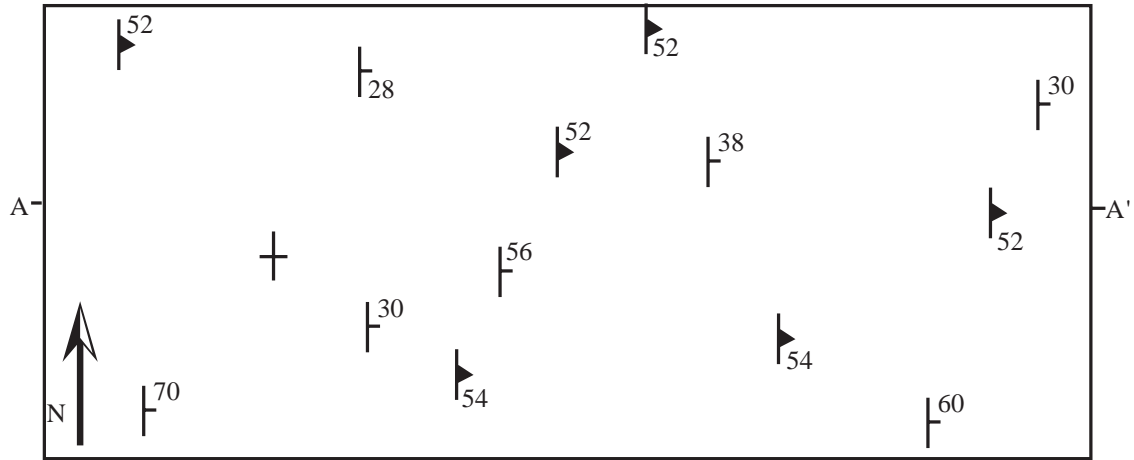
Name \_\_\_\_\_



**Fig. G-22** An outcrop in the Transantarctic Mountains of Antarctica, showing bedding (dipping toward the right) and well-developed cleavage. Arrow points to ice axe handle, which is about 90 cm long. For use in Problem 8.2. Photo by E. Duebendorfer.



Name \_\_\_\_\_



A ————— A'

**Fig. G-23** Geologic map showing attitudes of bedding and cleavage. For use in Problem 8.3.



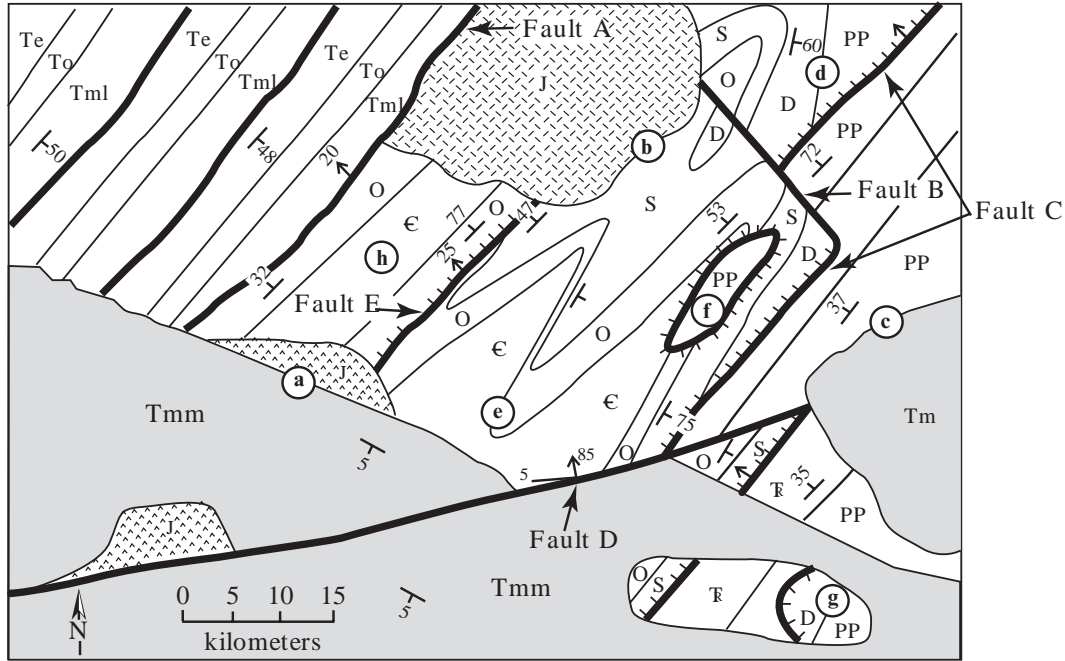
Name \_\_\_\_\_



**Fig. G-24** Slab of rock that experienced two generations of folding. For use in Problem 8.4. Photographed from the collection of O. T. Tobisch.







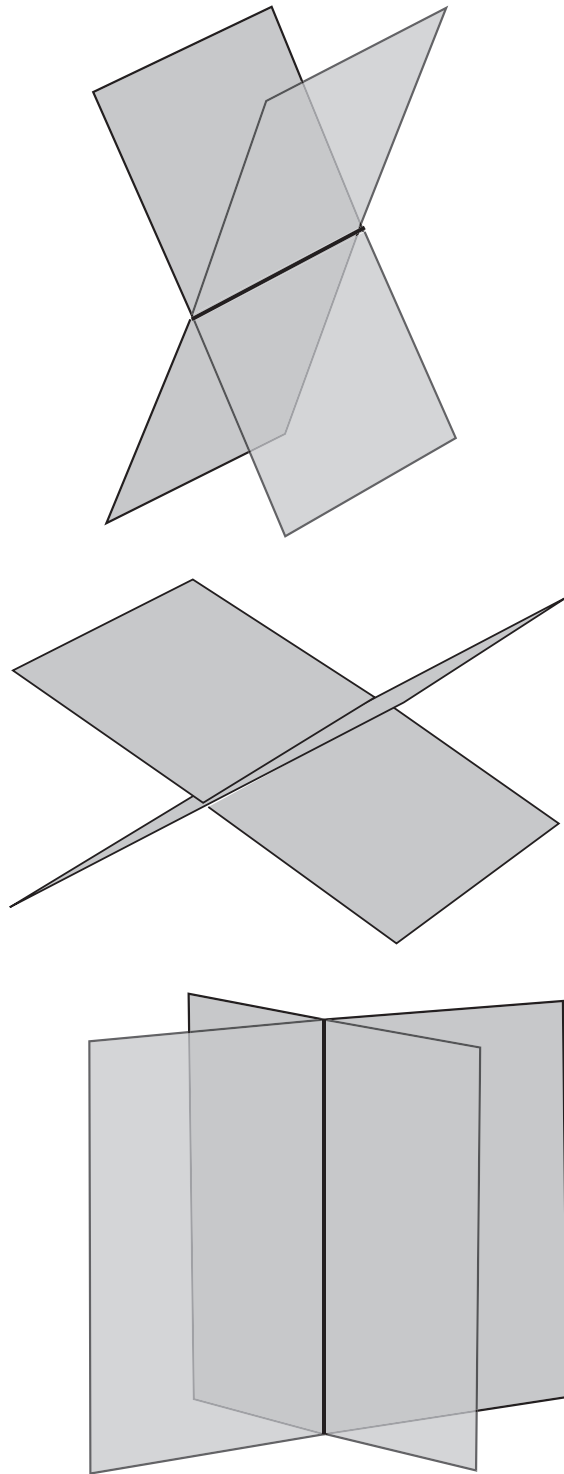
Tm - Miocene	Tr - Triassic	Strike and dip of bedding
Tmm - Middle Miocene	PP - Pennsylvanian	Dip of fault (arrow) and plunge of fault striae (line)
Tml - Lower Miocene	D - Devonian	Contact
To - Oligocene	S - Silurian	Fault, high angle
Te - Eocene	O - Ordovician	Fault, low angle (hachures on upper plate)
J - Jurassic	ε - Cambrian	

- |  |         |         |         |         |         |
|--|---------|---------|---------|---------|---------|
|  | Fault A | Fault B | Fault C | Fault D | Fault E |
|--|---------|---------|---------|---------|---------|
1. Type of fault: \_\_\_\_\_  
Age of faulting: \_\_\_\_\_
  - 2a. Type of contact: \_\_\_\_\_  
locality a                      locality b                      locality c                      locality d  
locality e                      locality f                      locality g                      locality h
  - 2b. Name the structure: \_\_\_\_\_
  4. \_\_\_\_\_  
\_\_\_\_\_
  5. Minimum amount of displacement on fault C: \_\_\_\_\_
  6. Geologic history: \_\_\_\_\_

**Fig. G-25** Geologic map for use in Problem 9.5.

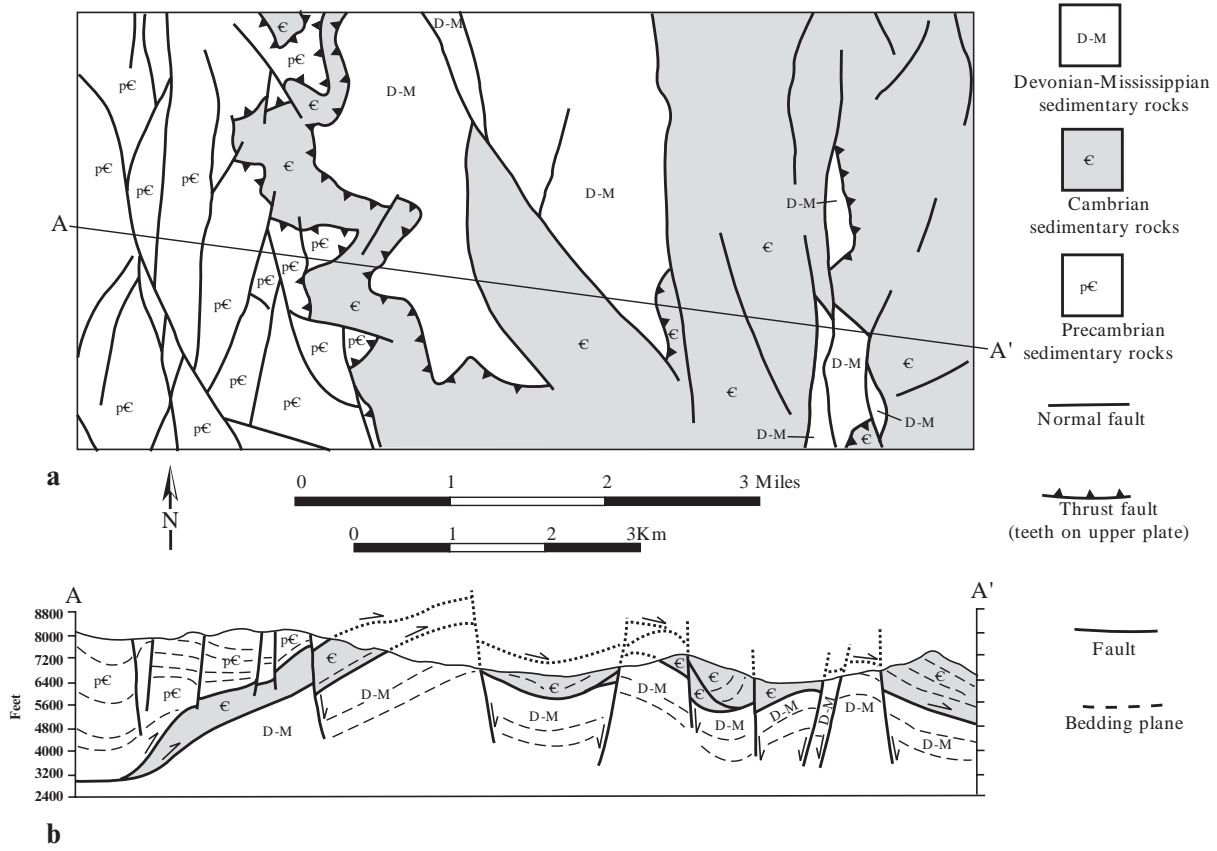


Name \_\_\_\_\_



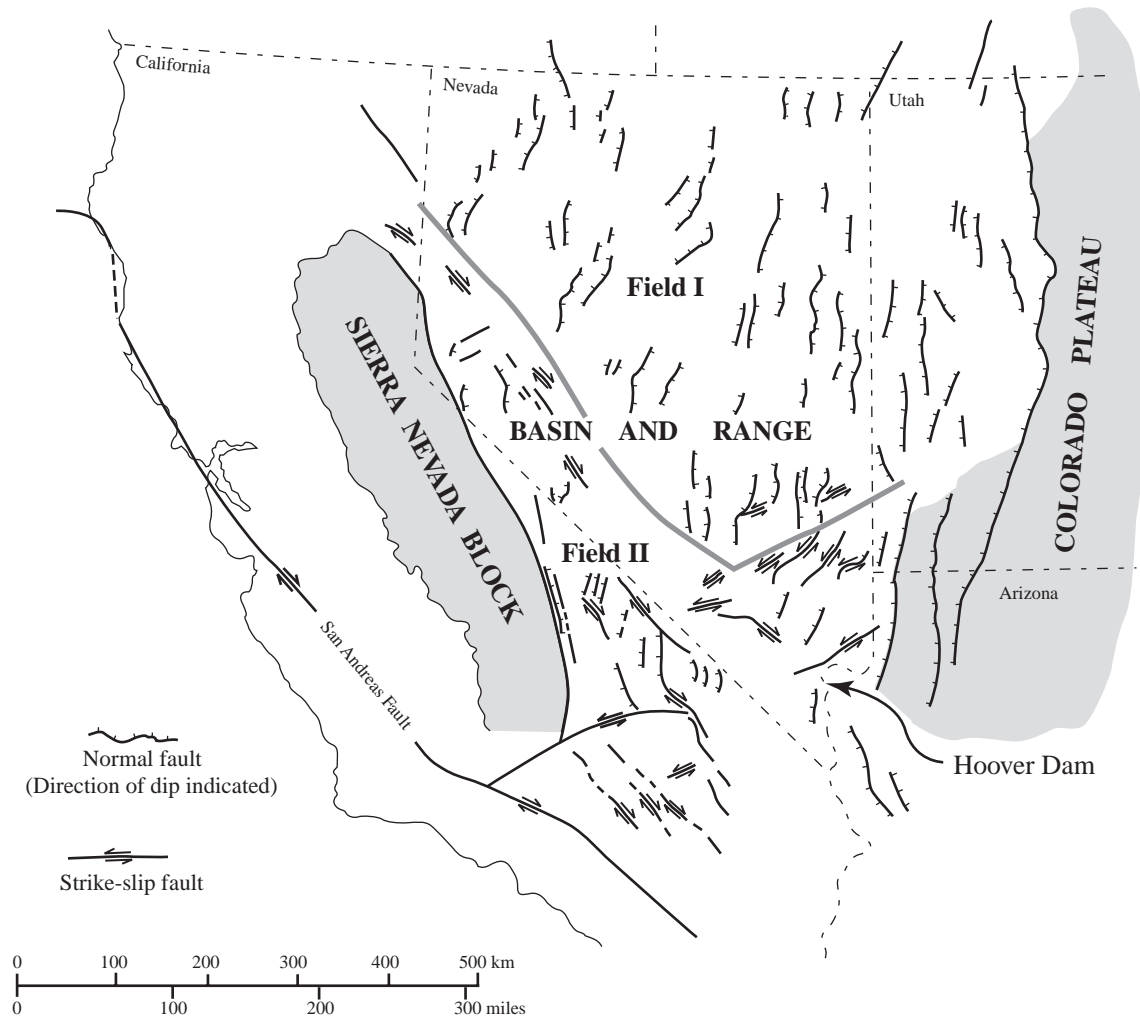
**Fig. G-26** Three pairs of conjugate shear surfaces. For use in Problem 10.1.





**Fig. G-27** (a) Generalized geologic map and (b) structure section of a portion of the Inyo Range of eastern California. For use in Problem 10.4. Generalized from Nelson (1971).

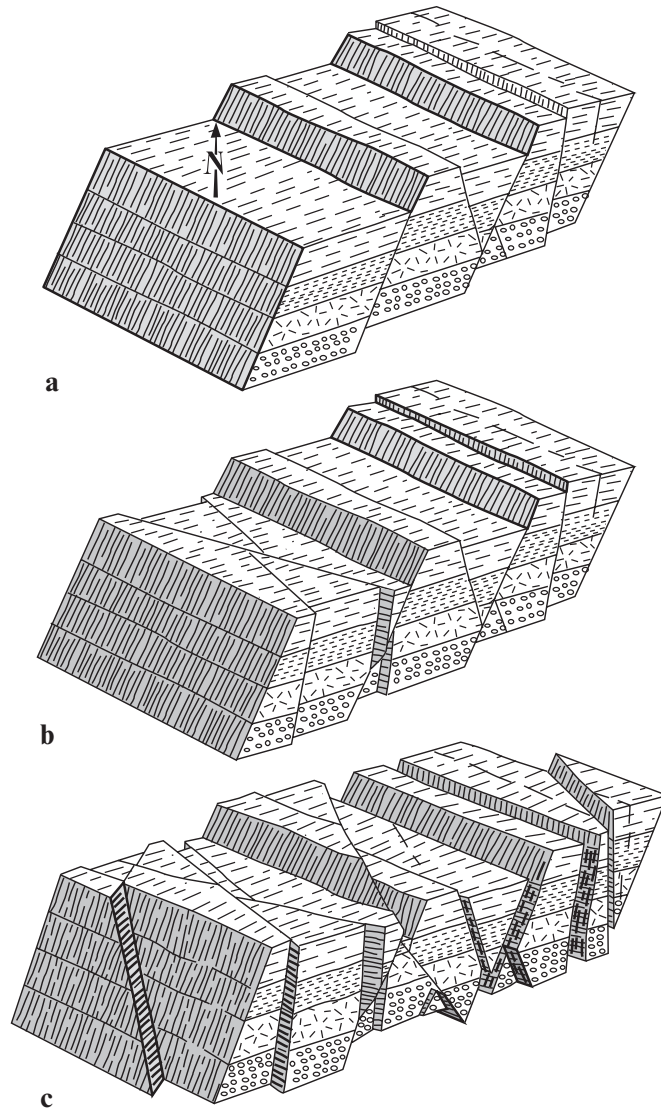




**Fig. G-28** Generalized map of late Cenozoic structural features of the Basin-and-Range province in the southwestern USA. Field I is characterized by listric normal faults. Field II is characterized by a combination of normal faults and sinistral and dextral strike-slip faults. For use in Problem 10.6. After Wright (1976).







Explanation for conversion of a strike-slip fault from sinistral to dextral during one tectonic episode: \_\_\_\_\_

\_\_\_\_\_

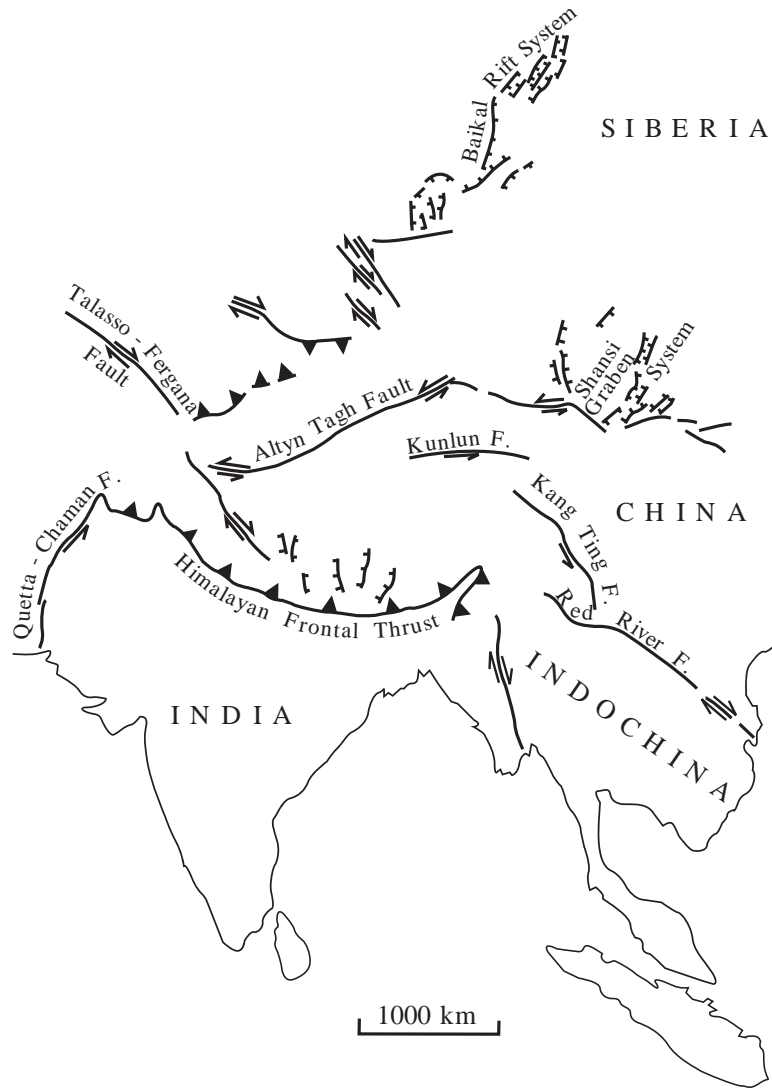
Speculations about the geologic factors involved in the structural development of this region: \_\_\_\_\_

\_\_\_\_\_

**Fig. G-29** Schematic block diagrams showing the main characteristics of faulting at Hoover Dam. For use in Problem 10.7. After Angelier *et al.* (1985).



Name \_\_\_\_\_



Summary of the evolution of the orientation of the stress ellipsoid in southeastern Asia in response to the collision of India: \_\_\_\_\_

\_\_\_\_\_

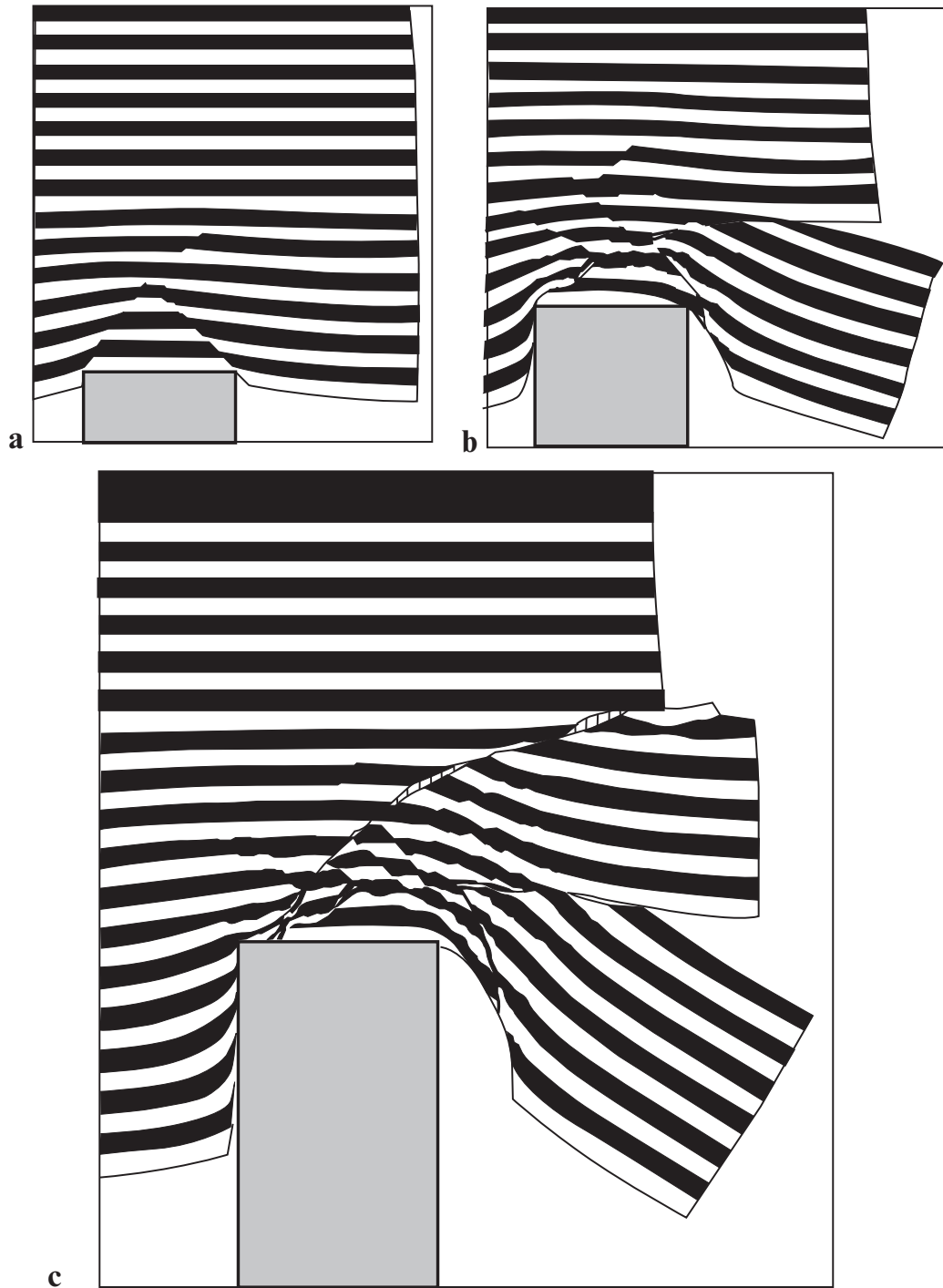
\_\_\_\_\_

\_\_\_\_\_

\_\_\_\_\_

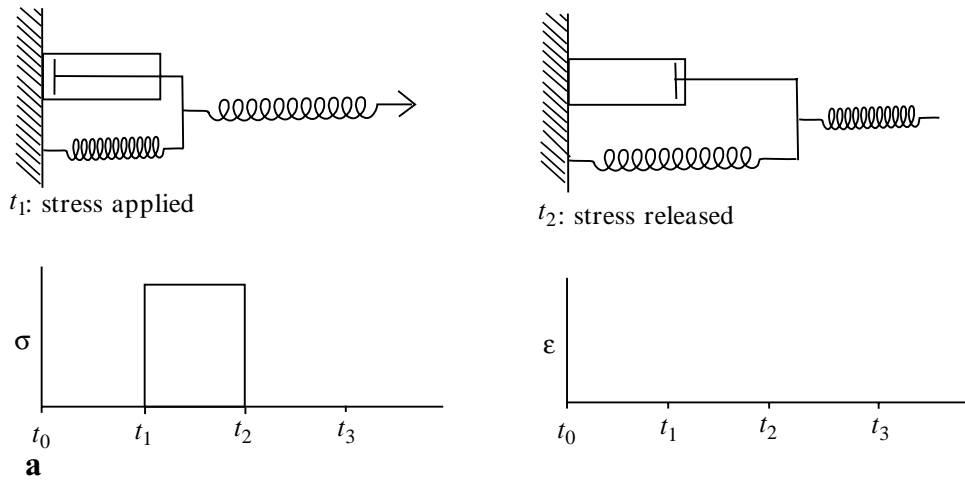
**Fig. G-30** Geologic map of southeastern Asia showing the major active faults. For use in Problem 10.8. After Molnar and Tapponnier (1975); Tapponnier et al. (1982).



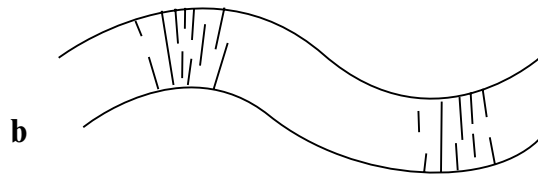


**Fig. G-31** Three stages of an experiment in which plasticine was deformed in a way to simulate the collision of India with Asia. In this particular experiment the layers of plasticine are confined at the top and on the left side, but they are unconfined on the right side. For use in Problem 10.8. After Tapponnier *et al.* (1982).





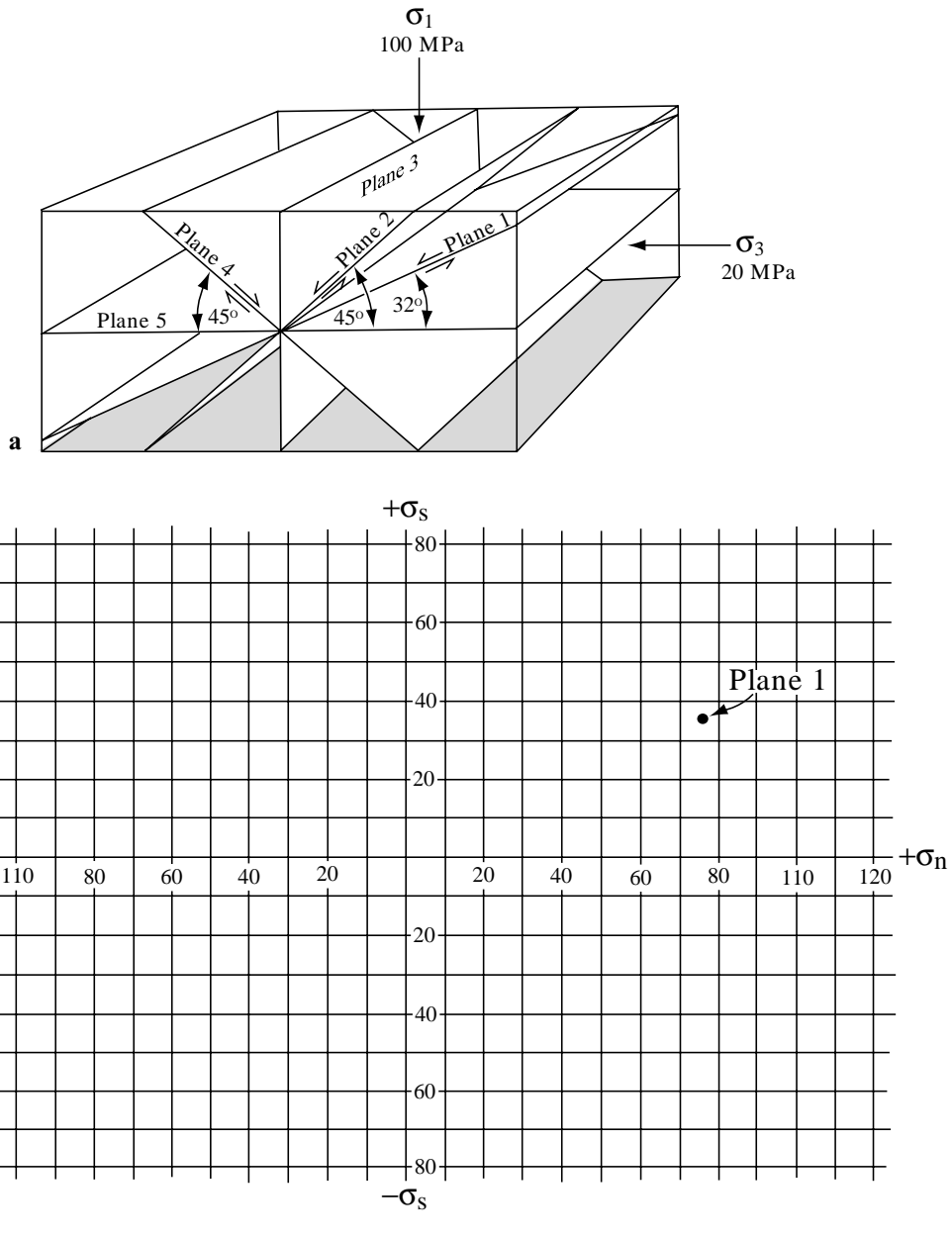
**Fig. G-32a** Rheologic model, stress-time graph, and strain-time graph for a standard linear solid. For use in Problem 12.1.



**Fig. G-32b** Sketch of a folded and fractured rock layer. For use in Problem 12.3.



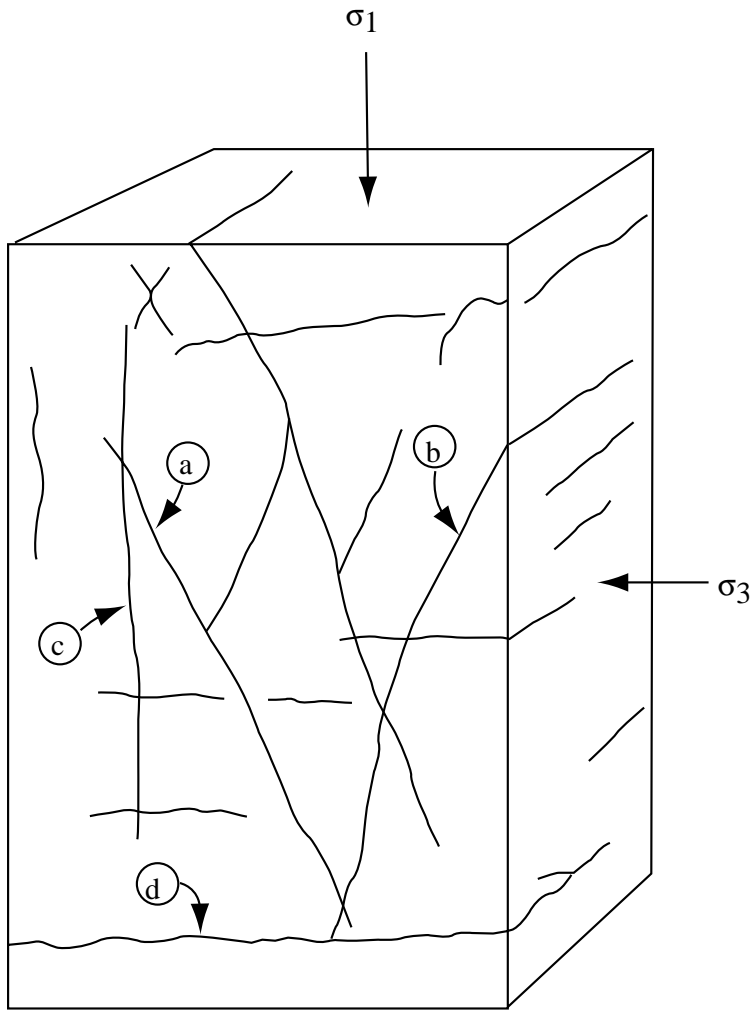




**Fig. G-33** (a) Five planes and the  $\sigma_1$  and  $\sigma_3$  stresses they are experiencing. (b) Mohr diagram on which to plot the normal and stresses experienced by the five planes shown above. Plane 1 has already been plotted. For use in Problem 13.2.



Name \_\_\_\_\_



Coulomb coefficient = \_\_\_\_\_

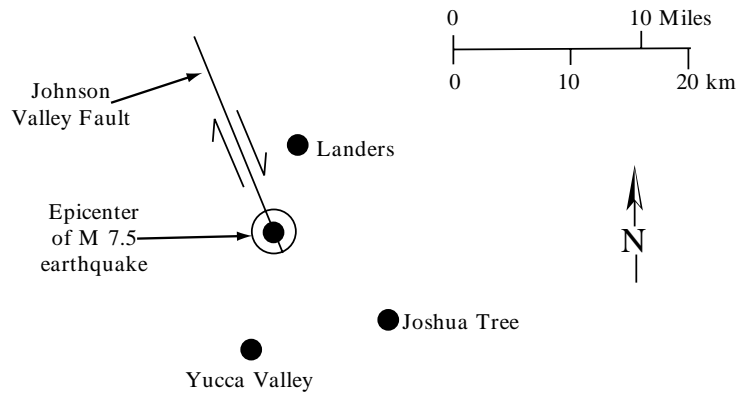
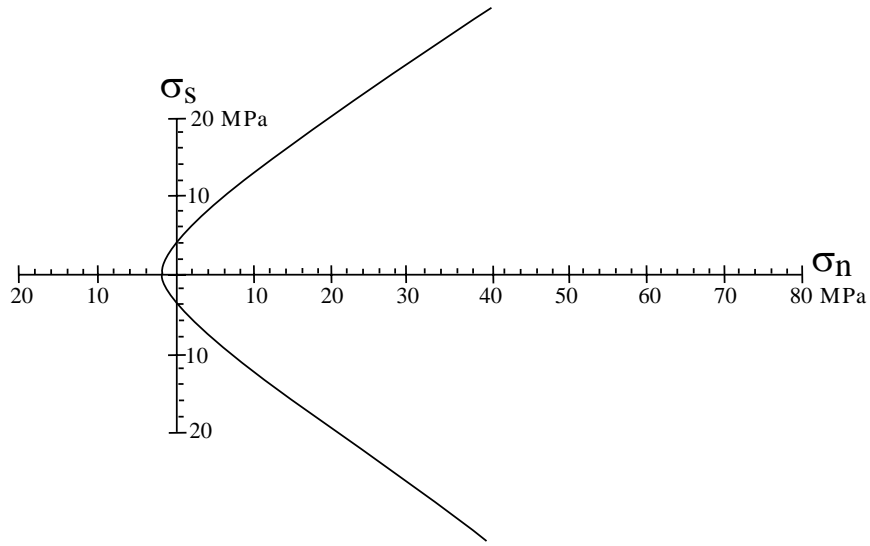
Explanation \_\_\_\_\_

\_\_\_\_\_

**Fig. G-34** Sketch of a block of fine-grained limestone that was experimentally shortened about 1% at room temperature. For use in Problem 13.6. After Hobbs *et al.* (1976).



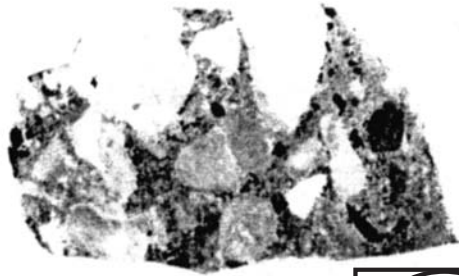
Name \_\_\_\_\_



**Fig. G-35** (a) Failure envelope of a petroleum reservoir rock. For use in Problem 13.7. (b) Map of the Johnson Valley Fault in southern California. For use in Problem 13.8.

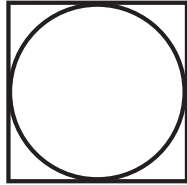


Name \_\_\_\_\_



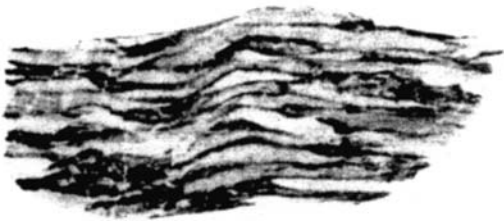
**a**

$$1 + e_1 : 1 + e_2 = 1.0 : 1.0$$



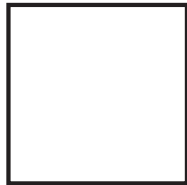
**b**

$$1 + e_1 : 1 + e_2 = \quad :$$



**c**

$$1 + e_1 : 1 + e_2 = \quad :$$



**d**

$$1 + e_1 : 1 + e_2 = \quad :$$



**Fig. G-36** Photographs, all at the same scale, of slabs of breccia from the Alps. Undeformed (a) and in varying stages of deformation (b–d). For use in Problem 14.2. Photographed from the collection of O. T. Tobisch.

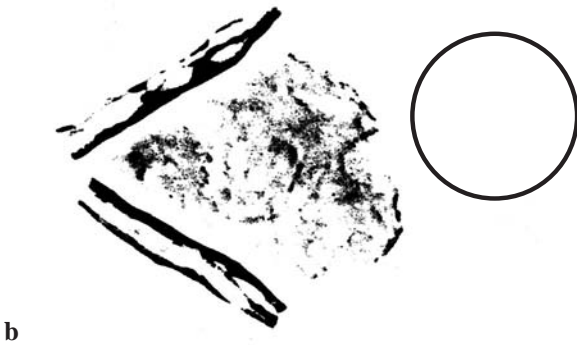




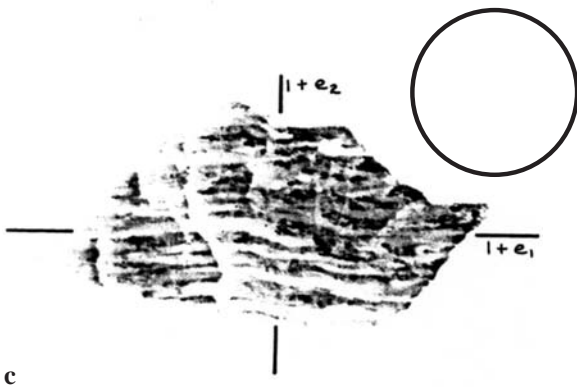
Name \_\_\_\_\_



The boomerang-shaped object in this rock slab is not a boudin; but a cross section through a dome.  
Field no. \_\_\_\_\_ because \_\_\_\_\_



This rock has a lumpy surface. Next to the main rock are two cross-section views cut at different angles.  
Field no. \_\_\_\_\_ because \_\_\_\_\_



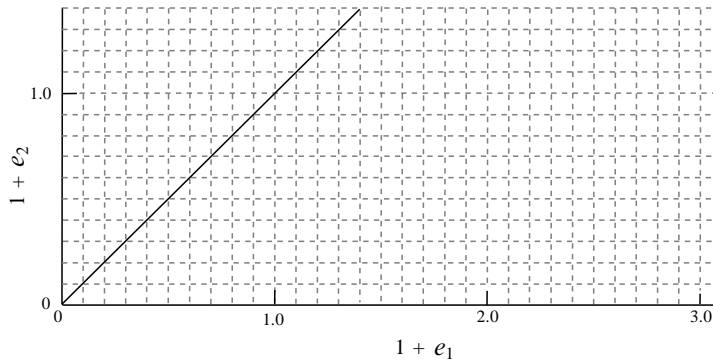
This is another sample of the deformed breccia seen in Fig. 14.13. Focus only on elongate grains; ignore fractures parallel to  $1 + e_2$ .  
Field no. \_\_\_\_\_ because \_\_\_\_\_

**Fig. G-37** Photographs of deformed structures. For use in Problem 14.3. Photographed from the collection of O. T. Tobisch.



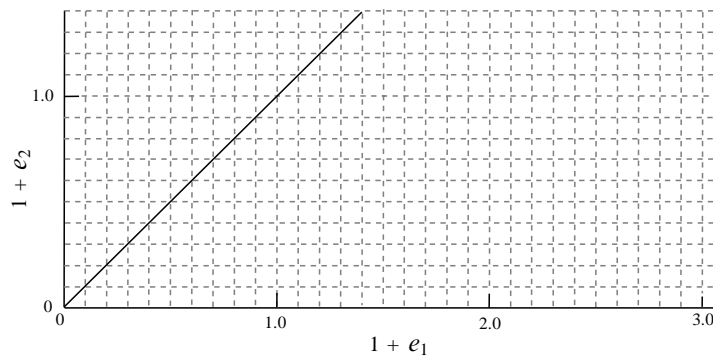
**Experiment 14.1: Coaxial strain**

Time	Length of semi-major axis	$e_1$	$1 + e_1$	Length of semi-minor axis	$e_2$	$1 + e_2$	$1 + e_1 : 1 + e_2$
$t_0$	$l_0 =$ _____	0	1.0	$l_0 =$ _____	0	1.0	1.0 : 1.0
$t_1$	_____	_____	_____	_____	_____	_____	_____
$t_2$	_____	_____	_____	_____	_____	_____	_____
$t_3$	_____	_____	_____	_____	_____	_____	_____
$t_4$	_____	_____	_____	_____	_____	_____	_____
$t_5$	_____	_____	_____	_____	_____	_____	_____
$t_6$	_____	_____	_____	_____	_____	_____	_____



**Experiment 14.4: Noncoaxial strain**

Time	Length of semi-major axis	$e_1$	$1 + e_1$	Length of semi-minor axis	$e_2$	$1 + e_2$	$1 + e_1 : 1 + e_2$	Angle of rotation
$t_0$	$l_0 =$ _____	0	1.0	$l_0 =$ _____	0	1.0	1.0 : 1.0	$0^\circ$
$t_1$	_____	_____	_____	_____	_____	_____	_____	_____
$t_2$	_____	_____	_____	_____	_____	_____	_____	_____
$t_3$	_____	_____	_____	_____	_____	_____	_____	_____
$t_4$	_____	_____	_____	_____	_____	_____	_____	_____
$t_5$	_____	_____	_____	_____	_____	_____	_____	_____
$t_6$	_____	_____	_____	_____	_____	_____	_____	_____



**Fig. G-38** Table for recording and graphing data from Experiments 14.1 and 14.4.



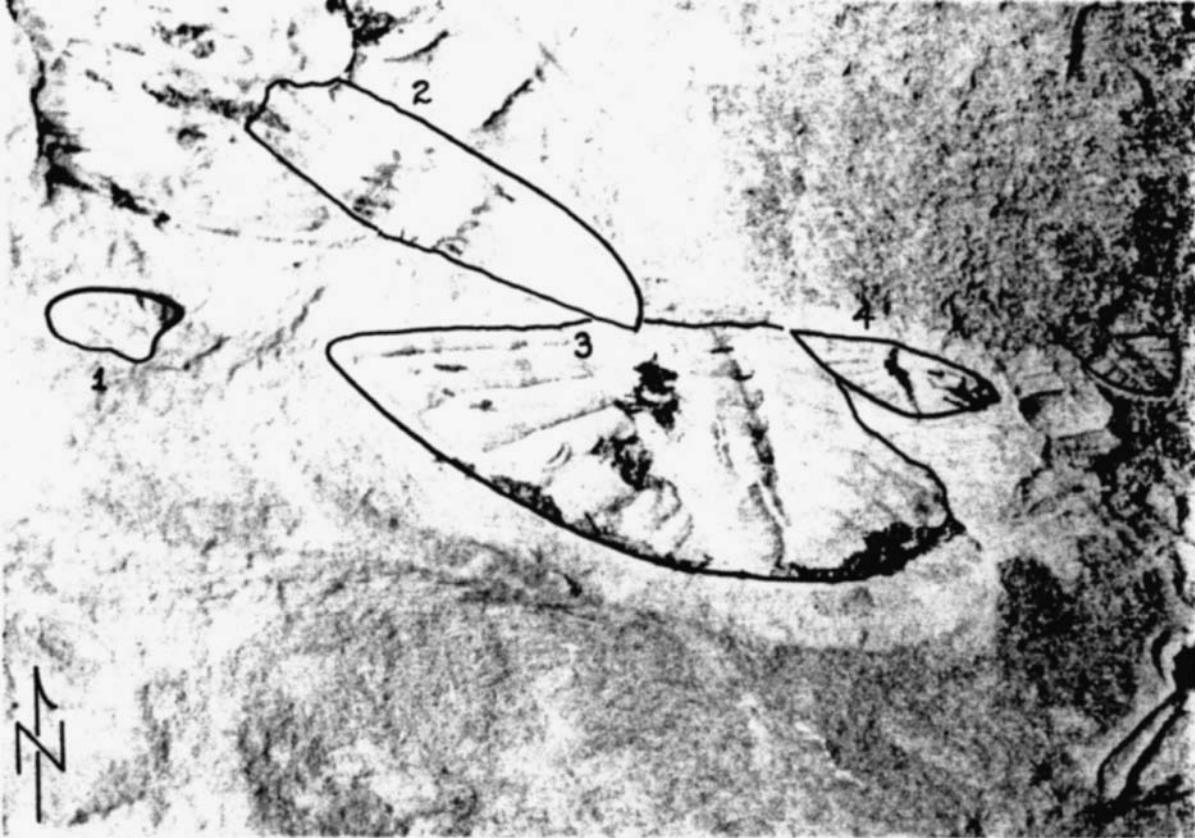
Name \_\_\_\_\_



**Fig. G-39** Sketch of a dike and sill complex. For use in Problem 14.4.



Name \_\_\_\_\_

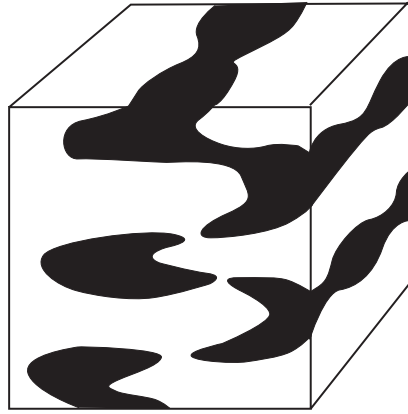
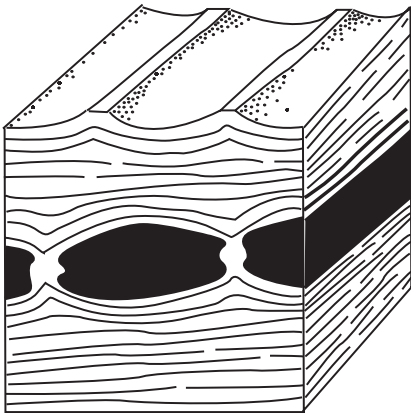
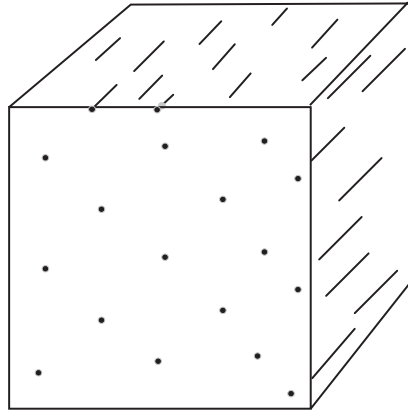
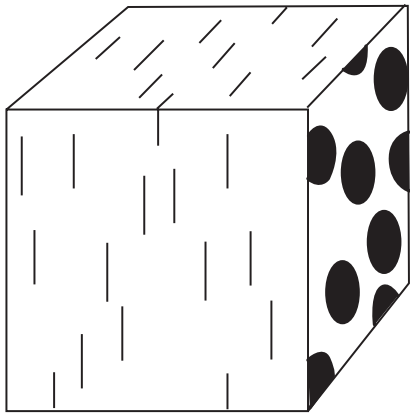


**Fig. G-40** Photograph of a slab of rock containing several pieces of deformed trilobites. For use in Problem 14.6.



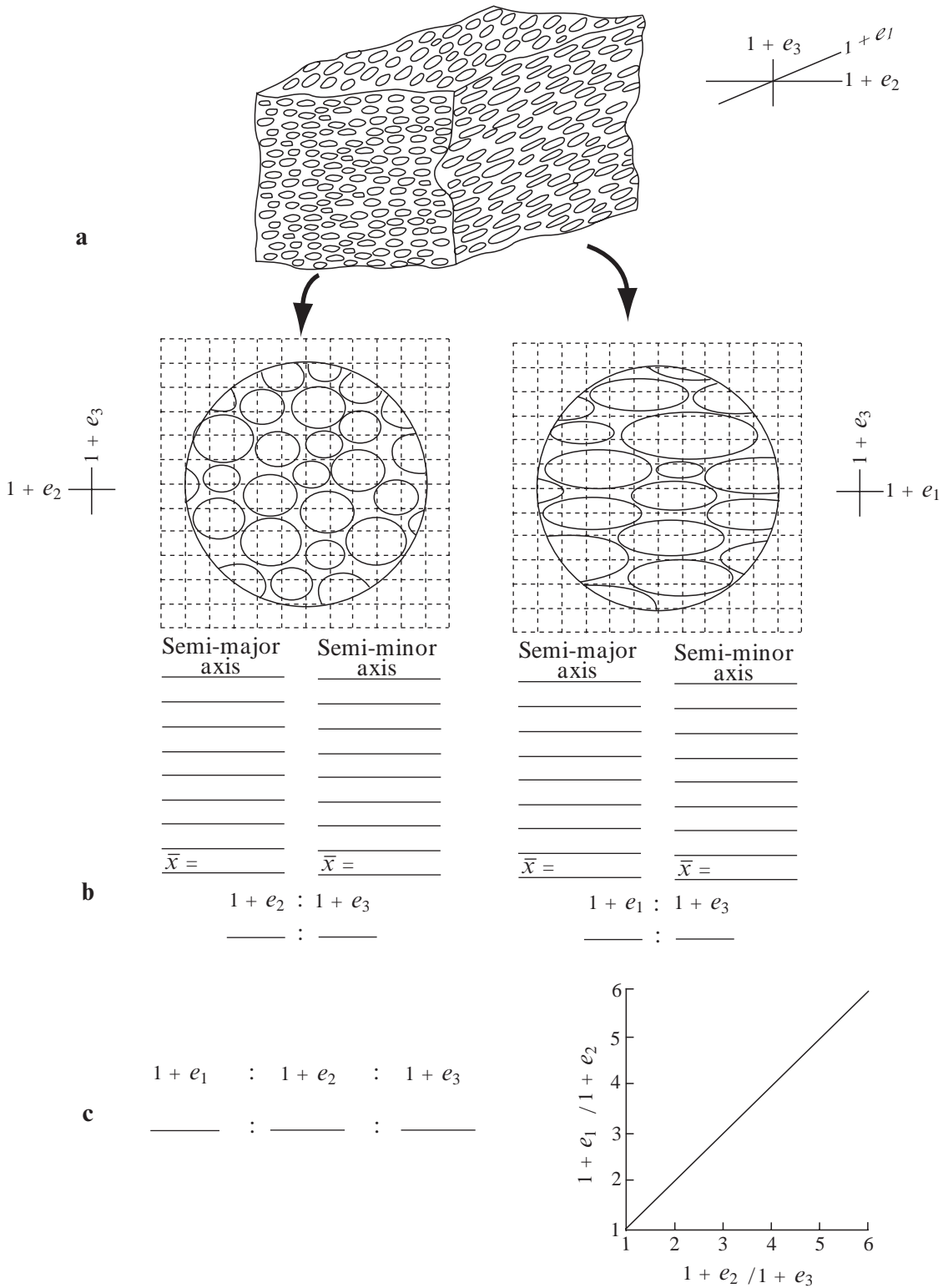


Name \_\_\_\_\_



**Fig. G-41** Four block diagrams of deformed rocks. For use in Problem 14.7.

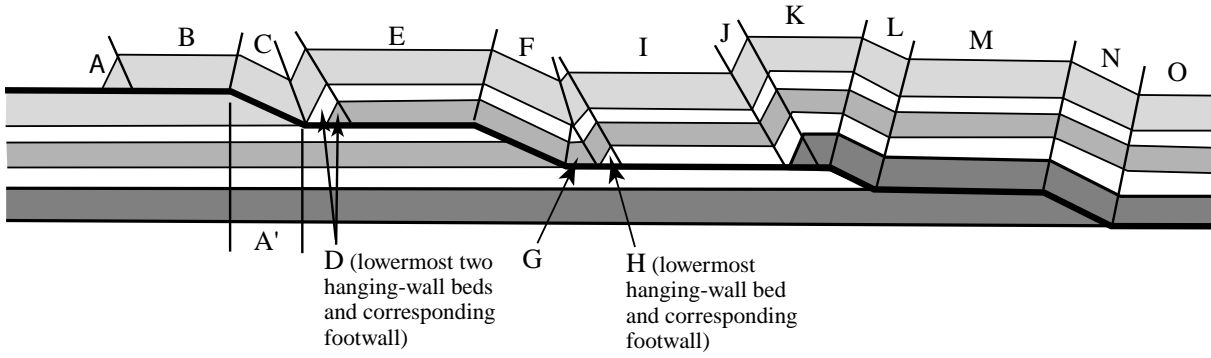




**Fig. G-42** Diagrams, tables, and graph for Problem 14.8.



Name \_\_\_\_\_



Panel	Hanging Wall	Footwall
A	Ramp	Flat
B		
C		
D		
E		
F		
G		
H		
I		
J		
K		
L		
M		
N		
O		

**Fig. G-43** For use in Problem 15.1. Adapted from Marshak and Woodward (1998).



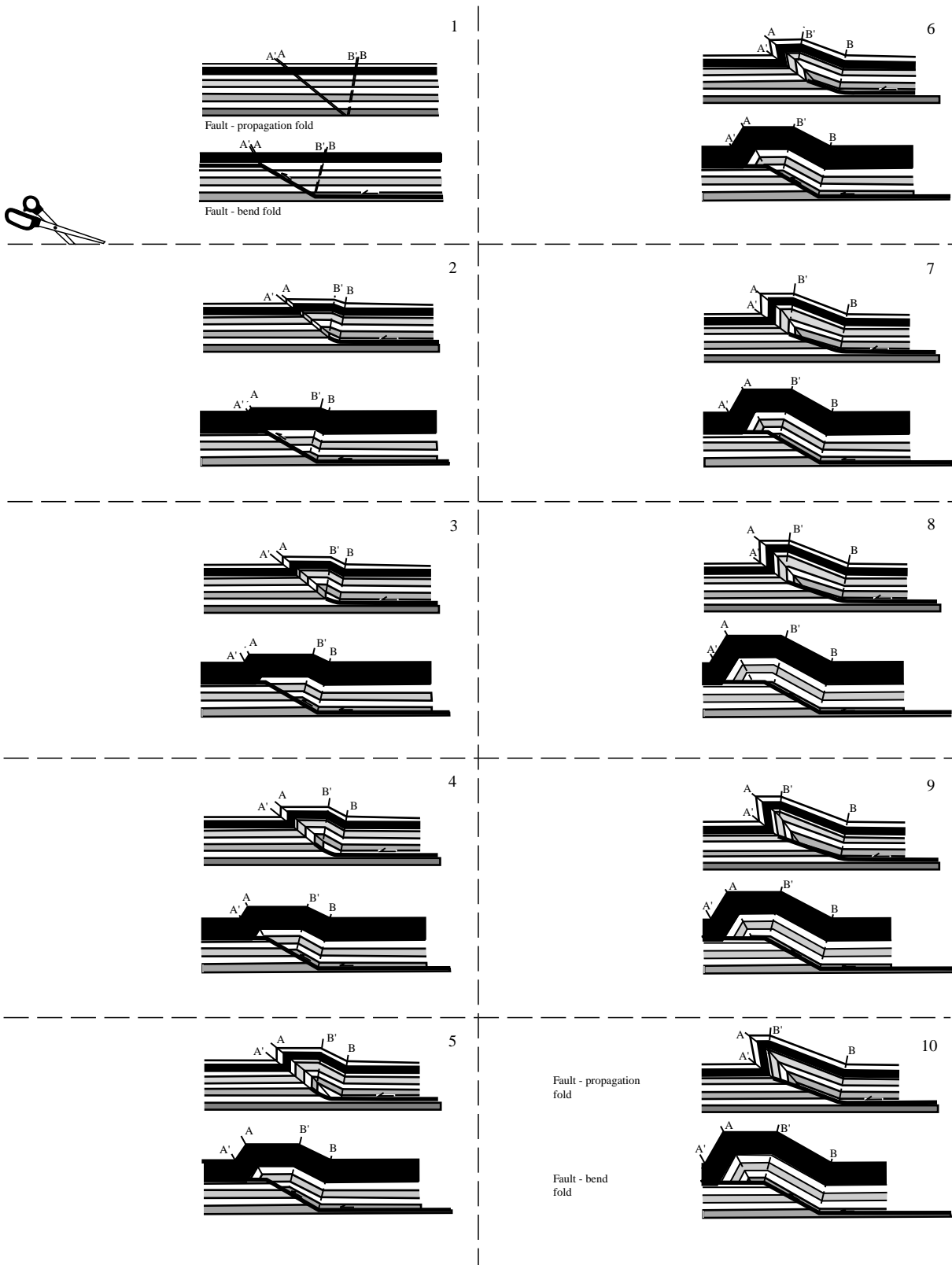
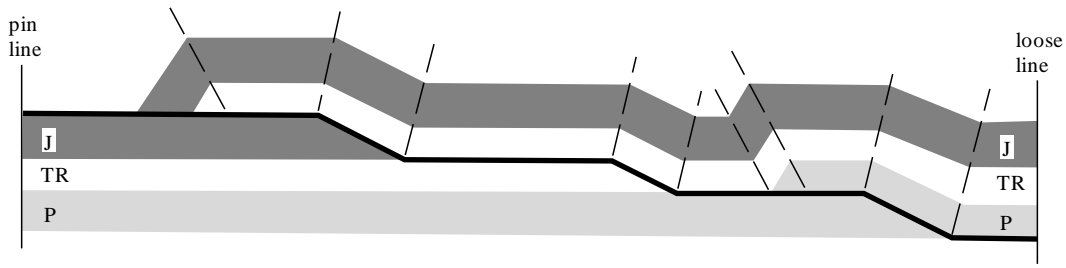


Fig. G-44 For use in Chapter 15.





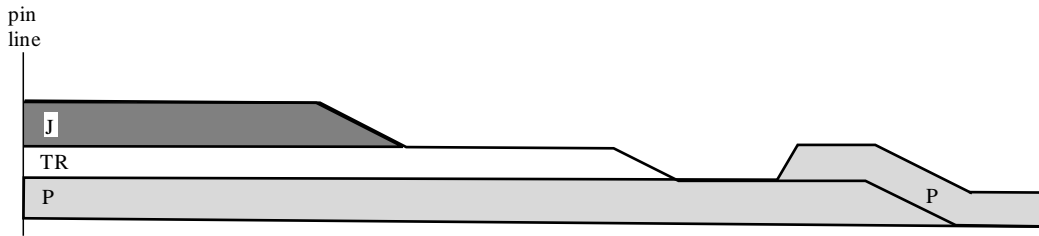
Name \_\_\_\_\_



**Fig. G-45** For use in Problem 15.3.



Name \_\_\_\_\_



**Fig. G-46** For use in Problem 15.4.



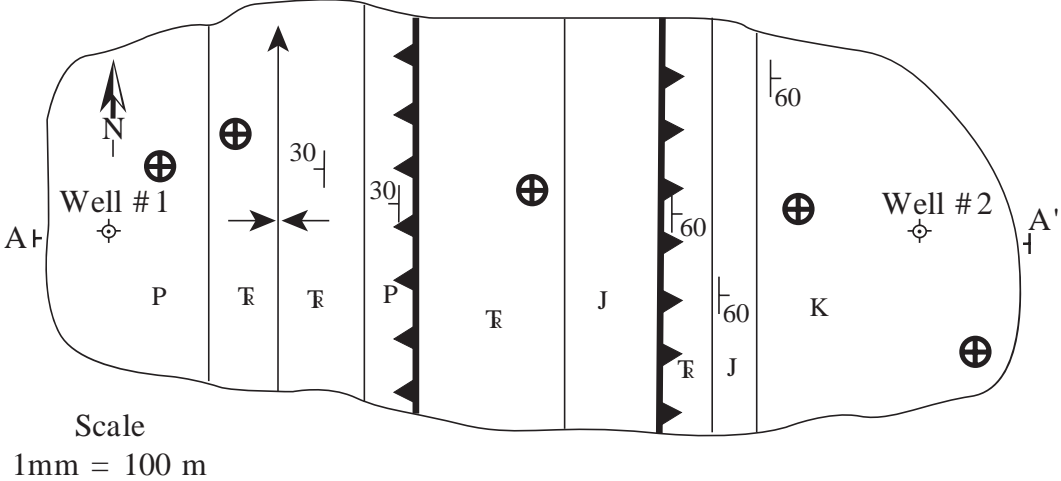
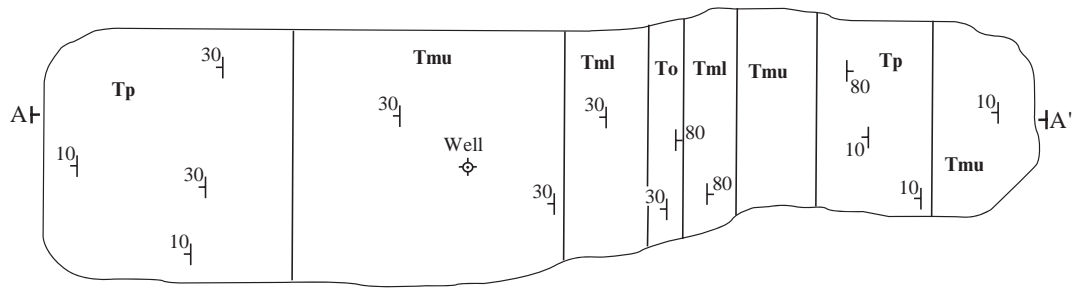


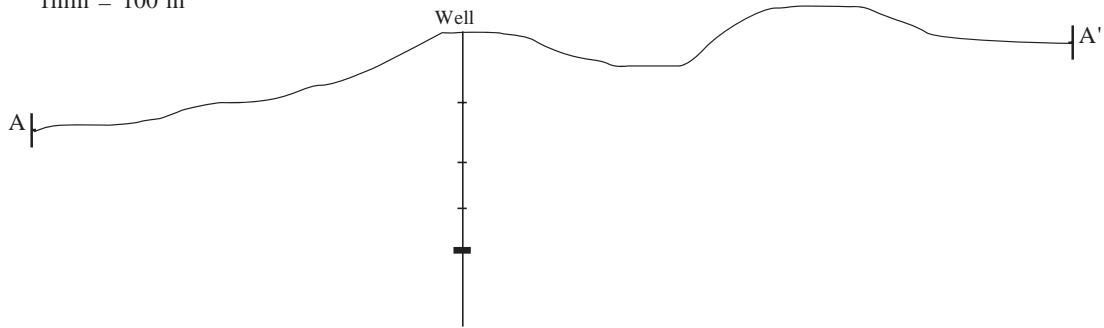
Fig. G-47 For use in Problem 15.5.



Name \_\_\_\_\_



Scale  
1mm = 100 m

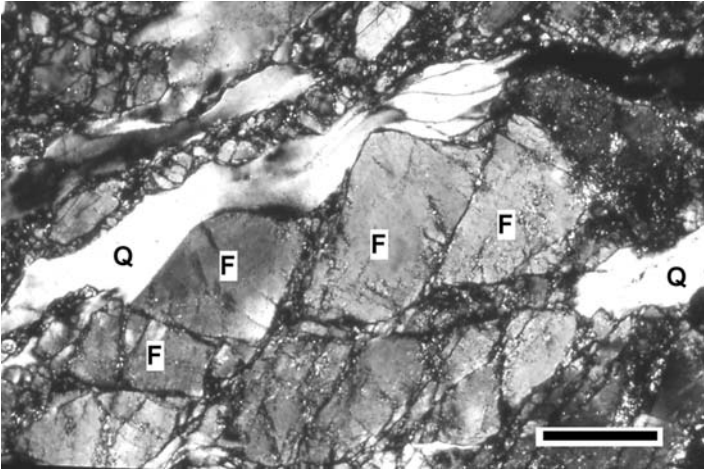


**Fig. G-48** For use in Problem 15.6. Tml, Tertiary lower Miocene; Tmu, Tertiary upper Miocene; To, Tertiary Oligocene; Tp, Tertiary Pliocene.

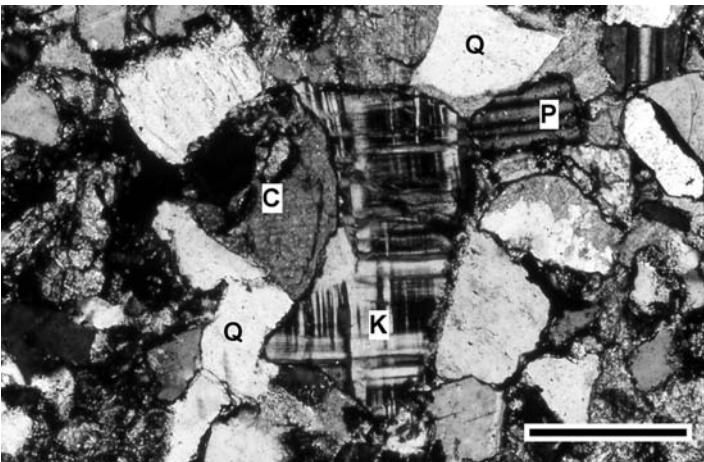




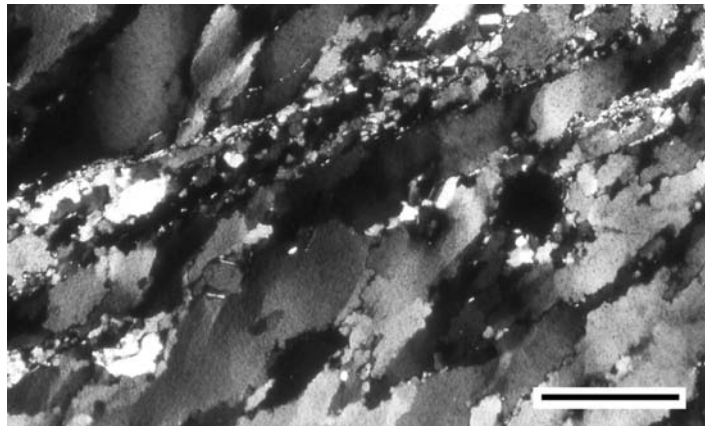
Name \_\_\_\_\_



**Fig. G-49** Photomicrograph for use in Problem 16.1. F, feldspar; Q, quartz. Crossed polars. Scale bar is 0.5 mm.



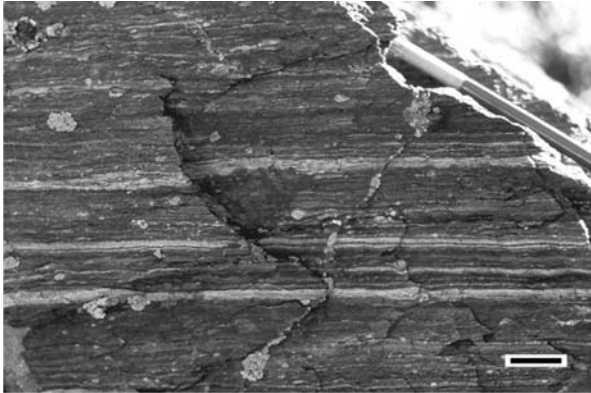
**Fig. G-50** Photomicrograph for use in Problem 16.2. C, calcite; K, potassium feldspar; P, plagioclase; Q, quartz. Crossed polars. Scale bar is 1 mm.



**Fig. G-51** Photomicrograph for use in Problem 16.3. Crossed polars. Scale bar is 1 mm.



Name \_\_\_\_\_



Type of fault rock: \_\_\_\_\_

Diagnostic features: \_\_\_\_\_

\_\_\_\_\_  
\_\_\_\_\_

**Fig. G-52a** Field photograph for use in Problem 16.4. The protolith of this rock was a coarse-grained granite. Scale bar is 2 cm.

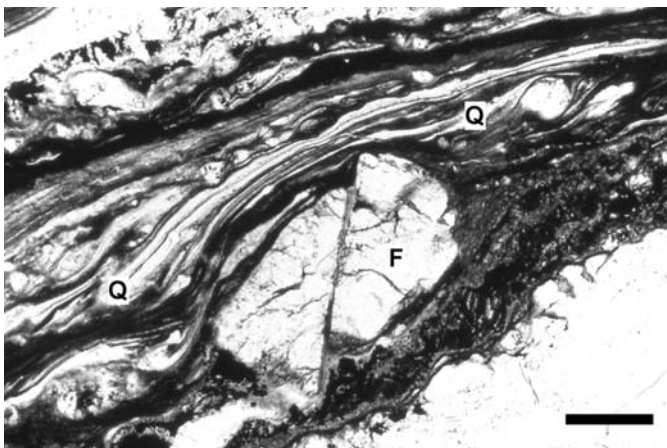


Type of fault rock: \_\_\_\_\_

Diagnostic features: \_\_\_\_\_

\_\_\_\_\_  
\_\_\_\_\_

**Fig. G-52b** Field photograph for use in Problem 16.5. The protolith of this rock was a porphyritic granite. Coin is 2.4 cm in diameter.



Description of principal microstructures in quartz and feldspar and interpretation of mechanisms:

Approximate range of temperatures and evidence:

Sense of shear:

**Fig. G-53** Photomicrograph for use in Problem 16.6. F, feldspar; Q, quartz. Plane polarized light. Scale bar is 0.5 mm.



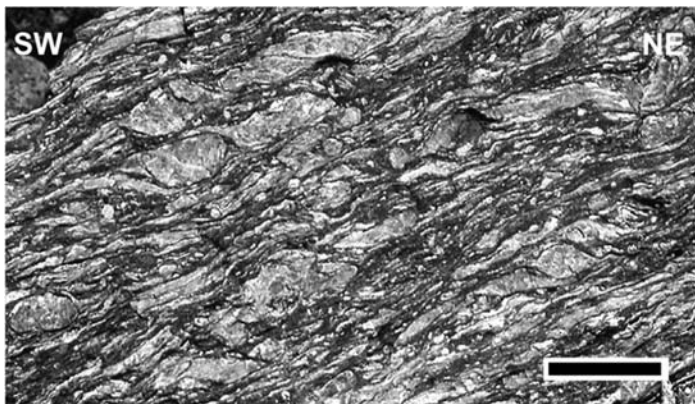
Name \_\_\_\_\_



Type of porphyroclast: \_\_\_\_\_

Description of type of movement  
in the shear zone:

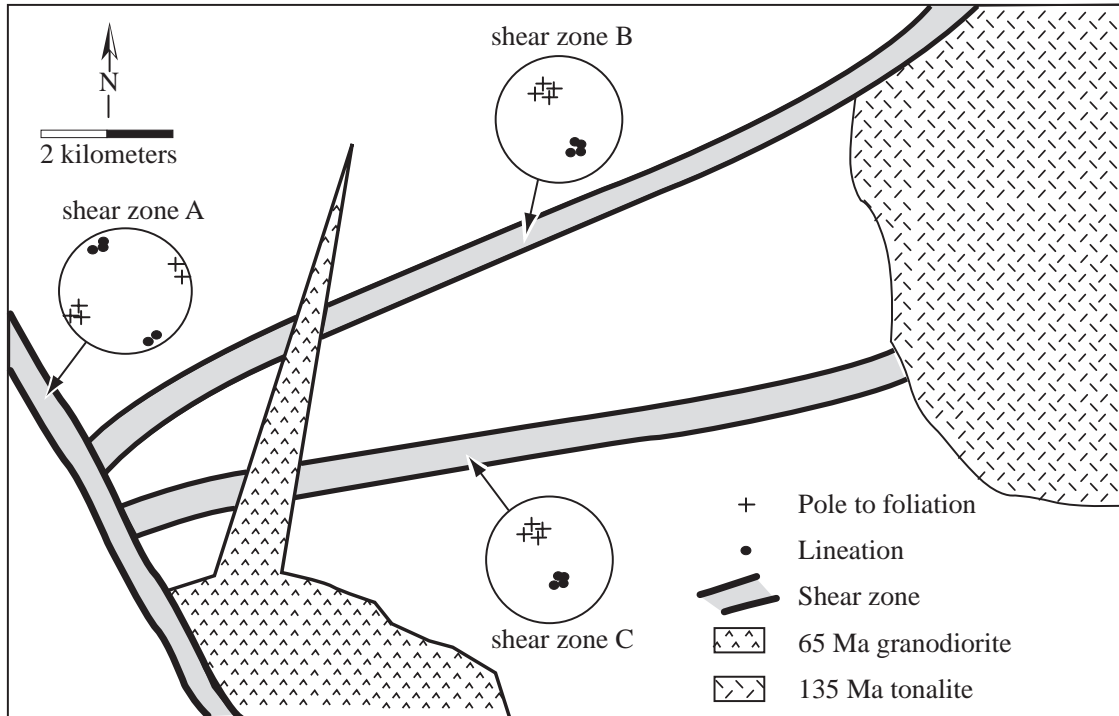
**Fig. G-54a** Field photograph of a large porphyroclast in a vertical cliff face, for use in Problem 16.7. You are looking parallel to the strike of the shear zone (toward  $050^\circ$ ). NW, northwest; SE, southeast. Scale bar is 5 cm.



Description of type of  
movement in the shear zone:

**Fig. G-54b** Field photograph of mylonitic megacrystic granite for use in Problem 16.8. You are looking parallel to the strike of the shear zone (toward  $330^\circ$ ). NE, northeast; SW, southwest. Scale bar is 2 cm.





Deformational history of map area:

**Fig. G-55** Tectonic map for use in Problem 16.9.



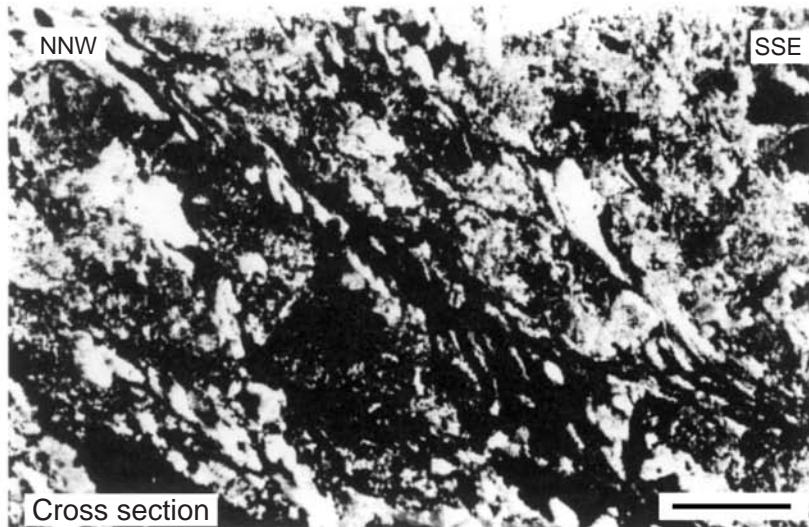




**a**



**b**

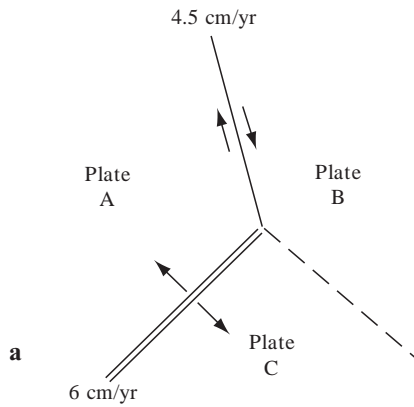


**c**

**Fig. G-56** Samples from shear zones for use in Problem 16.9. All views are of the XZ plane of the strain ellipsoid. (a) Quartz-feldspar mylonite from shear zone A. The view is of a horizontal outcrop surface with east on the right side of photo. Scale bar is 2 cm. (b) Mylonitic amphibolite from shear zone B. Cross-sectional view to the northeast. Scale bar is 2 cm. (c) Muscovite-quartz mylonite from shear zone C. Cross-sectional view to the east. Scale bar is 0.5 mm.



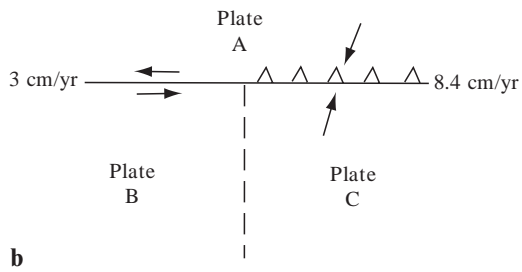
Name \_\_\_\_\_



Type of plate boundary between plates  
B and C: \_\_\_\_\_

Relative rate of motion between plates  
B and C: \_\_\_\_\_

**Fig. G-57a** For use in Problems 17.1 and 17.4.



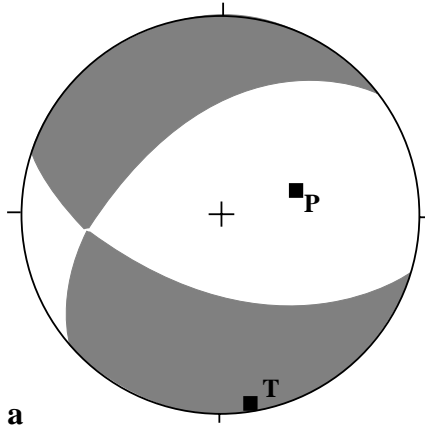
Type of plate boundary between plates  
B and C: \_\_\_\_\_

Relative rate of motion between plates  
B and C: \_\_\_\_\_

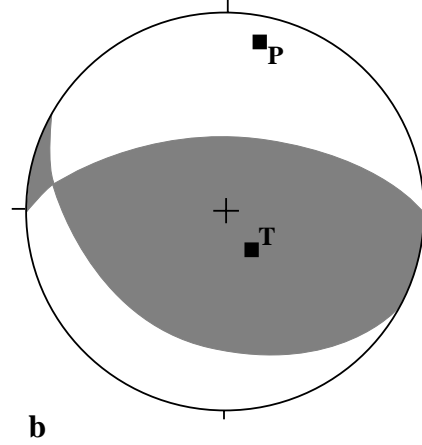
**Fig. G-57b** For use in Problems 17.2 and 17.4.



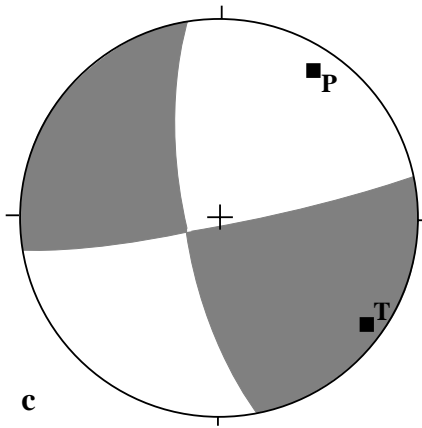
Name \_\_\_\_\_



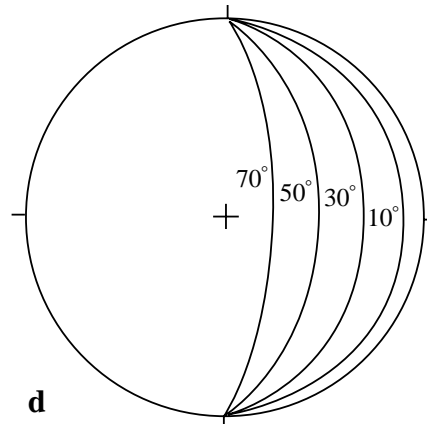
\_\_\_\_\_  
**or**  
\_\_\_\_\_



\_\_\_\_\_  
**or**  
\_\_\_\_\_



\_\_\_\_\_  
**or**  
\_\_\_\_\_

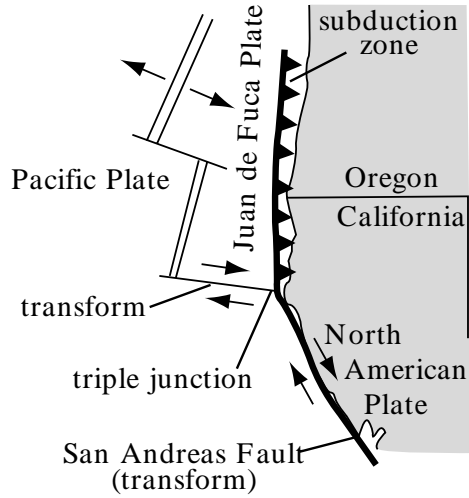


**Fig. G-58** For use in Problem 17.3.



Name \_\_\_\_\_

Data recorded at twenty-five seismic stations for two earthquakes with epicenters near the Mendocino triple junction.



Station	Azimuth (degrees)	Incidence (degrees)	First motion Event A	First motion Event B
1	269	45	D	N.D.
2	262	48	C	D
3	255	44	C	N.D.
4	256	31		C C
5	233	36	C	C
6	254	21	D	C
7	258	14	D	C
8	244	17	N	C
9	218	21	D	C
10	148	19	D	C
11	25	90	C	C
12	0	40	C	C
13	347	31	N.D.	C
14	66	73	C	D
15	290	51	D	D
16	46	14	C	C
17	271	85	C	D
18	275	61	D	D
19	261	64	C	D
20	266	50	N.C.	D
21	116	34	N.D.	C
22	101	51	C	N.C.
23	232	56	C	D
24	157	55	D	C
25	161	88	D	N.C.

C, compression first motion; D, dilational first motion; N, nodal; N.C., nodal (weakly compressional); N.D., nodal (weakly dilational)

	Event A	Event B
Plate boundary	_____	_____
Attitude of fault plane	_____	_____

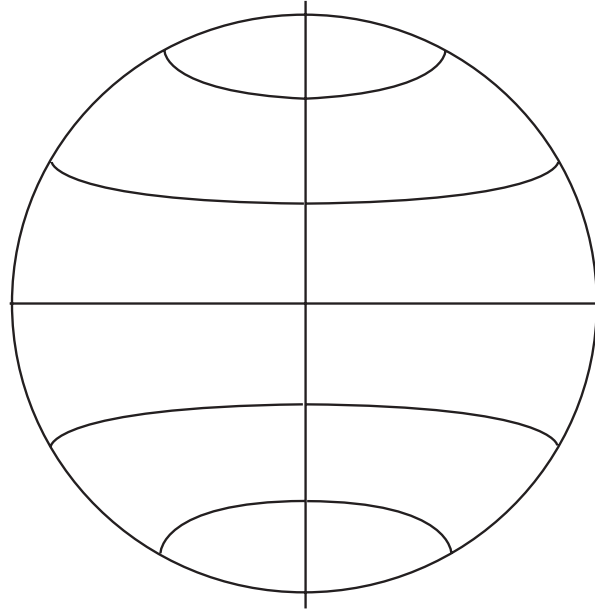
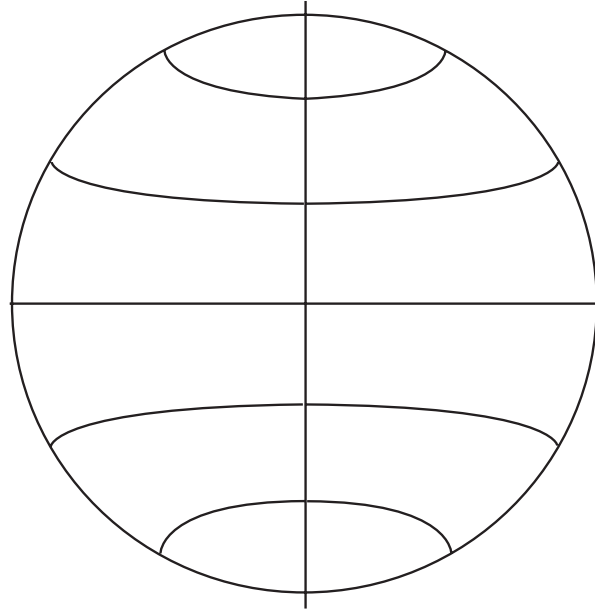
(attach focal-mechanism plots)

**Fig. G-59** For use in Problem 17.5.



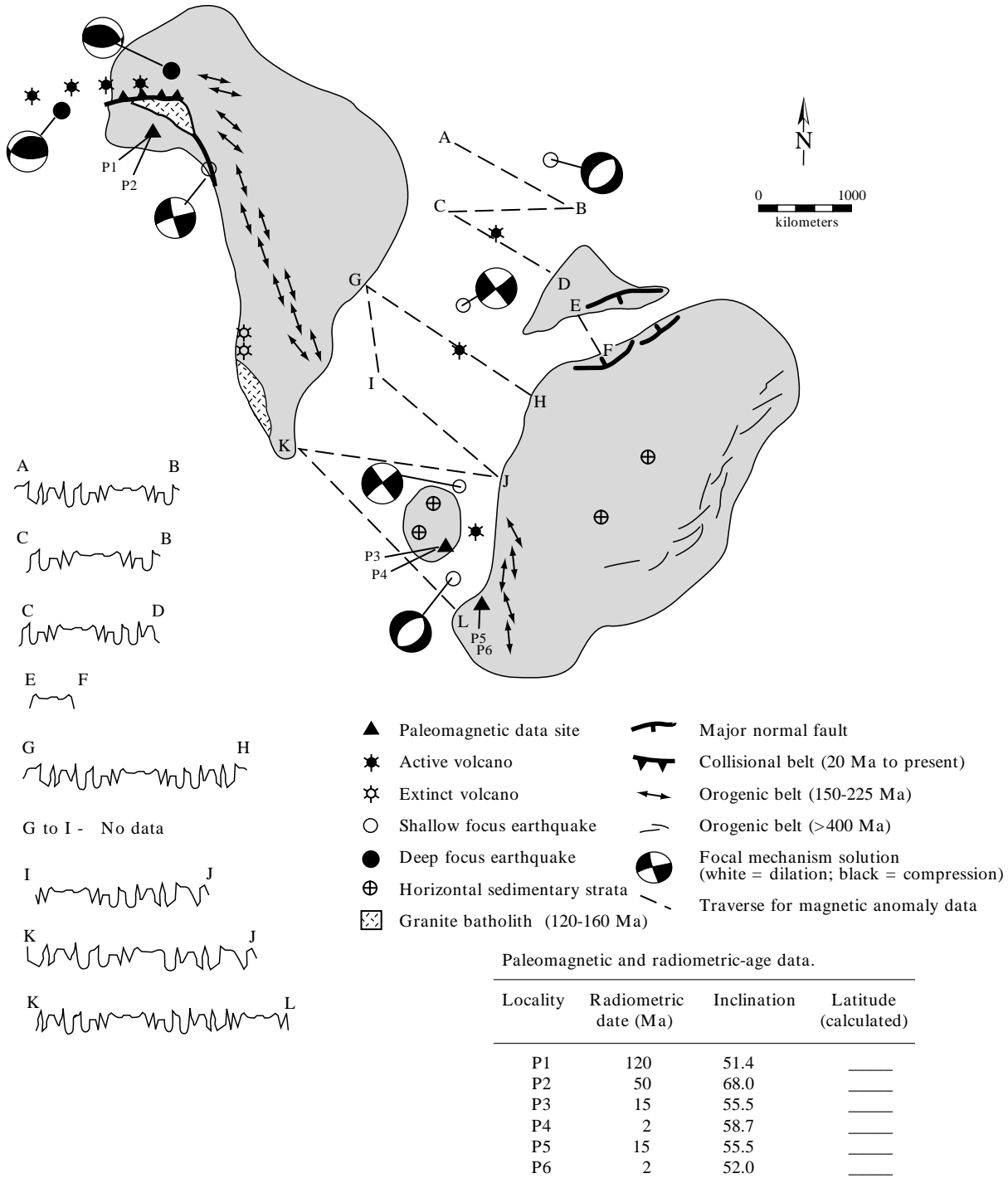


Name \_\_\_\_\_



**Fig. G-60** For use in Problem 17.8.





**Fig. G-61** For use in Problem 17.9.



# References

- Anderson, E.M. 1942. *The Dynamics of Faulting*. Edinburgh: Oliver & Boyd, 191 p. (2nd edn, 1952.)
- Angelier, J. 1979. "Determination of the mean principal directions of stresses for a given fault population." *Tectonophysics*, v. 56, T17–T26.
- Angelier, J., Colletta, B., and Anderson, R.W. 1985. "Neogene paleostress changes in the Basin and Range." *Geological Society of America Bulletin*, v. 96, 347–361.
- Aydin, A. and Reches, Z. 1982. "Number and orientation of fault sets in the field and in experiments." *Geology*, v. 10, 107–112.
- Compton, R.R. 1985. *Geology in the Field*. New York: Wiley, 398 p.
- Dahlstrom, C.D.A. 1954. "Statistical analysis of cylindrical folds." *Bulletin of the Canadian Institute of Mining and Metallurgy*, v. 57, 140–145.
- De Jong, K.A. 1975. "Electronic calculators facilitate solution of problems in structural geology." *Journal of Geological Education*, v. 23, 125–128.
- Dibblee, T.W., Jr. 1966. *Geologic Map and Sections of the Palo Alto 15' Quadrangle, California*. California Division of Mines and Geology, Map Sheet 8.
- Elliott, D. 1983. "The construction of balanced cross-section." *Journal of Structural Geology*, v. 5, 101.
- Gradstein, F.M., Ogg, J.G., and Smith, A.G. 2004. "Chronostratigraphy: Linking time and rock." In: Gradstein, F.M., Ogg, J.G., and Smith, A.G. (eds) *A Geologic Time Scale 2004*. Cambridge, UK: Cambridge University Press, 20–46.
- Hobbs, B.E., Means, W.D., and Williams, P.F. 1976. *An Outline of Structural Geology*. New York: Wiley, 571 p.
- Huber, N.K. and Rinehart, C.D. 1965. *Geologic Map of the Devils Postpile Quadrangle, Sierra Nevada, California*. U.S. Geological Survey Map GQ-437.
- Kamb, W.B. 1959. "Ice petrofabric observations from Blue Glacier, Washington in relation to theory and experiment." *Journal of Geophysical Research*, v. 64, 1891–1909.
- Marrett, R. and Allmendinger, R.W. 1990. "Kinematic analysis of fault-slip data." *Journal of Structural Geology*, v. 12, 973–986.
- Marshak, S. and Woodward, N. 1988. "Introduction to cross-section balancing." In: Marshak, S. and Mitra, G. (eds) *Basic Methods of Structural Geology*. Englewood Cliffs, NJ: Prentice Hall, 303–332.
- Molnar, P. and Tapponnier, P. 1975. "Cenozoic tectonics of Asia: Effects of a continental collision." *Science*, v. 189, 419–426.
- Nelson, C.A. 1971. *Geologic Map of the Waucoba Spring Quadrangle, Inyo County, California*. U.S. Geological Survey Map GQ-921.
- Palmer, H.S. 1918. "New graphic method for determining the depth and thickness of strata and the projection of dip." *US Geological Survey Professional Paper* 120-G, 123–128.
- Petit, J.P. 1987. "Criteria for the sense of movement on fault surfaces in brittle rocks." *Journal of Structural Geology*, v. 9, 597–608.
- Ragan, D.M. 1985. *Structural Geology: An Introduction to Geometrical Techniques* (3rd edn). New York: Wiley, 393 p.
- Raleigh, C.B., Healy, J.H., and Bredehoeft, J.D. 1972. "Faulting and crustal stress at Rangely, Colorado." In: Heard, H.C. and others (eds) *Flow and Fracture of Rocks*. Geophysical Monograph 16, 275–284. Washington, DC: American Geophysical Union.
- Ramsay, J.G. 1967. *Folding and Fracturing of Rocks*. New York: McGraw-Hill, 568 p.
- Ramsay, J.G. and Huber, M.I. 1983. *The Techniques of Modern Structural Geology, Volume I: Strain Analysis*. London: Academic Press, 307 p.
- Rowland, S.M. 1978. "Portable outcrops." *Journal of Geological Education*, v. 26, 109–110.

- Sherburne, R.W., and Cramer, C. 1984. "Focal mechanism studies: an explanation." *California Geology*, v. 37, no. 3, 54–57.
- Sibson, R.H. 1977. "Fault rocks and fault mechanisms." *Journal of the Geological Society of London*, v. 133, 191–213.
- Stein, R.S., King, G.C.P., and Lin, J. 1992. "Change in the failure stress on the southern San Andreas fault system caused by the 1992 magnitude 7.4 Landers earthquake." *Science*, v. 258, 1328–1332.
- Suppe, J. 1983. "Geometry and kinematics of fault-bend folding." *American Journal of Science*, v. 283, 684–721.
- Suppe, J. 1985. *Principles of Structural Geology*. Englewood Cliffs, NJ: Prentice Hall, 537 p.
- Tapponnier, P., Peltzer, G., Le Dain, A.Y., Armijo, R., and Cobbold, P. 1982. "Propagating extrusion tectonics in Asia: New insights from simple experiments with plasticene." *Geology*, v. 10, 611–616.
- The Course Team. 1972. *Internal Processes*. Bletchley, UK: Open University Press.
- Van der Pluijm, B.A., and Marshak, S. 1997. *Earth Structure: An Introduction to Structural Geology and Tectonics*. New York: WCB/McGraw-Hill, 495 p.
- Wang, J.N., Hobbs, B.E., Ord, A., Shimamoto, T., and Toriumi, M. 1994. "Newtonian dislocation creep in quartzites: Implications for the rheology of the lower crust." *Science*, v. 265, 1204–1206.
- Wellman, H.G. 1962. "A graphic method for analyzing fossil distortion caused by tectonic deformation." *Geological Magazine*, v. 99, 348–352.
- Weiss, L.E. 1954. "A study of tectonic style: structural investigation of a marble–quartzite complex in southern California." *University of California Publications in the Geological Sciences*, v. 30, no. 1, 1–102.
- Whitten, E.H.T. 1966. *Structural Geology of Folded Rocks*. Chicago: Rand McNally & Co, 663 p.
- Wright, L. 1976. "Late Cenozoic fault patterns and stress fields in the Great Basin and westward displacement of the Sierra Nevada block." *Geology*, v. 4, 489–494.
- Zalasiewicz, J., Smith, A., Brenchley, P., *et al.* 2004. "Simplifying the stratigraphy of time." *Geology*, v. 32, 1–4.

# Further Reading

## Chapter 1: Attitudes of Lines and Planes

- Bengtson, C.A. 1980. "Structural uses of tangent diagrams." *Geology*, v. 8, 599–602. An explanation of various uses of tangent diagrams, with several examples.
- De Jong, K.A. 1975. "Electronic calculators facilitate solution of problems in structural geology." *Journal of Geological Education*, v. 23, 125–128. A review of the use of pocket calculators in structural geology; includes an extensive bibliography.
- Dennison, J.M. 1968. *Analysis of Geologic Structures*. New York: Norton. A structural geology workbook emphasizing the trigonometric approach.

## Chapter 2: Outcrop Patterns and Structure Contours

- Bishop, M.S. 1960. *Subsurface Mapping*. New York: Wiley, 198 p. A good introduction to subsurface mapping, especially structure-contour maps.
- Dennison, J.M. 1968. *Analysis of Geologic Structures*. New York: Norton. Good discussion of outcrop patterns, three-point problems, and structure contours. Emphasis is on trigonometric solutions.
- Moody, G.B. (ed.) 1961. *Petroleum Exploration Handbook*. New York: McGraw-Hill. Much useful information on surface and subsurface maps applied to petroleum exploration.
- Ragan, D.M. 1985. *Structural Geology — An Introduction to Geometrical Techniques*. New York: Wiley. Good discussion of outcrop patterns, three-point problems, and structure contours. Emphasis is on graphical solutions.

## Chapter 3: Interpretation of Geologic Maps

- Bishop, M.S. 1960. *Subsurface Mapping*. New York: Wiley, 198 p. A good introduction to subsurface mapping, especially structure-contour maps.
- Blyth, F.G. 1965. *Geological Maps and their Interpretation*. London: Edward Arnold. Eighteen geologic maps with exercises and notes on interpretation.
- Dennison, J.M. 1968. *Analysis of Geologic Structures*. New York: Norton. Chapter 7 is devoted to the interpretation of geologic maps and contains exercises using geologic maps published by the United States Geological Survey.
- Lisle, R.J. 1988. *Geological Structures and Maps*. Oxford: Pergamon. Contains many useful examples and problems dealing with geological maps and structures.
- Roberts, J.L. 1982. *Introduction to Geologic Maps and Structures*. Oxford: Pergamon, 332 p.
- Spencer, E.W. 1993. *Geologic Maps*. New York: Macmillan. A guide to the interpretation and preparation of geologic maps. Includes several colored maps.

## Chapter 4: Geologic Structure Sections

- Owens, W.H. 2000. "An alternative approach to the Busk construction for a single surface." *Journal of Structural Geology*, v. 22, 1379–1384.
- Ragan, D.M. 1985. *Structural Geology—An Introduction to Geometrical Technique* (3rd edn). New York: Wiley. Chapter 19 is devoted to maps and cross sections.
- Suppe, J. 1985. *Principles of Structural Geology*. Englewood Cliffs, NJ: Prentice Hall. Pages 57–70 contain a discussion of retrodeformable or balanced cross sec-



tions, which allow the structure section to be undeformed for the purpose of analyzing earlier, less deformed states.

### Chapter 5: Stereographic Projection

- Dennison, J.M. 1968. *Analysis of Geologic Structures*. New York: Norton. Chapter 11 provides an introduction to stereographic projection, with numerous problems and an extensive bibliography.
- Hobbs, B.E., Means, W.D., and Williams, P.F. 1976. *An Outline of Structural Geology*. New York: Wiley. Appendix A contains a useful comparison of equiangular and equal-area projection.
- Phillips, P.C. 1960. *The Use of Stereographic Projection in Structural Geology* (2nd edn). London: Edward Arnold. Contains transparent overlays of sample problems.

### Chapter 6: Folds

- Cobbold, P.R. and Quinquis, H. 1980. "Development of sheath folds in shear regimes." *Journal of Structural Geology*, v. 2, 119–126.
- Huddleston, P.J. 1973. "Fold morphology and some geometrical implications of theories of fold development." *Tectonophysics*, v. 16, 1–46.
- Marjoribanks, R.W. 1974. "An instrument for measuring dip isogons and fold layer shape parameters." *Journal of Geological Education*, v. 22, 62–64. Design of an isogon plotter and discussion of procedure for measuring fold parameters.
- Ramsay, J.G. 1967. *Folding and Fracturing of Rocks*. New York: McGraw-Hill. A standard reference on the geometry and mechanisms of folding.
- Suppe, J. 1985. *Principles of Structural Geology*. Englewood Cliffs, NJ: Prentice Hall. Contains a good discussion of fold mechanics and mechanisms and many photographs and drawings of folds.
- The Course Team. 1972. *Internal Processes*. Bletchley, UK: Open University Press.

### Chapter 7: Stereographic Analysis of Folded Rocks

- Amenta, R.V. 1975. "Multiple deformation and metamorphism from structural analysis in the eastern Pennsylvania piedmont." *Geological Society of America Bulletin*, v. 85, 1647–1660. Good example of stereographic analysis of folds used to reconstruct the deformation history of an area.
- Ragan, D.M. 1985. *Structural Geology: An Introduction to Geometrical Techniques* (3rd edn). New York: Wiley. Good discussion of contoured equal-area diagrams and a description of an alternative method of counting points with the use of a Kalsbeek net.

Ramsay, J.G. and Huber, M.I. 1983. *The Techniques of Modern Structural Geology, Volume 2: Folds and Fractures*. New York: Academic Press.

Williams, P.F. 1985. "Multiply deformed terrains — problems of correlation." *Journal of Structural Geology*, v. 7, 269–280.

### Chapter 8: Parasitic Folds, Axial-Planar Foliations, and Superposed Folds

- Borradaile, G.J., Bayly, M.B., and Powell, C. McA. (eds) 1982. *Atlas of Deformation and Metamorphic Rock Fabrics*. New York: Springer-Verlag.
- Ramsay, J.G. 1967. *Folding and Fracturing of Rocks*. New York: McGraw-Hill. Chapter 10 is devoted to superposed folds.
- Simon, J.L. 2004. "Superposed buckle folding in the eastern Iberian Chain, Spain." *Journal of Structural Geology*, v. 26, 1447–1464.
- Suppe, J. 1985. *Principles of Structural Geology*. Englewood Cliffs, NJ: Prentice Hall. Contains a review of superposed folds with several examples at different scales.
- Thiessen, R.L. and Means, W.D. 1980. Classification of fold interference patterns: a reexamination. *Journal of Structural Geology*, v. 2, 311–316.
- Wilson, C. 1982. *Introduction to Small-scale Geological Structures*. London: George Allen & Unwin.

### Chapter 9: Faults

- Angelier, J., Colletta, B., and Anderson, R.W. 1985. "Neogene paleostress changes in the Basin and Range: A case study at Hoover Dam, Nevada-Arizona." *Geological Society of America Bulletin*, v. 96, 347–361. A good example of detailed analysis of faults and field criteria for determining sense of slip.
- Boyer, S.E. and Elliot, D. 1982. "Thrust systems." *American Association of Petroleum Geologists Bulletin*, v. 66, 1196–1230.
- Dennison, J.M. 1968. *Analysis of Geologic Structures*. New York: Norton. A structural geology workbook emphasizing the trigonometric approach to structural relationships.
- Peacock, D.C.P., Knipe, R.J., and Sanderson, D.J. 2000. "Glossary of normal faults." *Journal of Structural Geology*, v. 22, 291–306.
- Roberts, J.L. 1982. *Introduction to Geologic Maps and Structures*. Oxford: Pergamon. A textbook in structural geology emphasizing the interpretation of geology maps.
- Sylvester, A.G. 1988. "Strike-slip faults." *Geological Society of America Bulletin*, v. 100, 1666–1703.
- Wernicke, B. and Burchfiel, B.C. 1982. "Modes of extensional tectonics." *Journal of Structural Geology*, v. 4, 105–115.

## Chapter 10: Dynamic and Kinematic Analysis of Faults

- Anderson, E.M. 1952. *The Dynamics of Faulting*. London: Oliver & Boyd. A slightly revised edition of Anderson's very influential 1942 book. Mostly of historical interest.
- Angelier, J. 1994. "Fault slip analysis and paleostress reconstruction." In: Hancock, P.L. (ed.) *Continental Deformation*. Terrytown, New York: Pergamon, p. 53–100.
- Angelier, J., Colletta, B., and Anderson, R.W. 1985. "Neogene paleostress changes in the Basin and Range." *Geological Society of America Bulletin*, v. 96, 347–361. A good example of detailed analysis of paleostress.
- Dalziel, I.W.D. and Stirewalt, G.L. 1975. "Stress history of folding and cleavage development, Baraboo syncline, Wisconsin." *Geological Society of America Bulletin*, v. 86, 1671–1690. Good example of a study of the relationship between the stress ellipsoid and folds.
- Gapais, D., Cobbold, P.R., Bourgeois, O., Rouby, D., and de Urreiztieta, M. 2000. "Tectonic significance of fault-slip data." *Journal of Structural Geology*, v. 22, 881–888.
- Kamb, W.B. 1959. "Ice petrofabric observations from Blue Glacier, Washington in relation to theory and experiment." *Journal of Geophysical Research*, v. 64, 1891–1909.
- Marrett, R. and Allmendinger, R.W. 1990. "Kinematic analysis of fault-slip data." *Journal of Structural Geology*, v. 12, 973–986.
- Petit, J.P. 1987. "Criteria for the sense of movement on fault surfaces in brittle rocks." *Journal of Structural Geology*, v. 9, 597–608.

## Chapter 11: A Structural Synthesis

- Amenta, R.V. 1974. "Multiple deformation and metamorphism from structural analysis in the eastern Pennsylvania piedmont." *Geological Society of America Bulletin*, v. 85, 1647–1660. A good example of a structural synthesis of a region with several structural events. Note especially how diagrams and tables are used to display and summarize complex data.
- Cluff, J.L. 1980. "Time and time again." *Journal of Sedimentary Petrology*, v. 50, 1021–1022. A review of the correct usage of temporal and lithostratigraphic terminology. But also see Gradstein *et al.* (2004) and Zalasiewicz *et al.* (2004) on this topic; complete citations are provided in the References section.
- Cochran, W., Fenner, P., and Hill, M. (eds) 1984. *Geowriting—A Guide to Writing, Editing, and Printing in Earth Science* (4th edn). Falls Church, VA: American Geological Institute. A very useful handbook for geologists who are writing for publication.
- Davis, M. 1997. *Scientific Papers and Presentations*. San Diego, California: Academic Press, 296 p.

- Murray, M.W. 1968. "Written communication — A substitute for good dialog." *American Association of Petroleum Geologists Bulletin*, v. 52, 2092–2097. An excellent guide to effective organization of scientific reports.
- Norris, R.M. 1983. "Field geology and the written word." *Journal of Geological Education*, v. 31, 184–189. A detailed review of the method one instructor uses to teach report-writing skills in conjunction with field mapping.
- Strunk, W., Jr. and White, E.B. 2000. *The Elements of Style* (4th edn). Needham Heights, MA: Allyn & Bacon, 105 p.

## Chapter 12: Rheologic Models

- Dixon, J.M. and Summers, J.M. 1985. "Recent developments in centrifuge modelling of tectonic processes: equipment, model construction techniques and rheology of model materials." *Journal of Structural Geology*, v. 7, 83–102.
- Dixon, J.M. and Summers, J.M. 1986. "Another word on the rheology of silicone putty: Bingham." *Journal of Structural Geology*, v. 8, 593–595.
- Jaeger, J.C. and Cook, N.G.W. 1976. *Fundamentals of Rock Mechanics*. London: Chapman & Hall.
- Mansfield, C.E. 1985. "Modeling Newtonian fluids and Bingham plastics." *Journal of Geological Education*, v. 33, 97–100. A very readable summary of viscous and plastic behavior, with applications to sedimentology.
- McClay, K.R. "The rheology of plasticine." *Tectonophysics*, v. 33, T7–T15.
- Roper, P.J. 1974. "Plate tectonics: A plastic as opposed to a rigid body model." *Geology*, v. 2, 247–250. Implications of plastic behavior in plate tectonic reconstructions.
- Suppe, J. 1985. *Principles of Structural Geology*. Englewood Cliffs, NJ: Prentice Hall. A more mathematically rigorous review of rheological models is presented on p. 140–147.
- Turcotte, D.L. and Schubert, G. 1982. *Geodynamics: Applications of Continuum Physics to Geological Problems*. New York: Wiley & Sons.
- Walker, J. 1978. "Serious fun with Polyox, Silly Putty, Slime and other non-Newtonian fluids." *Scientific American*, v. 329, no. 5 (November), 186–196. An insightful discussion of non-Newtonian fluid flow; not specifically related to geologic phenomena.

## Chapter 13: Brittle Failure

- Bartley, J.M. and Glazner, A.F. 1985. "Hydrothermal systems and Tertiary low-angle normal faulting in the southwestern United States." *Geology*, v. 13, 562–564. Addresses the longstanding paradox of

- low-angle normal faults and the role of pore pressure in their development.
- Davis, G.H. 1978. "Experiencing structural geology." *Journal of Geological Education*, v. 26, 52–59. Reviews an integrated lab and field course in structural geology in which fracture strength experiments are combined with field analysis of structures.
- Donath, F.A. 1970. "Rock deformation apparatus and experiments for dynamic structural geology." *Journal of Geological Education*, v. 18, 3–13. Review of equipment and procedures necessary to carry out fracture strength experiments.
- Engelder, T. 1993. *Stress Regimes in the Lithosphere*. Princeton, NJ: Princeton University Press, 457 p.
- Means, W.D. 1976. *Stress and Strain*. New York: Springer-Verlag.
- Raleigh, C.B., Healy, J.H., and Bredehoeft, J.D. 1972. "Faulting and crustal stress at Rangely, Colorado." In: Heard, H.C., and others (eds) *Flow and Fracture of Rocks*. Geophysical Monograph 16, 275–284. Washington, DC: American Geophysical Union.
- Secor, D.T. 1965. "Role of fluid pressure in jointing." *American Journal of Science*, v. 263, 633–646.
- Stein, R.S., King, G.C.P., and Lin, J. 1992. "Change in failure stress on the southern San Andreas fault system caused by the 1992 magnitude 7.4 Landers earthquake." *Science*, v. 258, 1328–1332.
- Zoback, M.L. 1992. "First- and second-order patterns of stress in the lithosphere: the world stress map project." *Journal of Geophysical Research*, v. 97, no. B8, 11,703–11,728.
- Dahistrom, C.D.A. 1969. "Balanced cross-sections." *Canadian Journal of Earth Sciences*, v. 6, 743–757.
- DePaor, D.G. 1988. "Balanced sections in thrust belts, Part I: Construction." *American Association of Petroleum Geologists Bulletin*, v. 72, 73–91.
- Elliot, D. 1983. "The construction of balanced cross-section." *Journal of Structural Geology*, v. 5, 101.
- Marshak, S. and Woodward, N. 1988. "Introduction to cross-section balancing." In: Marshak, S. and Mitra, G. (eds) *Basic Methods of Structural Geology*. Englewood Cliffs, NJ: Prentice Hall, Chapter 14, 303–332.
- Mitra, S., and Namson, J. 1989. "Equal-area balancing." *American Journal of Science*, v. 289, 536–599.
- Suppe, J. 1983. "Geometry and kinematics of fault-bend folding." *American Journal of Science*, v. 283, 684–721.
- Wilkinson, M.S. and Dicken, C.L. 2001. "Quick-look techniques for evaluating two-dimensional cross sections in detached contractional settings." *American Association of Petroleum Geologists Bulletin*, v. 85, 1759–1770.

## Chapter 16: Deformation Mechanisms and Microstructures

### Chapter 14: Strain Measurement

- Compton, R.R. 1985. *Geology in the Field*. New York: Wiley. One chapter is devoted to field analysis of deformed rocks, including analysis of strain.
- Marrett, R. and Peacock, D.C.P. 1999. "Strain and stress." *Journal of Structural Geology*, v. 21, 1057–1063.
- Means, W.D. 1976. *Stress and Strain*. New York: Springer-Verlag.
- Ramsay, J.G. 1967. *Folding and Fracturing of Rocks*. New York: McGraw-Hill. A standard reference on strain analysis.
- Ramsay, J.G. and Huber, M.L. 1983. *The Techniques of Modern Structural Geology, Volume I: Strain Analysis*. London: Academic Press. A comprehensive coverage of strain analysis, suitable for the advanced structure student. Contains problems with answers and discussions.

### Chapter 15: Construction of Balanced Cross Sections

- Boyer, S.E. and Elliott, D. 1982. "Thrust systems." *American Association of Petroleum Geologists Bulletin*, v. 66, 1196–1230.
- Bell, T.H. and Ethendge, M.A. 1973. "Microstructure of mylonites and their descriptive terminology." *Lithos*, v. 6, 337–348.
- Berthe, D., Choukroune, P., and Jegouzo, P. 1979. "Orthogneiss, mylonite and noncoaxial deformation of granites: the example of the South Armorican Shear Zone." *Journal of Structural Geology*, v. 1, 31–42.
- Hanmer, S. and Passchier, C. 1991. "Shear-sense indicators: a review." *Geological Survey of Canada*, Paper 90–17, 72 p.
- Hirth, G. and Tullis, J. 1992. "Dislocation creep regimes in quartz aggregates." *Journal of Structural Geology*, v. 14, 145–159.
- Knipe, R.J. 1989. "Deformation mechanisms." *Journal of Structural Geology*, v. 11, 127–146.
- Lister, G.S. and Snoke, A.W. 1984. "S-C mylonites." *Journal of Structural Geology*, v. 6, 617–638.
- Passchier, C.W. and Simpson, C. 1986. "Porphyroclast systems as kinematic indicators." *Journal of Structural Geology*, v. 8, 831–843.
- Passchier, C. and Trouw, R.A.J. 1996. *Microtectonics*. Berlin, Heidelberg: Springer-Verlag, 289 p.
- Sibson, R.H. 1977. "Fault rocks and fault mechanisms." *Journal of the Geological Society of London*, v. 133, 191–213.
- Simpson, C. and Schmid, S.M. 1983. "An evaluation of the criteria to deduce the sense of movement in sheared rocks." *Geological Society of America Bulletin*, v. 94, 1281–1288.
- Snoke, A.W., Tullis, J.A., and Todd, V.R. 1998. *Fault-related Rocks: A Photographic Atlas*. Princeton, NJ: Princeton University Press, 617 p.

- Tullis, J., Snoke, A.W., and Todd, V.R. 1982. "Significance and petrogenesis of mylonitic rocks." *Geology*, v. 10, 227–230.
- Wise, D.U., Dunn, D.E., Engelder, J.T., *et al.* 1984. "Fault-related rocks: Suggestions for terminology." *Geology*, v. 12, 391–394.

### **Chapter 17: Introduction to Plate Tectonics (classic early papers)**

- Atwater, T. 1970. "Implications of plate tectonics for the Cenozoic tectonic evolution of western North America." *Geological Society of America Bulletin*, v. 81, 3513–3536.
- Atwater, T. and Stock, J. 1998. Pacific–North America plate tectonics of the Neogene southwestern United States — an update. *International Geology Review*, v. 40, 375–402.
- Condie, K.C. 1997. *Plate Tectonics and Crustal Evolution* (4th edn). Oxford: Butterworth-Heinemann, 282 p.
- Cox, A. and Hart, R.B. 1986. *Plate Tectonics: How It Works*. Palo Alto, CA: Blackwell Scientific Publications.
- Engebretson, D.C., Cox, A., and Gordon, R.G. 1985. "Relative motion between oceanic and continental plates in the Pacific Basin." *Geological Society of America Special Paper* 206, 1–59.
- Isacks, B., Oliver, J., and Sykes, L. 1968. "Seismology and the new global tectonics." *Journal of Geophysical Research*, v. 73, 5855–5899.
- McKenzie, D. and Morgan, W.J. 1969. "Evolution of triple junctions." *Nature*, v. 224, 125–133.
- Moore, E.M. and Twiss, R.J. 1995. *Tectonics*. New York: W.H. Freeman & Company, 415 p.
- Vine, F. and Matthews, D. 1963. "Magnetic anomalies over oceanic ridges." *Nature*, v. 199, 947–949.



# Index

- admissibility (of a balanced cross section) 136
- alignment diagrams (nomograms) 9–10
- Allmendinger, Richard 122
- Anderson, E.M. 86
- angle of incidence 156
- angles within a plane 43
- angular shear ( $\psi$ ) 119, 125–126
- angular unconformity 26–27
- anticline 55
- antiform 55
- antithetic shears 149
- apparent dip
  - alignment diagram, solution of 9
  - defined 2
  - orthographic projection solutions 4–7
  - plunge of ( $\alpha$ ) 4
- presentation in structure sections 32
- stereographic projection of 44
  - techniques for solving problems 3–9
  - trend of ( $\theta$ ) 4
  - trigonometric solutions 8–9
- apparent polar wander 162–163
- arc method 33
- asthenosphere 152
- asymmetric folds 54
- attitude 1
- auxiliary planes 157
- axial-planar foliations 70–71
- axial plane of a fold
  - defined 54
  - determination of through stereographic analysis 62
- axial surface of a fold 54
- axial trace of a fold
  - defined 54
  - determination of orientation 62
- azimuth method 2
- balanced cross sections (structure sections) 31
  - construction of 131–140
- Basin and Range Province 89
- beach-ball diagrams 155–158
- bearing 1
- bedding-cleavage angle 71
- beta axis 61
- beta diagrams 61
- Bingham plastic 102
- blind thrust 132
- boudins and boudinage 120
- Bree Creek Quadrangle map
  - introduction to 20
  - Neogene units 22–23, 26
  - Paleogene units 24
  - summary of exercises involving 95
- brittle failure 107–117
- brittle-plastic transition 105
- Brunton compass 165–166
- Busk method 33
- cataclasis 141, 145
- cataclasite 144–145
- cataclastic foliation 145
- Clar compass 165
- cleavage-bedding angle 71
- coaxial strain 121–125
- Coble creep 142
- compass use 165–166
- compressional first motion 156
- conformable contacts 26
- conjugate shear surfaces 86
- constricted ellipsoids 129
- contacts
  - angular unconformity 26–27
  - conformable 26

- contacts (*cont'd*)  
   defined 26  
   depositional 26–27  
   fault 26–27  
   intrusive 26–28  
 contoured equal-area diagrams 65–68  
 Coulomb coefficient ( $\mu$ ) 113–114  
 crest of a fold 53  
 crestral trace 54  
 crestral surface 54  
 cross sections, *see* structure sections  
   *see also* balanced cross sections  
 crust 152  
 crystal plasticity 142  
 Curie temperature 161  
 cutoff point and line 132  
 cylindrical fold 54
- dashpot 100  
 declination (magnetic) 160  
 décollement 77  
 deformation mechanisms 141–150  
 delta porphyroclasts 148–149  
 depositional contacts 26–27  
 detachment fault 77  
 dextral slip 76  
 differential stress 107  
 diffusive mass transfer 141–142  
 dilation in fault rocks 144  
 dilational first motion 156  
 dip  
   defined 1  
   determination from outcrop pattern 21–23  
   exaggeration of 36, 169  
   methods of expressing 3  
 dip isogons 56–57  
 dip separation 77  
 dip-slip fault 76  
 disconformity 26–27  
 dislocation glide and climb 143  
 down-plunge viewing of folds 59  
 drill-hole stereonet problem 48–51  
 dynamic analysis of faults 85–89  
 dynamic recrystallization 133
- effective stress 116  
 elastic deformation 99–100  
 elasticoplastic deformation 102  
 elasticoviscous deformation 102–103  
 emergent thrust 132  
 epicenter 155  
 equal-area net 38–39  
 Europa 105  
 extension 118–119  
 extension axis 91
- failure envelope 111–114  
 fault-bend fold 133–135  
 fault block tilting 82  
 fault breccia 144–145  
 fault contacts 26–27  
 fault gouge 145  
 fault plane 76  
 fault-plane solutions 157  
 fault-propagation fold 133, 135–136  
 fault rocks, classification of 144–145  
 fault slip, measurement of 78–79  
 fault tip 135  
 fault trace 77  
 fault zone 76  
 faults  
   defined 76, 144  
   description of 76–78  
   dip-slip 76  
   dynamic analysis of 85–89  
   kinematic analysis of 90–93  
   map patterns of 82–83  
   oblique-slip 76  
   strike-slip 76  
   timing of 83  
 finite strain ellipse  
   coaxial 124  
   noncoaxial 126  
 firmoviscous deformation 104  
 first motion studies 156  
 flats 131  
 Flinn diagram 129  
 focal-mechanism solutions 155–158  
 focal sphere 155  
 focus (of an earthquake) 155  
 fold axis  
   defined 54  
   determination through stereographic analysis 61–62  
 folds  
   asymmetric 54  
   axial plane of 54  
   axial surface of 54  
   classification based on dip isogons 56–57  
   descriptive terminology 53–55  
   down-plunge viewing of 59  
   fault-bend 133–135  
   fault-propagation 133, 135–136  
   interlimb angle of 55  
   kink 54  
   “M” folds 54  
   outcrop patterns of 57–58  
   overturned 55  
   parasitic 69–70  
   profile plane of 54  
   reclined 55  
   recumbent 55  
   “S” folds 54  
   vertical 55  
   “Z” folds 54  
 foliation  
   axial planar 69–70  
   cataclastic 145  
 footwall block 77  
 foreland 131  
 fossils (use in strain measurement) 127–128

- fracture processes 141  
fracture strength 112
- geologic map interpretation 21–30  
geologic time scale 167  
geometric lines 123  
girdle 67  
great circles 38–39  
Greek letters used in this book 168
- hanging-wall block 77  
heave 77  
hinge 132  
hinge line 53  
hinge point 53  
hinterland 133  
Hookean body 100  
Hooke's law 100  
hydraulic fracturing 116  
hypocenter 155
- incidence, angle of 156  
inclination (magnetic) 160  
incremental strain ellipse 123  
infinitesimal strain ellipse 123  
inflection, line of 53  
inflection point 53  
interlimb angle of a fold  
  defined 55  
  measurement of using stereographic  
  projection 67–68  
internal friction  
  angle of ( $\varphi$ ) 113  
  coefficient of 114  
intracrystalline plastic deformation 141–142  
intrusions  
  contacts of 26, 28  
  presentation on structure sections 33  
ionic diffusion within grains 142
- Kamb contouring method 93  
Kelvin body 104  
kinematic analysis of faults 90–93  
kinematic compatibility 92  
kinematic indicators 146–147  
kink fold 54  
kink-fold method of thrust-fault analysis 133  
klippe 83
- Lambert equal-area net 38–39  
listric fault 77  
lithosphere 152  
longitudinal strain 118–119  
loose line 137
- “M” folds 69  
magnetic reversals 160–161  
magnetic stripes 161  
magnetism 160–163  
mantle 152
- material lines 123  
Maxwell body 103  
median surface 53  
mica beards 142–143  
microstructures 141–150  
mid-ocean ridges 154  
Mohr, Otto 109  
Mohr circle 110  
Mohr diagram 109  
Mohr envelope of failure 111  
movement plane 91  
mylonite 145
- Nabarro–Herring creep 142  
neoblasts 144  
Newtonian fluids 100  
nodal planes 157–158  
nomograms 9–10  
noncoaxial strain 122, 125–127  
nonconformity 26–27  
noncylindrical fold 54  
non-Newtonian fluids 101  
normal faults  
  defined 77  
  map patterns of 82  
  stress orientation of 86  
normal stress 86, 107
- oblique-slip fault 76  
offset 77  
ooids (used in strain measurement) 129  
orthographic projection 3  
  use in apparent dip problems 4–7  
  use in thickness determinations 25  
outcrop patterns  
  description of 11  
  examples 12–14  
  use in determining attitude 31–33  
overturned fold 55
- P axis 157  
paleomagnetism 161  
panel 132  
parallel folds 57  
parasitic folds 69–70  
pi axis 62  
pi circle 62  
pi diagrams 62  
piercing points 76  
pin line 137  
pitch 1  
plane strain 129, 147  
plastic deformation 101  
plate tectonics 152–164  
  principles of 152–153  
play dough 118, 121–124  
plunge 1  
pore pressure 115–117  
porphyroclasts 145, 148–149  
preexisting planes of weakness 87



- pressure solution 142
- primitive circles 38–39
- principal strain axes 119
- principal stresses ( $\sigma_1, \sigma_2, \sigma_3$ ) 85–86
- profile plane of a fold 54
- protomylonite 145
- pure shear 122
  
- quadrant method 2
- quartz ribbons 142
- quicksand 101
  
- rake 1
- ramps 131
- Rangely experiment 116
- reclined fold 55
- recrystallization 141, 143–144
- recumbent fold 55
- report writing 95–98
- retrodeformability 31, 136
- reverse faults
  - defined 77
  - map patterns of 82–83
  - stress orientation of 86
- rheological models 99–106
- rheology 99
- right-hand rule 3
- rotational fault 77, 80
  
- “S” folds 69
- San Andreas fault 76, 157–158
- S-C fabric 147
- S-C mylonites 147
- Schmidt net 38–39
- scissor fault 77, 80
- shear
  - angular ( $\psi$ ) 119, 125–126
  - antithetic 149
  - pure 122
  - sense of 146–147
  - simple 125, 147
- shear fractures 86
- shear strain ( $\gamma$ ) 119
- shear stress ( $\sigma_s$  or  $\tau$ ) 86, 107
- shear surfaces, conjugate 86
- shear thickening and thinning 101
- shear zone 144
- shortening axis 91
- sigma porphyroclasts 148
- Silly Putty 99, 105
- similar folds 57
- simple shear 125, 147
- sinistral slip 176
- slickenlines 77, 146
- slickensides 77
- slip line 157
- slip vector 76
- small circles 38–39
- standard linear solid 105
- static recrystallization 144
- stereographic analysis of folds 61–68
- stereographic nets 38–39
- stereographic projection 38–51
  - angle within a plane 43
  - drill hole problem 48–51
  - line projection 40
  - line rotation 46–47
  - plane 40
  - plane intersection 42–43
  - pole 42
  - two-tilt problem 47
- strain ( $\epsilon$ ) 99
  - coaxial 121–125
  - longitudinal 118–119
  - measurement methods
    - fossils 127–128
    - ooids 129
  - noncoaxial 122, 125–127
  - plane 129, 147
  - shear ( $\gamma$ ) 119
- strain ellipse 119
  - incremental 123
  - infinitesimal 123
  - total (finite)
    - coaxial 124
    - noncoaxial 122, 125–127
- strain ellipsoid 128
- strain fields 120–121
- strain rate 102
- StrainSim 122
- stratigraphic column, construction of 28–30
- stratigraphic thickness, determination of 23–25
- stress ( $\sigma$ ) 99
  - differential 107
  - effective 116
  - normal ( $\sigma_n$ ) 86, 107
  - principal ( $\sigma_1, \sigma_2, \sigma_3$ ) 85–86
  - shear ( $\sigma_s$  or  $\tau$ ) 86, 107
- stress ellipsoid 86–87
- strike
  - defined 1
  - determination from outcrop pattern 21–23
  - methods of expressing 2–3
- strike separation 77
- strike-slip faults
  - defined 76
  - outcrop patterns of 83
  - stress orientation of 86
- structural synthesis 95–98
- structure contours 14–20
- structure sections 31–37
  - arc method 33
  - format of 36–37
  - involving folded layers 32–33
  - involving intrusive bodies 33
- stylolites 142
- subduction 154
- subgrains 143
- superimposed strain 124
- superposed folds 72

- symbols
  - used on geologic maps 171
  - used to characterize folds 70
- symmetric folds 54
- syncline 55
- synform 54
- synoptic diagram 96
  
- T axis 157
- tear (strike-slip) faults 76
- three-point problems 15–16
- throw 77
- thrust faults 77, 197
  - blind 132
  - emergent 132
  - map patterns of 82–83
  - stress orientation of 86
- tilting of fault blocks 82
- topographic profiles 34–36
- total strain ellipse
  - coaxial 124
  - noncoaxial 126
- transform boundaries 154
- translational faults 77
- trend
  - defined 1
  - methods of expressing 2
- trigonometry
  - use in analysis of geologic maps 21–24
  - use in apparent-dip problems 8–9
- triple junction 154
- trough 53
- trough surface 54
- trough trace 54
- true dip, plunge of ( $\delta$ ) 4
- twinning 143
- two-tilt stereonet problem 47
  
- ultramylonite 145
- unconformities 26–27
- undulose extinction 143
  
- V patterns in outcrop 11–14
- vertical exaggeration 36, 169
- vertical fold 55
- viscous deformation 100–101
  
- Weber Sandstone 116
- Wellman technique 128
- wrench (strike-slip) faults 76
- writing style for geologic reports 97–98
- Wulff net 38–39
  
- yogurt, rheological behavior of 101
  
- “Z” folds 69













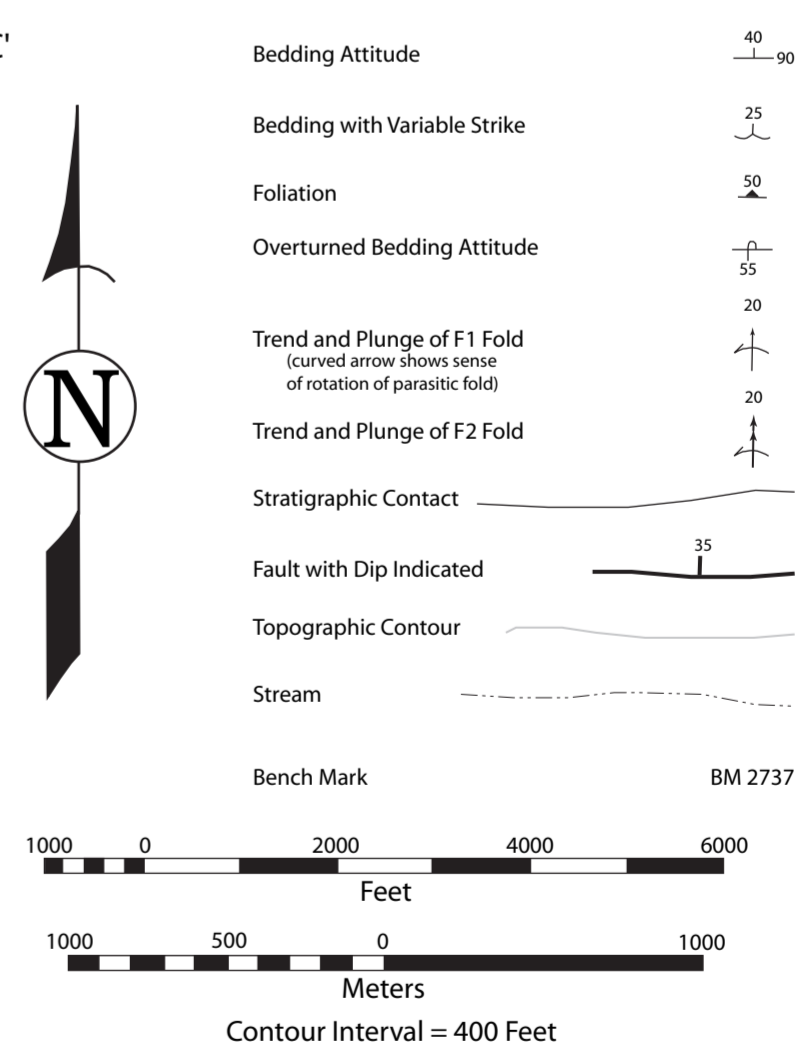






**Bree Creek Quadrangle**

Thd	Pliocene
Helm's Deep Sandstone	Miocene
Tr	
Rohan Tuff	
Tg	Tertiary
Gondor Conglomerate	
Tdd	
Dimill Dale Diatomite	
Tmm	
Misty Mountain Limestone	Eocene
Tm	
Mirkwood Shale	Paleocene
Tts	
The Shire Sandstone	
Tb	Paleocene
Bree Conglomerate	
Te	Paleocene
Edoras Formation (evaporites and nonmarine)	
Kdt	Cretaceous
Dark Tower Granodiorite	Mississippian
Mr	
Rivendell Dolomite	Devonian
Dlm	
Lonely Mountain Quartzite	Silurian
Sm	
Moria Slate	Ordovician
Omt	
Minas Tirith Quartzite	Ordovician
Omt	
Mt. Doom Schist	Ordovician



SMR©2007

